UNIVERSITY OF SOUTHAMPTON

FACULTY OF NATURAL AND ENVIRONMENTAL SCIENCES

Chemistry

Volume 1 of 1

Hyphenated Mass Spectrometry Methods for the Direct Characterisation and Quantification of Polar Molecules in Crude Oil or Modified Crude Oils

by

Ammar Nasif

Thesis for the degree of Doctor of Philosophy

December 2016

Abstract

UNIVERSITY OF SOUTHAMPTON

ABSTRACT

FACULTY OF NATURAL AND ENVIRONMENTAL SCIENCES

Chemistry

Thesis for the degree of Doctor of Philosophy

Hyphenated Mass Spectrometry Methods for the Direct Characterisation and Quantification of Polar Molecules in Crude Oil or Modified Crude Oils

Ammar Nasif

Crude oil is arguably one of the most complex organic mixture in nature. Therefore, crude oil characterisation requires the use of high resolution and high mass accuracy mass spectrometer such as FT-ICR MS; needed to resolve thousands of ions and assign their elemental formulae. Different heteroatom containing compounds classes are present in crude oil such as N_1, S_1 and O_2 containing compounds. These compounds cause variety of different problems such as N containing compounds cause catalyst deactivation for processes such as hydrodesulfurisation. The choice of the ionisation technique and its polarity is critical to the type of compounds that are observed in a crude oil mass spectrum. Two main studies for crude oil samples are covered in this thesis. The first is crude oil-1, 2 and 3 characterisation using ESI and APPI. The second is structural elucidation of nitrogen containing compounds in crude oil-2.

Positive ion ESI FT-ICR MS ionises basic molecules in crude oils. In the literature crude oil samples are dissolved using different ratios of toluene:methanol. The effect of using different solvent composition is often not regarded as important factor to consider. One of the reasons is the addition of ionisation enhancing additive such as formic acid, thought to normalise the ionisation response across different sample solvent composition. However, the solvent composition study data show that different toluene:methanol ratios play a critical role on the ionisation response of nitrogen containing compounds in different crude oils even with the addition of formic acid. Three different ratios were used which are toluene:methanol solvent ratios of 1:9, 3:7 and 6:4 with and without the addition of 0.1% formic acid for the analysis of crude oil-1, 2 and 3. The highest ionisation for N_1 containing compounds are achieved through using toluene:methanol ratio of 1:9 with 0.1% formic acid. Further to this the increase of toluene content in the

sample solvent decreased the ionisation of N_1 containing compounds in the analysed crude oils even with the addition of formic acid. However, the rate of decrease in the ionisation of N_1 containing compounds is more significant for crude oil-1 and 2 compared to crude oil-3. Thus, comparing nitrogen containing compounds among different crude oils should be undertaken using the solvent composition, toluene:methanol ratio of 1:9 with 0.1% formic acid. Another aspect for the solvent composition study is that multimer formation is not only concentration driven but as well sample solvent composition dependent. The data showed that multimer formation in N_1 DBE *versus* carbon number plots are reduced with acid addition and methanol content increase in the sample solvent.

The use of positive ion ESI allowed the ionisation of basic compounds in crude oil-1, 2 and 3. To ionise non-polar classes such as aromatics and thiophene containing compounds in crude oil-1, 2 and 3 positive ion APPI is used. Aromatics and thiophene were the most abundant ions in crude oil-1, 2 and 3 mass spectra. No significant difference in ion intensities for these ions were observed for crude oil-1, 2 and 3 mass spectra. However, the use of negative ion APPI showed major differences in the ions intensities of crude oil-1, 2 and 3 regarding HC, HC-R, N_1, S_1 and S_1-R classes. Further, comparable data for the O_2 class were obtained using negative ion ESI and APPI Orbitrap MS for crude oil-1, 2 and 3. Thus, negative ion APPI Orbitrap MS can be used to compare the O_2 class relative abundance among different crude oils.

Further to the characterisation study, structural elucidation of nitrogen containing compounds in crude oil-2 using positive ion ESI FT-ICR MS/MS was undertaken. Understanding the chemical structure might have applications in designing more effective catalysts for HDN process. At first a method development approach was undertaken to reduce the analysis time to 4.5 min and increase detection of low *m/z* low intensity fragment ions. This aim was achieved through increasing the ion accumulation time from 0.05 s to 5 s with averaging 40 spectra. Different N_1 precursor ions were isolated at different DBE values and degree of alkylation. A collision energy of 60 V was required to observe characteristic fragment ions such as N expulsion for N_1 precursor ion with DBE value of 13.5. While for N_1 precursor ion at DBE value of 6.5 a CE 40 V was enough to observe characteristic fragment ions. However, different approach was used for N_1 precursor ion with low DBE values, isolating the precursor ion with the lowest degree of alkylation. This approach was essential to observe N expulsion fragment ions for N_1 precursor ion with DBE value of 6.5. The core aromatic structure for N_1 precursor ions from DBE

values of 3.5 to 10.5 were suggested. This suggestion was based on N expulsion fragment ion and the dealkylated fragment ion. Furthermore, N expulsion from the aromatic ring supports the postulation that the nitrogen in the various precursor ions discussed is pyridinic. This was further confirmed for N_1 precursor ion with DBE value of 6.5 using a model compound, 2-butlyquinoline.

Table of Contents

List of Figures

Table of Figures

Table of Figures

Table of Figures

Table of Figures

Table of Figures

Table of Figures

Table of Figures

Table of Figures

List of Tables

List of Tables

DECLARATION OF AUTHORSHIP

I, Ammar Nasif declare that this thesis and the work presented in it are my own and has been generated by me as the result of my own original research.

Hyphenated Mass Spectrometry Methods for the Direct Characterisation and Quantification of Polar Molecules in Crude Oil or Modified Crude Oils

I confirm that:

1. This work was done wholly or mainly while in candidature for a research degree at this University;
2. Where any part of this thesis has previously been submitted for a degree or any other qualification at this University or any other institution, this has been clearly stated;
3. Where I have consulted the published work of others, this is always clearly attributed;
4. Where I have quoted from the work of others, the source is always given. With the exception of such quotations, this thesis is entirely my own work;
5. I have acknowledged all main sources of help;
6. Where the thesis is based on work done by myself jointly with others, I have made clear exactly what was done by others and what I have contributed myself;
7. None of this work has been published before submission:

Signed:.....

Date: 4/12/2016 .....

Acknowledgements

Professor John Langley has provided me great mentorship. In addition to the breadth of knowledge he shared with me, he shared invaluable skills both technical and transferrable. John has helped me become more attentive to details, a skill I was certainly lacking prior to my PhD. He taught me how a researcher and a mass spectrometrist approaches problems and how to solve them. I can go on for pages describing all that I have learnt from John over the past years. I shall always be so grateful to him. Most importantly, John has been the kind generous big brother when I needed someone the most especially in the last few months of the PhD journey and for this I shall always be indebted to him for his incredible support and patience.

I have been fortunate to be part of the Langley group at the university, of whom I would like to thank Julie Herniman for all her help and support in the lab. Julie is always calm, positive and willing to help and answer any questions. Thank you Julie.

I was fortunate to get the industrial exposure and experience and for that I would like to thank the team at BP; Mike Hodges, John Couves, Christianne Wicking and Huang Zeng. They were great help and added value input to the project. A special thanks to Christianne for her support and care during my secondment at BP and for all the training she gave me on how to use PetroOrg and the Orbitrap.

Special thanks to the support of my friends at Southampton Waraporn Ratsameepakai, Krina Patel and Efstathios Elia. I remember when I first met Stathis and he asked me where are you from? I said I am from Syria and he replied with a big smile I am from Cyprus. Usually when I tell people I am from Syria they get worried or scared but Stathis had a big smile on his face. Since then Stathis and I developed a friendship that will last beyond the PhD. Unfortunately, I didn't have the chance to live at Southampton but Stathis introduced me to all the places that serve good and cheap food. Thank you Stathis for being a good friend when I was in most need for one, I wish you all the best in the land of the Yankees.

I would like as well to thank Dr Francesco Cuda for all friendly advice. I met Francesco on the train and we became friends. Francesco, would come by my desk at the end of every day to leave together. I cherished our daily chats on

South West trains on the way back from Southampton. It was quite enjoyable and easing the boredom of the long commute.

I would like to thank my family for their endless support. I would like to thank my beloved Dima for what she endured of my mood swings. Dima was always helpful and positive and above all she trusted that I can do it all along the way. She was the most supportive. At the end when the writing started, she realised if I stayed at home I will start wasting my time. So every day she dragged me with her to Teddington where I will start writing till lunch time. Then we have lunch together and after that I continue writing till the end of the working day. Thank you Dima, without you I wouldn't have been able to develop a writing routine and I wouldn't have been able to finish my thesis. I would like to thank my parents' in-law and especially my mother in law, Amal for all the good food and motherly caring she offered me.

Finally, I would like to thank my parents and brothers to whom I belong and forever thankful to all what they have done for me.

Definitions and Abbreviations

ADC	Analog-to-digital converter
AGC	Automatic Gain Control
APCI	Atmospheric pressure chemical ionisation
API	Atmospheric pressure ionisation
APPI	Atmospheric pressure photoionisation
B	Strength of the magnetic field
CAD	Collisionally activated dissociation
CE	Collision energy
CID	Collision-induced dissociation
CRM	Charge residue model
DBE	Double bond equivalents
DC	Direct potential
DART	Direct analysis in real time
ECD	Electron capture dissociation
EE^+	Even-electron ion
EI	Electron ionisation
ES	Electrospray
ESI	Electrospray ionisation
f_c	Cyclotron frequency
FID	Free induction decay
f_m	Magnetron frequency
FIA	Flow injection analysis
GC	Gas chromatography
GC × GC	Two-dimensional gas chromatography

List of Abbreviations

HR MS	High-resolution mass spectrometry
HDS	Hydrodesulfurisation
HDN	Hydrodenitrogenation
HPLC	High performance liquid chromatography
ICR	Ion cyclotron resonance
IE	Ionisation energy
IEM	Ion evaporation model
IP	Ionisation potential
isCID	In-source CID
IUPAC	International Union of Pure and Applied Chemistry
LC	Liquid chromatography
LC-MS	Liquid chromatography-mass spectrometry
LEVI	Low-voltage electron ionisation
MMBPD	Million Barrels of Oil Per Day
m	Mass of the ion
min.	Minute
MALDI	Matrix-assisted laser desorption/ionisation
MS/MS	Tandem mass spectrometry
NPD	Nitrogen phosphorus detector
NMR	Nuclear magnetic resonance
NCE	Normalised collision energy
NIST	National Institute of Standards and Technology
OPEC	Organisation of Petroleum Exporting Countries
OSPW	Oil sands process-affected water
$OE^{+\cdot}$	Odd-electron radical cation

PA	Proton affinity
QqQ	Triple quadrupole
R	Resolving power
RF	Radio frequency
$RL^{\cdot}$	Radical loss
SORI-CID	Sustained-off resonance irradiation/CID
S/N	Signal-to-noise
T	Temperature
t	Time
TOF	Time-of-flight
U	Amplitude of DC
V	Amplitude of RF (electric potential)
v	Velocity of the ion
VPO	Vapour pressure osmometry
z	Number of charges

Chapter 1: Introduction

1.1 Crude oil

Crude oil is also referred to as petroleum. The etymology of the word petroleum is from Latin *petra* means rock and *oleum* means oil.[1] The inferred meaning is rock-oil which means that the oil is accumulated in subterranean reservoir, sedimentary rock. There are three types of petroleum; crude oil is a liquid that contains varying amounts of hydrocarbons, bitumens and impurities; natural gas which consists of light hydrocarbon predominantly methane; and semi-solid to solid forms which contains a high concentration of asphaltenes.[2]

Despite the attempt of countries around the world to diversify their energy sources, fuels that are derived from crude oil remains the most used energy source for cars, buses, tractors and airplanes. It is expected that global demand for crude oil will rise to 99 MMBPD by 2030, a 9% increase from current demand.[3] Conventional crude oil reserves are being depleted for Organisation of Petroleum Exporting Countries (OPEC) at rate of 1.25% per annum and for non-OPEC at 5.6% per annum based on 2005 production and recovery techniques.[4] Thus, to meet energy demands the oil and gas industry is resorting to unconventional sources of crude oils. It is expected that unconventional crude oil supply will approximately account for 15% of global crude oil production by 2035.[5]

Unconventional crude oils include shale oil[6], oil sands[7] and heavy crude oils[8]. These sources of crude oils have production related problems such as flowability[9], metal corrosion[10] and catalyst deactivation[11,12]. For example naphthenate[13] deposits have been frequently reported for heavy crude oils (immature) in different regions of the world, such as offshore production sites in Norway, Great Britain and the Gulf of Mexico.[14] This has resulted in more frequent obstruction of production pipelines that may result in shutdown until cleaning is undertaken. Other problems for oil sands include environmental concerns, such as the oil sands process-affected water (OSPW) resulted from extracting bitumen.[15]

1.1.1 Crude oil formation

Petroleum is derived from the thermal decomposition of kerogen, an organic macromolecule in sedimentary rock. (See Figure 1 for crude oil formation)[16]. Kerogen is insoluble in most organic solvents and its fragment, asphaltene, is present in crude oil.[17]

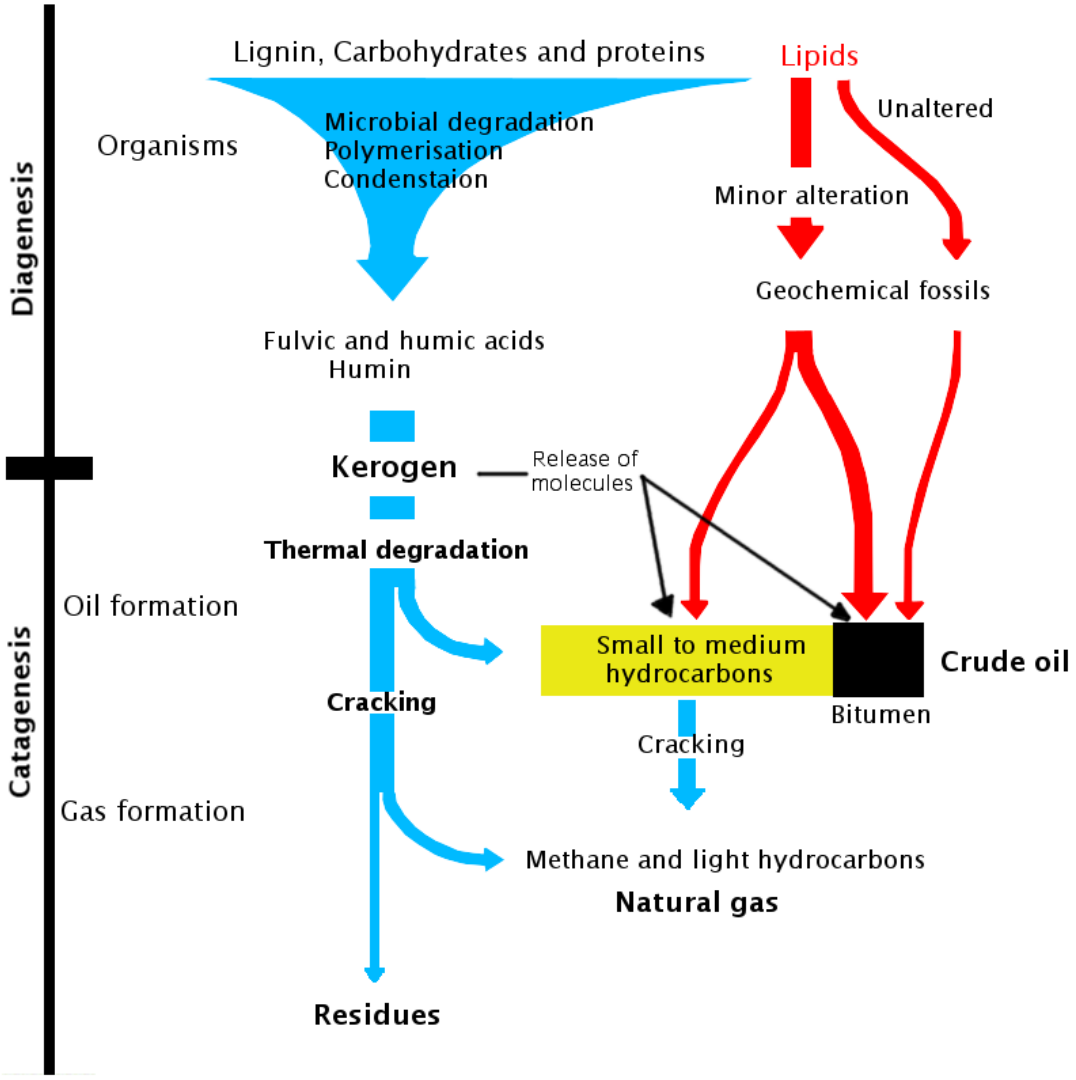

Figure 1 Crude oil formation and occurrence. Modified and reproduced from Tissot and Welte, 1984, summary of the oil process.[16]

Kerogens are derived from three main sources; Type I kerogen, hydrogen-rich, derived from algal and bacterial organic matter; Type II from sapropelic marine organics; and Type III from higher plant debris. Organic sulfur concentration in crude oil depends on the type of kerogen and its stage of evolution; immature Type II kerogen contains the highest amount of sulfur compared to Type I and III. This originates from the reaction of organic matter, the building blocks of kerogen, with hydrogen sulfide and elemental sulfur. .[18]

It should also be noted that iron in clastic sedimentary rock such as sandstone or siltstone competes with the organic matter for sulfur. Therefore, non-clastic derived kerogen such as carbonates, siliceous oozes and evaporites are rich in sulfur.

Mature crude oil is the result of a high thermal exposure (deeply buried for long times). This is reflected on the low content of sulfur because high temperature breaks the weak bond between C and S producing hydrogen sulfide gas (H_2S). Having a low S content crude is favourable because sulfur-containing compounds are catalysts poisons.[19] Further, nitrogen containing compounds and metals in crude oil cause catalyst deactivation. Trace elements in crude oils are also present such as nickel, vanadium and iron.[20]

1.1.2 Crude oil composition

Crude oil is one of the most complex natural mixtures. It is mainly composed of a certain set of elements ($C_cH_hN_nO_oS_s$). The mix of different hydrocarbons of different carbon chain length accounts approximately for 90% of the mixture, and is composed of alkanes (paraffins), cycloalkanes (naphthenes), aromatic hydrocarbons and asphaltenes.[1] Each different petroleum reserve contains different proportions of these types of hydrocarbons and this is reflected in the physical property of crude oil, such as viscosity and colour. High quality crude oils are of low viscosity and golden or amber in colour. An indication of the reserve maturation that translates into its rich content of desirable low molecular weights alkanes. While the remaining 10% (varies according to the type of crude oil) of compounds are the heteroatomic contaminants, containing nitrogen, oxygen and sulfur ($N_nO_oS_s$). The sulfur containing compounds are the most varied across different geographical origin and they give an indication of the quality of the crude.[21]

Saturates, also called paraffins, are aliphatic compounds that have the general formula of C_nH_{2n+2}, where n is the number of carbon atoms. Paraffins from C_1 to C_{40} usually appear in crude oil where more than 20 carbons are present are called paraffin waxes. Different paraffins are produced from crude oil *via* distillation. Isoparaffins, branched paraffins, are also present and they have a lowerboiling point than paraffins. Since they are saturated, paraffins are molecules that are stable over long periods of geological times.[22]

Cycloparaffins, also called naphthenes, are cyclic saturated hydrocarbons with the general formula of C_nH_{2n}. The most abundant are the most stable naphthenic rings which are those that contain 5 (cyclopentane) or 6 (cyclohexane) carbon atoms. Aromatic fractions contain mono-aromatics and polycyclic aromatics compounds. Common aromatics, found in crude oil are benzene and its analogues alkylbenzenes. Resins contain -NSO compounds such as acids, bases, phenolics and naturally occurring compounds such as humic acids.

The asphaltene fraction contains complex high-molecular weight hydrocarbons mixture and it is the heaviest and most polar fraction of crude oil, hence it can cause fouling problems. Asphaltenes are soluble in petroleum fluids and toluene, however it precipitates by the addition of an excess of n-heptane, is predominantly aromatic and decomposes on heating.[23,24] Asphaltenes can adsorb small aromatic hydrocarbons leading to the formation of micelles and hence the formation of colloidal system. (See Figure 2)

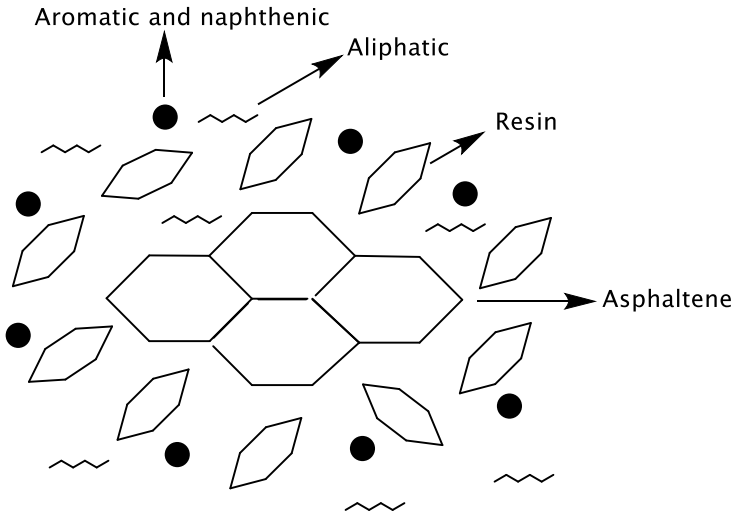

Figure 2 Asphaltene micelles. [25]

1.1.3 Crude oil classification

Crude oil is classified according to the American Petroleum Institute gravity, which measures its heaviness with respect to water and it is calculated from this equation: American Petroleum Institute gravity = 141.5/specific gravity (SG) – 131.5.[26] (See Table 1)

Bulk properties of crude oil are dependent on its American Petroleum Institute gravity value. Light crudes are rich with low-boiling compounds where as heavy crudes are the opposite.

Table 1 Crude oil classification according to American Petroleum Institute gravity.

American Petroleum Institute gravity	Crude Oil Classification
> 31.1	Light Crude Oil
22.3 - 31.3	Medium Crude Oil
10 - 22.3	Heavy Crude Oil
< 10	Extra Heavy Crude Oil

Crude oil is characterised as well depending on the sulfur content into sweet crude (< 1 percentage by weight wt%) and sour crude (> 0.5wt%) and can also be described depending on the predominant hydrocarbon either paraffinic or naphthenic crude oils.[27]

One of the most important classifications is based on crude oil compounds solubility in different solvents. Depending on this four fractions are obtained which are Saturates, Aromatics, Resins and Asphaltenes (SARA).[28] (See Table 2)

Table 2 SARA fractionation properties.

Fraction	Polarity	Characteristics	Colour
Saturate	Non-polar	Viscous oil	White
Aromatic	Non-polar	Viscous liquid	Dark brown
Resin	Highly-polar	Semi-solid	Dark brown
Asphaltene	Highly-polar	Solid	Brown

Figure 3 shows that when n-heptane is added to crude oil a precipitate is formed, asphaltene. The liquid fraction, referred to as maltene, contains the saturates, aromatics and resins. The separation of this fraction is undertaken using high performance liquid chromatography (HPLC). Alumina or silica packed column is used to achieve this separation.[29] Saturates are non-polar and therefore are not retained by the chromatographic column. While aromatics and resins, composed

of $C_cH_hN_nO_oS_s$ containing compounds, are eluted from the chromatographic column by increasing the percentage of the polar mobile phase.

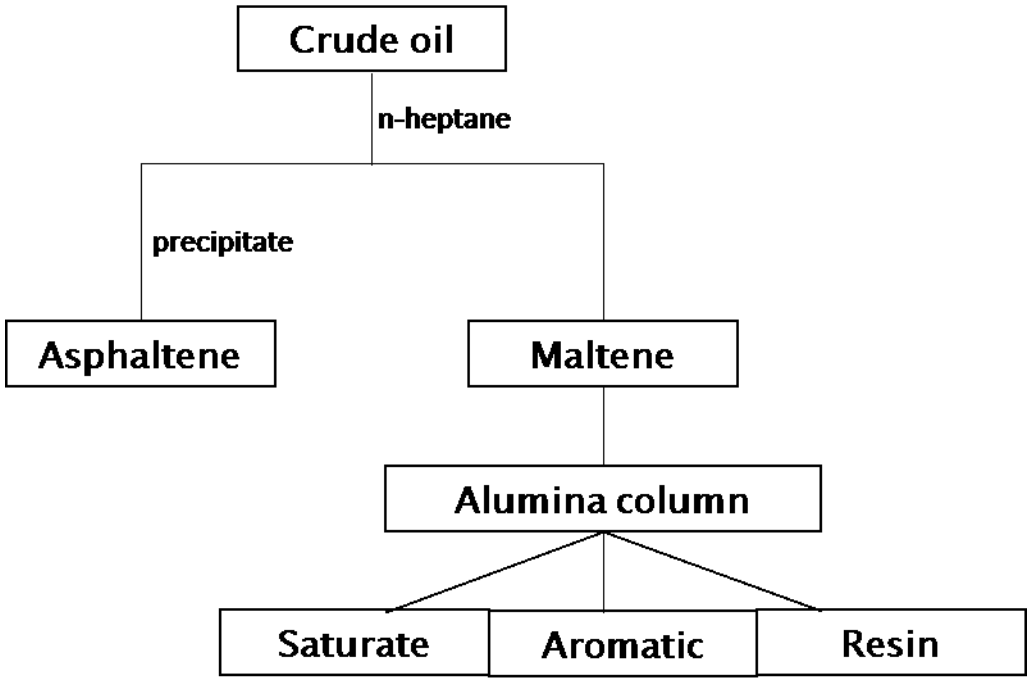

Figure 3 SARA fractionation.

1.1.4 Crude oil refining

Crude oil continues to be one of the most important energy source, however crude oil in its raw form is not usually used for an industrial application. It contains thousands of different molecules where methane (CH_4) is the simplest with a molar mass of 16 g/mol. These molecules have different boiling points, thus refining process is undertaken *via* distillation. The refining is a process in which different fractions are obtained from petroleum. These fractions undergo conversion processes such as cracking and reforming where the size and chemical structure of the molecule is changed. The refinery process can be divided into three main categories: first, distillation, is the separation of petroleum into different fractions in a distillation column. Second, conversion, is the chemical alteration of petroleum fractions. The third, treatment and purification, is removing impurities from the hydrocarbon fraction.[30-32] (See Table 3)

Table 3 Refining processes.

Process	Action	Reason	Result
Distillation	Vacuum and atmospheric columns	Different chains of hydrocarbons	Butane and propane, petrol, kerosene, diesel and *etc*.
Conversion	Decomposition	Cracking	Breaking large molecules to smaller ones
	Unification	Alkylation and polymerisation	Building larger molecules
	Reforming	Isomerisation and catalytic reforming	Changing geometric structure
Treatment	Purification	Desalting	Remove salt
		Hydrodesulfurisation	Remove sulfur
		Dewaxing	Improve pour point
		Sweetening	Reduce sulfur and odour

1.1.5 Polar molecules in crude oil

Heteroatoms containing compounds (N, O and S) are polar molecules and are classed as contaminants in crude oils.[33] (See Table 4). These compounds are present at high amount in immature crude oils. Although these compounds account for approximately 10% they cause a variety of different problems. For example –NSO containing compounds have many associated problems regarding the refinery process, thus influencing the cost of the process. Sulfur containing compounds are one of the most undesirable contaminants as they are transferred to diesel during the refining process. The Environmental Protection Agency (EPA) states that these compounds must be removed as they are one of the contributing factor of acidic rain. Acidic rain is caused when sulfur compounds in

diesel are converted to sulfur oxides during the combustion process. However, different countries have different limits for S and N containing compounds in fuels. Sulfur is removed by a hydrotreatment processes, *e.g*. hydrodesulfurisation (HDS).[34,35] However, the presence of small amount of nitrogen containing compounds in the feedstock (< 50 ppm) causes catalysts deactivation for HDS and other processes such as hydrocracking and reforming.[36] The deactivation mechanism involves the preferential adsorption of nitrogen containing compounds on catalysts that therefore hinders adsorption of other reactants. Therefore, the solution is hydrodenitrogenation (HDN), removes nitrogen containing compounds. However, conventional catalysts are not adequately effective for heavy crude oils.[11] Thus, designing more specific catalysts require detailed understanding of the chemical composition of crude oils. Furthermore, removal of N-containing compounds are a requisite from the EPA to limit the emission of nitrogen oxides, further N-containing compounds affects fuel stability during storage. These compounds are divided in crude oils into basic and non-basic materials. However, during hydroprocessing non-basic N-containing compounds are hydrogenated to basic compounds.[36]

Table 4 Possible heteroatoms (-NSO) containing compounds in crude oils.

Heteroatom	**Amount (wt %) in crude oils**	**Compounds**
Nitrogen	0.1%-0.9%[1]	Basic: amines, aniline, pyridines, quinolines, isoquinolines, benzoquinoline, acridines Non-basic including neutrals: pyrroles, indoles, carbazoles
Oxygen	< 2%[1]	carboxylic acids, phenols, cresols naphthenic acids
Sulfur	0.05%-14%[37]	hydrogen sulfide, organic sulfides and disulfides, benzothiophene, dibenzothiophene, thiols

Figure 4 shows an example of different structures that might be found in crude oils. Compounds containing more than one heteroatom can also be found. The R, attached to the aromatic or naphthenic ring or the alicyclic structure, is an alkyl chain that can be at different chain length and can be attached at different positions.

Asphaltene has a high content of heteroatoms (N, O and S) and metals (Ni and V). Asphaltene has many associated problems such as precipitation during hydroconversion. Asphaltene increases the viscosity of crude oil. This increases the difficulty of transporting crude oil with high content of asphaltene. Further, asphaltene can cause catalysts deactivation [38,39]

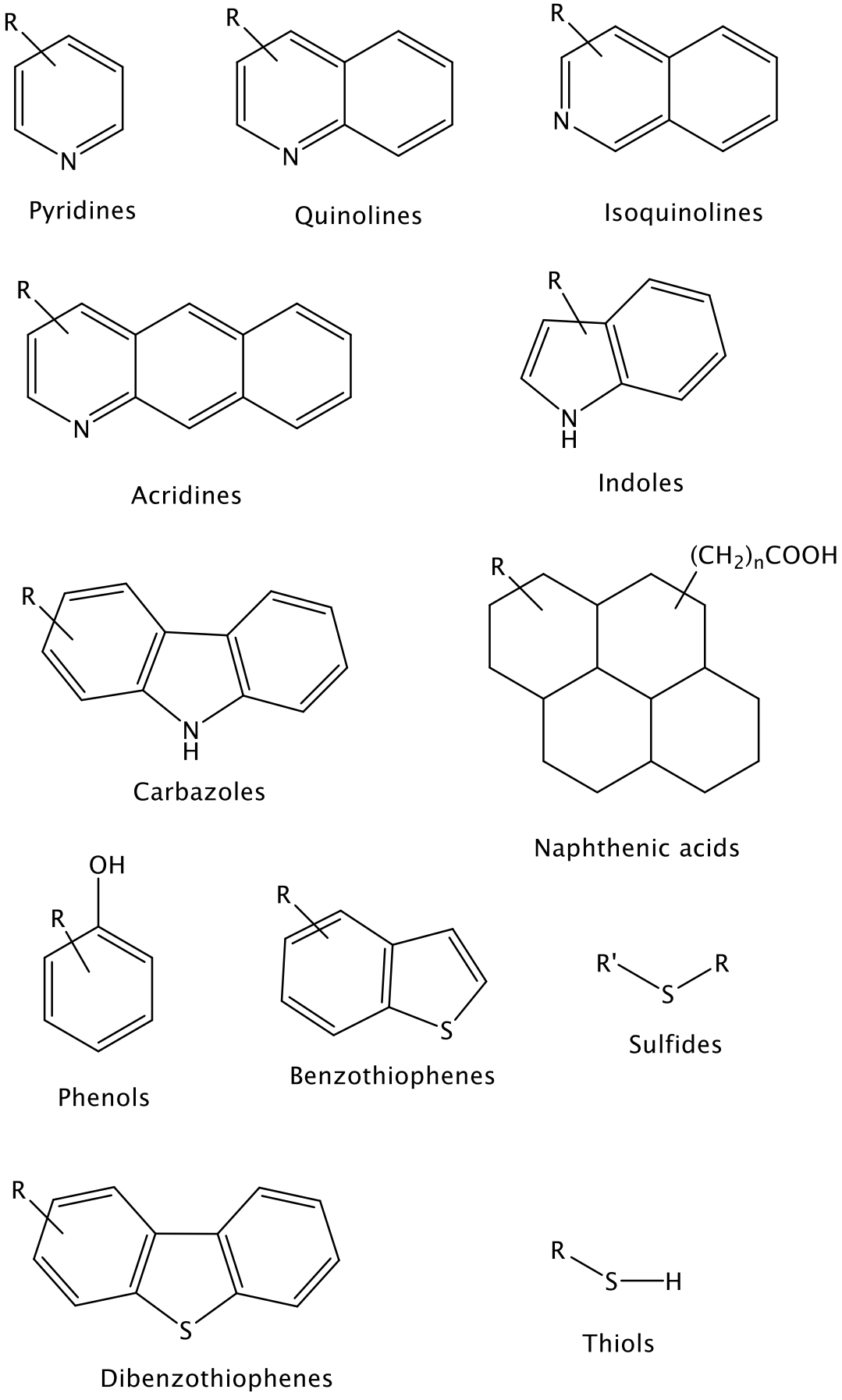

Figure 4 Example of heteroatom containing compounds present in crude oils

The presence of naphthenic acids (NAs) in crude oils, classified as part of the polar molecules content of crude oil, have many associated problems. NAs can cause corrosion in refineries, called naphthenic acid corrosion, and is one of the major problem for crude oil processing.[40] Steel corrosion is the result of the reversible binding of the carboxylate ion with the metal ion. This process is favourable at temperature between 220 and 400 ºC. However, for temperature higher than 400 ºC NAs decompose and a layer of coke is formed on the steel.

The acidity of crude oil is measured using the total acid number (TAN). TAN is determined by the amount of potassium hydroxide in milligrams that is required to neutralise the acids in one gram of crude oil. Measurement of TAN cannot be reliably used as an indicator of NAs induced corrosion. This is because crude oils with high TAN have shown similar corrosiveness compared to crude oils with low TAN number.[41] However generally crude oil with a TAN of more than 0.5 has a high level of corrosion. NAs corrosion is dependant as well on the chemical structure of the molecule. For example, the adsorption of carboxylic acids on the metal surface is influenced by the number of methylene units $(-CH_2)_n$ in the carbon chain. Adsorption is increased at n = 3 to 4 but above these values steric hindrance decreases the adsorption to the metal surfaces.[42] Corrosion can be induced as well by the content of sulfur species and chloride. Corrosion induced by sulfur contents is proportional with the increase in temperature.[41] The NAs and sulfur corrosion are two competing processes that can be explained according to the following Equation 1:

$$Fe + 2RCOOH \rightarrow Fe(RCOO)_2 + H_2$$

$$Fe + H_2S \rightarrow FeS + H_2$$

$$Fe(RCOO)_2 + H_2S \rightarrow FeS + 2RCOOH$$

The difference between iron naphthenate and iron sulfide is that the first is soluble in crude oil whereas the latter forms a protective layer on the metal surface. NAs can be regenerated by the reaction of iron naphthenate with hydrogen sulfide. Thus, a crude oil with high content of naphthenic acids and low amount of sulfur is more corrosive compared to crude oil with the same amount of NAs but with higher amount of sulfur.[40] Characterisation of polar molecules in different crude oils compounds will be the focus of this thesis.

Chapter 2: Instrumentation

2.1 Mass spectrometry (MS)

Mass spectrometry is an analytical tool where molecules are ionised using an ionisation source. Then, ions are separated in the mass analyser depending on their mass and charge. Thus, MS is an instrument that measures *m/z*. *m/z* definition according to the IUPAC represents the dimensionless quantity formed by dividing the ratio of the mass of an ion to the unified atomic mass unit, by its charge number (regardless of sign).[43] The data is presented by plotting *m/z* on the abscissa and the relative abundance of the ions on the ordinate.

According to the IUPAC mass-to-charge ratio is sometimes used instead of *m/z*. However, the term mass-to-charge ratio is deprecated. This is because the quantity measured is not the mass of the ion divided by it electric charge. Further, *m/z* should not be used in mathematical equation but instead the variables mass (m) in kg and charge (q) in C should be used.

The mass spectrometer is composed of three main components; the ionisation source generates gas phase ions through use of different ionisation techniques, such as electron ionisation (EI) and electrospray ionisation (ESI); the mass analyser, such as quadrupole and FT-ICR, separates the ions according to their *m/z* values; the detector, *e.g.* an electron multiplier registers the ion current. The mass spectrometer operates under vacuum. (See Figure 5). MS is capable of generating rich information content about gas phase ions such as accurate mass and structural information in the case of tandem MS.

The rationale for tandem MS is the introduction of soft ionisation technique where little or no fragmentation is observed for the protonated/deprotonated molecule.

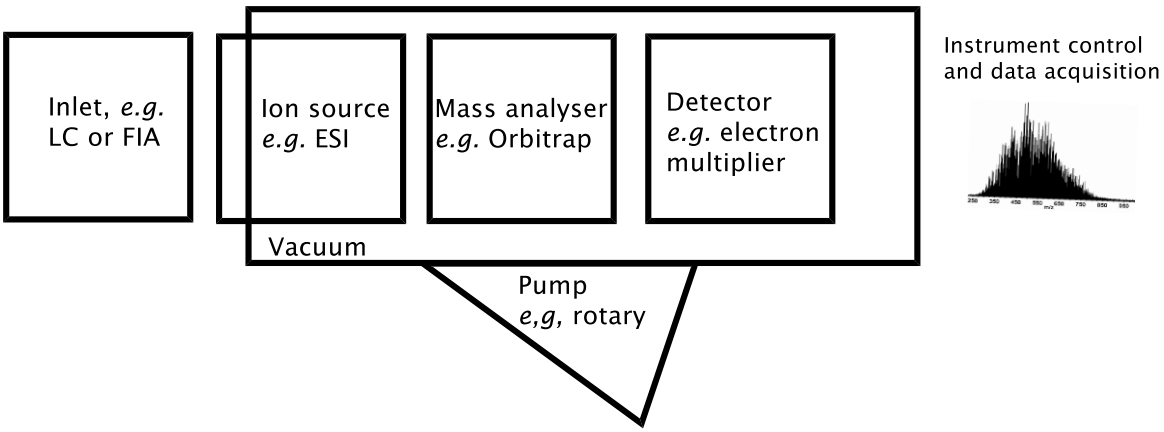

Figure 5 The main components of a mass spectrometer.

2.1.1 Ionisation techniques

2.1.1.1 Electrospray ionisation

Electrospray ionisation, (ESI), is an ionisation method that is widely used for ionising polar high and small molecular weight compounds producing the ionised form of the neutral molecule. Factors govern the ionisation mechanism of an ESI source; charged droplets are produced; desolvation of these charged droplets, are aided through stream of nitrogen and temperature, results in Coulombic fission yielding the gas phase ions.[44,45] Figure 6 shows how the analyte is introduced into the desolvation chamber by either flow injection analysis (FIA) through a syringe pump or as an eluent from a chromatographic column. The dissolved analyte in solution then passes through the ESI needle. The high potential difference, 2 to 4 kV, is applied between the ESI needle and the counter electrode. The dispersion of the liquid is caused by the electric field forming highly charged droplets, the process is described in details in Figure 8.

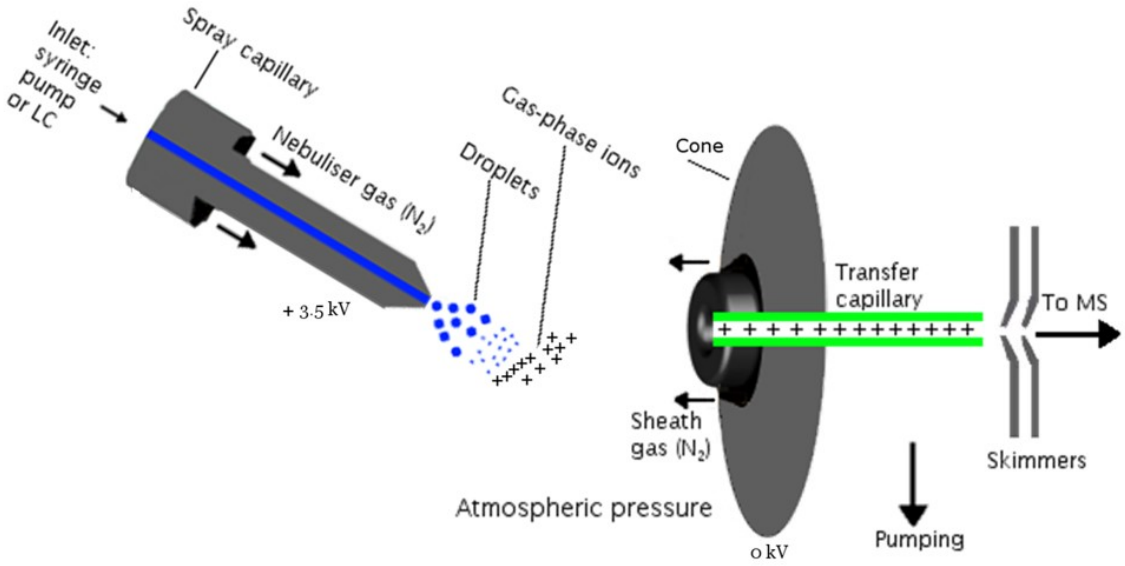

Figure 6 Schematic of an ESI source is shown.

The polarity of the ESI source can be switched depending on the analyte chemistry. In positive ion ESI basic compounds with a protonation site can be ionised producing $[M + H]^+$. Ions are repelled from the capillary (positive electrode) and elecrophoretically move toward the tip of the needle whereas the negative electrode is the sampling cone. For negative ion ESI the reverse is true where acidic compounds can be detected as they deprotonate, producing negative ions, $[M - H]^-$.

Taylor cone formation[46] is described by the process of which the charge density of the meniscus, has formed at the capillary tip, is raised due to an increase in Coulombic repulsions of ions. The meniscus shape is changed to a cone like shape because Coulombic repulsions is greater than Rayleigh instability limit (surface charge repulsion equals surface tension of the solvent). Taylor cone acts as producer of a stream of smaller droplets containing either an excess amount of anions or cations.[46] See Figure 8, illustrates the Taylor cone and the produced droplets. This process is aided by a stream of nitrogen which acts as the drying gas causing droplets to shrink in size. Thus, the charge density in droplets is further increased leading to Coulombic fission. At this point the electrostatic repulsion forces, has overcome surface tension, lead to smaller droplets.[47] From these droplets gas phase ions are introduced to the orifice of the mass analyser. Two main theories have been proposed to describe the process; the first by Iribarne and Thomson[48]; and the second by Dole *et al*.[49] The first is the ion evaporation (IE) model which proposes that small droplets (less than 10 nm in diameter) can evaporate leading to gas phase ion. However, this model can only

describe small ion gas formation whereas for larger biomolecule the second model is used, the charge residue model (CRM). CRM is defined as a single ion contained in a small droplet, a by-product of Coulombic fission and solvent evaporation. (See Figure 7)

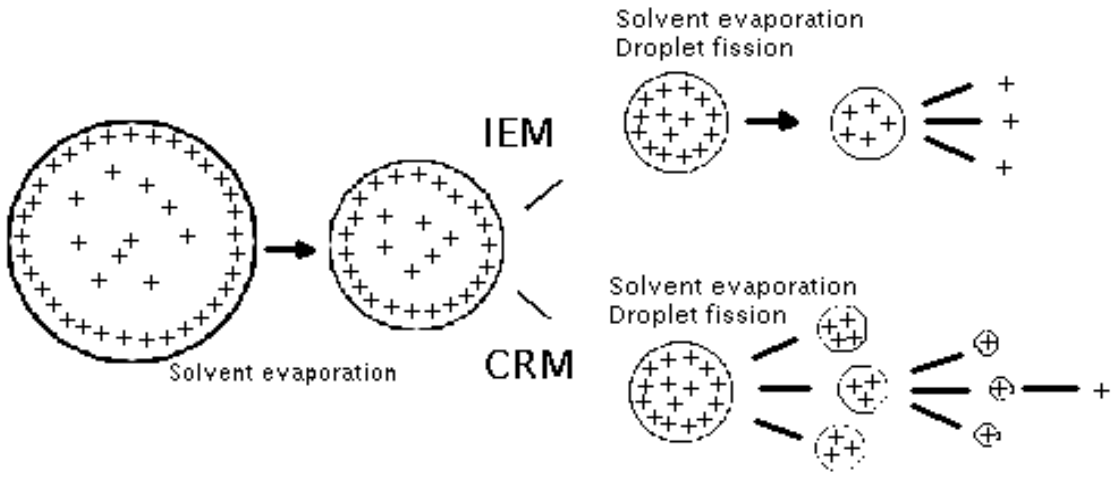

Figure 7 Ion evaporation model and charge residue model are shown.

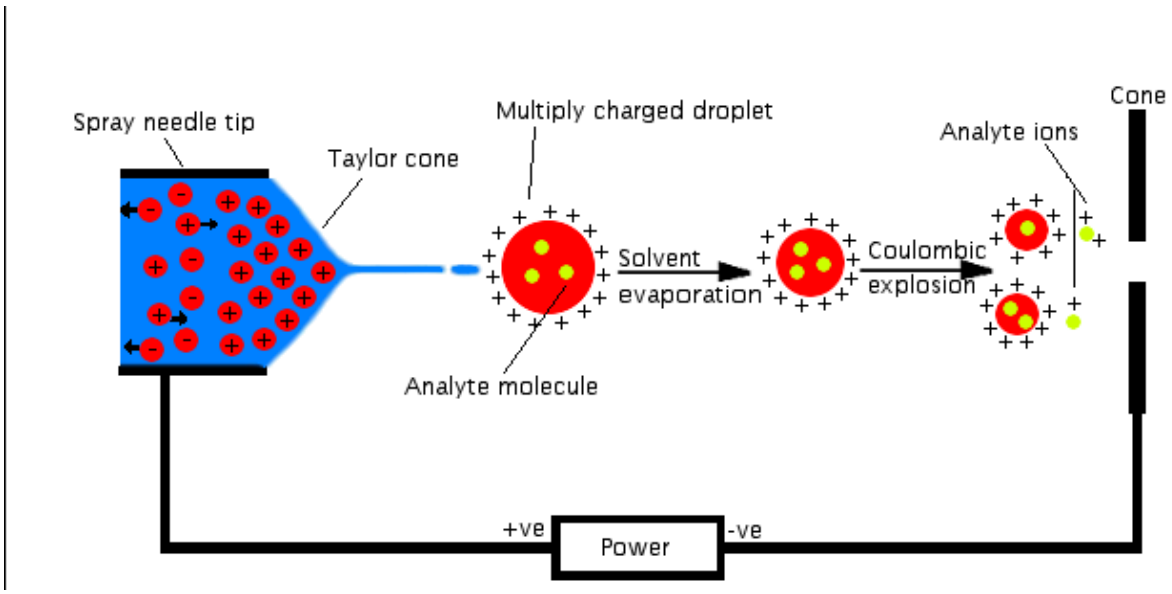

Figure 8 The desolvation mechanism is illustrated starting from the formation of the Taylor cone to the final stage of gas phase ion production. Positive ion ESI.

ESI is ionisation technique of choice for ionising polar molecule and large biomolecule with no or little fragmentation. Thus, ESI is classified as a soft

ionisation technique where ionisation takes place at atmospheric pressure. Protonated species can be detected in positive ion ESI such as basic compounds $[M + nH]^{n+}$ whereas deprotonated species are detected using negative ion ESI such as acidic compounds $[M - nH]^{-n}$. n>1 is usually associated with biomolecule which has multiple protonation site producing multiple charged species complicating the mass spectrum which requires additional processing software to process the data. However, for small molecules such as small polar molecules in crude oil singly charge species are produced (n = 1). Adduct formation such as $[M + Na]^+$, $[M + K]^+$ and $[M + NH_4]^+$ can be produced depending on the ions present in the solvent.[50] ESI is prone to ion suppression and enhancement depending on the nature of the matrix that coelute with the analyte.[51] ESI is prone as well to contaminants such as alkali metals and solvent clusters. As was mentioned previously ESI is used for ionising polar molecules, however for ionising non-polar compounds atmospheric pressure photo ionisation is used.

2.1.1.1.1 Analysis of polar molecules in crude oil *via* electrospray ionisation

ESI has enabled the analysis of polar compounds in crude oil.[44,52] Crude oil is composed of 90% hydrocarbon (C_cH_h) which are not ionised under ESI conditions. This can be considered as an advantage as it adds specificity to the technique where the $C_cH_hN_nO_oS_s$ containing compounds are the most problematic with regard to pollution, deposit formation and refinery corrosion.

The ionisation step in ESI is achieved in the liquid phase by the addition of a weak acid such as formic acid in the case of positive ion ESI or weak base such ammonium hydroxide in the case of negative ion ESI. Thus, ionisation in ESI requires a relatively strong acidic or basic site such as carboxylic acid or pyridinic nitrogen respectively. Extending the range of ionisation to include aromatic hydrocarbon, thiophenes and furans will be advantageous.[53] Accessibility of these species using ESI can be through chemical derivatisation to methylated species. Further, thiophenes and furans in crude oil can be ionised using alternative ionisation techniques such as APPI.[54,55]

Table 5 Compounds that are ionised by positive and negative ion ESI

Neutral molecule	Negative ion ESI	Positive ion ESI
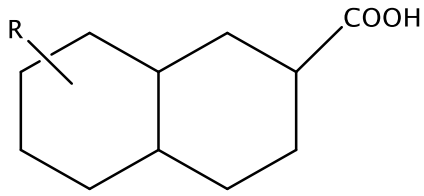	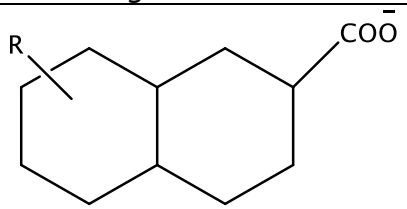	
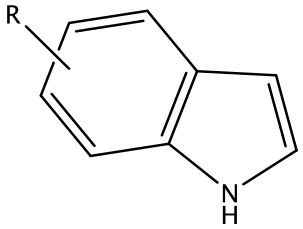	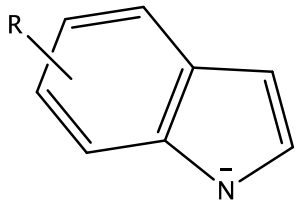	
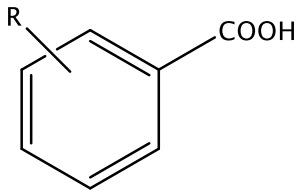	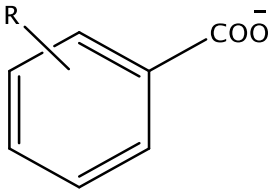	
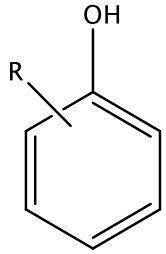	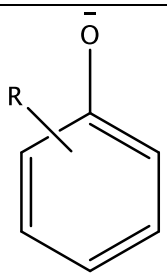	
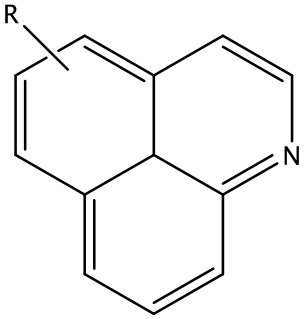		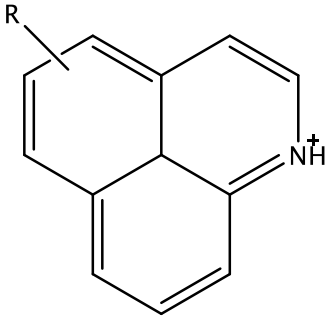
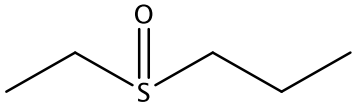		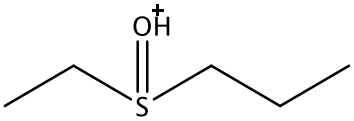
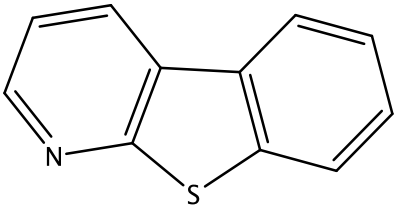		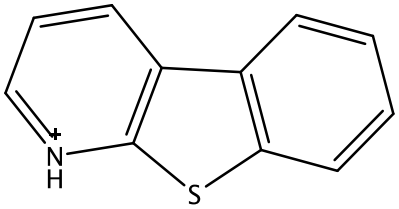

More than 17,000 different organic acids and bases have been resolved and identified using ESI FT-ICR MS.[56] The complexity of the mixture of crude oil translates into a complex mass spectrum. Hence the need is to arrange these compounds into different classes.[53] Petroleum is composed of homologous series that are defined by heteroatom class, double bond equivalents (DBE) and carbon number. Hsu *et al*. have shown[57] the advantage of using FT-ICR MS in analysing North American crude oil and Chinese crude oil. Chinese crude oil contained mostly the corrosive O_2 class species (naphthenic acid). While the North American crude oil contained mostly the N_1 class, pyrrole. However, pyrrole-containing compounds are of less interest in the deactivation of catalysts than basic nitrogen compounds.

2.1.1.2 Atmospheric pressure photoionisation

Atmospheric pressure photo ionisation (APPI) is a recently introduced ionisation technique, capable of ionising non-polar sulfur and hydrocarbons.[58] APPI is developed to broaden the range of ionisable compounds to include non-polar and polar and it's regarded as a complementary technique to ESI and APCI. For example, non-polar compounds such as PAHs or sulfur containing compounds in crude oil are usually unobservable by electrospray. A krypton UV discharge lamp is used to emit photons at 10.6 eV. Droplets are photoirradiated and molecular ions are produced if the irradiating photon energy ($h\nu$) exceeds the ionisation potential (IP) of the molecule. See Figure 9 for an APPI source schematic where its main components are illustrated. However, LC solvents such as methanol and acetonitrile can deplete the photon flux resulting in poor analyte ionisation. That is why the use of a photoionisable dopant, such as toluene or acetone, is sometimes necessary.[59-61]

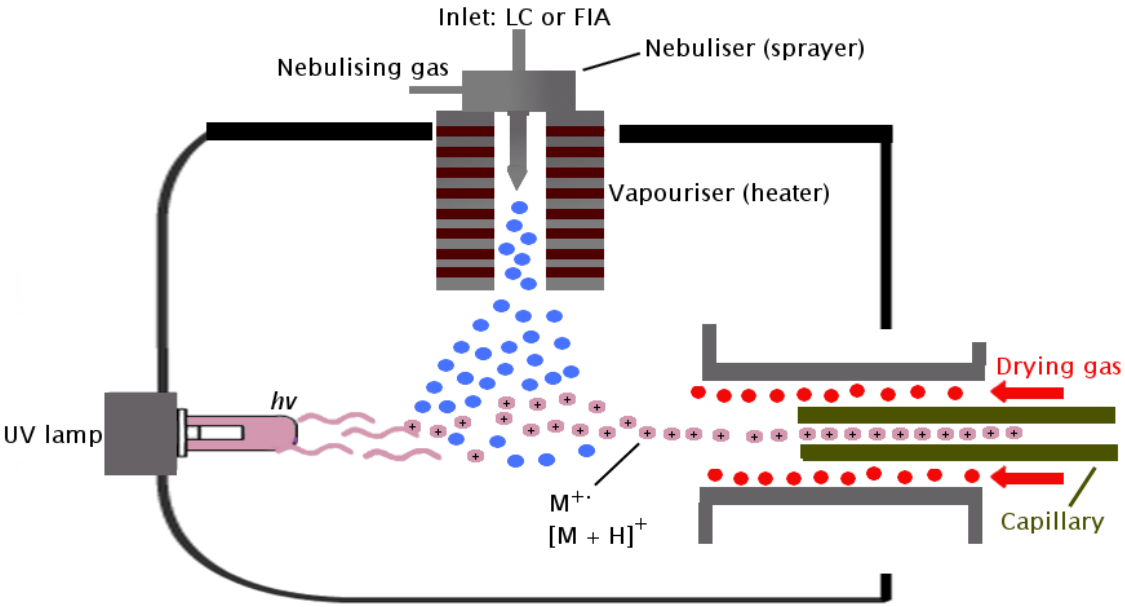

Figure 9 Schematic of an APPI source.

Usually a dopant is added when LC is coupled to an APPI source. The dopant is introduced directly into the solvent flow post-column or infused into a stream of hot gas through the auxiliary gas port of the APPI source heated nebuliser.

Toluene has a first IE of 8.3 eV, lower than that of the photons from the UV lamp (10.6 eV) and is typically infused at a flow rate that results in a relative molar concentration much higher than that of the analyte.

The combination of low first ionisation energy and high molar concentration increases the statistical probability that an analyte ion will form because the abundant dopant radical molecular ions interact reactively with the analyte.[58,62]

With toluene as a dopant two ionisation products can be observed. If the proton affinity of the analyte is higher than the proton affinity of the toluene, a protonated molecule is formed. Radical molecular ion can form as well if the electron affinity of the toluene radical cation is higher than the electron affinity of the analyte. It's possible to form these two species, radical cation and protonated molecule in the same analysis complicating the mass spectrum.

Robb *et al* have proved that the addition of a dopant increases sensitivity by promoting charge exchange reactions.[58] The experiment was conducted on 4 compounds with and without dopant. A 100-fold increase in signal intensity is observed for some of the compounds when the dopant is added.

In direct APPI the solvent and the analyte molecules are exposed to the UV light. A fraction of the analyte (M) is ionised directly by photons (hv). As a result, the analyte molecule is excited and an electron (e^-) is lost producing a radical cation ($M^{+\cdot}$).

Another pathway for the ionisation in direct APPI is possible. The analyte molecules can be ionised through proton transfer from the solvent molecules. The photons (hv) can excite the solvent molecules. Since the ionisation takes place at atmospheric pressure billions of molecular collisions per second is possible between the abundant solvent and the analyte molecules. The result is solvent-assisted chemical ionisation in which a proton is donated from the solvent molecule to the analyte.

The end result is the formation of two types of ions from the neutral compound, $M^{+\cdot}$ and $[M + H]^+$. These are shown below:

Equation 2

Direct APPI[59]:

$$M + hv \rightarrow M^{+\bullet} + e^-$$

$$M + S + hv \rightarrow [M + H]^+ + [S - H]^-$$

The dopant assisted APPI is similar to direct APPI where two types of ions are produced. The dopant molecules (D) are ionised first by the photons because they outnumber the analyte molecules (M). Then two ionisation pathways are possible for the analyte molecules. The dopant can either donate a proton to the analyte molecule or receive an electron from the analyte molecule. The two ionisation pathways for the analyte molecules are shown below;

Equation 3

Dopant assisted APPI[59]:

$$D^{+\bullet} + M \rightarrow [M + H]^+ [D - H]^\bullet$$

$$D^{+\bullet} + M \rightarrow M^{+\bullet} + D$$

2.1.1.2.1 Analysis of non-polar and low-polarity compounds in crude oil *via* APPI

Crude oil analysis by APPI can be challenging because of the complexity of the sample producing protonated molecule and radical cation from the same compound. Calculation of the double bond equivalent (DBE) for a protonated molecule results in a non-integer value. Hence, by simply calculating the DBE value from the molecular formula, determined by ultrahigh-resolution and mass accuracy MS of detected ion, the type of ion formed in the APPI source can be determined. Purcell *et al.*[63] have analysed crude oil mixture using atmospheric pressure photoionisation (APPI) coupled to a 9.4 T FT-ICR MS. APPI produces protonated, deprotonated, and cation radical molecular ion in a single run. This makes the crude oil mass spectra of APPI even more complex compared to ESI mass spectra of crude oil. The APPI source is capable of ionising non-polar classes in the crude such as S_1, S_2, HC and S_3 classes of compounds that are not ionisable by ESI. Some of these compounds are benzothiophenes, furans, cycloalkanes and polycyclic aromatic hydrocarbons (PAHs).[64]

The addition of a dopant such as toluene is essential when using APPI as it increases ionisation efficiency by promoting charge exchange reactions. The need for high resolution MS is important because of the two different ionisation events that can occur producing the ^{13}C molecular radical cation and the ^{12}C protonated molecular molecule with *m/z* difference of 4.5 m*m/z* units. The required resolution is 130000 at *m/z* 600 and higher at high molecular weight to separate these isobars. The isobar at 3.4 m*m/z* units ($^{12}C_3$ *vs* $^{32}SH_4$) is observed by ESI and APPI source however the 1.1 m*m/z* units isobar (C_4 vs. $SH_3{}^{13}C$) is only observed by APPI emphasising even more the need of high resolution mass measurement when an APPI source is employed. This is because when APPI is used a broader range of compounds are ionised in crude oil compared to ESI.

2.1.2 Mass analysers

2.1.2.1 Fourier transform ion cyclotron resonance mass spectrometry (FT-ICR MS)

FT-ICR MS was developed by Comisarov and Marshall.[65] The instrument is capable of performing high mass accuracy and high mass resolution experiments. A detailed description of the operating principles of FT-ICR MS is discussed in two detailed reviews by Marshall and co-workers.[66,67]

In FT-ICR MS, a spatially uniform superconducting magnet is used to trap ions in the ICR cell. The Penning trap, the ICR cell, can have different configurations such as cubic or cylindrical cell shape. Usually the ICR cell is composed of three pair of plates but there are other configurations such as dynamically harmonized cell. (See Figure 10) The plates at the front and the end of the ICR cell is the trapping plates, used to trap ions in the horizontal axis. The two excitation plates are connected with a radio frequency generator that is used to excite ions. The detection plates are used for the image current detection of current induced by ions.

A brief description of ions separation, excitation and detections can be described as; ions separation occur in the ICR cell according to their frequencies, associated to their *m/z* values[68] where the fixed magnetic field causes ions oscillation depending on their unique *m/z* values; a perpendicular oscillating electric field is applied to cause further oscillation of ions; a current is induced at the detection plates; Fourier transform is then applied to convert from cyclotron frequency to *m/z* value.

The high resolving power of FT-ICR MS is because the measured *m/z* value of ions is a function of frequency, and frequency is a parameter that can be measured with high accuracy by modern instruments. Peak resolution is proportional to the cyclotron frequency.

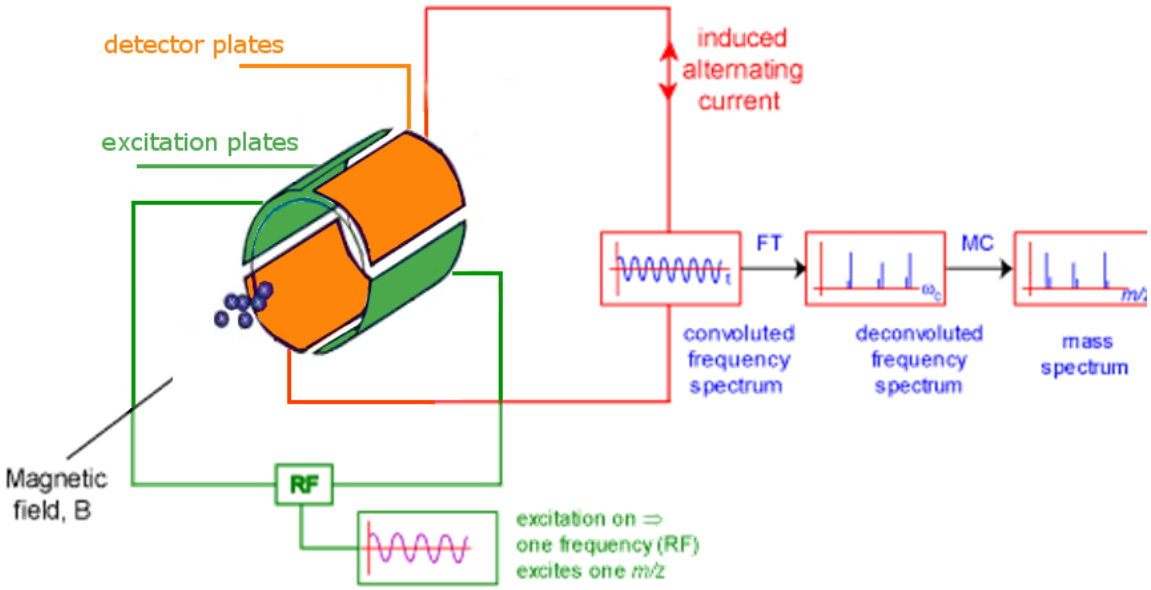

Figure 10 Schematic of a cylindrical ICR cell. Fourier transform and mass conversion are abbreviated as FT and MC respectively.

2.1.2.1.1 Ion motion

The FT-ICR cell is positioned at the centre of the magnet. Ions are introduced to the FT-ICR cell where they rotate around the magnetic field with a cyclotron frequency proportional to z/m where z is the number of charges per ion and m is the mass of the ion. The trapping mechanism of ions is affected by two forces; radial trapping of ions by the magnetic field; and axial trapping by quadrupolar electrostatic field. Because of the electrostatic fieldand the Coulombic contribution of ions in the FT-ICR cell the cyclotron frequency is shifted by a constant amount for all trapped ions.[66]

These effects are combined in a quadratic equation where the cyclotron frequency is computed as *m/z*. The calibration step is important when using FT-ICR MS instrument which can correct for the shift in the cyclotron frequency. Three or more ions of known *m/z* values are used to calibrate the instrument.[69] The intensity of the ions used for calibration should have the same intensity for the measured ions to correct for space charge effect and achieve sub 1 ppm mass accuracy.

Ion cyclotron motion of ions is derived from the interaction of ions with a spatially uniform magnetic field. The Lorentz force (F_L), perpendicular to the ion motion and the magnetic field, is responsible for the circular motion of ions.

Equation 4

$$F_L = qv \times B$$

Where: q = ionic charge, v = velocity and B is the magnetic field.

Equation 5

$$v_{xy} = \sqrt{v_x^2 + v_y^2}$$

Equation 6

$$\left[\frac{dv}{dt}\right] = v_{xy}^2/r$$

Substitution of the velocity (v) in the *xy* plane Equation 5 and the angular acceleration [dv/dt] Equation 6 with F_L Equation 4 to give:

Equation 7

$$qv_{xy}B_0 = mv_{xy}^2/r$$

where B_0 is the magnetic field in tesla, m is the ionic mass in dalton and r is the ion cyclotron orbital radius.

In Equation 7 v_{xy}/r is the angular velocity (ω) in radians/s, thus Equation 7 can be written as:

The unperturbed ion cyclotron frequency (ω_c):

Equation 8

$$\omega_c = qB_0/m$$

According to Equation 8, the circular motion of ions in the ICR cell depends on the strength of the magnetic field (B) and mass of the ion (m) and its charge (q). However, the radius of the cyclotron motion of the ion depends on its kinetic energy.[70] Each ion with a specific mass and charge has a unique cyclotron frequency (ω_c). This cyclotron frequency is proportional to the strength of the magnetic field (B). Thus, a stronger magnetic field provides a higher frequency. Thus, measurements of ions are more accurate with higher cyclotron frequencies.[70]

However, the motion of ions in the ICR cell are not circular but more similar to a spiral. [71] This is because other motions of ions than the cyclotron motion are present in the ICR Cell. The magnetron motion is dependent on the three-dimensional field that is formed from the strength of the magnetic field (B) and the electric potential (V). The magnetron motion is independent of the mass of the ion and its charge. However, the magnetron motion is dependent on the geometry of the ICR cell and the distance between the trapping plates of the ICR cell.[70]

Further, the axial trapping of ions using an applied DC voltage to the trapping plate produces another motion of ions in the ICR cell. This motion of ions is described as having harmonic oscillations between trapping plates in the ICR cell. Further, the trapping motion of the ions is affected by the low negative potential (if negative ions are stored). This negative potential is applied to the trapping plates of the ICR cell where three dimensional potential is produced due to the presence of the excitation/detection electrodes and the use of the trapping electrodes.

Ion cyclotron motion of ions cannot be detected because the cyclotron radius of ions is too small and ions are not coherent in the ICR cell. Thus, ions are stored in the ICR cell. Further, a radio frequency (RF) excitation pulse is applied, oscillating at or near the value of the cyclotron frequency. Therefore, ions that have the same cyclotron frequency as the oscillating RF gain energy and move to a bigger detectable orbit. The cyclotron cell has two excitation plates that emit a sweep of RF ranging from few kHz to lower MHz region. Thus, this generated RF sweep, called chirp, is used to excite ions with different *m/z* simultaneously. Coherent excited ions induce a current at the detection plates of the cyclotron cell which is proportional to the total charge. This acquired transient signal of all ions is in the time domain. A Fourier transform algorithm is used to convert time domain signal to a frequency spectrum and then mass conversion is applied resulting in a mass spectrum with *m/z* value on the *x*-axis and ion intensity on the *y*-axis.

Using image current detection in FT-ICR MS have the advantage of non-destructive detection of ions. Thus, the sensitivity and the resolution of the experiment can be increased through repeated measurements of the frequency of ions in the ICR cell. The performance of the ICR mass analyser depends on the use of high vacuum. For optimum performance and to achieve high resolution and mass accuracy the vacuum should be less than 10^{-8} torr to avoid collisions during the acquisition time with air molecules. Otherwise collisions with air molecules can cause broadening of the ICR peaks. For example, ions at *m/z* value of 1,000 analysed using 9.4 T FT-ICR MS should be trapped for ~4 s without colliding with air molecules to achieve a mass resolving power of ~480,000 and substantially less (<400,000) if apodization is applied afterwards.[72]

2.1.2.2 Quadrupole mass analyser

The operating principles of the quadrupole mass analyser was first described by Paul and Steinwedel in the 1950s.[73] Commercialisation of quadrupole *m/z* analyser began in the mid-1960s. The quadrupole was hyphenated to gas chromatography (GC) because it allowed rapid data acquisition. The quadrupole is classified as a filter type *m/z* analyser. Fixed or direct current (DC) and alternating current (AC or RF) (where radiofrequency is changing) are applied to the four parallel rods that the *m/z* analyser is composed of. The stable trajectory of a selected mass of an ion is dependent on the values of these voltages where unstable trajectory of an ion causes the ion to collide with the rods. Thus, these ions are filtered out and only ions with a stable trajectory pass through the *m/z* analyser and to the detector. (See Figure 11).[74]. The quadrupole is a scanning *m/z* analyser where the potentials are increased from a minimum to maximum value but at fixed DC/RF ratio. The *m/z* range of the mass spectrum is scanned with the potentials increase. The scanning can be as well undertaken from high to low potentials. Thus, a mass spectrum is obtained by decreasing or increasing the magnitude of the RF amplitude and DC potential at a fixed ratio

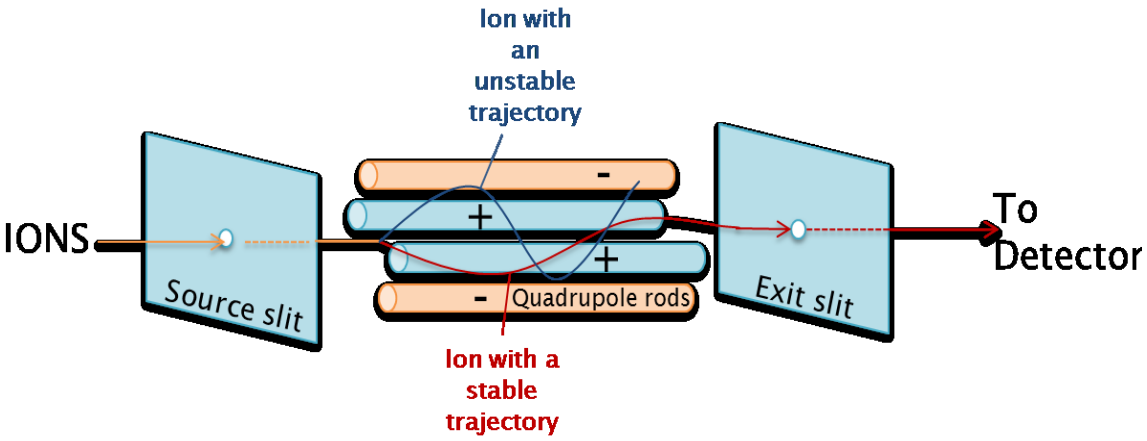

Figure 11 Schematic diagram of a quadrupole mass analyser showing ions with a stable and unstable trajectory and their path through the quadrupole rods

Ions are constantly repelled and attracted to the quadrupole rods because these rods are successively negatively and positively charged. The motion of ions is governed by the generated quadrupolar field. See Table 6 for rods potential equation where each rod is coupled with its diametric opposite.

The ion trajectory equation in Table 6 was deduced by Mathieu based on Newton second law of motion. The equation explains the variables that influence the electric fields that ions are experiencing in a hyperbolic mass filter. The ion

trajectory equation is used to calculate the produced electric field along the *x-y-z* axes. It can be concluded that the applied DC and RF potentials at fixed ratio to the rods has no effect on increasing ions acceleration in the *z* direction. This is because the equation is not dependent on the movement ions along the *z* axis, between the ionisation source and the detector.

The equations of ion motion or Mathieu equations are shown in Table 6, The definition of the two parameters (a_u and q_u) enabled the simplification of equation of ion motion. (See Table 6). This is because the parameter a_u is linked to DC and q_u is linked to RF. For ions to have a stable trajectory and finally reach the detector the solution of Mathieu equations is bounded. The result is little displacement along the x- or y- axis. Therefore, a_u and q_u have stable trajectories in the quadrupole *m/z* analyser. Figure 12 shows Mathieu stability diagrams where a_u is plotted against q_u. Region A represents the first stability region of a specific *m/z* value. For collisional trajectory for ions in the quadrupole *m/z* filter the solution for Mathieu equation is unbounded. Therefore, ions are neutralised through colliding with the quadrupole rods surfaces and thus they do not reach the detector. The a_u and q_u reduced parameters in Figure 12 are plotted in two-dimensional plot to simplify parameters affecting motion of ions in quadrupole *m/z* analyser.

Table 6 Quadrupole equations of rod potential, ion trajectory and ion motion.

Rod potential	+(U+Vcos(ωt)) or -(U+Vcos(ωt))	
Ion trajectory	$\theta = [U + Vcos(\omega t)]\frac{x^2 - y^2}{r_0^2}$	
Ion motion (IM)	$a_{u=\frac{8eU}{mr_0^2\omega^2}}$	$q_{u=\frac{4eV}{mr_0^2\omega^2}}$
Simplified (IM)	$\frac{a_u}{q_u} = \frac{2U}{V}$	

u	DC voltage which has a negative or positive value
Vcos	voltage with an oscillating radio frequency (ω) in the time domain (t)
x and y	The distance from the coordinate
r_0	The distance from the z axis which is from the centre.
$_u$	Position along the y and x coordinate
e	Charge of electron
m	Mass of the ion

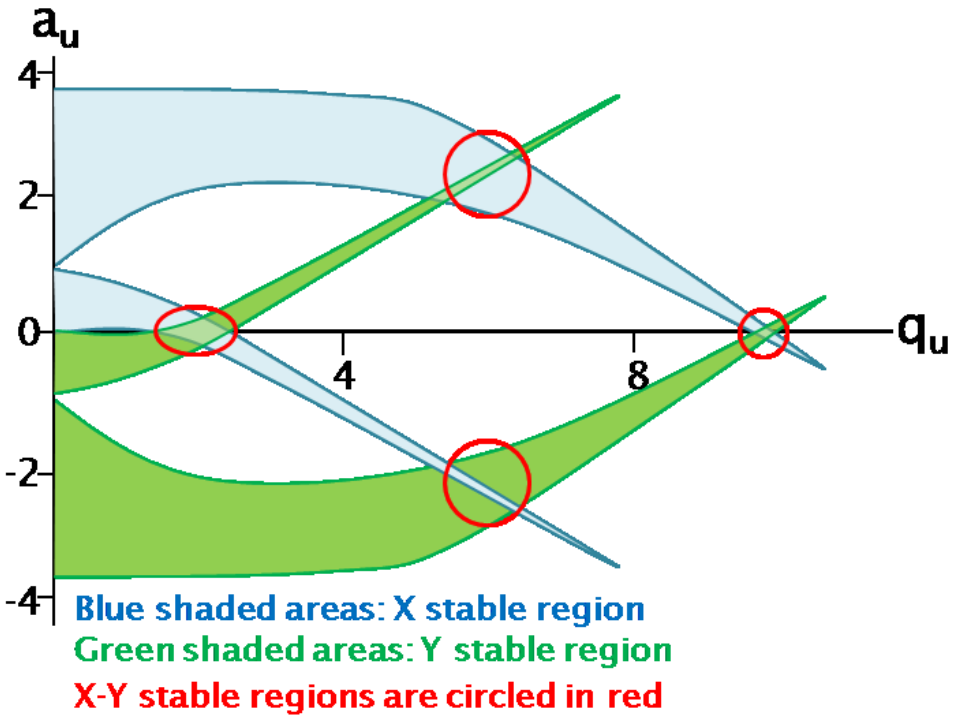

Figure 12 Mathieu stability diagrams for quadrupole mass analyser showing the stability regions (colour coded).[73]

The main advantages of using quadrupole type *m/z* analyser are: relatively inexpensive compared to other *m/z* analysers due to short flight path of ions, the size is relatively small, has fast scan rate and the transmission efficiency of ions is high. Quadrupole can be coupled in space to another two quadrupoles leading to a triple quadrupole mass analyser. The first and the third quadrupole are mass analysers while the middle one is an RFonly quadrupole where collision induced dissociation (CID) occurs leading to a tandem MS experiment. Quadrupole can be hyphenated to chromatography with different ionisation techniques equipped such as ESI, APCI and APPI. The resolution of the instrument is limited from half to one *m/z*. The quadrupole in this study is used in tandem MS experiments for the isolation of precursor ions. The FT-ICR MS instrument that is used for crude oil analysis is mainly composed of a quadrupole, collision cell and the ICR cell. Precursor ions can be isolated using the quadruple. Then, ion activation is undertaken in the collision cell. This is followed by *m/z* analysis of fragment ions in the ICR cell.

The reason for tandem MS experiment is that the use of soft ionisation techniques had little or no dissociation occurs for the ions due to the low amounts of energy imparted. Thus, little or no structural information is observed

in the mass spectrum. The limitation is overcome by the use of two stage of mass analysis, (MS/MS). [75]

2.1.2.3 The Orbitrap

Orbitrap is a relatively new trap mass analyser that was developed by Alexander Makarov at HD Technologies, Ltd, in the United Kingdom.[76] The Orbitrap principle of operation was demonstrated by Makarov and co-workers in the late 1990s.[77] The improvement in Orbitrap technology led to its commercialisation by Thermo Fisher Scientific in 2005.[78,79] The instrument was first introduced at the 2005 *ASMS meeting on Mass Spectrometry and Allied Topics* held in San Antonio, Texas, June 5 – 9.

A similar concept to the Orbitrap mass analyser was introduced in 1922 by K. H. Kingdon at the Research Laboratories of General Electric Company in Schenectady, New York.[80] The Kingdon trap design consisted of an electrically isolated thin wire in the centre and an outer cylindrical electrode. Trapping of ions is through an electrostatic field, a radial nonlinear electric field, that is generated by applying a DC voltage between the outer and the wire electrodes.

In 1981, a modified version of the Kingdon trap was introduced by R. D. Knight where the outer electrode included an axial quadrupole term.[81] Thus, ions are confined on the trap *z*-axis (axial direction) with harmonic oscillations. However, neither the Kingdon trap or its newer modified design by Knight could generate a mass spectrum. One of the technical difficulties that prevented the Knight trap to function as an *m/z* analyser is ion injection into the mass analyser.

The Orbitrap, is the latest development of trapping mass analysers, is composed of an outer electrode that is shaped like a barrel and a coaxial inner electrode that is shaped like a spindle.[78,82] Thus, the Orbitrap can be viewed as a modified version of the Knight-style Kingdon trap. The opposing surfaces of the electrodes are nonparallel as shown in Figure 13. Thus, the electric field between the two electrodes varies according to the position on the *z*-axis.

The operational stages of the Orbitrap can be divided into; ion trapping, injection, excitation and detection. Ions trapping in orbit is due to the electrostatic attraction of ions to the inner spindle-like electrode balanced by the ions centrifugal forces. Ions follows a circular orbit around the inner electrode (spindle) but below the outer electrode (barrel). The radius of the circular orbit is

not dependent on mass. Thus, ions are trapped radially in the Orbitrap with the amplitude of the orbit for all trapped ions with different *m/z* values is the same.

However, another naturally produced ion motion is along the *z*-axis, back and forth along the inner electrode analogous to the motion of an oscillating pendulum bob. This motion of ions is the result of the inhomogeneous electric filed, an electrostatic electric field with quadro-logarithmic potential, between the electrodes surfaces.[82] This harmonic motion (along the *z*-axis) is independent from all initial parameters of ions including the motion around the inner electrode. However, the harmonic motion of ions is dependent on the ion *m/z* value.[77]

To conclude, the observed helical motion of ions is the result of ions elliptical trajectories, trapping of ions around the central electrode, and the harmonic motion of ions which gives *m/z* separation. The oscillating frequencies of ions along the *z*-axis are detected using image current detection as a time-domain signal. Fourier transform is used to convert the detected image current to a mass spectrum which is similar to the process used in FT-ICR MS.

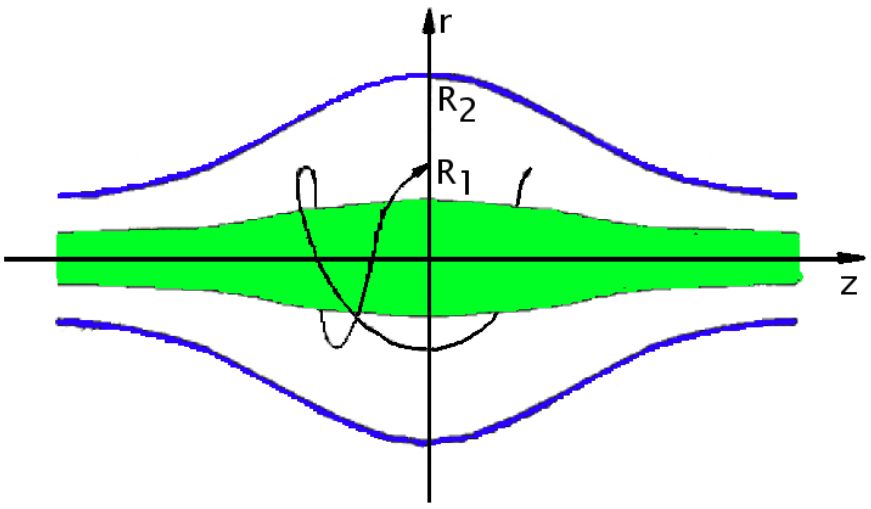

Figure 13 Stable ion trajectory is shown inside an Orbitrap mass analyser.

2.1.2.3.1 The C trap

One of the problem associated with static electric field, used in the Orbitrap, is the ion injection. Thus, the injected ion packet is not trapped and will pass through the *m/z* analyser.[83] The design of the C trap was essential for the

Orbitrap to become a functional mass analyser. Radial trapping of ions in the Orbitrap requires the use of dynamic electric field. The applied electric field between the electrodes of the Orbitrap is increased for > 300 ns during the ion injection from the C trap. Thus, the timing of the process is essential to ensure efficient trapping of ions in the mass analyser.[77,84] Prior to ion injection from the C trap, curved linear trap, into the Orbitrap the ion packet is electrodynamically focussed in time and space.[85] Ions are transferred in space to the Orbitrap *m/z* analyser through decreasing the RF and increasing the DC potential to accelerate ions out form the C trap and into the Orbitrap.[85] This process of ions ejection from the C trap is undertaken in line with another process in the Orbitrap where the electric field potential on the central electrode is increased. The end result is high transmission efficiency of ions (approx. 30%) into the Orbitrap and radial trapping of ions around the central electrode of the Orbitrap.[85]

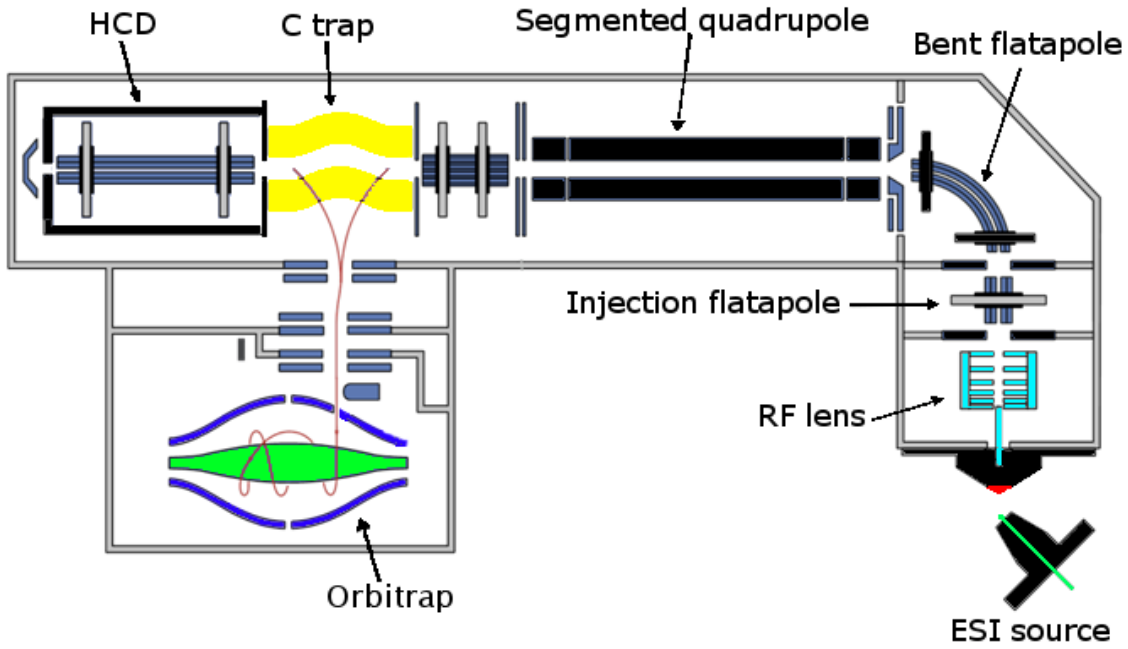

Figure 14 Schematic of Thermo Scientific™ Q Exactive™ Orbitrap instrument. Reproduced and modified from ASMS 2016 Thermo Fisher Scientific, Enabling Mass Spectrometric Analysis of Intact Proteins in Native Conditions on A Hybrid Quadrupole-Orbitrap Mass Spectrometer

Scheffler K, Damoc E, Bailey A, Josephs J.

An Orbitrap Q Exactive™ schematic is shown in Figure 14. The different compartments of the instrument are illustrated. Ions are squeezed in the C trap and *m/z* analysis is undertaken in the Orbitrap. Collision-induced dissociation experiment (CID) can be undertaken in the C trap, HCD cell or the Orbitrap.[86]

However, using the Orbitrap for CID experiment is not recommended because of inefficient trapping of product ions. The trapping trajectories of product ions, the motion of ions around the inner electrode, are unstable because product ions have similar velocity compared to their precursor ions. Therefore, a CID experiment is first undertaken either in the C trap or the HCD cell followed by *m/z* analysis in the Orbitrap.

2.1.3 Crude oil analysis

Crude oil is arguably one of the most complex organic mixture. Different analytical tools have been used for crude oil analysis.[87] Ultimately the goal is to go beyond the batteries of bulk physical testing such as viscosity measurement of crude oils and gain an in depth understanding of the different elemental compositions of the mixture. This will have a direct effect on extraction, refining, recovery, oil fingerprinting and effective cleaning of spillages. Crude oil has been characterised using HPLC with different stationary phases[88-90], field ionisation MS, vapour pressure osmometry (VPO) and ^{13}C nuclear magnetic resonance spectroscopy[91-93]. Other techniques include the use of gas chromatography (GC) coupled to different detectors such as flame ionisation detector (FID)[94], nitrogen phosphorus detector (NPD)[94] and mass spectrometry (MS)[95,96]. The use of two-dimensional gas chromatography (GC × GC) has many advantages compared to GC for complex mixture analyses in increasing the peak capacity and the accurate identification of compounds. Furthermore, the peak width for compounds that are eluted from the second chromatographic column can be 50-100 times narrower compared to the first column.[97,98] Advances in mass spectrometry and the inception of atmospheric pressure ionisation (API) sources paved the way for mass spectrometry to become one of the most used analytical tool for detailed understanding of the chemical composition of crude oils. At the early stage of MS development in the1940s and 1950s magnetic sector instrument with 10,000 resolving power was not sufficient for resolving commonly found isobars in petroleum. Isobars are ions with the same nominal mass but have different exact mass. *E.g.* one of the most common found isobar in crude oil sample is observing two isobaric ions where three carbons from one ion is exchanged with one sulfur and four hydrogens for the second ion. The *m/z* difference between the two isobars is at 3.4 m*m/z* units. Thus, the minimum required resolving power at *m/z* 400 is approximately 118,000 for peaks with equal intensities.

However, the resolving power of magnetic sector instrument can be increased through narrowing the slits. Narrowing the slits allow ions with specific *m/z* value to pass through the mass analyser. However, increasing the restriction results in fewer ions passing through the mass analyser. This comes at the expense of decreasing signal-to-noise ratio (S/N).[99] Different mass analysers have been introduced since the 1950s such as time-of-flight (TOF)[100], quadrupole[101], ion trap[102], Fourier transform ion cyclotron (FT-ICR)[103] and Orbitrap[82]. FT-ICR and Orbitrap offer the highest resolving power and are suitable for complex mixture

analysis with sufficient mass accuracy for elemental composition assignment. Different mass analysers have different resolving power. For comparison purpose an Orbitrap QExcative have similar resolving power to a 4.7 T FT-ICR MS instrument, 400,000 at *m/z* 400. Both of these instruments were used Chapter 4 for crude oil characterisation. However, FT-ICR MS is the tool of choice of complex mixture analysis if a more powerful magnet was used. For example, recently a 21 T FT-ICR MS was developed at National High Magnetic Field Laboratory.

However, MS alone cannot distinguish different isomers in a mixture. The number of isomers for a given molecule is greatly affected by the degree of its unsaturation. For example, saturated $C_{13}H_{28}$ has an 802 possible isomers while $C_{13}H_{22}$ at DBE = 3 has 1.7×10^5 isomers.[104]

Different ionisation techniques ionise different molecules in crude oils producing different mass spectra. Volatile species, low in molecular weight and non-polar, can be ionised using electron ionisation (EI) or chemical ionisation (CI), a softer gas phase ionisation technique. CI is a softer gas phase ionisation because little fragmentation is observed in CI mass spectra compared to EI mass spectra.

Analysing aliphatic hydrocarbon mixtures by EI without a gas chromatography step is problematic because of the extensive fragmentation of the hydrocarbon molecular ion making the identification of the molecular ion in the mass spectrum problematic.[105] In EI energetic electrons (70 eV) interact with gas phase atoms or molecules to produce ions. EI is considered a hard (fragmentation) ionisation, since it uses high energetic electrons to produce ions. This leads to fragmentation of the molecular ion, which can be used for structure elucidation. However, aliphatic hydrocarbons are for example not as stable as aromatic hydrocarbons. This results in extensive fragmentation of the aliphatic hydrocarbon molecular ion. Alternative ionisation method for aliphatic hydrocarbons is low-voltage electron ionisation (LEVI) which was introduced to reduce the fragmentation of the molecular ion.[106] Heteroatom containing compounds of nitrogen, oxygen and sulfur in crude oil distillate were analysed using LEVI FT-ICR MS.[107] Another ionisation technique that is used for crude oil analysis is field desorption (FD). In a study by Schaub *et al.* FD FT-ICR MS was used for analysing non-polar molecules in petroleum distillate.[108] Matrix-assisted laser desorption/ionisation (MALDI) is not frequently used for crude oil analysis.[109] This is also true when using direct sample introduction into an EI source installed where no chromatographic separation step is undertaken. Atmospheric pressure

soft ionisation techniques such as electrospray ionisation (ESI)[52], atmospheric pressure photoionisation (APPI)[63] and atmospheric pressure chemical ionisation (APCI)[110] are routinely becoming used for crude oil analysis. These ionisation techniques are usually used for the characterisation of heteroatom containing compounds in crude oil.

2.2 Data analysis

2.2.1 Resolving power

Resolving power (R) equals (m/Δm) and it is considered a performance parameter for the mass spectrometer.[43] The definition of resolution depends on Δm. The 10% valley definition is calculated by subtracting two resolved peaks with a 10% valley. If one peak is to be used for R calculation then Δm is calculated by taking peak width at 5% peak height. (See Figure 15). These two approaches are used to calculate resolution in magnetic sector instrument. The other approach is the full width at half maximum (FWHM) which is used to calculate $\Delta m_{50\%}$ for quadrupole MS, FT-ICR MS and TOF MS.[111] FWHM definition can be used to calculate the resolving power for one peak as $m/\Delta m_{50\%}$, shown in Figure 16. Or R (FWHM) can be calculated for two peaks of equal heights as m_2/m_2-m_1.[112]

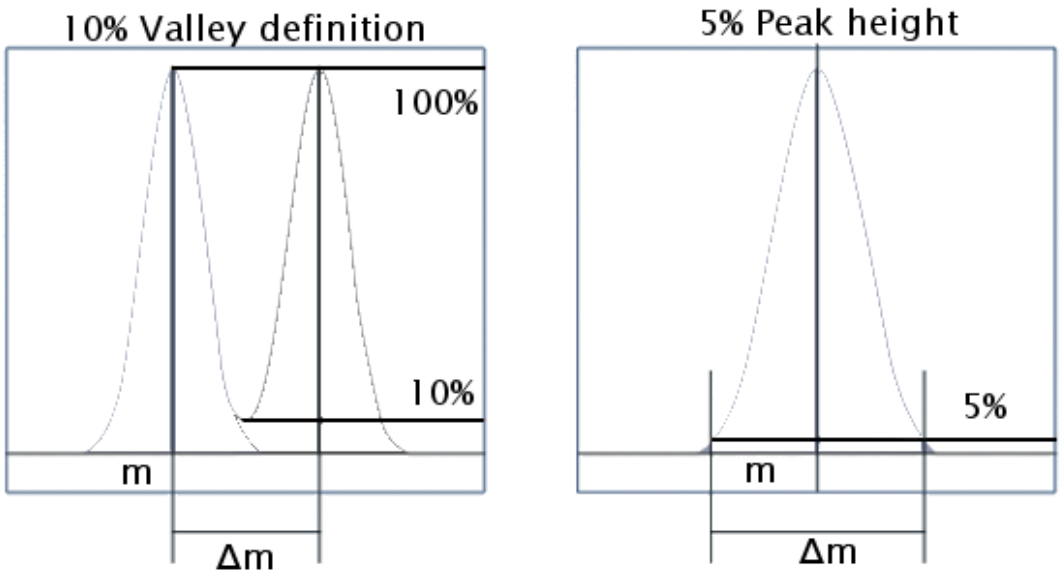

Figure 15 10% valley resolution definition for two peaks with equal magnitude and width. 5% valley resolution definition is shown.

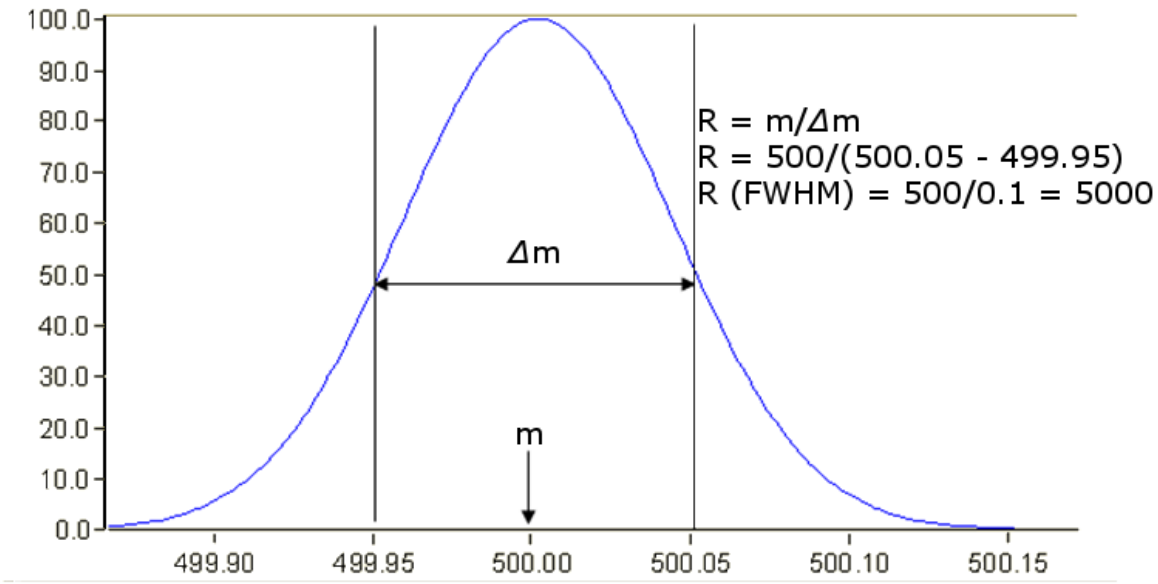

Figure 16 Peak width at half maximum FWHM definition.

Resolution depends on the type of the mass analyser. In ion trap and quadrupole mass analysers resolution is defined as unit mass resolution (usually *m/z* 0.5).

In TOF instrument the mass resolving power of the mass spectrometer is constant.

Equation 9

$$R_{FWHM} = \frac{m}{\Delta m} = \frac{t}{2\Delta t} \approx \frac{L_{eff}}{2\Delta Z}$$

Where m = mass, t = flight time of the ion, Δm and Δt = peak widths, L_{eff} = effective length of the TOF analyser, ΔZ = ion's packet thickness.The number 2 in R time definition is reducing resolution and it is derived from the square root dependence of the flight time on mass.[113] For quantification, resolution becomes important as insufficient mass resolution produces false negative or false positive.

However, for FT-ICR MS instrument the relationship between cyclotron frequency (ω_c) and the magnetic field (b) is shown below: (See Figure 17)

Equation 10

$$\omega_c = \frac{q}{m} B$$

Where q is the ionic charge, b is the magnetic field and m is the ionic mass. From the equation mass is inversely proportional to frequency, thus at higher *m/z* a decrease in mass resolution is observed which is one of the limitation of FT-ICR MS. (See Figure 17).

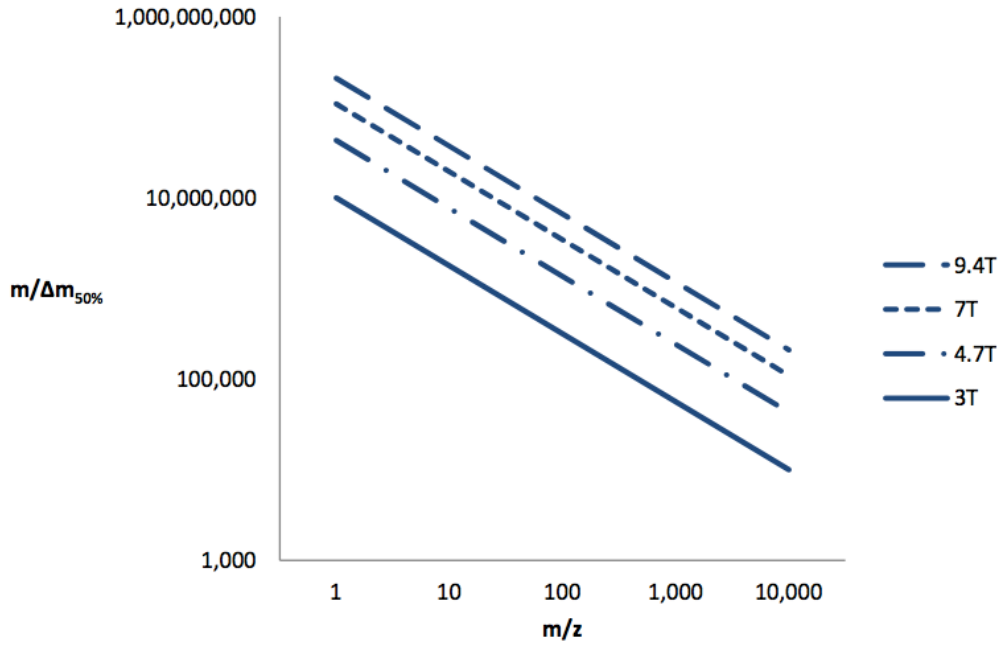

Figure 17 Resolution (R) as a function of *m/z* for different magnets. T_{acq}=1 s (Adapted)[66].

The angular frequency (ω) in rad/s is calculated from as

Equation 11

$$\omega = \left(\frac{kq}{m}\right)^{\frac{1}{2}}$$

Where m is the ion mass and q its charge. The frequency (ω) is the axial oscillation of ions that is only dependent on the *m/z* value of ions.[83]

The resolving power can be calculated as $m/\Delta m_{50\%}$ or as $\omega/\Delta\omega_{50\%}$, the full width of the ion peak at half maximum peak height (FWHM). Because of Equation 11the resolving power is multiplied by 2.

Equation 12

$$\frac{\omega}{\omega_{50\%}} = 2\frac{m}{m_{50\%}}$$

The resolving power for the Orbitrap is decreased as the square root of *m/z*. It can be calculated from the equation below:

Equation 13

$$\frac{m}{\Delta m_{50\%}} = \frac{1}{2\Delta\omega_{50\%}}\left(\frac{kq}{m}\right)^{\frac{1}{2}}$$

The harmonic axial frequency (ω) of ions in the Orbitrap in Equation 11 is inversely proportional to $(m/q)^{1/2}$. Where as in the FT-ICR MS the cyclotron frequency (ω_c) in Equation 10 is inversely proportional to (m/q). The drop in *m/z* resolution at high *m/z* is less for Orbitrap compared to FT-ICR MS. *E.g.* The Orbitrap with a mass resolving power of 100,000 at *m/z* 400 will outperform a 7 T FT-ICR MS at *m/z* 800 and 12 T FT-ICR MS at *m/z* 2500 respectively.[114] However, experimental parameters for FT-ICR MS such as acquisition time and low *m/z* cut off should be considered. For example, if the low *m/z* cut off is increased, the 7 T FT-ICR will again outperform the Orbitrap at *m/z* 400.

2.2.2 The need for ultra-high resolution and high mass accuracy mass spectrometer for crude oil analysis

The advent of high resolution high mass accuracy mass spectrometers, such as FT-ICR MS, has enabled crude oil analysis to be undertaken on the molecular level. The high resolution is needed for resolving isobars that found in crude oil sample.

Resolving isobars in crude oil sample is necessary for accurate elemental composition assignment of the different heteroatom containing compounds. High resolving power is example required for assignment of sulfur containing compounds.[24] Table 7 shows common isobars encountered in crude oil sample. Resolving these isobars requires high resolution high mass accuracy mass spectrometer such as FT-ICR MS or Orbitrap-MS.

In petroleomics, the *m/z* value of an ion is often reported in Da as all the observed ions in the mass spectrum are singly charged ($z = 1$). The charge state of ions is defined from the use of isotopologue spacing. One *m/z* is observed between the ^{12}C and ^{13}C isotope of an ion for different classes of compounds in crude oil mass spectrum acquired using different ionisation sources and polarities such as positive ion ESI, negative ion ESI and positive ion and negative ion APPI.[85,86,115]

The use of high resolution high mass accuracy mass spectrometer in crude oil analysis has enabled mass spectrometrists to characterise crude oil sample. The prediction of properties and behaviour of crude oil is aided with the previous knowledge regarding the elemental composition of the crude oil sample. Elemental composition assignment of crude oil sample is constrained to hydrogen, carbon, nitrogen, oxygen and sulfur. This is because elemental analysis of different crude oils confirmed that the presence of the previous elements. Further, nickel, vanadium and iron are also present but in heavy fraction at concentrations less than 300 ppm.[1]

Table 7 The required resolution to seperate common isobars in crude oil.

Isobars	Mass difference (Δm) m*m/z* units	Resolution (m/Δm) × 10^3
SH_4/C_3	3.4	130
$C_2H_3/^{13}CN$	17	27
O/CH_4	36.4	13
H_{12}/C	93.9	5

The elemental composition search algorithm for a measured *m/z* value in crude

oil mass spectrum is constrained to certain set of elements ($C_cH_hN_nO_oS_s$) and their corresponding isotopes. Thus, *m/z* assignment of ions is aided by prior knowledge of crude oil elemental composition and as well the use of homologous series and DBE value information.

Further FT-ICR signal is usually displayed in the magnitude-mode, however displaying the signal in the absorption mode improves both mass accuracy (two fold) and mass resolution (40-100%). This has allowed to resolve two species with approximately the mass of an electron (548 μ m*m/z* units) using 9.4 T FT-ICR MS.[116]

2.2.3 Mass calibration

External and internal mass calibration are used in petroleum analysis. External calibration with known masses is undertaken as an experiment prior to running the sample. An approximately ±5 ppm mass accuracy can be obtained with this method.[117] This mass accuracy is sufficient for determination of elemental compositions of alkylation series across the mass range. This step is followed by an internal calibration using the analysed sample where sub 1 ppm mass accuracy can be obtained because all ions are under the influence of the same magnetic, electric fields and space charge effect. This method is used in assigning the elemental compositions of compounds to up to 400 Da with high confidence. However, for compounds, bigger than 400 Da, the exploitation of other useful information in the mass spectrum can be used to determine elemental formula such as the spacing between compounds (differing by two hydrogens) and alkylation series (Kendrick normalisation) can be used as well. This is carried out by identifying series below *m/z* 400 depending on accurate mass measurements with high degree of confidence as stated above and then the subsequent addition of $-CH_2$ should be able to identify the homologous series at high *m/z* values.

In addition, an important factor to consider in internal or external calibration is the peak shape and ion abundance of the different ions with known *m/z* values that are used for mass calibration. External calibration of the instrument should be undertaken with the ion abundance for the external calibration matching the ion abundance of the analysed sample. This has significant effect on the mass accuracy of the analysed sample.[118]

In crude oil analysis internal mass calibration is undertaken using a homologous series that belong to a DBE of a certain class of compound. For example, in positive ion ESI FT-ICR MS of crude oil-1 the N_1 class is the most abundant class in the mass spectrum. Thus the N_1 homologous series with DBE value of 9 can be used to internally calibrate crude oil-1 mass spectrum.

2.2.4 Mass accuracy

A mass spectrometer that is capable of performing high mass accuracy measurement is regarded to have mass accuracy measurement reported to the fourth decimal place for *m/z* of an ion. The mass accuracy can be calculated by subtracting the observed *m/z* from the theoretical *m/z* divided by the observed *m/z*.[112] The definition of exact mass for an element is different from the chemical definition of weighted average of the isotopes of that element. The integer value for the isotopic mass of an element is not an accurate representation of the mass of that element as the strong nuclear forces that bind the atomic nucleus vary. Thus, high resolution high mass accuracy mass spectrometer measures the *m/z* values to the four decimal place relative to ^{12}C which has an exact mass of 12.0000. Table 8 shows the theoretical exact masses of different monoisotopic elements in which crude oil is composed of, $C_cH_hN_nO_oS_s$.

Table 8 Exact masses of elements found in crude oil and the isotopic abundance of the most abundant naturally occurring isotope.

Element	Symbol	Exact mass	Abundance
Hydrogen	^{1}H	1.0078	99.99
	^{2}H	2.0141	0.015
Carbon	^{12}C	12.0000	98.90
	^{13}C	13.0033	1.10
Nitrogen	^{14}N	14.0031	99.63
	^{15}N	15.0001	0.37
Oxygen	^{16}O	15.9949	99.76
	^{18}O	17.9991	0.20
Sulfur	^{32}S	31.9721	95.02
	^{34}S	33.9679	4.21

The exact mass for a molecule is calculated based on the combined monoisotopic atomic masses. *E.g.* the monoisotopic exact mass for methane is equal to C (12.0000) + H_4 (4.0312) = 16.0313 Da.

Assigning accurate mass in complex mixture analysis by FT-ICR MS is only possible when method optimisation is applied to reduce the space-charge effects within the ICR cell. (See Figure 18).

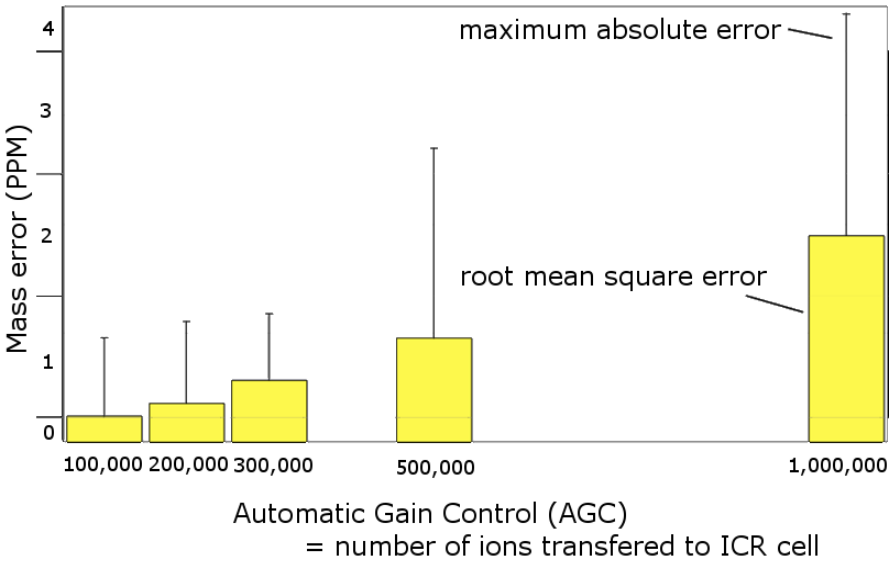

Figure 18 The relationship between mass accuracy and the number of ions inside the ICR cell.[119] (Adapted)

Figure 18 shows that ion population at high density in the ICR cell affects mass accuracy as a result of Coulombic repulsion between ions in the ICR cell. The resulted error in the measurement of the mass accuracy of ions from space-charge effects is considered a systematic error. This systematic error can result between measurements of different mass spectra or within a mass spectrum between measured ions with different *m/z* values. that can be resulted across different acquired mass spectra or in the same mass spectrum between different measured *m/z* values. The error in mass accuracy from space-charge effects is minimised through maintaining approximately the same ion population in each acquired mass spectrum.[120]

Table 9 shows that assigning elemental composition for C, H, N, O, and S depending solely on high mass accuracy is not sufficient even with 0.1 ppm mass accuracy especially for compounds with molecular mass above 300 Da. The elemental constrains are sat to C = 50, H = 100, N = 5, O = 5 and S = 3. However, filtering the results with isotopic abundance improve elemental composition assignment. For example, in positive ion APPI S1 containing compounds are ionised. The elemental composition assignment of the S1 class is improved when ^{34}S isotope assignment and abundance of 4.25% compared to ^{32}S is taken into account.

Table 9 Different sets of mass accuracies with the possible elemental composition for each one. The inclusion of isotopic abundance filtering significantly reduces the number of possibilities.

Without the contribution of isotope abundance (IA)						**2% IA**	**5% IA**
Molecular mass (Da)	10 ppm	5 ppm	3 ppm	1 ppm	0.1 ppm	3 ppm	5 ppm
150	2	1	1	1	1	1	1
200	3	2	2	1	1	1	1
300	20	9	6	2	1	1	5
400	65	31	19	6	1	2	11
500	221	96	53	18	2	3	28
600	421	214	129	42	4	3	30
700	872	448	268	90	8	8	81
800	1637	810	499	167	16	11	93
900	2873	1427	871	288	27	15	163

2.2.5 Rings plus double bonds (DBE) and Z number

Both terminology, DBE and Z number, are used to express the hydrogen deficiency of a compound. Mass spectrometrists prefer to use DBE while petrochemists use Z number. These values are reported for the neutral form of the observed ion.

The general formula is used to calculate both DBE and Z number.

DBE general formula = $C_cH_hN_nO_oS_s$ is calculated by the nitrogen rule:[121]

Equation 14

$$DBE = c - h/2 + n/2+1$$

The conversion between DBE and Z number is calculated from the following equation:

Equation 15

$$Z = -2(DBE) + n + 2$$

Table 10 Double bond equivalents (DBE) example compounds

DBE 0	DBE 1	DBE 1
 hexane Chemical Formula: C_6H_{14}	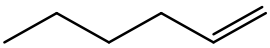 hex-1-ene Chemical Formula: C_6H_{12}	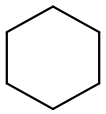 cyclohexane Chemical Formula: C_6H_{12}
DBE 2	**DBE 3**	**DBE 4**
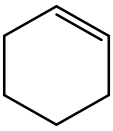 cyclohexene Chemical Formula: C_6H_{10}	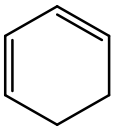 cyclohexa-1,3-diene Chemical Formula: C_6H_8	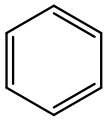 benzene Chemical Formula: C_6H_6

2.2.6 Kendrick mass and Kendrick plots

Crude oil mass spectrum analysed using high resolution and high mass accuracy mass spectrometer contains thousands of ions. Crude oil as a sample is considered to be one of the most complex organic mixture in nature. See Figure 19 as an example for crude oil mass spectrum acquired using positive ion ESI FT-ICR MS. However, not all the compounds in crude oil sample are ionisable under one ionisation technique. *E.g.* basic compounds such as pyridine containing compounds are observed as protonated molecules in positive ion ESI and acidic compounds such as naphthenic acids are observed in negative ion ESI.[122] Regardless of the ionisation source or the polarity switch that is being used any crude oil mass spectrum contains repeated spacing across the *m/z* range.

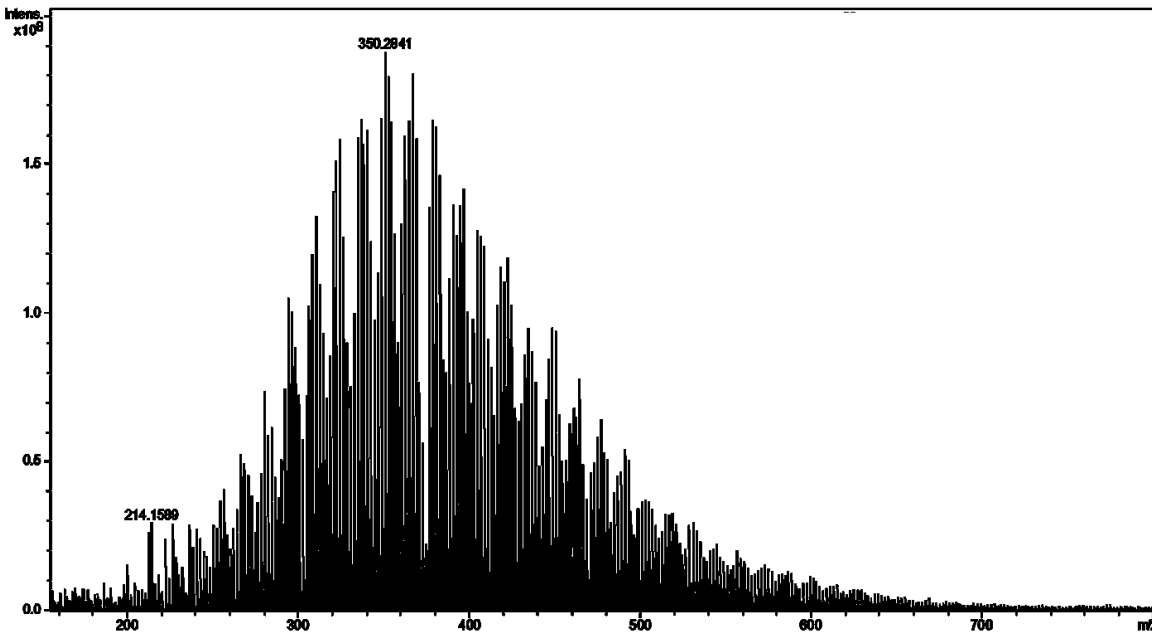

Figure 19 Positive ion ESI FT-ICR MS mass spectrum of Crude oil-2.

Figure 20 A shows an expanded *m/z* range of the crude oil mass spectrum shown in Figure 19. *m/z* 14 unit spacing in the mass spectrum is observed, related to -CH_2 (exact mass of *m/z* 14.0157). Thus an alkyl series (homologous series) is defined as ions having the same heteroatom content and the same DBE value but differing only by the number of -CH_2 groups. Further, all elemental composition assignments will be categorised according to three criteria: heteroatom content, carbon number, and DBE.

In Figure 20 B another spacing is observed in the mass spectrum which corresponds to the accurate mass of two hydrogen atoms. Therefore, these spacings belong to the same class and carbon number but differ only in the number of rings plus double bonds. The addition of ring or double bond lowers the ion mass by 2.0157 *m/z* units and the addition of –CH_2 increases the ion mass by 14.0157 *m/z* units.

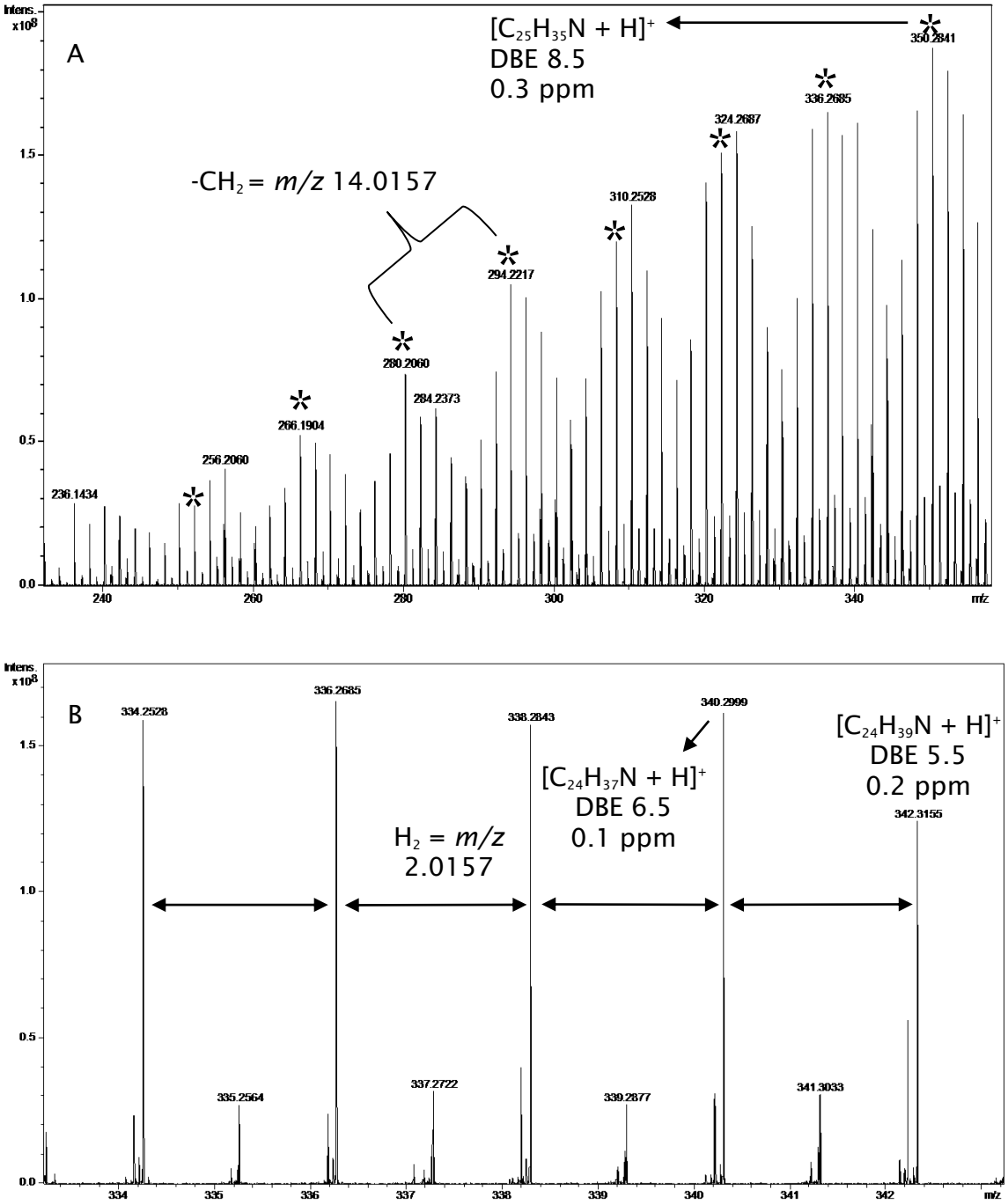

Figure 20 Positive ion ESI FT-ICR MS of crude oil-2 showing 14.0157 *m/z* unit spacing and 2.0157 *m/z* unit spacing .

Carbon-12 is defined as having an accurate mass of 12.0000 Da on the IUPAC scale. The Kendrick scale converts the IUPAC mass of CH_2 14.0157 Da to 14.000 Da.

The IUPAC mass of methylene (CH_2) is converted to the Kendrick scale by using the following equation:

Equation 16

$$\text{Kendrick mass} = \text{IUPAC mass} \times (14/14.01565)$$

Kendrick mass facilitate the identification of the same class of compound, the same heteroatom content, with the same number of rings plus double bonds but with different degree of carbon number.[123]

From the previous equation the IUPAC mass of $-CH_2$ at 14.0157 Da is converted to 14.0000. Thus, the same heteroatom content and same DBE value have the same Kendrick mass defect (KMD).

Equation 17

$$\text{KMD} = (\text{Nominal mass} - \text{Kendrick mass}) \times 1000$$

Abbreviation is commonly used to express compound classes and DBE. The $1O_2$ abbreviation would refer to the O_2 class of compounds and rings plus double bonds equal to 1. Therefore, a saturated fatty acid such as pentadecanoic ($C_{15}H_{30}O_2$), hexadecanoic ($C_{16}H_{32}O_2$) and heptadecanoic acid ($C_{17}H_{34}O_2$) would be classified as $1O_2$, and the conversion of IUPAC $-CH_2$ of the saturated fatty acids to Kendrick mass normalises the values of the series to give identical Kendrick mass defect (KMD). These results are plotted as KMD *versus* nominal Kendrick mass where equally distant dots differing by 14 Da are displayed horizontally where it indicates the successive increase in the number of $-CH_2$. KMD is displayed vertically where different KMDs are equally distant reflecting the increase of numbers of rings plus double bonds. Different classes of compounds as well have different KMDs where this can be exploited to plot different classes in a single Kendrick plot.

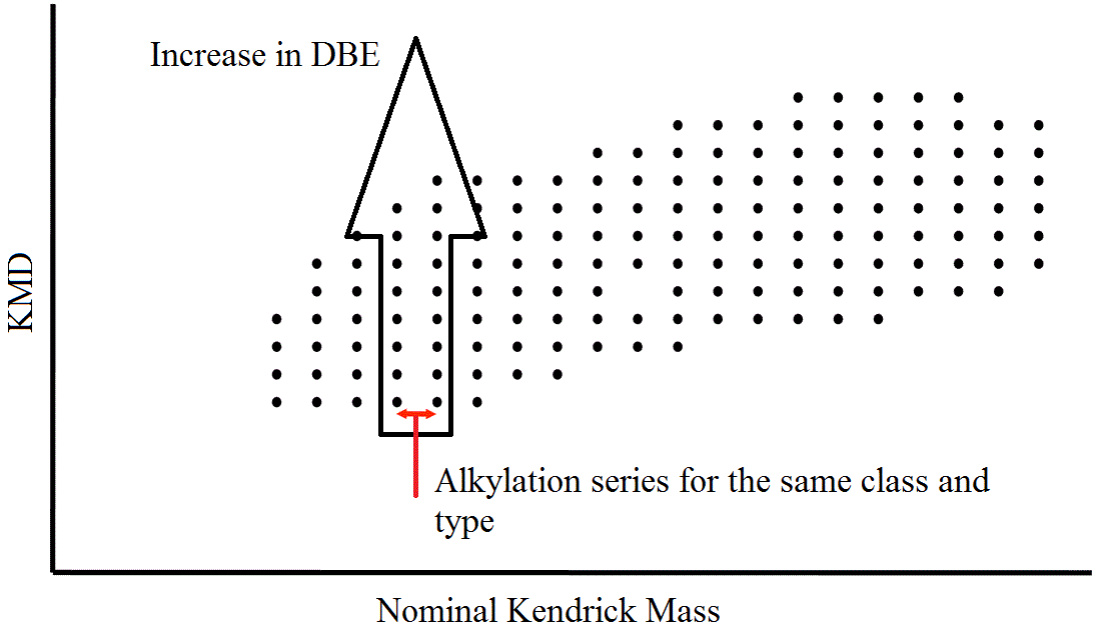

Figure 21 Schematic of a Kendrick plot for x class of compound, the increase in DBE is displayed vertically and each additional $-CH_2$ is displayed horizontally.

The Kendrick plot shown in Figure 21 is useful for identification of a homologous series for a class of compound over a particular *m/z* range. At low *m/z* value (up to 400 *m/z* units) the elemental formula can be assigned unambiguously depending on accurate mass measurements. Then subsequent unambiguous assignment of elemental formula at high *m/z* (going horizontally through the data points) for the same KMD is conducted through the use of Kendrick plot. This process of *m/z* assignment aided by the use of Kendrick plot at high *m/z* cannot be provided with high confidence if the process was only dependant on accurate mass measurement.[124] Therefore, the use of Kendrick mass normalisation allows for approximately a threefold increase in the mass limit for unique elemental composition assignment.

The level of information provided by the different ions in a crude oil mass spectrum can be sorted according to class, type (DBE or KDM) and carbon number (homologous series). Therefore, three levels of information are obtained from a crude oil mass spectrum. Bottom left plot A in Figure 22 shows that different classes of compounds are plotted on the *x*-axis where the normalisation on the *y*-axis is performed by summing the abundance of a certain class divided by the sum of all identified peaks in the mass spectrum. In Figure 22 plot (A) any class that has a relative abundance less than 1% is not shown. The N_1 class is the most

abundant class relative to other classes of compounds such as NS or NO that are present in positive ion ESI FT-ICR MS of crude oil-2 mass spectrum. The plot (B) in Figure 22 shows that N_1 class has a range of different DBE values from 4 up to approximately 25. The most abundant DBE value for crude oil-2 N_1 class is DBE 9. Further, an additional level if information is observed which is the carbon number distribution for N_1 at DBE 7 (see Figure 22 plot C). The type (DBE) and carbon number are scaled to the abundance of the highest member.

It should be noted that when the N1 class is mentioned is referred to the protonated species of the N1 class. While if the N1-R is mentioned it refers to N1 radical ion class.

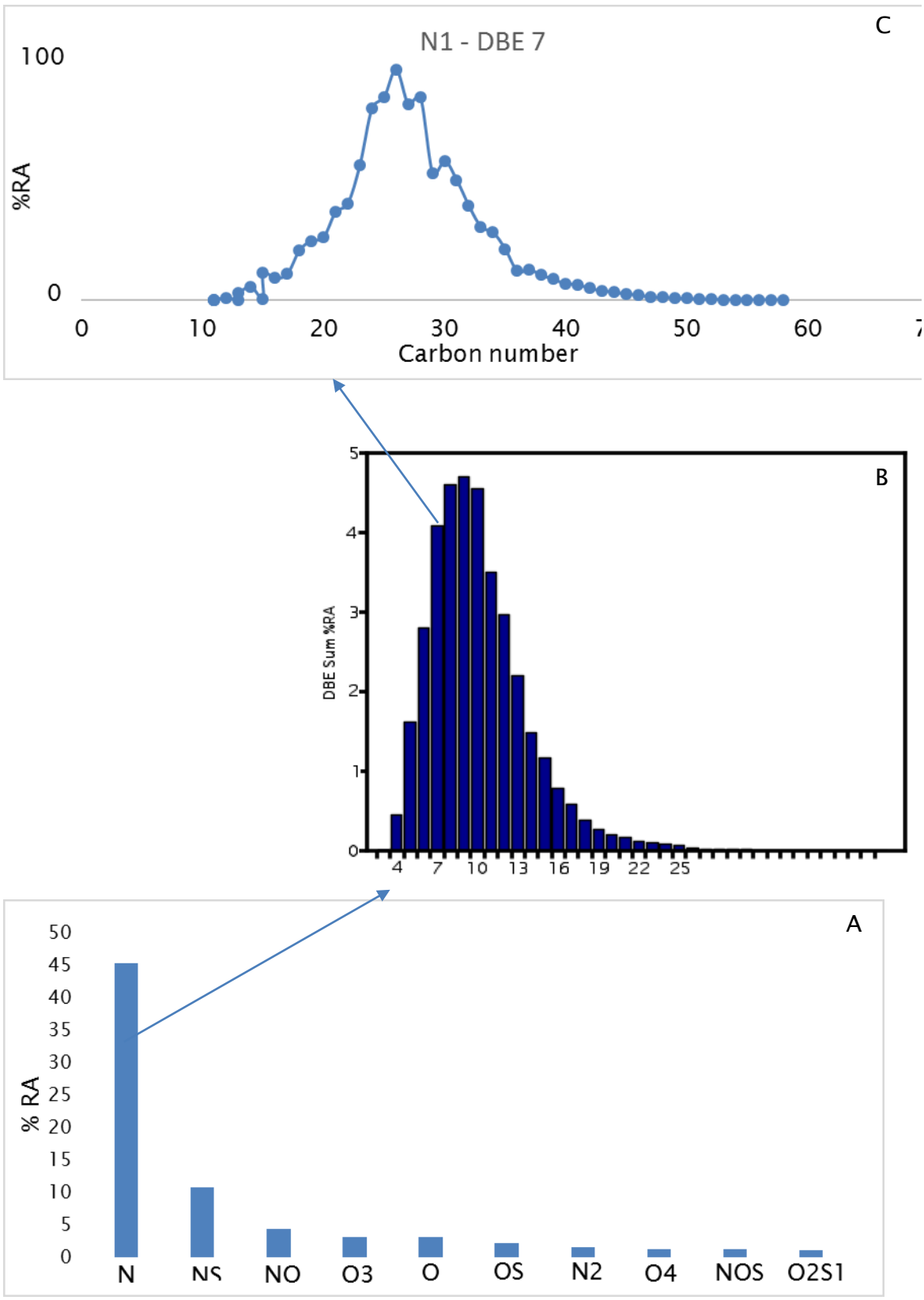

Figure 22 Class distribution plot for different classes of compounds from positive ion ESI FT-ICR MS data of crude oil-2 is shown in A. The B plot represents the DBE distribution of the N_1 class. The A plot represents the carbon number distribution of the N_1 class with DBE 7.

2.2.7 PetroOrg™

PetroOrg is a software developed at the Florida State University in collaboration with Future Fuels Institute and the National High Magnetic Field laboratory.[125] In the field of crude oil analysis development of instrumentations in terms of resolution has exceeded the much needed development of data interpretation software packages. PetroOrg is a commercial software that is used to facilitate the data interoperation of crude oil mass spectra. A text file containing the *m/z* values and ion intensities is loaded into the software. Then, the software calibrates the data based on a selected ion series in the crude oil mass spectrum. This previous step is followed by automatically assigning the elemental formulae of the different *m/z* values and sort these assigned elemental formulae according to heteroatom class, DBE value and carbon number. The software is capable of visualising the data according to the three different levels of chemical information that was discussed in Figure 22. Further, different plots can be generated such as DBE *versus* carbon number plot for a certain class of compound with the intensity of the ion is colour coded (red being the most intense ion). However, checking the raw data is still essential at this stage of the software development as mis-assignment by the software can result in false characterisation of a certain class of compound.

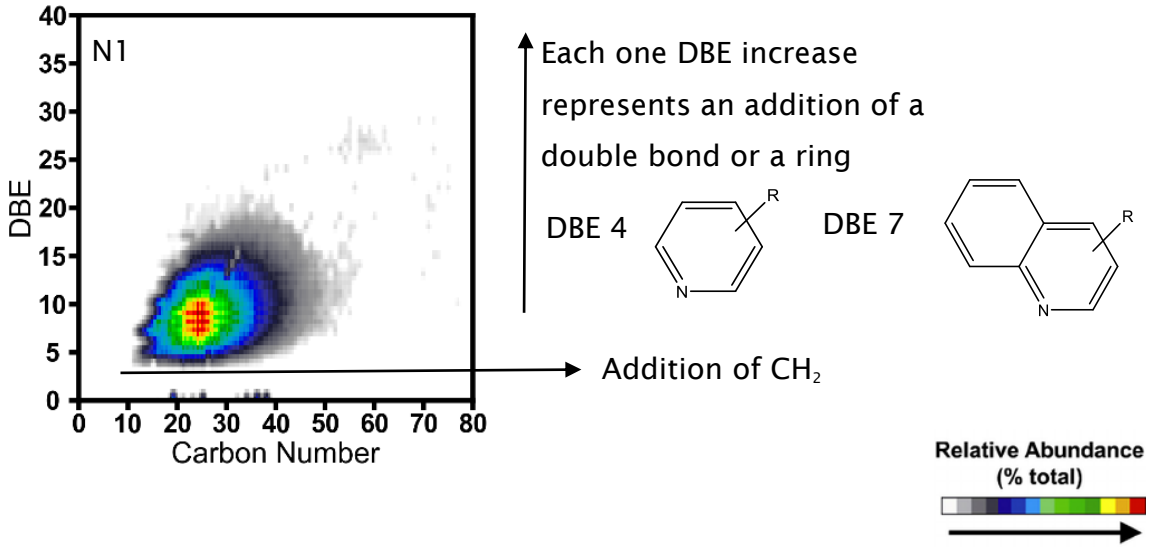

Figure 23 DBE *versus* carbon number plot is shown for the N1 class present in the positive ion ESI FT-ICR MS of crude oil-2.

Chapter 3: Experimental details

3.1 Samples and chemicals

Three crude oils were investigated. (See Table 11). LC-MS grade methanol, HPLC grade toluene, reagent grade formic acid and ammonium hydroxide were purchased from Fisher Scientific (Loughborough, UK). Methanol and toluene were used for diluting the crude oil samples. Formic acid and ammonium hydroxide were used as ionisation enhancing additives in positive and negative ion ESI respectively. Formic acid salt (sodium formate) has a purity of ≥ 99.0% and was purchased from Sigma Aldrich (Gillingham, UK).

Table 11 Crude oil samples

Given name	Source
Crude oil-1	BP Pangbourne Technology Centre, Pangbourne, UK
Crude oil-2	BP Pangbourne Technology Centre, Pangbourne, UK
Crude oil-3	NIST crude oil

3.2 Calibration solutions

FT-ICR MS:

FT-ICR MS was externally calibrated in positive and negative ion ESI with 5 µg/mL sodium formate solution in methanol, where sub 2 ppm mass accuracy was obtained for *m/z* 150 to 800. Agilent APCI tune mix was used (without dilution) for positive ion APPI FT-ICR MS calibration.

Orbitrap MS:

Orbitrap Q Exactive™ Plus (Thermo, MA, USA) was used for crude oil analysis in positive and negative ion ESI. Pierce™ LTQ Velos ESI Positive Ion Calibration Solution and Pierce™ Negative Ion Calibration Solution were used to calibrate the Orbitrap in positive and negative ion ESI respectively.

3.3 Sample preparation

3.3.1 Positive ion electrospray ionisation

Stock solutions of 10 mg/mL in toluene were prepared based on the mass of the original weighted crude oil sample. Then for each crude oil (crude oil-1, 2 and 3) dilutions solutions were prepared from the stock at 0.3 and 0.1 mg/mL in toluene:methanol (t:m) ratios of 1:9, 3:7 and 6:4 with and without 0.1% formic acid (FA).

3.3.2 Negative ion electrospray ionisation

10 mg/mL stock solutions of each crude oil sample were prepared in toluene based on the mass of the original weighted crude oil samples. Then 6:4 toluene:methanol (t:m) dilution solutions from the stock of each crude oil (crude oil-1, 2 and 3) were prepared at 0.3 mg/mL with 0.1% ammonium hydroxide.

3.3.3 Positive and negative ion atmospheric pressure photoionisation

10 mg/mL stock solutions of each crude oil sample were prepared in toluene based on the mass of the original weighted crude oil samples. Then toluene solutions of each crude oil (crude oil-1, 2 and 3) were prepared at 0.5 mg/mL.

3.4 Fourier transform ion cyclotron resonance mass spectrometry

Mass spectra were acquired using a Bruker 4.7 T FT-ICR MS (Bruker Daltonics, Billerica, MA). The superconducting magnet is actively shielded. Data acquisition was undertaken using solariXcontrol version 1.5.0. and data processing was using Bruker DataAnalysis and PetroOrg™. At the centre of the superconducting magnet the ICR cell design is a cylindrical infinity cell. The infinity cell is employed to avoid ion ejection in the *z*-direction while ions are excited by the broadband radio frequency.[126]

Ions were accumulated externally to the ICR cell using a multipole and transferred using an RF only hexapole to the cylindrical ICR cell.[127] The hexapole operated at a frequency of 5 MHz and rf amplitude (peak to peak voltage) of 300 V_{pp}.[128] After ions transfer to the ICR cell through the ion optic region ions are trapped due to the use of the trapping potentials and the magnetic field. This is followed by broadband frequency-sweep excitation (chirp) of the trapped ions form *m/z* 100 to 1500.[129] The excitation stage of ions is followed by image current detection that resulted in 2 Mword time-domain data. 300 time-domain data were averaged to increase ions signal intensity as small number of ions were transferred to the ICR cell to minimise peak coalescence and space-charge effects.[130] The time-domain signal was apodized which reduces peaks overlapping near the baseline but at the expense of peak broadening at the peak width at half maximum peak height. This was followed by zero filling, Fourier transform and magnitude mode calculation. Mass spectra were generated by converting the frequency to *m/z* using quadrupolar electric trapping potential approximation.[69,117] Table 12 list the values of parameters that are used in the acquisition, accumulation, transfer and analysis of ions in the FT-ICR MS.

Table 12 List of parameters (except the ionisation source) are used in FT-ICR MS

Parameter	Value	Parameter	Value	Parameter	Value
Acquisition Mass Control					
Detection	Broadband	TD	2 M	*m/z* range	*m/z* 100 to 1500
Accumulation					
Average spectra	32 or 300	Source accumulation	0.001 s	Ion accumulation	0.050 s or indicated
Ion cooling	0.001 s	Time of flight	0.750 ms		
Ion transfer - source optics + for positive ion and – for negative ion					
Capillary exit	+220.0 V/-180 V	Deflector plate	+/-200.0 V	Funnel 1	+/-150 V
Skimmer	+15 V/ -50 V	Funnel RF amplitude	150 V_{pp}		
Ion transfer – collision cell					
Collison voltage	-0.5 V pos. ion/+0.5 V neg. ion	DC extract bias	+0.5 V pos. ion/-0.6 V neg. ion	RF frequency	2 MHz
Collision RF amplitude	1600 V_{pp}				
Ion transfer – transfer optics and gas control					
Time of flight	0.750 ms	Frequency	4 MHz	RF amplitude	350 V_{pp}
Gas control flow	40%				
Mass analyser					
Transfer exit lens	-15 V pos. ion/+15 V neg. ion	Analyser entrance	-8 V pos. ion/+8 V neg. ion	Side kick	-5 V pos. ion/+5 V neg. ion
Side kick offset	-2 V pos. ion/ 5 V neg. ion	Front trap plate	0.950 V pos. ion/ -0.650 V neg. ion	Back trap plate	0.850 V pos. ion/-0.700 V neg. ion
Sweep excitation power	15 %				

Fragmentation of the precursor ion can be undertaken either in the collision cell as collision-induced dissociation experiment (CID) or inside the ICR cell as sustained off-resonance irradiation (SORI) CID experiment. In CID experiments the precursor ion is isolated using the quadrupole at isolation window to $m/z \geq \pm 0.5$ and it is indicated in the Figure legend. The CID experiment is undertaken in the collision cell with argon as the collision gas at different collision energies indicated in the Figure legend. Collision rf amplitude and rf frequency are 1600 V_{pp} and 2 MHz respectively.

For SORI CID experiment, ions at a desired *m/z* can be isolated using the quadrupole or inside the ICR cell using an RF-sweep followed by single-frequency excitation pulses. The isolated precursor ions are excited by a rf-field having a frequency of 500 MHz below the ICR frequency of ions with SORI power at 1.2% and pulse length at 0.15 s. Precursor ions collided with argon inside the ICR cell at pressure reservoir of 10 mbar. Argon was introduced into the ICR cell *via* a pulsed valve. The purpose of argon is to act as a neutral collision gas. Upon collisions between ions and argon gas molecules the kinetic energy of ions is converted into internal energy which results in bond breakage and fragmentation of the precursor ion.

3.4.1 Positive and negative ion ESI FT-ICR MS conditions

Diluted crude oil samples were infused into the ionisation source using a Harvard syringe infusion pump at a flow rate of 2 µL/min. Hamilton syringe (100 µL) was used to infuse the diluted crude oil samples into the ionisation source. (See section 3.3.1 and 3.3.2)

Positive and negative ion ESI conditions were the followings: the stainless steel capillary is held at ground potential relative to the end-plate electrode at capillary voltage - 4000 V for positive ion ESI and +4000 V for negative ion ESI. Nitrogen (N_2) was used as both a drying gas (temperature 200 °C, 4 L/min.) and nebulising gas with pressure at 1.2 bar.

For the positive ion ESI mass spectra internal *m/z* calibration was applied using the homologous series for DBE 9 of the N_1 class of compounds (See Table 13) .

For the negative ion ESI mass spectra internal *m/z* calibration was applied using the homologous series for DBE 3 of the O_2 class of compounds (See Table 14).

Table 13 List of ions that are used for internal *m/z* calibration in positive ion ESI FT-ICR MS

Protonated molecule	Theoretical *m/z*	Protonated molecule	Theoretical *m/z*	Protonated molecule	Theoretical *m/z*
$[C_{14}H_{11}N + H]^+$	194.0965	$[C_{31}H_{45}N + H]^+$	432.3625	$[C_{48}H_{79}N + H]^+$	670.6286
$[C_{15}H_{13}N + H]^+$	208.1121	$[C_{32}H_{47}N + H]^+$	446.3782	$[C_{49}H_{81}N + H]^+$	684.6442
$C_{16}H_{15}N + H]^+$	222.1278	$[C_{33}H_{49}N + H]^+$	460.3938	$[C_{50}H_{83}N + H]^+$	698.6599
$C_{17}H_{17}N + H]^+$	236.1434	$[C_{34}H_{51}N + H]^+$	474.4095	$[C_{51}H_{85}N + H]^+$	712.6755
$[C_{18}H_{19}N + H]^+$	250.1591	$[C_{35}H_{53}N + H]^+$	488.4251	$[C_{52}H_{87}N + H]^+$	726.6912
$[C_{19}H_{21}N + H]^+$	264.1747	$[C_{36}H_{55}N + H]^+$	502.4408	$[C_{53}H_{89}N + H]^+$	740.7068
$[C_{20}H_{23}N + H]^+$	278.1904	$[C_{37}H_{57}N + H]^+$	516.4564	$[C_{54}H_{91}N + H]^+$	754.7225
$[C_{21}H_{25}N + H]^+$	292.2060	$[C_{38}H_{59}N + H]^+$	530.4721	$[C_{55}H_{93}N + H]^+$	768.7381
$[C_{22}H_{27}N + H]^+$	306.2217	$[C_{39}H_{61}N + H]^+$	544.4877	$[C_{56}H_{95}N + H]^+$	782.7538
$[C_{23}H_{29}N + H]^+$	320.2373	$[C_{40}H_{63}N + H]^+$	558.5034	$[C_{57}H_{97}N + H]^+$	796.7694
$[C_{24}H_{31}N + H]^+$	334.2530	$[C_{41}H_{65}N + H]^+$	572.5190	$[C_{58}H_{99}N + H]^+$	810.7851
$[C_{25}H_{33}N + H]^+$	348.2686	$[C_{42}H_{67}N + H]^+$	586.5347	$[C_{59}H_{101}N + H]^+$	824.8007
$[C_{26}H_{35}N + H]^+$	362.2843	$[C_{43}H_{69}N + H]^+$	600.5503	$[C_{60}H_{103}N + H]^+$	838.8164
$[C_{27}H_{37}N + H]^+$	376.2999	$[C_{44}H_{71}N + H]^+$	614.5660	$[C_{61}H_{105}N + H]^+$	852.832
$[C_{28}H_{39}N + H]^+$	390.3156	$[C_{45}H_{73}N + H]^+$	628.5816	$[C_{62}H_{107}N + H]^+$	866.8477
$[C_{29}H_{41}N + H]^+$	404.3312	$[C_{46}H_{75}N + H]^+$	642.5973	$[C_{63}H_{109}N + H]^+$	880.8633
$[C_{30}H_{43}N + H]^+$	418.3469	$[C_{47}H_{77}N + H]^+$	656.6129	$[C_{64}H_{111}N + H]^+$	894.87890

Table 14 List of ions that are used for internal *m/z* calibration in negative ion ESI FT-ICR MS

Deprotonated molecule	Theoretical *m/z*	Deprotonated molecule	Theoretical *m/z*	Deprotonated molecule	Theoretical *m/z*
$[C_9H_{14}O_2 - H]^-$	153.0921	$[C_{23}H_{42}O_2 - H]^-$	349.3112	$[C_{37}H_{70}O_2 - H]^-$	545.5303
$[C_{10}H_{16}O_2 - H]^-$	167.1078	$[C_{24}H_{44}O_2 - H]^-$	363.3269	$[C_{38}H_{72}O_2 - H]^-$	559.5460
$[C_{11}H_{18}O_2 - H]^-$	181.1234	$[C_{25}H_{46}O_2 - H]^-$	377.3425	$[C_{39}H_{74}O_2 - H]^-$	573.5616
$[C_{12}H_{20}O_2 - H]^-$	195.1391	$[C_{26}H_{48}O_2 - H]^-$	391.3582	$[C_{40}H_{76}O_2 - H]^-$	587.5773
$[C_{13}H_{22}O_2 - H]^-$	209.1547	$[C_{27}H_{50}O_2 - H]^-$	405.3738	$[C_{41}H_{78}O_2 - H]^-$	601.5929
$[C_{14}H_{24}O_2 - H]^-$	223.1704	$[C_{28}H_{52}O_2 - H]^-$	419.3895	$[C_{42}H_{80}O_2 - H]^-$	615.6086
$[C_{15}H_{26}O_2 - H]^-$	237.1860	$[C_{29}H_{54}O_2 - H]^-$	433.4051	$[C_{43}H_{82}O_2 - H]^-$	629.6242
$[C_{16}H_{28}O_2 - H]^-$	251.2017	$[C_{30}H_{56}O_2 - H]^-$	447.4208	$[C_{44}H_{84}O_2 - H]^-$	643.6399
$[C_{17}H_{30}O_2 - H]^-$	265.2173	$[C_{31}H_{58}O_2 - H]^-$	461.4364	$[C_{45}H_{86}O_2 - H]^-$	657.6555
$[C_{18}H_{32}O_2 - H]^-$	279.2330	$[C_{32}H_{60}O_2 - H]^-$	475.4521	$[C_{46}H_{88}O_2 - H]^-$	671.6712
$[C_{19}H_{34}O_2 - H]^-$	293.2486	$[C_{33}H_{62}O_2 - H]^-$	489.4677	$[C_{47}H_{90}O_2 - H]^-$	685.6868
$[C_{20}H_{36}O_2 - H]^-$	307.2643	$[C_{34}H_{64}O_2 - H]^-$	503.4834	$[C_{48}H_{92}O_2 - H]^-$	699.7025
$[C_{21}H_{38}O_2 - H]^-$	321.2799	$[C_{35}H_{66}O_2 - H]^-$	517.4990	$[C_{49}H_{94}O_2 - H]^-$	713.7181
$[C_{22}H_{40}O_2 - H]^-$	335.2956	$[C_{36}H_{68}O_2 - H]^-$	531.5147	$[C_{50}H_{96}O_2 - H]^-$	727.7338

3.4.2 Positive ion APPI FT-ICR MS conditions

Diluted crude oil samples were infused into the ionisation source using a Harvard syringe infusion pump at a flow rate of 5 µL/min. Hamilton syringe (100 µL) was used to infuse the diluted crude oil samples into the ionisation source. (See section 3.3.3). Crude oil-1, 2 and 3 were analysed using positive ion APPI FT-ICR MS. (See Table 15 for positive ion APPI conditions).

Table 15 Positive ion APPI-FT-ICR MS conditions.

Parameter	Value
Capillary voltage	- 1000 V
N_2 – drying gas temperature	200 ˚C
N_2 – drying gas flow rate	3 L/min
N_2 – nebulising gas pressure	2.5 bar
Vaporiser temperature	370 ˚C

In positive ion APPI internal *m/z* calibration was applied using the homologous series for DBE 9 of the HC class of compounds. (See Table 16).

Table 16 List of ions that are used for internal *m/z* calibration in positive ion APPI FT-ICR MS

Radical cation	Theoretical *m/z*	Radical cation	Theoretical *m/z*	Radical cation	Theoretical *m/z*
$C_{26}H_{36}^{+\cdot}$	348.2823	$C_{35}H_{54}^{+\cdot}$	474.4231	$C_{44}H_{72}^{+\cdot}$	600.5640
$C_{27}H_{38}^{+\cdot}$	362.2979	$C_{36}H_{56}^{+\cdot}$	488.4388	$C_{45}H_{74}^{+\cdot}$	614.5796
$C_{28}H_{40}^{+\cdot}$	376.3136	$C_{37}H_{58}^{+\cdot}$	502.4544	$C_{46}H_{76}^{+\cdot}$	628.5953
$C_{29}H_{42}^{+\cdot}$	390.3292	$C_{38}H_{60}^{+\cdot}$	516.4701	$C_{47}H_{78}^{+\cdot}$	642.6109
$C_{30}H_{44}^{+\cdot}$	404.3449	$C_{39}H_{62}^{+\cdot}$	530.4857	$C_{48}H_{80}^{+\cdot}$	656.6266
$C_{31}H_{46}^{+\cdot}$	418.3605	$C_{40}H_{64}^{+\cdot}$	544.5014	$C_{49}H_{82}^{+\cdot}$	670.6422
$C_{32}H_{48}^{+\cdot}$	432.3762	$C_{41}H_{66}^{+\cdot}$	558.5170	$C_{50}H_{84}^{+\cdot}$	684.6579
$C_{33}H_{50}^{+\cdot}$	446.3918	$C_{42}H_{68}^{+\cdot}$	572.5327	$C_{51}H_{86}^{+\cdot}$	698.6736
$C_{34}H_{52}^{+\cdot}$	460.4075	$C_{43}H_{70}^{+\cdot}$	586.5483	$C_{52}H_{88}^{+\cdot}$	712.6892

3.5 The Orbitrap

Orbitrap Q Exactive Plus mass spectrometer (Thermo, MA, USA), operated in negative ion and positive ion ESI-MS (ESI-MS/MS) or +/-APPI-MS. The mass spectrometer instrumental parameters were: AGC target 1e6 and *m/z* range is mentioned below for each ionisation technique. For all experiments (MS or MSMS) the analysis time was for 0.5 min for each analysis.

3.5.1 Positive and negative ion ESI conditions

Diluted crude oil samples were infused into the ionisation source using Unimetrics syringe at a flow rate of 10 µL/min. (See section 3.3.1 and 3.3.2 for sample preparation in positive and negative ion ESI respectively). Scan range of the mass spectrometer was from *m/z* 100–1000. Positive and negative ion ESI operating parameters are listed in Table 17.

Table 17 Positive and negative ion ESI conditions.

Parameter	Value
Spray voltage	+ESI 4000 V –ESI 3000 V
Capillary temperature	+ESI 300 ˚C –ESI 350 ˚C
Sheath gas flow rate	+/- ESI 10
Auxiliary gas heater temperature	-/+ ESI 50 ˚C
S-lens rf	-/+ ESI 60

For tandem MS experiments the isolation of the precursor ion was undertaken using the segmented quadrupole with an isolation window of ± 0.2 *m/z* units. The fragmentation of the precursor ion was undertaken in the higher-energy collisional dissociation (HCD) cell at different collision energies and the fragment ions were transferred back to the c trap followed by injection into the Orbitrap. The parameters regarding the collision energy value and the selected precursor ion are shown in the Figure legend of tandem mass spectra in the results and discussion section.

3.5.2 Positive and negative ion APPI conditions

Diluted crude oil samples were infused into the ionisation source using Unimetrics syringe at a flow rate of 100 µL/min. (See section 3.3.3 for sample preparation in positive and negative ion APPI). Scan range of the mass spectrometer was from *m/z* 175–1200. Positive and negative ion APPI parameters values are listed in Table 18).

Table 18 Positive and negative ion APPI conditions.

Parameter	Value
Spray voltage	+/- APPI 0.7 V
Capillary temperature	+/- APPI 270 ˚C
Sheath gas flow rate	+/- APPI 50
Auxiliary gas flow rate	+/- APPI 35
Auxiliary temperature	+/- APPI 400 ˚C
S-lens rf	+/- APPI 90
Vaporiser temperature	+APPI 400 ˚C -APPI 360 ˚C

Chapter 4: Characterisation of polar and non-polar molecules in crude oils

4.1 Positive ion ESI FT-ICR MS analysis of nitrogen containing compounds in crude oils

The world's light sweet crude oil reserve is being depleted.[1] The alternative to this is the heavy crude oils with higher amounts of heteroatom containing compounds. Nitrogen containing compounds in crude oil can cause variety of different problems such as catalyst deactivation by forming a layer of coke on the catalyst surface.[131,132] Zhan and co-workers proved that electrospray ionisation can be used to analyse fossil fuels samples such as crude oil, jet fuel and gasoline.[52] Thus, polar molecules in various hydrocarbon matrices are ionisable under ESI conditions. However, Zhan *et al.* used a triple quadrupole mass analyser which is unable to resolve isobaric ions, commonly found in crude oil sample. Further, triple quadrupole mass spectrometer cannot provide accurate mass measurements.

Miyabayashi and co-workers used positive ion ESI FT-ICR MS (7 T magnet) for the analysis of an Arabian mix vacuum residue. The observed mass spectrum contained predominantly even mass ions that were mis-assigned as hydrocarbon radical cations rather than basic nitrogen protonated molecules.[133] Direct analysis of crude oil sample *via* flow injection analysis has the advantage of avoiding any chemical modification of the sample such as oxidation of certain classes of compounds. Thus, the analysis of crude oil samples using positive ion ESI FT-ICR MS was conducted using flow injection analysis, without prior chromatographic separation stage.

The aim is to apply positive ion ESI-MS to study the different compound classes that are ionised in crude oils using this ionisation conditions. The upper *m/z* range was up to *m/z* 1000 in crude oils mass spectra analysed using positive ion ESI FT-ICR MS. The most abundant ions in the mass spectra of crude oil-1,2 and 3 were even mass ions. Figure 24 (A) shows a positive ion ESI FT-ICR mass spectrum for crude oil-2. The expanded *m/z* region in Figure 24 (B) shows that even mass ions are the most abundant ions. Close inspection of the entire mass spectrum of crude oil-2 in Figure 24 (A) confirms that even mass ions are the most abundant in the mass spectrum.

In Table 19 even mass ions that are shown in Figure 24 (B) are assigned as singly charged protonated molecules containing one nitrogen atom. Thus, their neutral molecules have odd masses. The nitrogen rule states that molecules with odd masses contain odd number of nitrogen atoms.[134] It should be noted that nitrogen containing compounds constitute a small percentage of the total crude oil. However, these compounds are basic and therefore ionisable under ESI conditions producing protonated molecules $[M + H]^+$. The major constituent of crude oil is straight and branched chain hydrocarbons, aromatics and thiophene containing compounds. These compounds cannot be ionised using ESI as the ionisation source.

In Table 19 five ions were assigned as protonated molecules containing one nitrogen atom, taken from expanded *m/z* range in Figure 24 (B). These ions differ only by two hydrogens from each other which is reflected in their corresponding DBE values. This is why the DBE value is from 5.5 to 9.5, an increase of one DBE for each ion represents either an addition of a double bond or a ring.

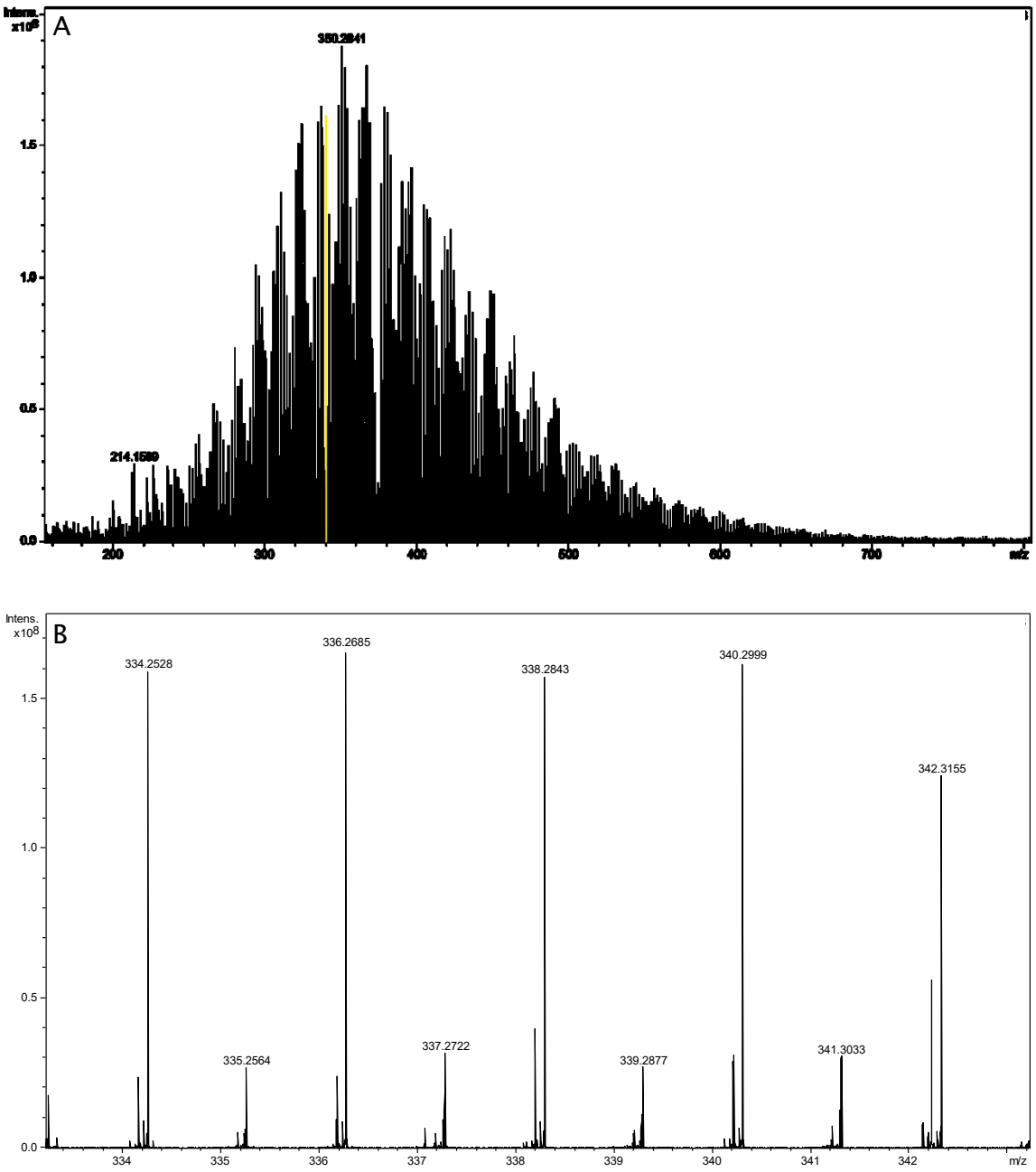

Figure 24 0.3 mg/mL solution of crude oil-2 was dissolved in toluene:methanol ratio of 6:4 with 0.1% formic acid was added to aid the ionisation. isCID 40 V. (A) is showing the entrire mass spectrum for crude oil-2 which was acquired using flow injection analysis in positive ion ESI FT-ICR MS. While (B) is expanded *m/z* of (A) showing different DBEs for the N_1 class.

Table 19 List of assigned protonated molecules containing one nitrogen atom of the expanded *m/z* of Figure 24 (B).

Protonated molecule	Measured *m/z*	DBE	Mass accuracy in ppm
$[C_{24}H_{39}N + H]^+$	342.3155	5.5	0.2
$[C_{24}H_{37}N + H]^+$	340.2999	6.5	0.1
$[C_{24}H_{35}N + H]^+$	338.2843	7.5	0.1
$[C_{24}H_{33}N + H]^+$	336.2685	8.5	0.2
$[C_{24}H_{31}N + H]^+$	334.2528	9.5	0.2

The different ions in the mass spectrum of crude oil-2, see Figure 24 (A), can be grouped together according to heteroatom class, DBE and degree of alkylation. Figure 25 shows the relative percentage contribution of all classes of compounds that are present in crude oil-2. The most abundant class is N_1 followed by N_1S_1, N_1O_1 and O_1 class of compounds. The shown no hit are ions that could not be assigned to any compound classes using PetroOrg™.

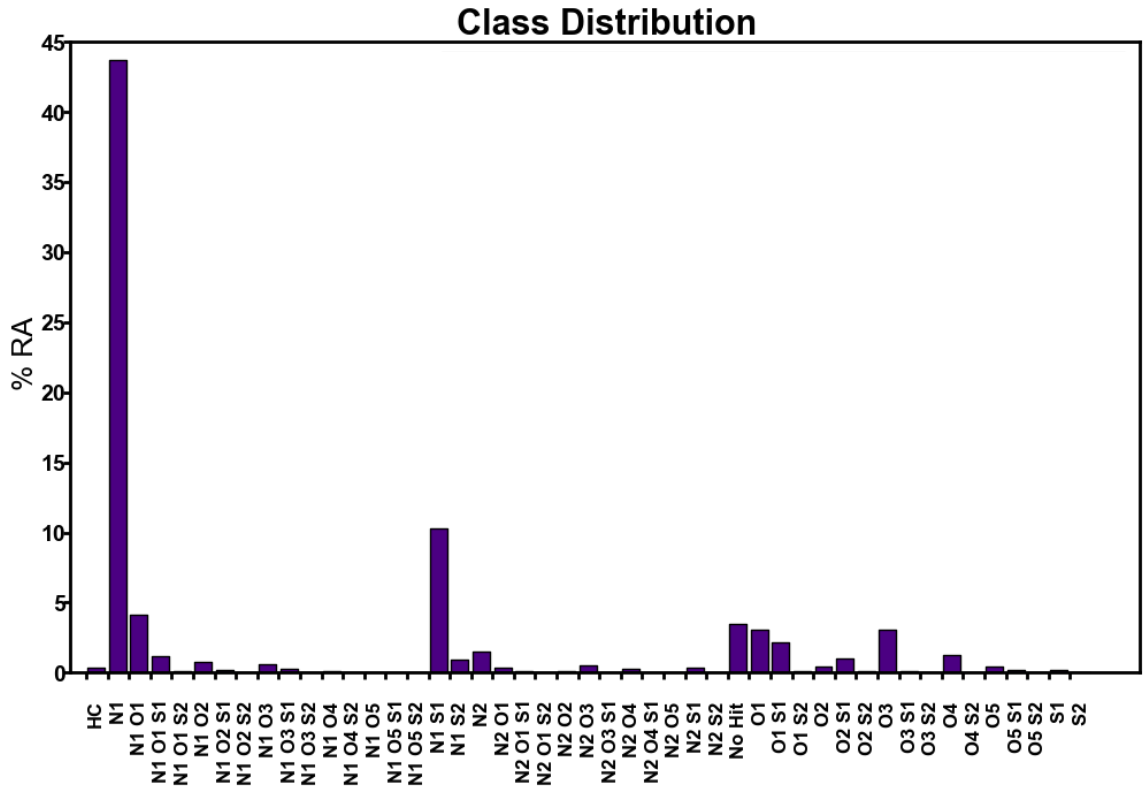

Figure 25 Per cent relative abundance (%RA) is shown for the different compound classes of crude oil-2. The N_1 class is the most abundant compared to other compound classes. The data was plotted using PetroOrg™. *m/z* values with their intensities were taken from crude oil-2 mass spectrum analysed using positive ion ESI FT-ICR MS. (See Figure 24 A).

The most abundant classes of compounds, N_1 and N_1S_1, differ only by 3.4 m*m/z* units which results from the substitution of C_3 with SH_4 requires high *m/z* resolution to distinguish between the two isobaric *m/z* values. The expanded *m/z* mass spectrum of Figure 24 (A) yellow highlighted region in Figure 26 shows that different compound classes are present at the expanded *m/z* region such as N_1, N_1O_1, N_1O_2 and N_1S_1. Two protonated molecules, N_1 and N_1S_1 class, that differ by C_3/SH_4 are $[C_{25}H_{23}N + H]^+$ and $[C_{22}H_{27}NS + H]^+$ respectively.

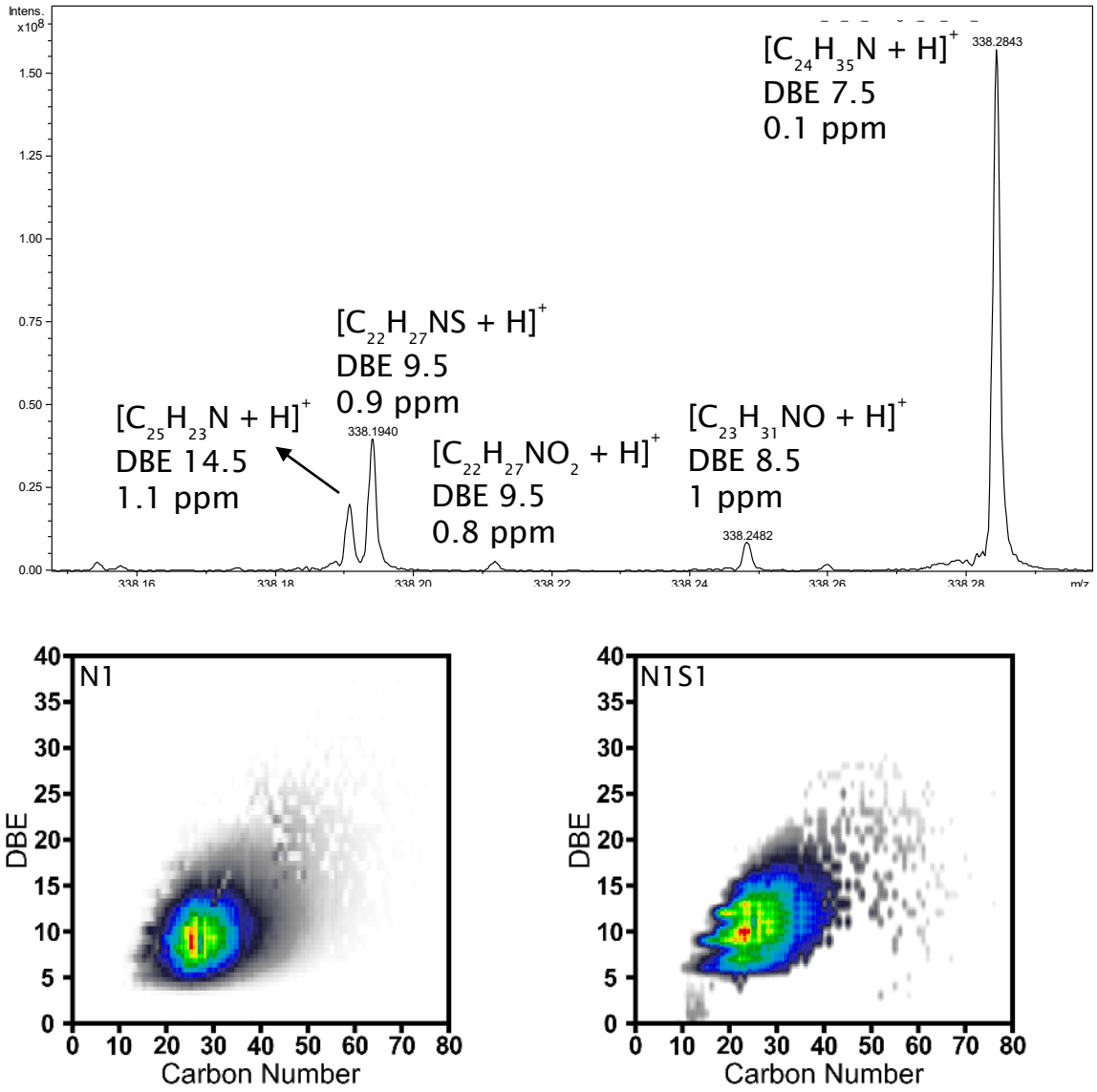

Figure 26 Expanded *m/z* of positive ion ESI FT-ICR MS crude oil-2 mass spectrum from Figure 24 (A) yellow highlighted *m/z* region. DBE *versus* carbon number plot is shown for N_1 class and N_1S_1 class of crude oil-2.

The second part of Figure 26 is DBE *versus* carbon number plots for N_1 and N_1S_1 class. Without a high resolution mass spectrometer correct assignment of N_1 and N_1S_1 class is not possible. The combination of resolution and correct *m/z* assignments are essential for producing different plots using PetroOrg such as the presented DBE *versus* carbon number plot for different compound classes. It should be noted that the comparison of intensities between N1 and N1S1 would be possible if the DBE plots used an absolute intensity scale, instead of normalising to the most intense peak within a given class.

Further, when the data is presented using PetroOrg™ the correct elemental formulae assignment of ions can be confirmed by checking the isotope fingerprint of crude oil. The observed odd mass ions in Figure 24 (B) is the corresponding ^{13}C isotope of the even mass ions (N_1 class). The exact *m/z* difference between ^{13}C and ^{12}C is 1.003 *m/z* units at a ^{13}C abundance of 1.1%. Therefore, *m/z* elemental formulae assignments can be validated using these isotopic *m/z* differences within a crude oil mass spectrum. A DBE *versus* carbon number plot is shown for monoisotopic ^{12}C N_1 class and the corresponding ^{13}C N_1 class in Figure 27.

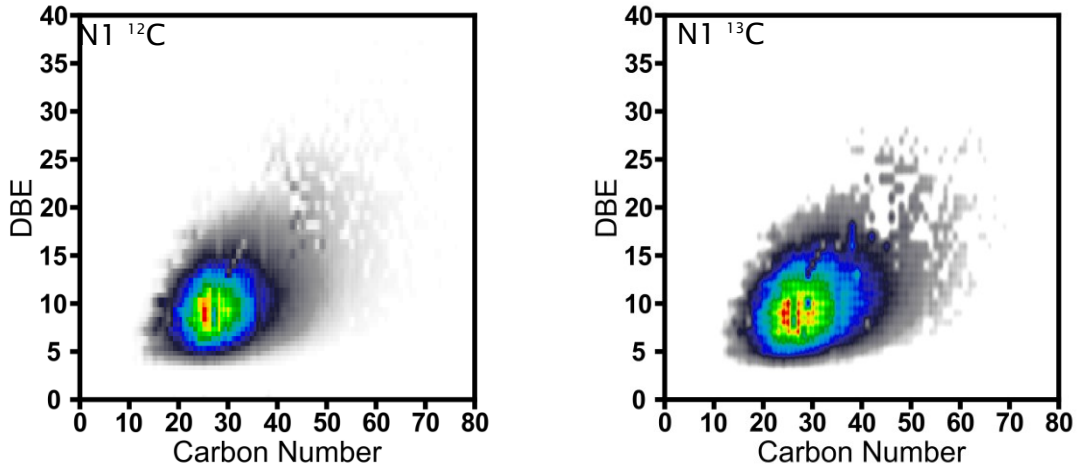

Figure 27 N_1 class ^{12}C and ^{13}C DBE *versus* carbon number plot for crude oil-2.

In addition, ^{34}S isotope fingerprint within a crude oil mass spectrum can be used to aid in the assignment of sulfur containing compounds. The exact *m/z* difference between ^{32}S and ^{34}S isotope is 1.9956 *m/z* units.

4.1.1 Effect of sample solvent and additive on multimer formation and signal intensity of the N_1 class in crude oil-1, 2 and 3

The first step of any analysis undertaken using the ESI source is the choice of a suitable dilution solvent for the analysed sample. In crude oil analysis the most common used dilution solvent is a mixture of toluene and methanol. This is because toluene can dissolve all the different compounds in crude oil. However, if the crude oil sample was dissolved in 100% toluene in positive ion ESI no ions can be observed in the crude oil mass spectrum. Thus, methanol is added as it is first miscible with toluene and second, the addition of methanol (MeOH) is essential because it acts as a source of protons in positive ion ESI that is needed to form protonated molecules $[M + H]^+$. However, 100% toluene as a sample solvent for crude oil analysis can be used in other ionisation techniques such as APPI.[63] The ratio at which methanol is added can vary among different laboratories around the world and even within the same laboratory.

Comparing data among different laboratories becomes troublesome if the data were acquired using either different dilution solvents or different ratios of toluene:methanol. Hughey and co-workers were able to characterise 11,000 compositionally distinct components in crude oil using positive ion ESI FT-ICR MS where crude oil was dissolved in toluene:methanol at a ratio of 3:7.[135] Within the same laboratory Marshall and co-workers used a toluene:methanol ratio of 1:1 for the positive ion ESI FT-ICR MS analysis of crude oil .[53] Further in different laboratory, Pakarinen and co-workers have used toluene:methanol ratio of 1.5:8.5 for positive ion ESI FT-ICR MS characterisation of Russian and North sea crude oils and their distillation fractions.[136] Guricza and co-workers have also used a mixture of 1:1:1 toluene:dichloromethane:chloroform to dissolve an asphaltene extract. This was followed by further dilution in a mixture of acetonitrile and methanol for positive ion ESI FT-ICR MS analysis .[137]

This variation in the used sample solvent also extends to other ionisation techniques such as APPI. Bae and co-workers have used 1:1 toluene:methanol ratio as a sample solvent for the analysis of conventional crude oil at concentration of 1 mg/mL using APPI 15 T FT-ICR MS.[138] Sim and co-workers have fractionated two different de-asphalted crude oil samples into 4 fractions using reversed phase HPLC. The collected fractions were analysed using positive ion APPI FT-ICR MS.[139] However, fractions corresponding to one sample were dissolved in 100% toluene while the other sample was dissolved in 1:1 toluene:methanol. Further, contribution of each compound class for collected fractions were

compared between the two samples. The N_1 class was claimed to be higher in one of the sample fraction that 1:1 toluene:methanol was used as a sample solvent compared to the other sample fraction that only toluene was used as a sample solvent. The possible reason for this variation in N_1 class relative abundance is probably due to variation in the ionisation efficiency across different sample solvent.

However, other ambient ionisation techniques such as direct analysis in real time (DART) does not require sample dissolution into suitable solvent.[140] Crude oil in its crude form can be directly analysed without the need for any sample preparation. The DART ionisation source was successfully hyphenated to FT-ICR MS for the analysis of complex organic mixtures such as de-asphalted crude oil and bio-tar.[141]

In this work, the effect of sample solvent composition and concentration will be investigated through analysing three different crude oil samples in positive ion ESI FT-ICR MS. Crude oil-1,2 and 3 were analysed using positive ion ESI FT-ICR MS *via* direct infusion analysis using 100 µL Hamilton syringe. Each crude oil sample was analysed at two different concentrations, 0.1 and 0.3 mg/mL. For each concentration, the crude oil sample was analysed using different toluene:methanol ratio of 1:9, 3:7 and 6:4. Further, the effect of ionisation enhancing additive such as formic acid was investigated for the different crude oil samples at different toluene:methanol ratios at 0.1 and 0.3 mg/mL. 300 spectra were averaged for each acquired crude oil-1, 2 and 3 mass spectra using positive ion ESI FT-ICR MS.

Crude oil-1, 2 and 3 mass spectra were internally *m/z* calibrated using the homologous series for DBE 9 of the N_1 class compounds. Then the data, *m/z* values and their signal intensities, were imported to PetroOrg without further calibration. N_1 DBE *versus* carbon number plots were generated from crude oil-1, 2 and 3 mass spectra in positive ion ESI FT-ICR MS using PetroOrg™. These plots are used to compare the distribution of ion series (DBE *versus* carbon number) across different types of crude oils, different sample solvent ratios, concentrations and with and without the addition of ionisation enhancing additive. The ion intensity in DBE *versus* carbon number plot is colour coded (red being the most intense ion in a certain class of compounds). However, the colour coding of DBE *versus* carbon number plot is assigned based on the most intense ions within a certain assigned class. Thus, for example contaminants assigned as N_1 will make the colour distribution in DBE *versus* carbon number plot according

to the intensity of the contaminant. Further comparing ion intensity for compounds in the same class across different types of crude oils, sample solvent compositions, concentrations and with and without addition of formic acid is not possible using DBE *versus* carbon number plot.

The comparison is undertaken by using the raw mass spectra data. This was conducted by focusing on specific *m/z* to show differences in the ion intensity across different crude oils samples, concentrations, sample solvents and the addition of formic acid. The comparison was conducted using N_1 class as it is the most abundant species in the positive ion ESI FT-ICR mass spectra for crude oil-1, 2 and 3.

0.1 mg/mL of crude oil-1 was analysed using positive ion ESI FT-ICR MS. Different sample solvents were used at toluene:methanol ratios of 1:9, 3:7 and 6:4. Addition of 0.1% formic acid, an ionisation enhancing additive, was added to the three different solvent ratios was investigated. (See Figure 28 for the design of the solvent composition experiment for 0.1 mg/mL crude oil-1. The same experimental design applies to 0.3 mg/mL crude oil-1 and to crude oil-2 and 3). Figure 29 shows DBE *versus* carbon number plots for the N_1 class of crude oil-1. N_1 DBE *versus* carbon number plots for toluene:methanol ratios of 1:9, 3:7 and 6:4 show a DBE distribution from DBE 4 to approximately DBE 25. The same DBE *versus* carbon number distribution plots for N_1 class is observed when 0.1% formic acid is added to the different ratios of toluene:methanol. The possible reason why 3:7 and 6:4 toluene:methanol N_1 plots have different colour distribution compared to the remaining plots is probably due to the presence of containment assigned as a compound of the N_1 class. At 0.1 mg/mL, Figure 29, no multimer formation was observed in the DBE *versus* carbon number plots for with and without the addition of formic acid for the different sample solvent ratios.

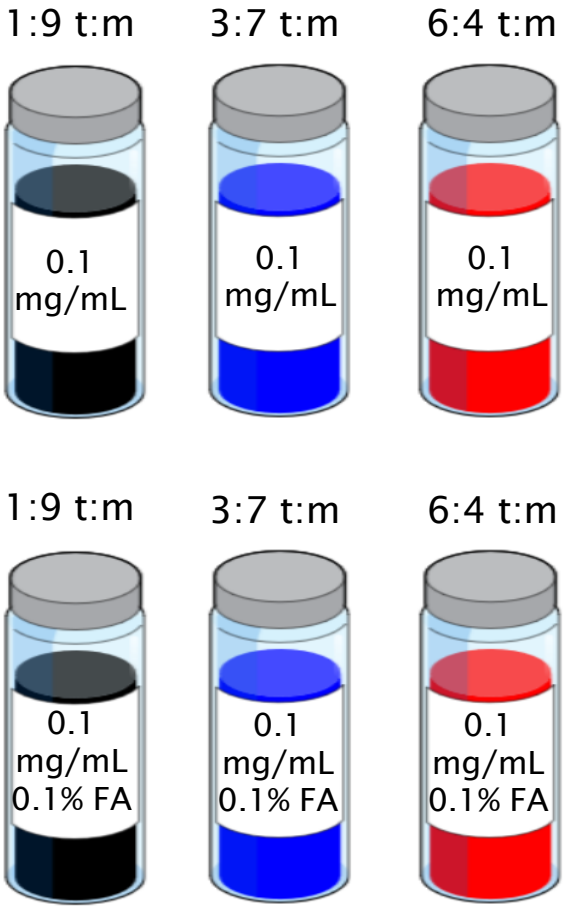

Figure 28 0.1 mg/mL crude oil-1 in different solvent ratios of toluene:methanol (t:m).

Figure 30 shows an expanded *m/z* region at nominal *m/z* 404 of 6 mass spectra for crude oil-1 analysed using positive ion ESI FT-ICR MS. Three ions are shown, protonated molecules $[C_{29}H_{41}N + H]^+$, $[C_{30}H_{29}N + H]^+$ and $[C_{27}H_{33}NS + H]^+$. The most intense ion of these is $[C_{29}H_{41}N + H]^+$. This protonated molecule, is used to visualise the changes in signal intensity across different sample solvent ratios with and without the addition of 0.1% formic acid. The top three mass spectra in Figure 30 are for crude oil-1 analysed at toluene:methanol ratio of 1:9, 3:7 and 6:4. The protonated molecule, $[C_{29}H_{41}N + H]^+$, has a higher signal intensity in the mass spectrum that was acquired using toluene:methanol solvent ratio of 1:9 compared to toluene:methanol solvent ratio of 3:7 and 6:4. The decrease in the signal intensity of $[C_{29}H_{41}N + H]^+$ is more significant at toluene:methanol solvent ratio of 6:4 compared to 3:7.

This can be explained that the sample solvent at toluene:methanol ratio of 6:4 contains the least amount of protons in solution compared to toluene:methanol ratio of 3:7 and 1:9 respectively.

The source of protons in the sample solvent is originating from the methanol content in the sample solvent. In positive ion ESI, protons in solution are needed to protonate a basic site that is available in compounds of the N_1 class such as the observed ion at *m/z* 404.332 with elemental formula of $[C_{29}H_{41}N + H]^+$ in Figure 30.

0.1% formic acid was added to 0.1 mg/mL crude oil-1 at toluene:methanol solvent ratio of 1:9, 3:7 and 6:4, shown in the bottom three mass spectra in Figure 30. The addition of formic acid, a source of protons, should have an effect on increasing the ionisation of basic nitrogen containing compounds in the crude oil-1 such as the N_1 containing compounds. Figure 30 shows that the addition of 0.1% formic acid increases the ion intensity of $[C_{29}H_{41}N + H]^+$ compared to $[C_{29}H_{41}N + H]^+$ without formic acid addition of the top three mass spectra in Figure 30. This increase in signal intensity when formic acid is added is attributed to ionising more of $[C_{29}H_{41}N + H]^+$ at toluene:methanol ratio of 1:9, 3:7 and 6:4. However, variations in the ion intensity of $[C_{29}H_{41}N + H]^+$ at toluene:methanol ratio of 1:9, 3:7 and 6:4 is observed even when formic acid is added. Signal intensity of $[C_{29}H_{41}N + H]^+$ at toluene:methanol ratio of 1:9 with formic acid is significantly greater compared to toluene:methanol ratio of 3:7 and 6:4. This means that the addition of formic acid aided the ionisation of protonated molecule, $[C_{29}H_{41}N + H]^+$. However, this addition to the different toluene:methanol ratios showed that differences in the ion intensity is still observed even when formic acid is added. Figure 30 shows that the trend in ion intensity decrease of $[C_{29}H_{41}N + H]^+$ followed by the increase of toluene ratio in the sample solvent whether formic acid is added or not. This shows that for crude oil-1 analysed at 0.1 mg/mL using positive ion ESI FT-ICR MS the effect of sample solvent composition is regardless of the additive addition,

It can be argued that $[C_{29}H_{41}N + H]^+$ is more soluble in this solvent composition of toluene:methanol ratio of 1:9. However, $[C_{29}H_{41}N + H]^+$ has DBE value of 9.5 which suggests that the core aromatic structure might be acridine $[C_{13}H_9N + H]^+$ or other isomers could be possible. Acridine is soluble in organic solvent such as toluene.[142] Further, $[C_{29}H_{41}N + H]^+$ has a long alky chain of $-CH_3(CH_2)_{15}$ which affects the overall hydrophobicity of the molecule increasing its solubility in toluene.

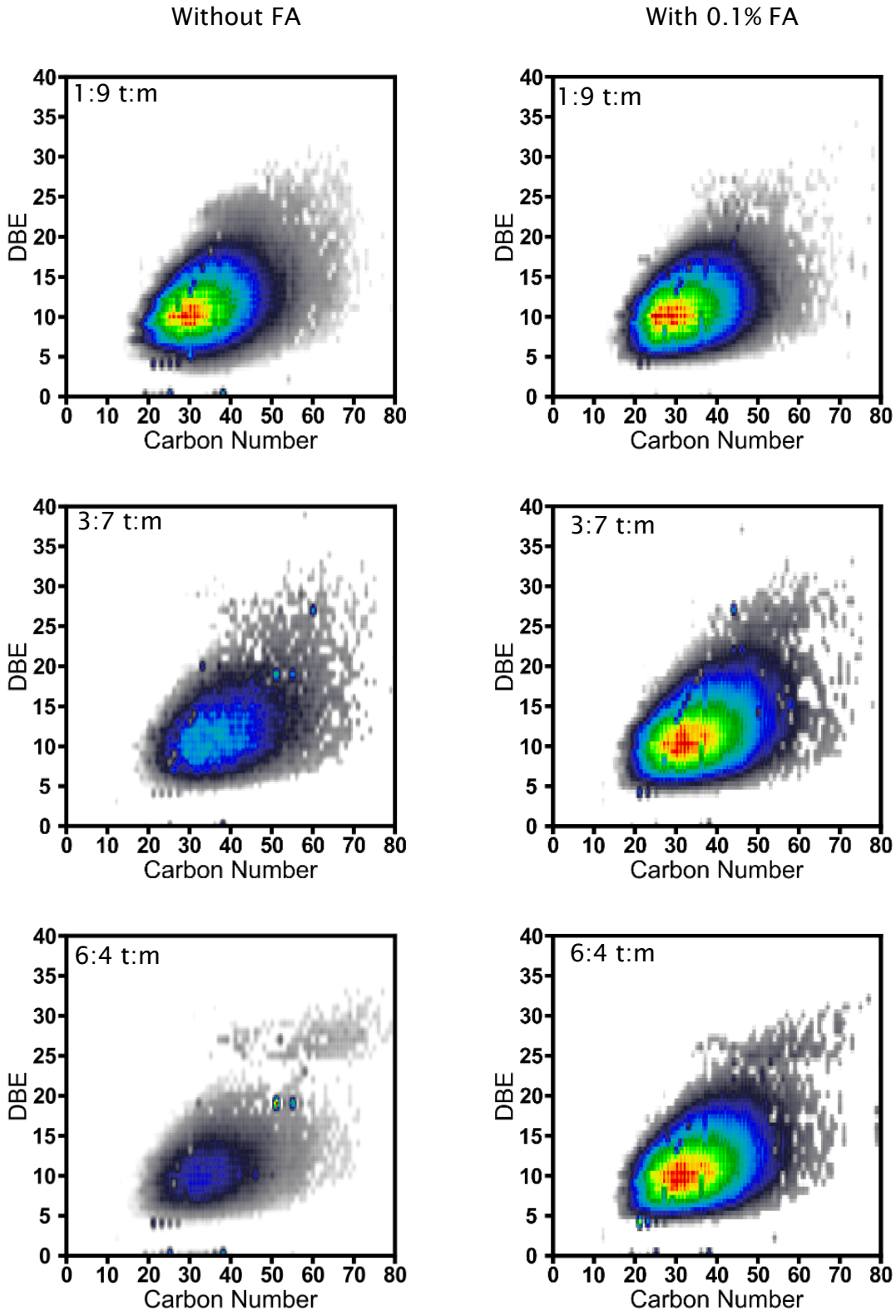

Figure 29 0.1 mg/mL solution of crude oil-1 was dissolved in toluene:methanol (t:m) solvent ratio of 1:9, 3:7 and 6:4 with and without the addition of 0.1% formic acid (FA). Crude oil-1 was analysed using positive ion ESI FT-ICR MS. DBE *versus* carbon number plot is shown for the N_1 class. See appendix for mass spectra, Figure 113.

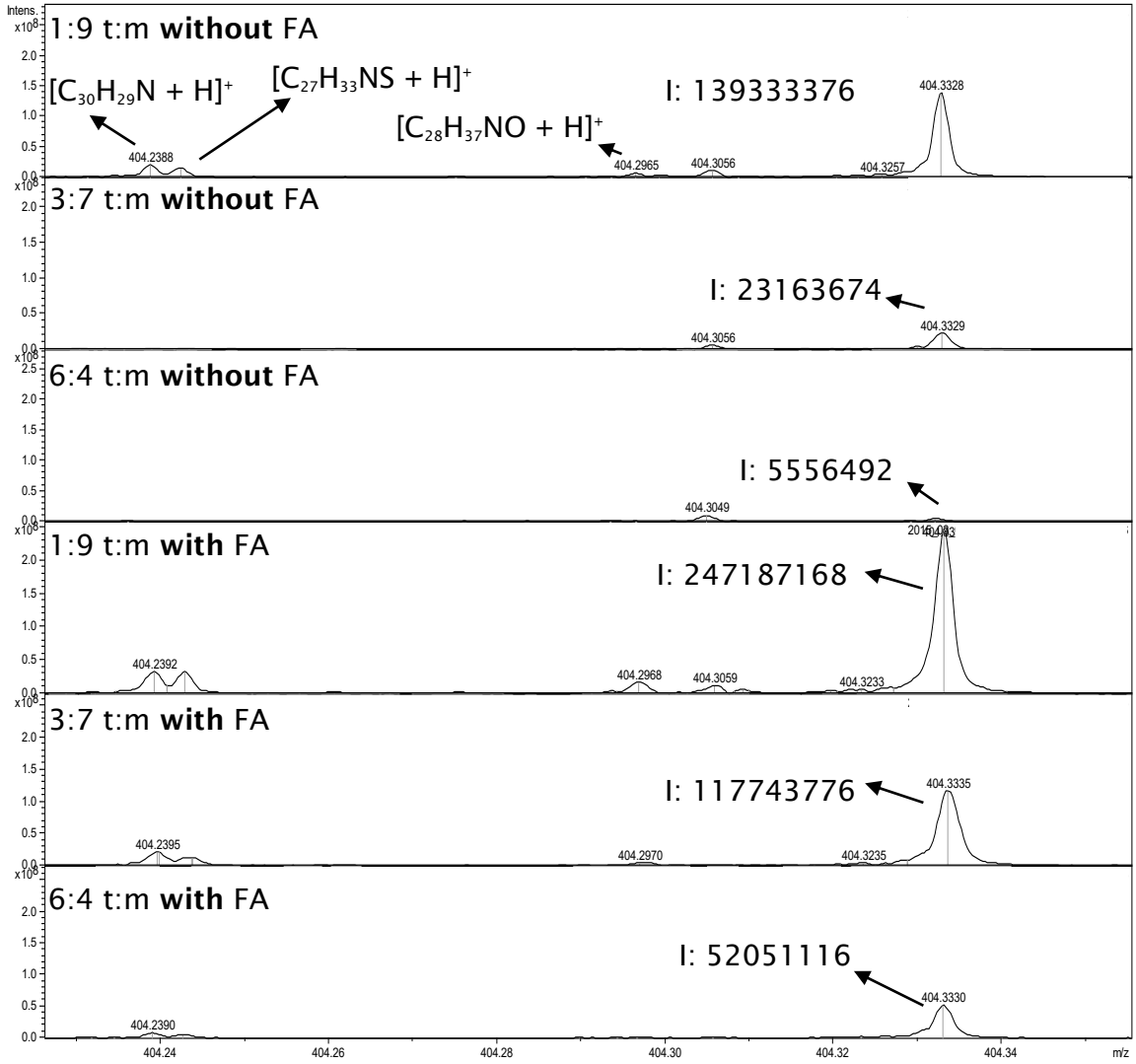

Figure 30 Positive ion ESI FT-ICR MS of 0.1 mg/mL solution of crude oil-1 at nominal *m/z* 404. The *y*-axis, intensity, is set at approximate value of 2×10^8 (intens.) for all mass spectra. I: abbreviation represents signal intensity. See appendix for mass spectra, Figure 113.

Previously, Figure 29 showed the N_1 class DBE *versus* carbon number plots distribution for 0.1 mg/mL crude oil-1 at different sample solvent compositions. The DBE value for the N_1 class was up to 25. No multimers were formed during the electrospray ionisation process at 0.1 mg/mL for crude oil-1 at the different sample solvent compositions with and without the addition of formic acid. Figure 31 shows the same analysis for crude oil-1 as Figure 29 but at higher concentration, 0.3 mg/mL rather than 0.1 mg/mL respectively. The monomeric distribution for the N_1 class DBE *versus* carbon number plots, up to DBE 25, for 0.3 mg/mL crude oil-1 in Figure 31 is the same as 0.1 mg/mL crude oil-1 in Figure 29.

The molecular weight of a compound does not change with concentration. However, one of the caveats of using electrospray ionisation is the formation of dimers or multimers in the gas phase ions, $[2M + H]^+$ and $[xM + H]^+$ respectively. Multimers are formed above the critical concentration of multimer formation in the ESI source. The ESI source is prone to form multimers as the ionisable compounds are polar molecules which tend to non-covalently aggregate. The formation of multimers in positive ion ESI FT-ICR MS of crude oil analysis hinders the correct assignment of the monomeric distribution of DBE and carbon number for a certain class of compound. Ions aggregation are probably due to Coulombic repulsion in the gas phase of the ESI source.

Figure 31 shows that multimer formation was observed in 0.3 mg/mL crude oil-1 N_1 DBE *versus* carbon number plot. These multimers are highlighted in red circle in N_1 DBE *versus* carbon number plots at toluene:methanol ratio of 3:7 and 6:4. However, these multimers are not observed in Figure 29 N_1 DBE *versus* carbon number plots for 0.1 mg/mL crude oil-1. The molecular weight distribution does not change with concentration which proves that these multimers are formed in the gas phase as a result of increase in concentration. It should be noted that these multimers are not aggregate of N1 as it would be shown as N2 class rather than N1.Figure 31 shows that no multimers were formed for 0.3 mg/mL crude oil-1 sample analysed using toluene:methanol ratio of 1:9 without the addition of formic acid. However, in Figure 31 at the same concertation, 0.3 mg/mL for crude oil-1, multimers were formed at toluene:methanol ratio of 3:7 and 6:4 without the addition of formic acid. This suggests that multimer formation is not only concentration driven but also solvent composition dependent. A high content of methanol in the sample solvent, toluene:methanol ratio of 1:9, reduced multimer formation which might be due to the acidity of methanol.

Further, if the hypothesis is correct the addition of an acid such as formic acid should reduce multimer formation for 0.3 mg/mL crude oil-1 analysed with high toluene content in the sample solvent. This is confirmed in Figure 31 where the addition of 0.1% formic acid to sample analysed using toluene:methanol ratio of 3:7 and 6:4 reduced multimer formation. Figure 32 compares the signal intensity of $[C_{29}H_{41}N + H]^+$ across different sample solvent composition with and without the addition of formic acid for 0.3 mg/mL crude oil-1. Figure 32 is similar to Figure 30 where $[C_{29}H_{41}N + H]^+$ ion intensity is the highest when toluene:methanol ratio of 1:9 with 0.1% formic acid is used compared to other toluene:methanol ratios of 3:7 and 6:4.

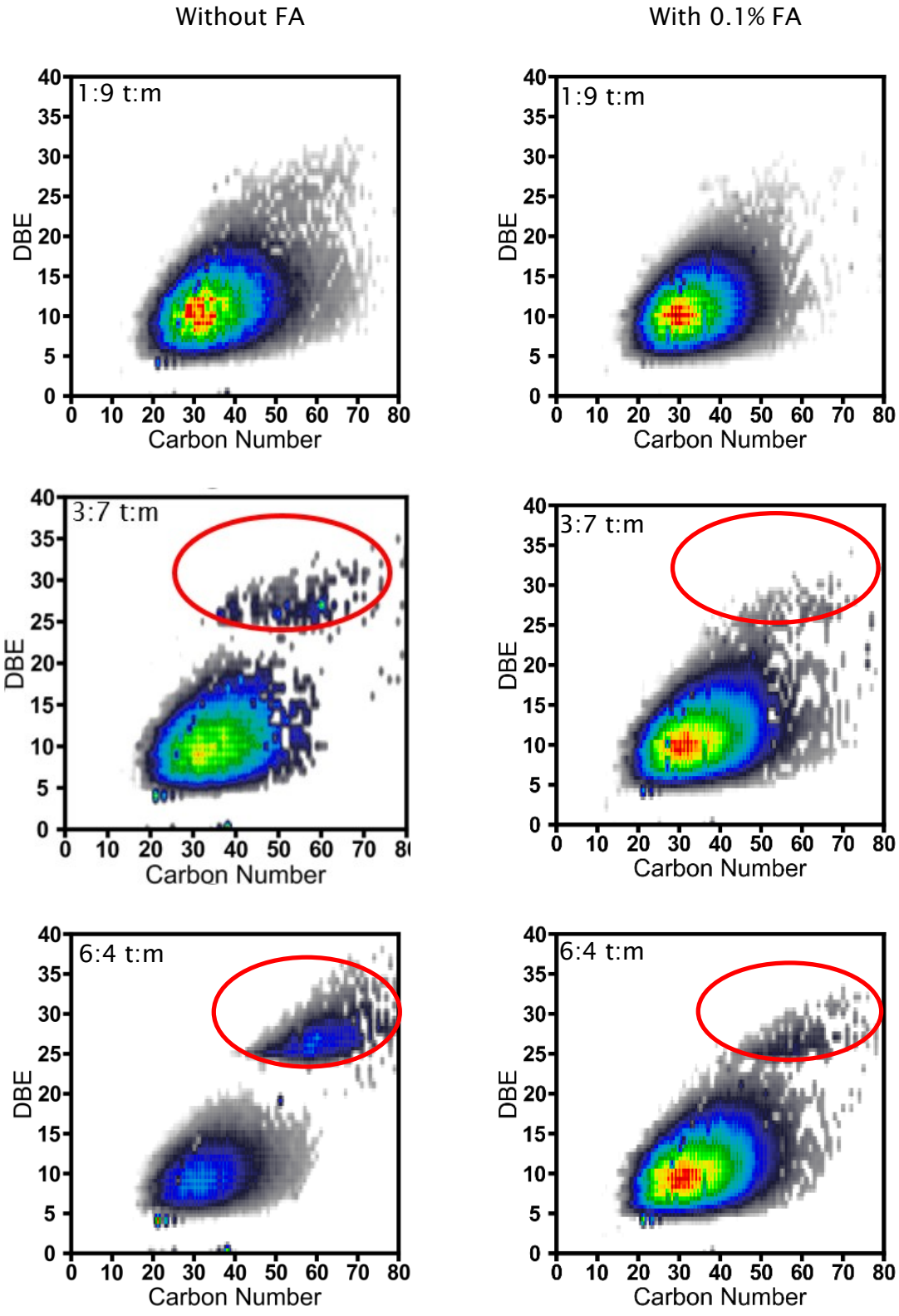

Figure 31 0.3 mg/mL solution of crude oil-1 was dissolved in toluene:methanol (t:m) solvent ratio of 1:9, 3:7 and 6:4 with and without the addition of 0.1% formic acid (FA). Crude oil-1 was analysed using positive ion ESI FT-ICR MS. DBE *versus* carbon number plot is shown for the N_1 class. See appendix for mass spectra, Figure 114.

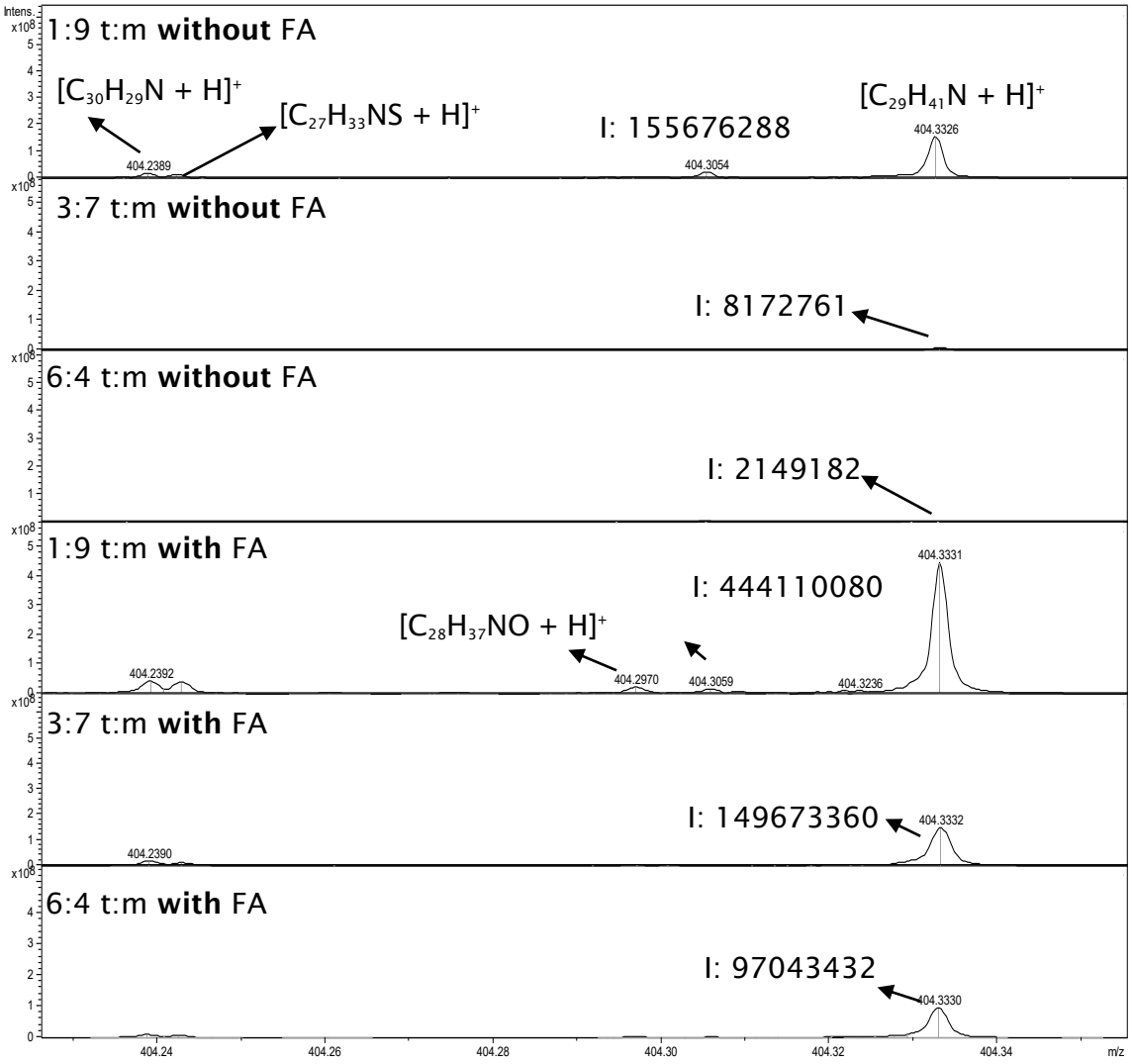

Figure 32 Positive ion ESI FT-ICR MS of 0.3 mg/mL solution of crude oil-1 at nominal *m/z* 404. The *y*-axis, intensity, is set at approximate value of 5×10^8 (intens.) for all mass spectra. I: abbreviation represents signal intensity. See appendix for mass spectra, Figure 114.

Crude oil-2, different in its content of heteroatoms containing compounds compared to crude oil-1, was as well analysed using positive ion ESI FT-ICR MS. In Figure 29 DBE *versus* carbon number plot for N_1 class for 0.1 mg/mL crude oil-1 analysed using different toluene:methanol ratios with and without the addition of formic acid was shown. Similarly, Figure 33 shows the N_1 class DBE *versus* carbon number plots for 0.1 mg/mL crude oil-2.

However, the main difference is that crude oil-1 in Figure 29 compared to crude oil-2 showed no multimer formation at 0.1 mg/mL for the different toluene:methanol ratios of 1:9, 3:7 and 6:4 with and without the addition of formic acid. The observed multimers in N_1 class plots in Figure 33 is for 0.1

mg/mL crude oil -2 at toluene:methanol ratio of 3:7 and 6:4 with DBE value > 25. These multimers were not formed when the analysis was undertaken at toluene:methanol ratio of 1:9.

The addition of 0.1% formic acid to 0.1 mg/mL crude oil-2 analysed with toluene:methanol ratio of 3:7 and 6:4 resulted in multimers dissociation compared to toluene:methanol ratios of 3:7 and 6:4 analysed without the addition of formic acid. It should be noted that multimers formed at 0.3 mg/mL for crude-1 in Figure 31 were not completely dissociated when formic acid was added for toluene:methanol ratio of 3:7 and 6:4.

In comparison, 0.1 mg/mL crude oil-1 in Figure 29 showed no multimer formation in N_1 class plots. But 0.1 mg/mL crude oil-2 N_1 class plots in Figure 33 showed multimer formation at toluene:methanol ratio of 3:7 and 6:4. This suggests that crude oil-2 is more prone to form multimers which is reflected in its different content of heteroatoms compared to crude oil-1.

Figure 34 shows an expanded *m/z* region for 0.1 mg/mL crude oil-2 mass spectra analysed using positive ion ESI FT-ICR MS at different sample solvent compositions. The effect of sample solvent compositions on the ionisation of *m/z* 404.333 with elemental formula of $[C_{29}H_{41}N + H]^+$ is illustrated. The ion intensity for *m/z* 404.333 is the highest at toluene:methanol ratio of 1:9 with 0.1% formic acid compared to the other used ratios. This observation of ion intensity increase is in accordance with 0.1 and 0.3 mg/mL crude oil-1, shown in Figure 30 and Figure 32 respectively. Figure 34 shows that the addition of formic acid to 0.1 mg/mL crude oil-2 at toluene:methanol ratio of 1:9. 3:7 and 6:4 did not result in the same ion intensities despite the addition of the ionisation enhancing additive. The reduction in signal intensity of $[C_{29}H_{41}N + H]^+$ at *m/z* 404.333 follows according to the toluene:methanol ratio of 1:9 to 3:7 and to 6:4.

This reduction in ion intensity can be observed as well for other protonated molecules in Figure 33. In the *m/z* expanded region in Figure 33 other protonated molecules are observed, $[C_{30}H_{29}N+H]^+$ and $[C_{27}H_{33}NS+H]^+$ with DBE 16.5 and 11.5 respectively. In Figure 33 the reduction in ion intensity when toluene content is increased is observed for different DBEs of the N_1 class, DBE 9.5 for $[C_{29}H_{41}N+H]^+$ and DBE 16.5 for $[C_{30}H_{29}N+H]^+$. Further, the decrease in ion intensity is observed as well for the protonated molecule $[C_{27}H_{33}NS + H]^+$ belonging to the N_1S_1 class.

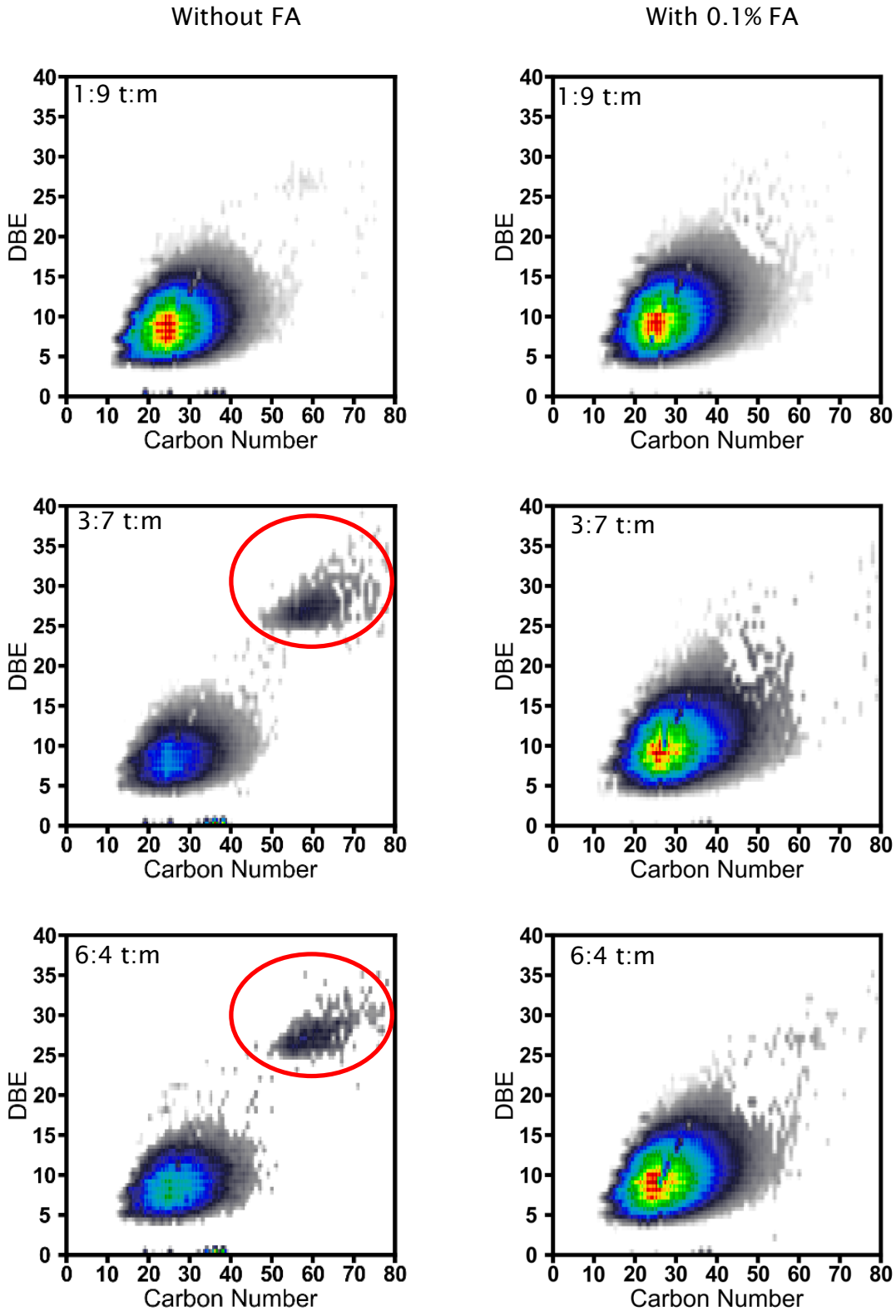

Figure 33 0.1 mg/mL solution of crude oil-2 was dissolved in toluene:methanol (t:m) solvent ratio of 1:9, 3:7 and 6:4 with and without the addition of 0.1% formic acid (FA). Crude oil-2 was analysed using positive ion ESI FT-ICR MS. DBE *versus* carbon number plot is shown for the N_1 class. See appendix for mass spectra, Figure 115.

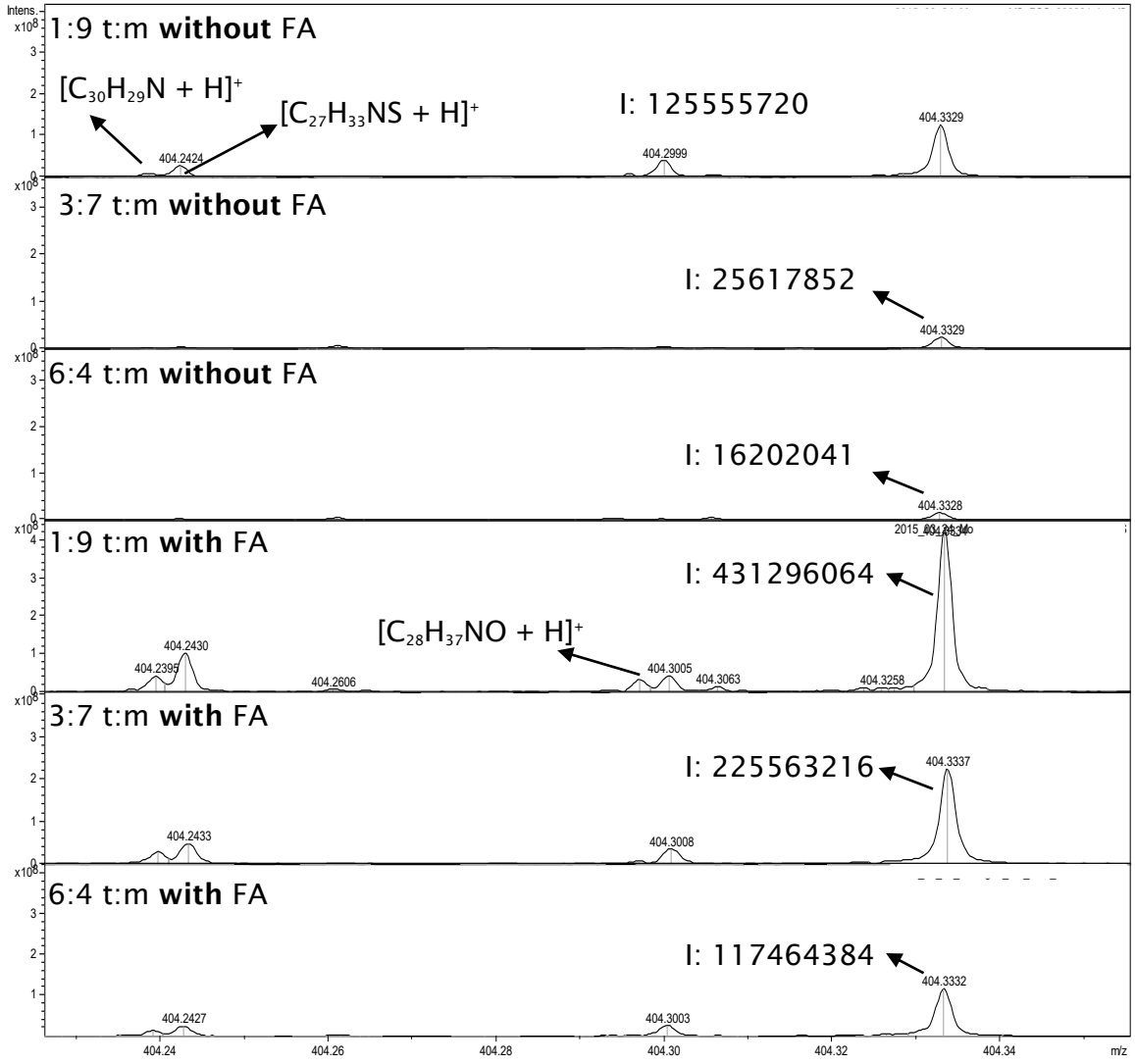

Figure 34 Positive ion ESI FT-ICR MS of 0.1 mg/mL solution of crude oil-2 at nominal *m/z* 404. The *y*-axis, intensity, is set at approximate value of 3×10^8 (intens.) for all mass spectra. I: is an abbreviation for signal intensity. See appendix for mass spectra, Figure 115.

The analysis of 0.3 mg/mL crude oil-2 using positive ion ESI FT-ICR MS at different toluene:methanol ratios was undertaken. DBE *versus* carbon number plots for the N_1 class are shown in Figure 35. Multimers were observed in N_1 plots for 0.3 mg/mL crude oil-2 at toluene:methanol ratio of 1:9, 3:7 and 6:4 without the addition of formic acid, highlighted using red circles. However, 0.1 mg/mL crude oil-2 showed no multimer formation in N_1 DBE *versus* carbon number plot at toluene:methanol ratio of 1:9 without the addition of formic acid. (See Figure 33). Thus, at 0.3 mg/mL crude oil-2 in Figure 35 multimers were observed in N_1 DBE *versus* carbon number plot at toluene:methanol ratio of 1:9 without the addition of formic acid. These multimers were not observed at 0.1 mg/mL crude oil-2 in Figure 33 at the same toluene:methanol ratio of 1:9 without the addition

of formic acid. This further proves that one of the factors of forming these multimers is concentration driven.

When 0.1% formic acid was added to 0.3 mg/mL crude oil-2 multimers were dissociated at toluene:methanol ratio of 1:9 and 3:7 and reduced at 6:4. (See Figure 35). This could be explained that the formation of these multimers could be due to the lack of protons in the sample solvent and/or hydrogen bonding between molecules. Thus, two molecules are joined non-covalently to share a proton. The addition of 0.1% formic acid, a source of protons, to 0.3 mg/mL crude oil-2 analysed at toluene:methanol ratio of 1:9 and 3:7 dissociated these multimers, observed in N_1 DBE *versus* carbon number plots. (See Figure 35). However, in Figure 35 multimers formation were reduced for 0.3 mg/mL crude oil-2 at toluene:methanol ratio of 6:4 when formic acid was added.

At 0.1 mg/mL crude oil-2 multimers were dissociated at toluene:methanol ratio of 6:4 when formic acid was added. (See Figure 33). But at 0.3 mg/mL crude oil-2 the formations of these multimers were reduced at toluene:methanol ratio of 6:4 when formic acid was added. (See Figure 35). This could be explained that in Figure 35 at 0.3 mg/mL crude oil-2 toluene:methanol ratio of 6:4 more acid is required to dissociate these multimers that was not required in Figure 33 at 0.1 mg/mL crude oil-2 toluene:methanol ratio of 6:4. This is because of the concentration increase form 0.1 mg/mL to 0.3 mg/mL for crude oil-2. This hypothesis is further proved that at 0.3 mg/mL crude oil-2 at toluene:methanol ratio of 1:9 and 3:7 with formic acid multimers were dissociated because of the higher content of methanol in the sample solvent compared to toluene:methanol ratio of 6:4 with formic acid. Figure 36 is similar to Figure 34 but crude oil-2 mass spectra were analysed at 0.3 mg/mL instead of 0.1 mg/mL at different sample solvent ratios of toluene:methanol. The expanded *m/z* region at *m/z* 404 shows three major protonated molecules. In Figure 36, $[C_{29}H_{41}N+H]^+$ at *m/z* 404.333 has the same trend in signal intensity at different sample solvent composition compared to Figure 34 at 0.1 mg/mL crude oil-2 and crude oil-1 at 0.1 mg/mL in Figure 30 and 0.3 mg/mL in Figure 32. The trend is that the signal intensity of *m/z* 404.333 is decreased when the toluene content is increased in the sample solvent. Further, the addition of formic acid to toluene:methanol ratio of 1:9, 3:7 and 6:4 aided the protonation of $[C_{29}H_{41}N+H]^+$.

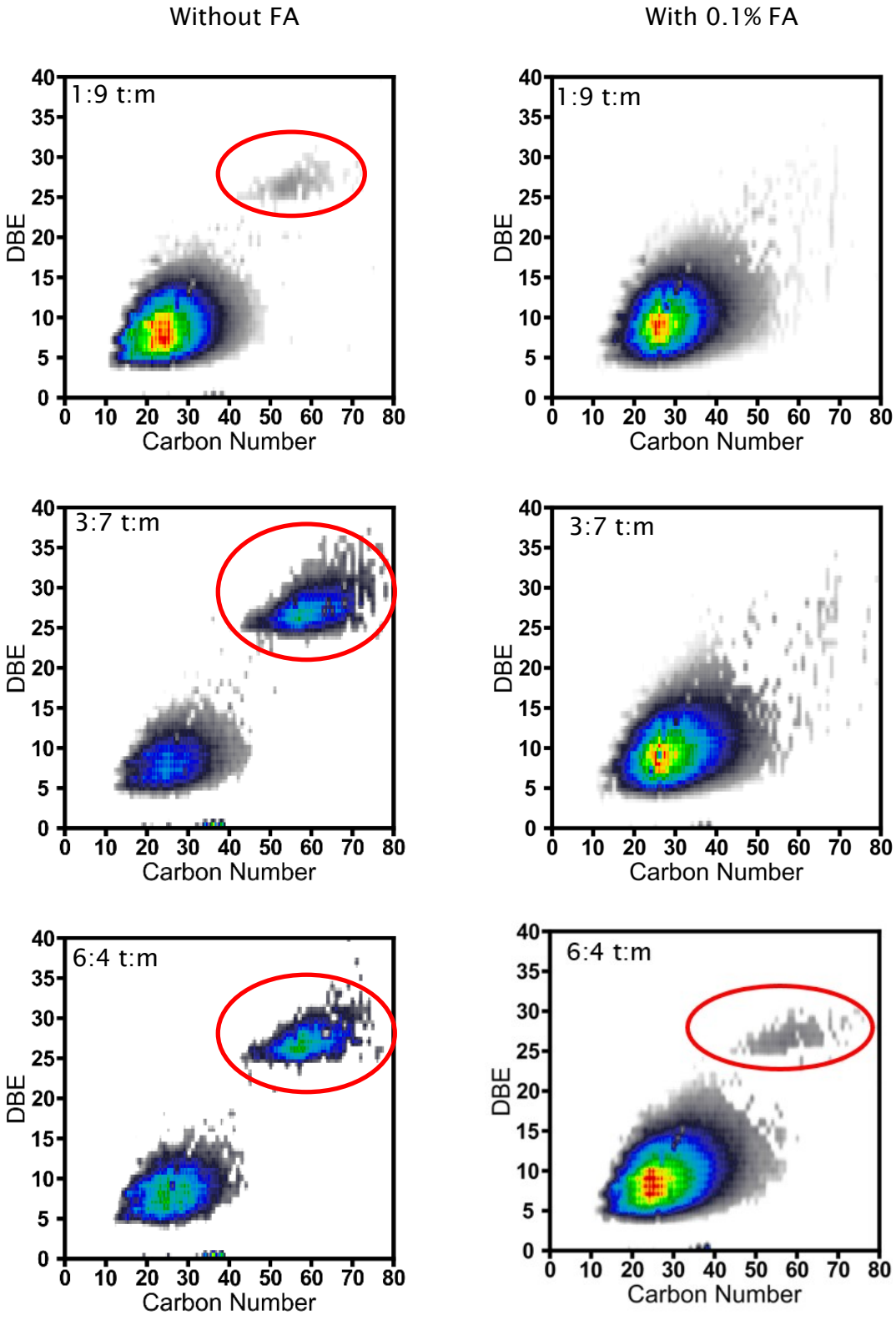

Figure 35 0.3 mg/mL solution of crude oil-2 was dissolved in toluene:methanol (t:m) solvent ratio of 1:9, 3:7 and 6:4 with and without the addition of 0.1% formic acid (FA). Crude oil-2 was analysed using positive ion ESI FT-ICR MS. DBE *versus* carbon number plot is shown for the N_1 class. See appendix for mass spectra, Figure 116.

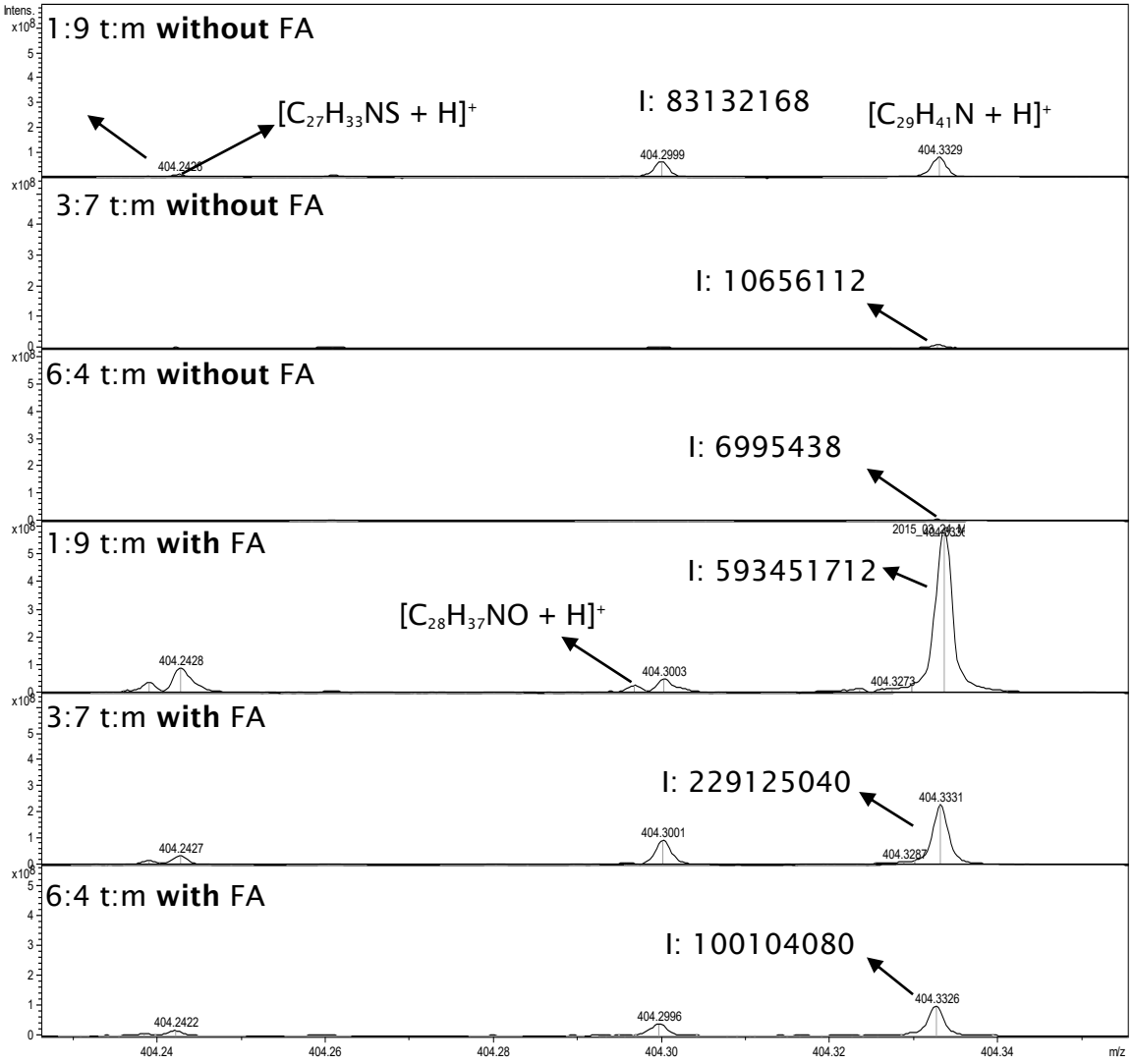

Figure 36 Positive ion ESI FT-ICR MS of 0.3 mg/mL solution of crude oil-2 at nominal *m/z* 404. The *y*-axis, intensity, is set at approximate value of 5×10^8 (intens.) for all mass spectra. I is for signal intensity. See appendix for mass spectra, Figure 116.

0.1 and 0.3 mg/mL solutions of crude oil-3 were analysed using positive ion ESI FT-ICR MS at different toluene:methanol ratios with and without the addition of formic acid. N_1 DBE *versus* carbon number plots are shown in Figure 37 and Figure 39 for 0.1 and 0.3 mg/mL respectively. Crude oil-3 is a light sour crude oil which has a rich amount of light weight hydrocarbons and sulfur containing compounds. In N_1 DBE *versus* carbon number plots of crude oil-3 no multimers were formed at 0.1 mg/mL or 0.3 mg/mL in Figure 37 and Figure 39 respectively for the different toluene:methanol ratios. This might indicate that this type of crude oil, light and sour, is less prone to form multimers in the gas phase. The other types of crude oils that were previously discussed showed multimer formation at different concentrations in N_1 DBE *versus* carbon number plots.

Crude oil-1 showed no multimers at 0.1 mg/mL in Figure 29 N_1 DBE *versus* carbon number plots at different toluene:methanol ratios. But multimers were observed at 0.3 mg/mL for crude oil-1 in Figure 31 N_1 DBE *versus* carbon number plots at toluene:methanol ratio of 3:7 and 6:4. Crude oil-2 multimers were observed starting from 0.1 mg/mL in Figure 33 N_1 DBE *versus* carbon number plots at toluene:methanol ratio of 3:7 and 6:4. In conclusion, multimers in N_1 DBE *versus* carbon number plots were only observed for crude oil-1 and crude oil-2. No multimers were observed for 0.1 mg/mL or 0.3 mg/mL crude oil-3 in N_1 DBE *versus* carbon number plots at different toluene:methanol ratios. This suggest that multimer formation is affected by the property of the analysed crude oil sample. This information can be linked back to the physical properties of crude oil as crude oil-1 and 2 are heavy crude oils whereas crude oil-3 is light and sour crude oil. See Table 1 Crude oil classification according to American Petroleum Institute gravity. Expanded *m/z* mass spectra comparison at *m/z* 404 was undertaken for crude oil-3 at 0.1 mg/mL and 0.3 mg/mL in Figure 38 and Figure 40 respectively for the different toluene:methanol ratios with and without the addition of formic acid. This same comparison of different expanded crude oils mass spectra was undertaken for crude oil-1 at 0.1 mg/mL and 0.3 mg/mL in Figure 30 and Figure 32 respectively. And as well was undertaken for crude oil-2 at 0.1 mg/mL and 0.3 mg/mL in Figure 34 and Figure 36 respectively. For crude oil-1 and 2 the signal intensity of *m/z* 404.332 with elemental formula $[C_{29}H_{41}N + H]^+$ is most intense at toluene:methanol ratio of 1:9 with the addition of 0.1% formic acid. The signal intensity of *m/z* 404.332 is decreased with increasing the toluene content in the sample solvent even with the addition of formic acid. Thus, *m/z* 404.332 ion intensity is decreased from toluene:methanol ratios of 1:9 to 3:7 to 6:4. However, this trend in the ion signal intensity of *m/z* 404.332 that was observed for crude oil-1 and 2 was not observed for crude oil-3. The ion intensity of *m/z* 404.332 for 0.1 mg/mL and 0.3 mg/mL crude oil-3 in Figure 38 and Figure 40 respectively did not decrease from toluene:methanol ratio of 1:9 to 3:7 with the addition of formic acid. However, the ion intensity of *m/z* 404.332 was decreased at toluene:methanol ratio of 6:4 compared to 1:9 and 3:7 in Figure 38 and Figure 40. The data suggest that the effect of changing the sample solvent composition of toluene:methanol ratios is not the same for all types of crude oils. This further complicates the comparison among different types of crude oils. As the data suggest that light and sour crude oil-3 is less affected by sample solvent variations of toluene:methanol with the formic acid compared to crude oil-1 and 2.

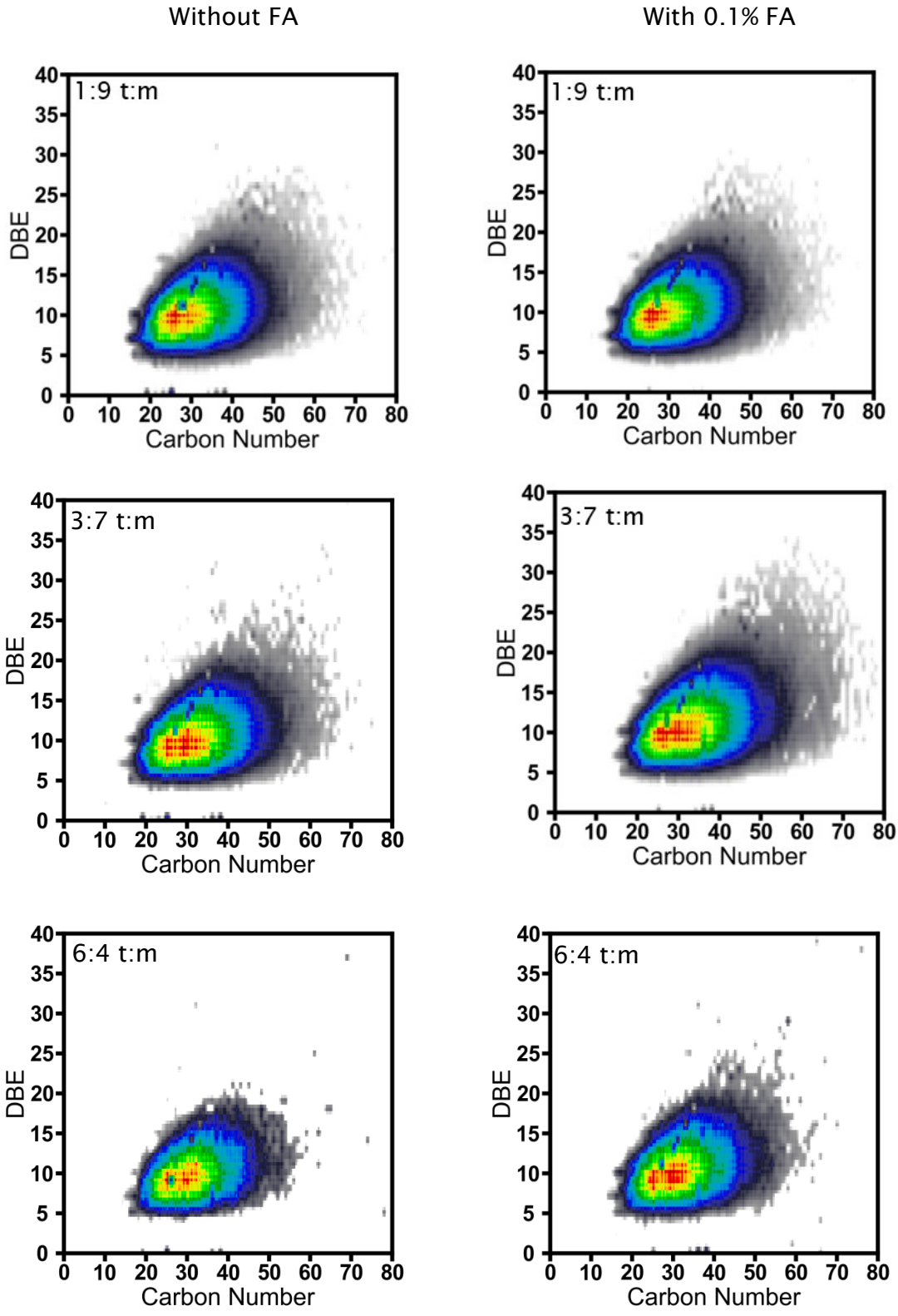

Figure 37 0.1 mg/mL solution of crude oil-3 was dissolved in toluene:methanol (t:m) solvent ratio of 1:9, 3:7 and 6:4 with and without the addition of 0.1% formic acid (FA). Crude oil-3 was analysed using positive ion ESI FT-ICR MS. DBE *versus* carbon number plot is shown for the N_1 class. See appendix for mass spectra, Figure 117.

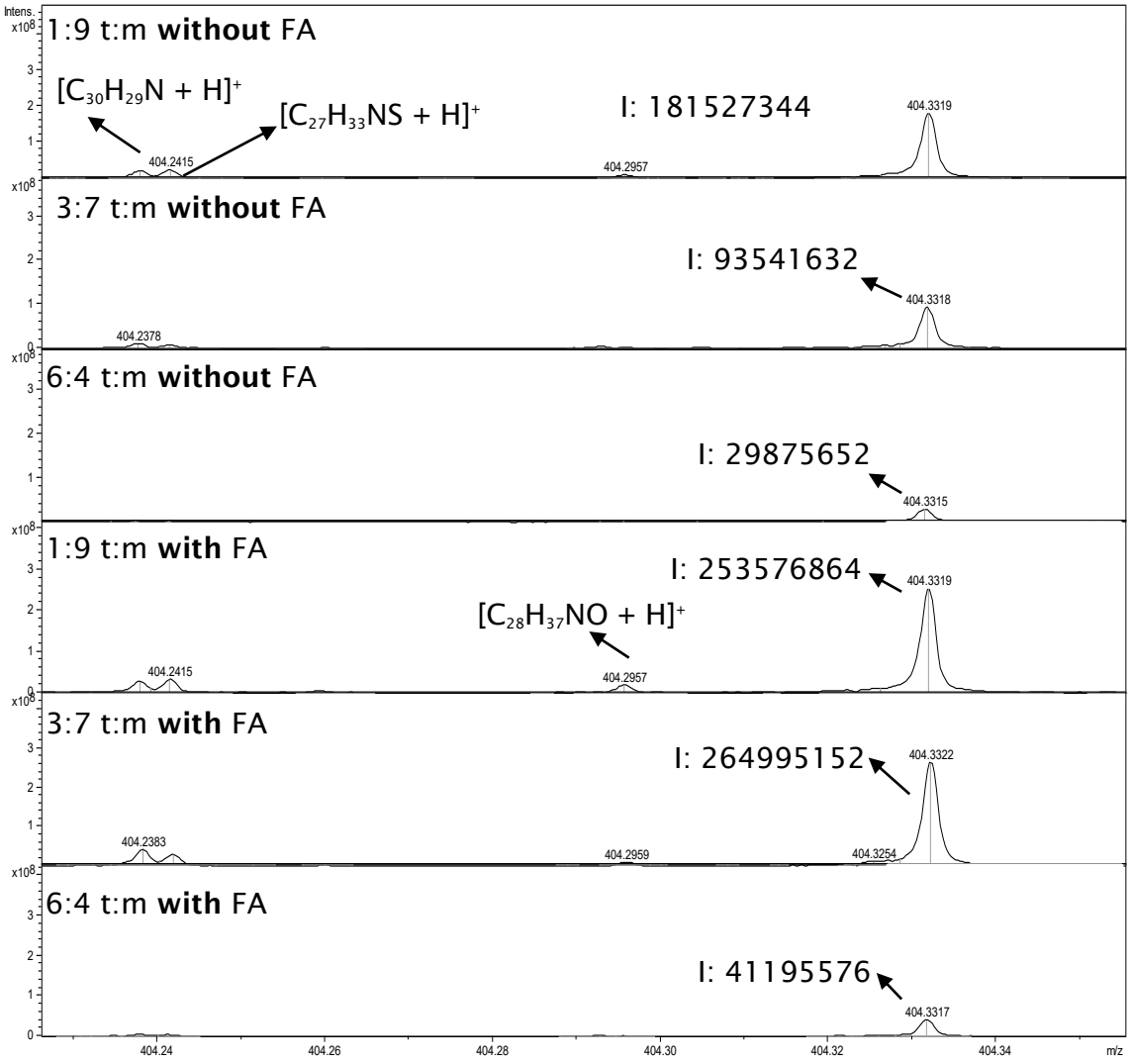

Figure 38 Positive ion ESI FT-ICR MS of 0.1 mg/mL solution of crude oil-3 at nominal *m/z* 404. The *y*-axis, intensity, is set at approximate value of 3×10^8 (intens.) for all mass spectra. I: abbreviation represents signal intensity. See appendix for mass spectra, Figure 117.

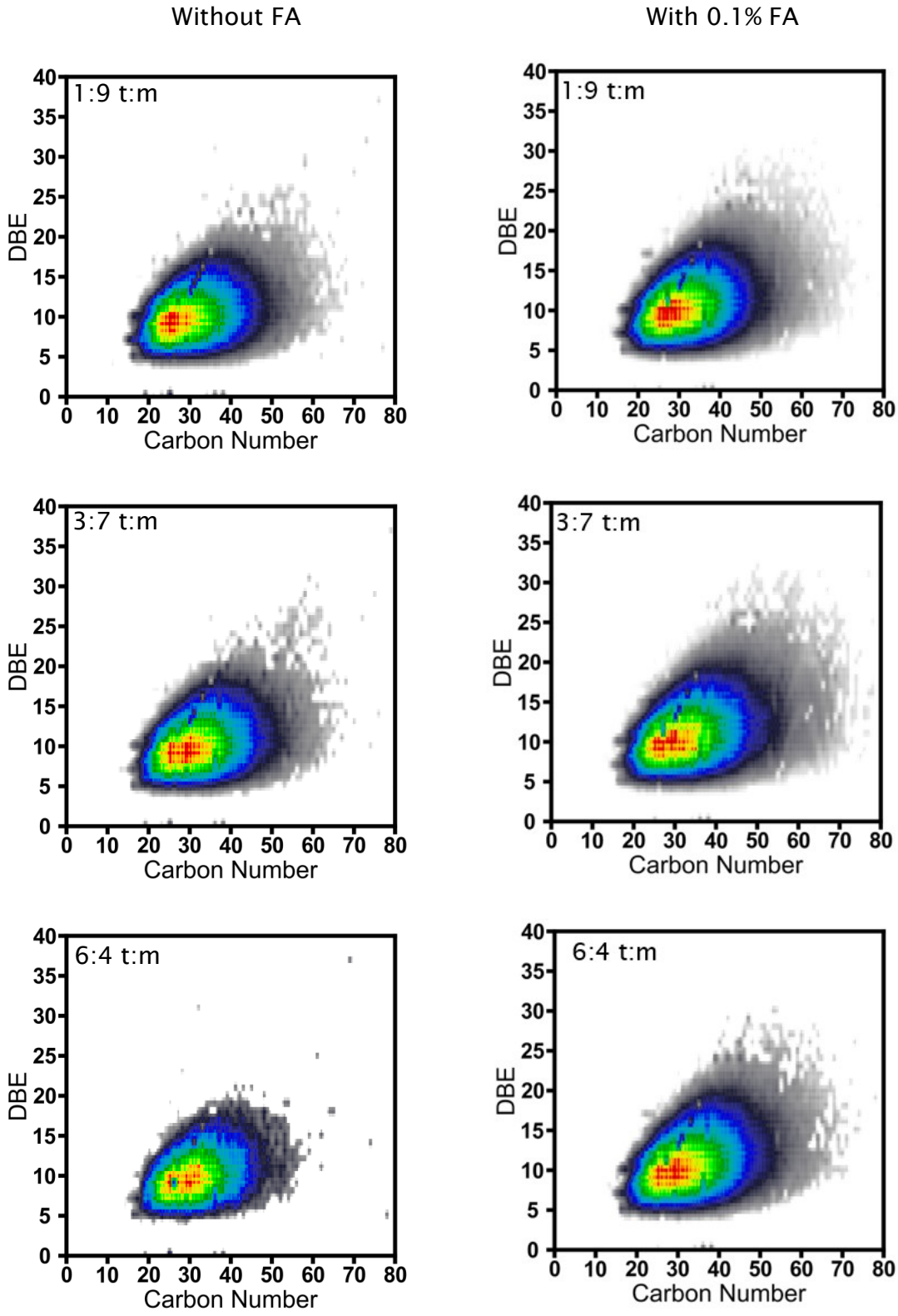

Figure 39 0.3 mg/mL solution of crude oil-3 was dissolved in toluene:methanol (t:m) solvent ratio of 1:9, 3:7 and 6:4 with and without the addition of 0.1% formic acid (FA). Crude oil-3 was analysed using positive ion ESI FT-ICR MS. DBE *versus* carbon number plot is shown for the N_1 class. See appendix for mass spectra, Figure 118.

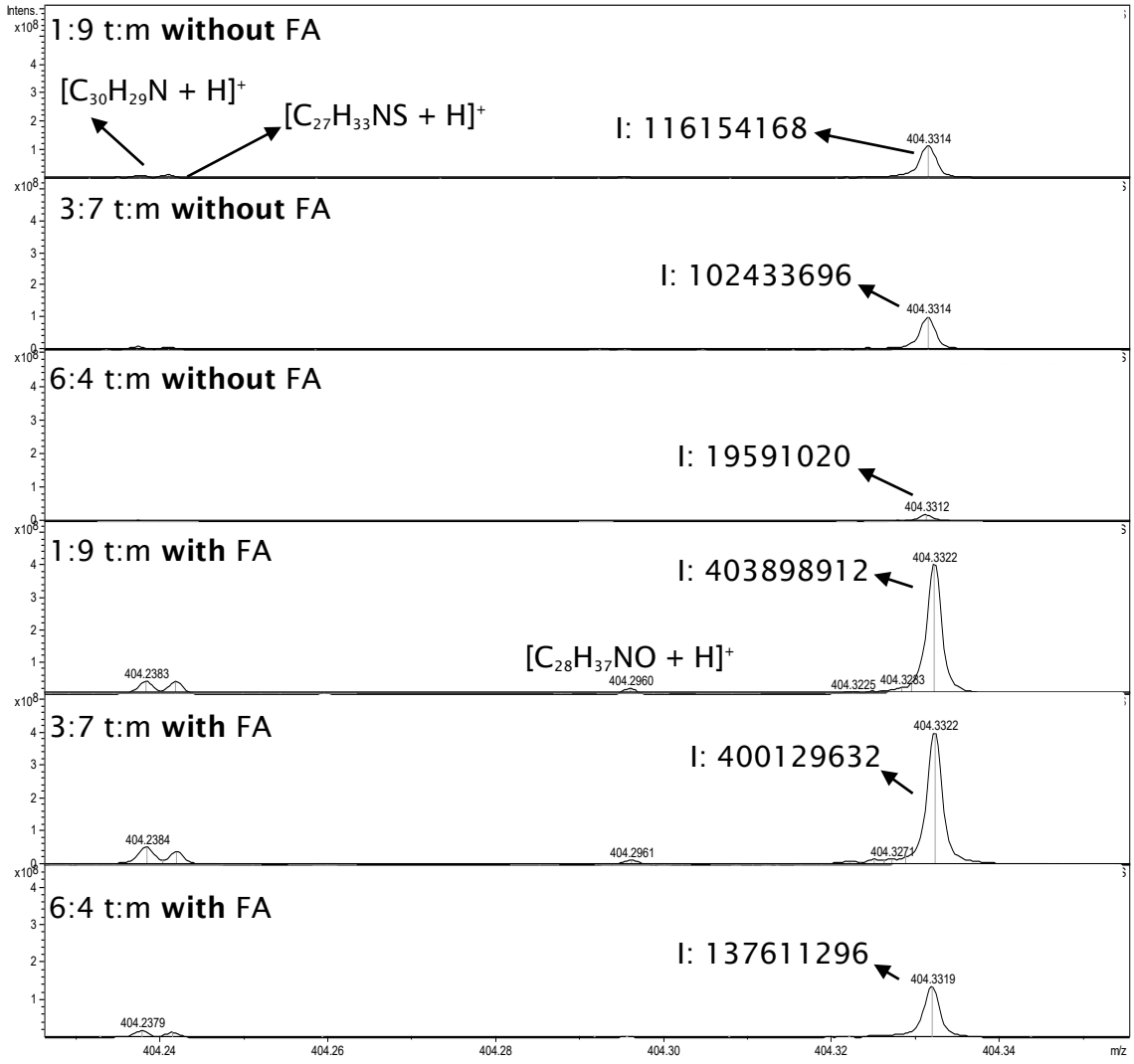

Figure 40 Positive ion ESI FT-ICR MS of 0.3 mg/mL solution of crude oil-3 at nominal *m/z* 404. The *y*-axis, intensity, is set at approximate value of 4×10^8 (intens.) for all mass spectra. I: abbreviation represents signal intensity. See appendix for mass spectra, Figure 118.

4.1.2 Comparing N_1 combined ion intensities of crude oil-1, 2 and 3

Previously, the N_1 class for crude oil-1, 2 and 3 were compared using DBE *versus* carbon number plots for the different toluene:methanol ratios with and without the addition of 0.1% formic acid. These N_1 plots were used to compare the effect of sample solvent composition and additive addition on multimer formation and dissociation. However, to compare the effect of sample solvent composition and addition of additive on ion intensity the crude oil mass spectra were used. An expanded region of the crude oil mass spectrum at *m/z* 404 was viewed. *m/z* 404.332 with elemental formula of $[C_{29}H_{41}N + H]^+$ was used to compare the effect of sample solvent composition and addition of formic acid on its ion intensity across different types of crude oils. However, it can be argued that one ion at *m/z* 404.332 with elemental formula of $[C_{29}H_{41}N + H]^+$, related to the N_1 class, cannot be used to reliably assess the effect of sample solvent composition and additive addition on the N_1 class as a whole.

Thus, in Figure 41 the ion intensities that are related to the N_1 class are combined for 0.1 mg/mL crude oil-1, 2 and 3 at different toluene:methanol ratios of 1:9, 3:7 and 6:4 with the addition of 0.1 % formic acid. The analysis was undertaken in triplicates and the error bars are shown. The triplicate, shown in Figure 41, are resulted for measuring the same sample solution. Figure 41 shows only the data that was acquired with the addition of 0.1% formic acid. This is because the comparison in section 4.1.1 undertaken using *m/z* 404.332 confirmed that the addition of formic acid aided the ionisation of *m/z* 404.332 in crude oil-1, 2 and 3 mass spectra using toluene:methanol ratios of 1:9, 3:7 and 6:4. Despite the addition of formic acid *m/z* 404.332 ion intensity was reduced when the toluene content was increased for crude oil-1 and 2. However the reduction in ion intensity of *m/z* 404.332 was not observed for crude oil-3 when the toluene content was increased from toluene:methanol ratio of 1:9 to 3:7. This showed that the trend in ionisation response for *m/z* 404.332 in crude oil-3 is different from crude oil-1 and 2. The aim of Figure 41 is to show that these differences in ion intensities are not only observed for *m/z* 404.332 but as well for the N_1 class as a whole across different toluene:methanol ratios.

In Figure 41 the N_1 class ion intensities for crude oil-2 (grey colour) is the highest at toluene:methanol ratio of 1:9 with 0.1% formic acid. The combined ion intensities for N_1 class is reduced when the toluene content is increased to toluene:methanol ratio of 3:7 and 6:4 respectively with 0.1% formic acid. N_1 class combined ion intensities of crude oil-1, black colour, is the highest at

toluene:methanol ratio of 1:9 with 0.1% formic acid. The N_1 class ion intensities for crude oil-1 is reduced at toluene:methanol ratios of 3:7 and 6:4 compared to 1:9. However the reduction that was observed for N_1 combined ion intensities for crude oil-2 from toluene:methanol ratio of 3:7 to 6:4 was not observed for crude oil-1. The N_1 class combined ion intensities for crude oil-3 in Figure 41, blue colour, has the highest intensity at toluene:methanol ratio of 1:9 with 0.1% formic acid. The reduction in N_1 class combined ion intensities when the toluene is increased in the sample solvent is less for crude oil-3 compared to crude oil-1 and 2. Further a slight reduction in N_1 combined ion intensities is observed for crude oil-3 when the toluene content in the sample solvent is increased from toluene:methanol ratio of 3:7 to 6:4 with 0.1% formic acid.

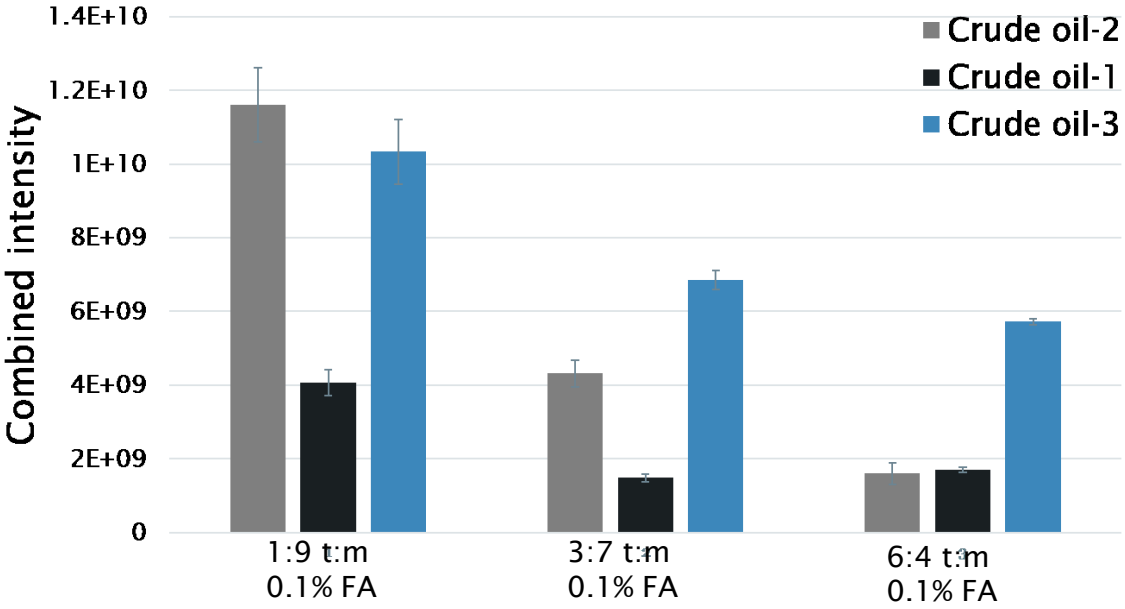

Figure 41 0.1 mg/mL solution of crude oil was analysed using positive ion ESI FT-ICR MS. The N_1 class combined ion intensities at different toluene:methanol (t:m) ratios is shown for crude oil-2, 1 and 3.

Comparing the N_1 combined intensities of crude oil-1, 2 and 3 can be undertaken using Figure 41. Comparing crude oil-1, 2 and 3 N_1 combined ion intensities at toluene:methanol ratio of 1:9 with 0.1% formic acid was first undertaken. The highest N_1 combined ion intensities is for crude oil-2 then followed by crude oil-3 and 1. Thus, at toluene:methanol ratio of 1:9 the crude oil-2 N_1 class combined ion intensities is the most intense compared to the other crude oils. This was most evident in crude oil-1 which has less than half of the N_1 combined ion intensities compared to crude oil-2.

The N_1 combined ion intensities in Figure 41 for crude oil-2 was significantly decreased from toluene:methanol ratio of 1:9 to 3:7 with 0.1% formic acid. However, the decrease in the N_1 class combined ion intensities for crude oil-3 at toluene:methanol ratio of 3:7 from 1:9 was not as significant as the decrease for crude oil-2. This has resulted that at toluene:methanol ratio of 3:7 the combined ion intensities of the N_1 class of crude oil-3 is greater than crude oil-2. However, at toluene:methanol ratio of 1:9 the reverse is true, crude oil-2 N_1 class combined ion intensities is greater than crude oil-3. This is because the effect of toluene increase in the sample solvent on the decrease of the N_1 class combined ion intensities is more significant for crude oil-2 compared to crude oil-3. The data presented in Figure 41 can be argued with two points; the first is that the N_1 class combined ion intensities is decreased with increasing the toluene content in the sample solvent for crude oil-1, 2 and 3; and the second is that the rate of decrease in N_1 combined ion intensity is different for different types of crude oils.

In Figure 41 the comparison for different crude oils at toluene:methanol ratio of 6:4 with 0.1% formic acid was undertaken for 0.1 mg/mL crude oil-1, 2 and 3. The first observation is that the N_1 class combined ion intensities for crude oil-2 is further reduced at toluene:methanol ratio of 6:4 compared to toluene:methanol ratio of 1:9 and 3:7 respectively. However, there is no decrease for the N_1 class combined ion intensities for crude oil-1 when the toluene content is increased from toluene:methanol ratio of 3:7 to 6:4. This has resulted in approximately equal N_1 class combined ion intensities for crude oil-1 and 2 at toluene:methanol ratio of 6:4. However, the comparison between crude oil-1 and 2 at toluene:methanol ratio of 1:9 and 3:7 shows that N_1 class combined ion intensities for crude oil-2 is greater than crude oil-1. Crude oil-3 N_1 class combined ion intensities is decreased at toluene:methanol ratio of 6:4. The rate of decrease in combined ion intensities of N_1 class when the toluene content is increased in the sample solvent for crude oil-3 is significantly less compared to crude oil-2.

The result shows that at toluene:methanol ratio of 6:4 crude oil-3 N_1 combined ion intensities is greater than crude oil-2. This was true as well for toluene:methanol ratio of 3:7. But at toluene:methanol ratio of 1:9 crude oil-2 N_1 combined ion intensities is the most intense compared to crude oil-1 and 3.

In conclusion, crude oil-1, 2 and 3 were analysed using positive ion ESI FT-ICR MS. The focus was on the N_1 class because it is the most abundant class for the crude oils studied in positive ion ESI. Variations in the ionisation at different sample

solvent composition of toluene:methanol ratios were first confirmed by observing the change in the ion intensity of *m/z* 404.332 with elemental formula $[C_{29}H_{41}N + H]^+$ for crude oil-1, 2 and 3. (See Figure 30 and Figure 32 for crude oil-1, Figure 34 and Figure 36 for crude oil-2, Figure 38 and Figure 40 for crude oil-3 in section 4.1.1). The rate of change in ion intensity of *m/z* 404.332 was different across different toluene:methanol ratios even with the addition of the ionisation enhancing additive, 0.1% formic acid. Further, the ion intensity of *m/z* 404.332 was affected by different rates when the toluene content was increased in the sample solvent in different crude oils. The decrease in ion intensity of *m/z* 404.332 was less for crude oil-3 compared to crude oil-1 and 2. Further, not only $[C_{29}H_{41}N + H]^+$ ion intensity was observed but all the ions that are assigned as N_1 class in the mass spectrum were combined and compared for crude oil-1, 2 and 3. The data presented in Figure 41 confirmed the preliminary observation made using *m/z* 404.332. It showed that the solvent composition that should be used for the analysis and comparison of nitrogen containing compounds in different crude oils is at toluene:methanol ratio of 1:9 with 0.1% formic acid.

According to Figure 41 crude oil-2 is the most affected by the variation of sample solvent composition of toluene:methanol. It can be argued that at toluene:methanol ratio of 1:9 with 0.1% formic acid the source of protons are coming from methanol and the addition of formic acid. These protons are needed to protonate a basic site such as the nitrogen containing compounds in crude oil-2 analysed using positive ion ESI. Thus, the N_1 class combined ion intensities is the most abundant at toluene:methanol ratio of 1:9 with 0.1% formic acid. The increase in toluene content from toluene:methanol ratio of 1:9 to 6:4 with 0.1% formic acid resulted in a decrease in the concentration of protons in the sample solvent that are needed for protonation. This has resulted in the decrease of N_1 class combined ion intensities of crude oil-2 at toluene:methanol ratio of 6:4 with 0.1% formic acid. Figure 36 shows that the ion intensity of *m/z* 404.332, $[C_{29}H_{41}N + H]^+$, in crude oil-2 is decreased at toluene:methanol ratio of 6:4 compared to 1:9 with 0.1% formic acid. It showed as well that the addition of 0.1% formic aided the ionisation across different toluene:methanol ratios. According to the previous discussion an increase in the formic acid concentration at toluene:methanol ratio of 6:4 should increase the ion intensity of *m/z* 404.332. Figure 42 shows the analysis of crude oil-2 at toluene:methanol ratio of 6:4 with 0.1%, 0.2% and 0.3% formic acid. The data in Figure 42 shows that there is no increase in the ion intensity of *m/z* 404.332 when the formic acid is increased from 0.1% to 0.2% and 0.3%.

This suggests that the effect of the sample solvent composition on ion intensity in positive ion ESI is regardless of the concentration of formic acid. The decrease in the ionisation response of *m/z* 404.332 is either attributed to the increase of toluene content or the decrease in methanol content in the sample solvent. This further proves that the analysis in positive ion ESI for the crude oils studied should be undertaken at toluene:methanol ratio of 1:9 with 0.1% formic acid. This is because the ionisation response for nitrogen containing compounds, most abundant ions in positive ion ESI, are most intense a toluene:methanol ratio of 1:9 with 0.1% formic acid.

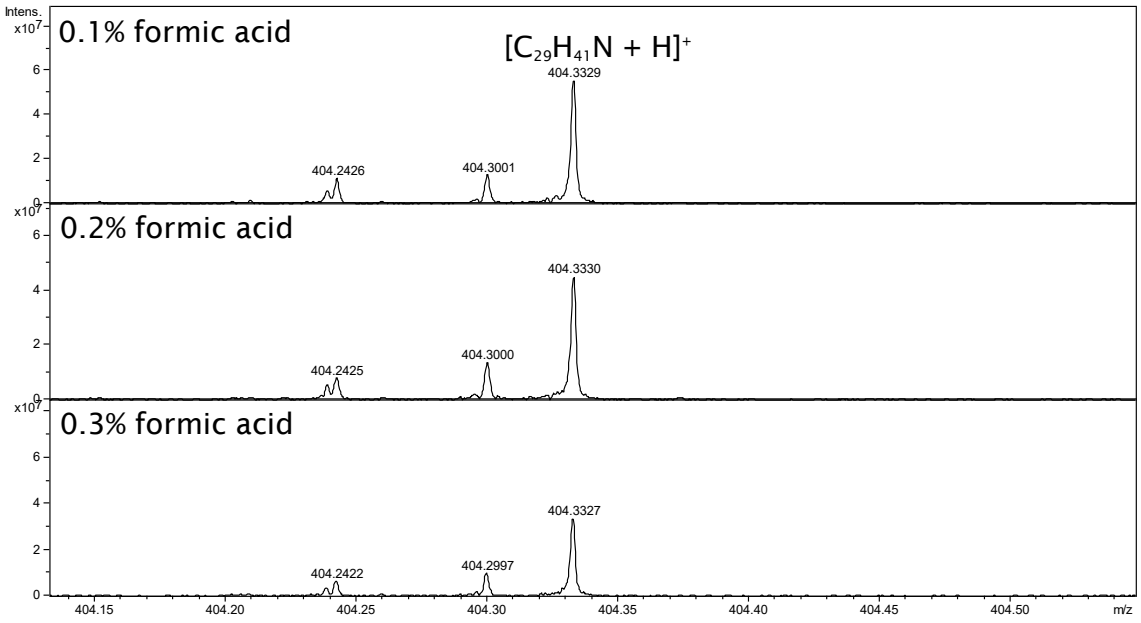

Figure 42 0.3 mg/mL solution of crude oil-2 in toluene:methanol ratio of 6:4 analysed using +ESI FT-ICR MS. *m/z* is expanded. Ion intensity is 6 × 10^7.

4.1.3 Sample concentration and multimer formation

The effect of sample solvent composition, addition of formic acid and sample concentration were previously illustrated in section 4.1.1 for crude oil-2. Multimers observed in N_1 DBE *versus* carbon number plots for crude oil-2 are affected by sample solvent composition, addition of formic acid and concentration of crude oil-2. However, other heterogeneous multimers are formed in the gas phase of the ESI source that are not affected by sample solvent composition of toluene:methanol ratios. 0.1 and 0.3 mg/mL crude oil-2 were analysed using positive ion ESI FT_ICR MS. Figure 43 and Figure 44 show crude oil-2 mass spectra at 0.1 mg/mL and 0.3 mg/mL respectively analysed using toluene:methanol ratios of 1:9, 3:7 and 6:4 with 0.1% formic acid. The mass spectra in Figure 43 and Figure 44 show that there are two *m/z* distributions that are observed. The multimer region is highlighted using red boxes. In Figure 43 and Figure 44 the *m/z* region from *m/z* 150 to approximately *m/z* 480 which is not highlighted represent the monomeric distribution of the crude oil mass spectra at different toluene:methanol ratios. This region is the most affected in the variation of sample solvent composition of toluene:methanol ratios. This is because this region contains predominantly ions that are related to the N_1 class. (This issue was discussed in details in section 4.1.1).

The crude oil mass spectra that are shown in Figure 43 and Figure 44 for crude oil-2 can be processed using PetroOrg for elemental formulae assignments. For example 0.3 mg/mL crude oil-2 mass spectra in Figure 44 at toluene:methanol ratio of 1:9 and 6:4 are processed using PetroOrg and shown in Figure 45. Not all classes of compounds for crude oil-2 are shown in Figure 45. The N_1 class in Figure 45 is shown in blue colour for crude oil-2 at toluene:methanol ratio of 1:9 and 6:4. The N_1 class signal intensity is reduced from approximately 7×10^8 to 1.5×10^8 from toluene:methanol ratio of 1:9 to 6:4 respectively. This further confirms the observation made about crude oil-2 mass spectra in Figure 43 and Figure 44. The multimer region that was identified using red boxes in crude oil-2 Figure 43 and Figure 44 were assigned as multimers containing one nitrogen, oxygen and sulfur in its elemental formula. Figure 45 shows $N_1O_1S_1$ crude oil-2 multimers highlighted in red. Regardless of the used toluene:methanol ratio the signal intensity of $N_1O_1S_1$ multimers in Figure 45 is at approximately 2×10^8 for 0.3 mg/mL crude oil -2.

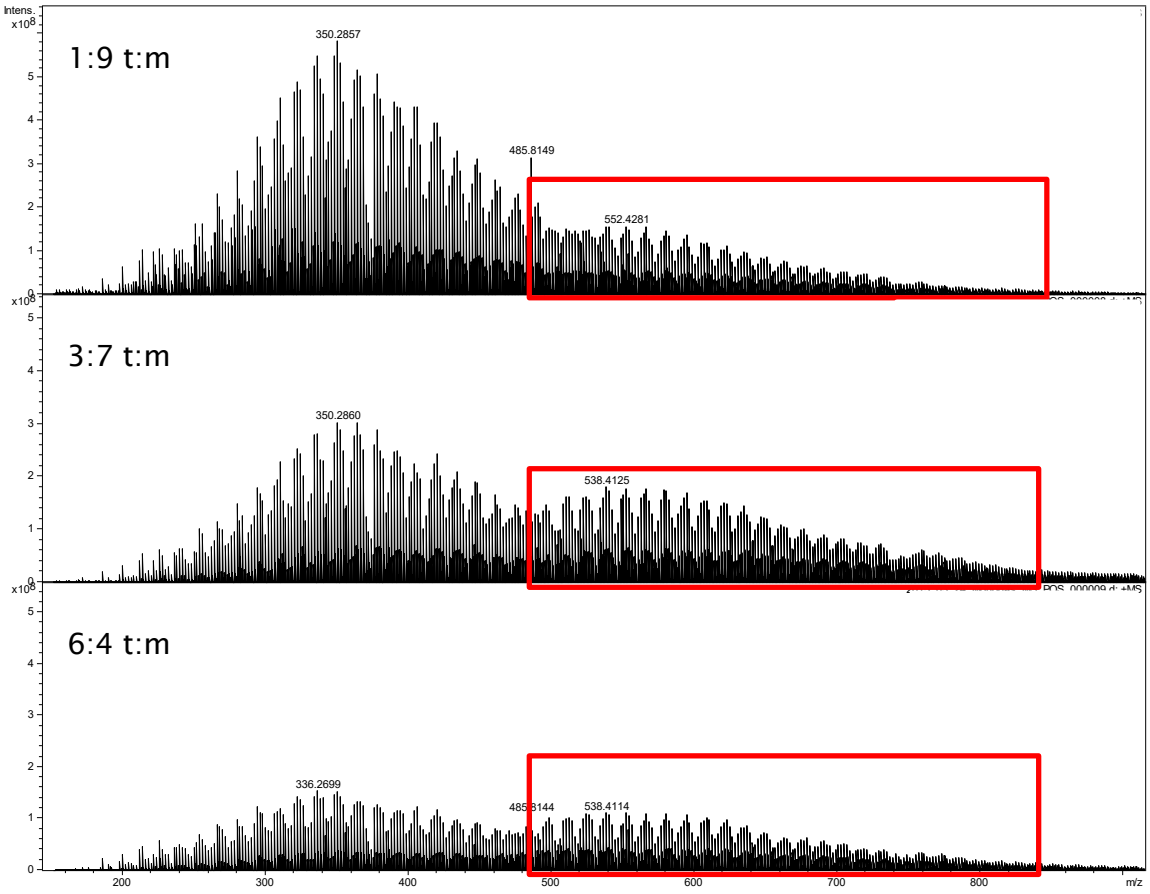

Figure 43 0.1 mg/mL solution of crude oil-2 analysed using positive ion ESI FT-ICR MS with 0.1% formic acid. Intensity scale is at 5×10^8.

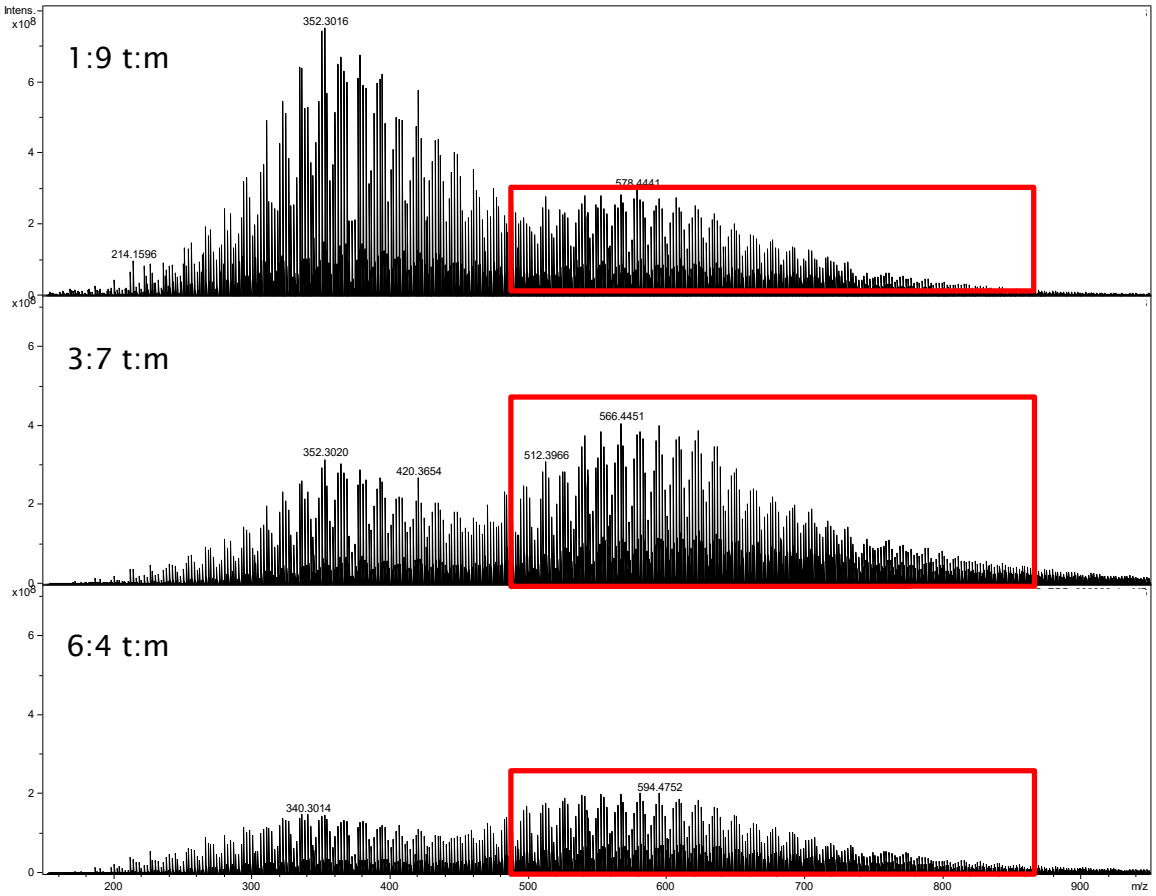

Figure 44 0.3 mg/mL solution of crude oil-2 analysed using positive ion ESI FT-ICR MS with 0.1% formic acid. Intensity scale is at 6×10^8.

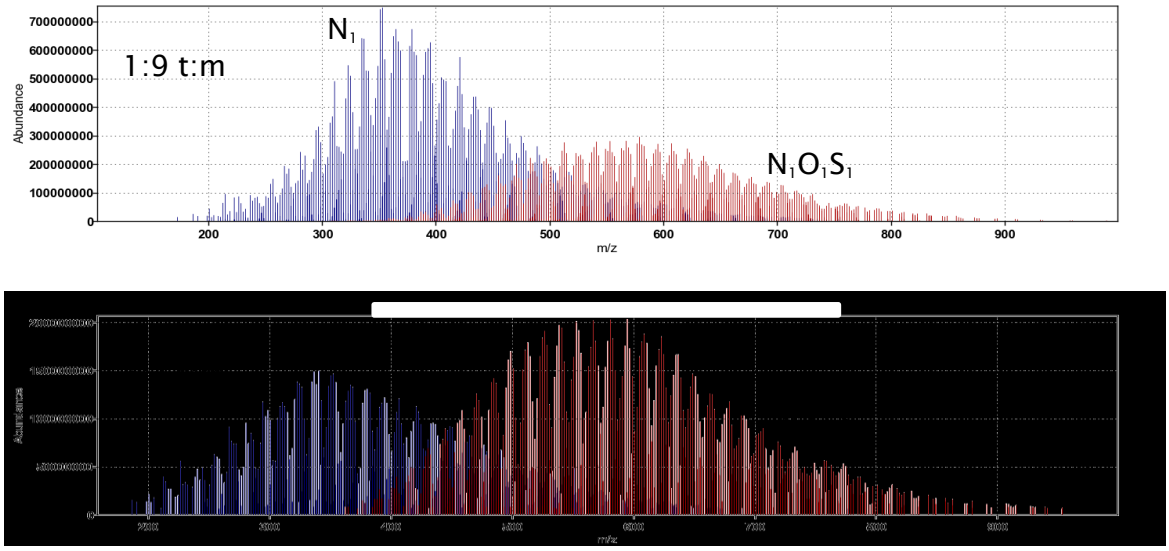

Figure 45 PetroOrg mass spectra for 0.3 mg/mL solution of crude oil-2 dissolved in 6:4 t:m and 1:9 t:m analysed using positive ion ESI FT-ICR MS. 0.1% formic acid was added. PetroOrg assigned N_1 class in blue and $N_1O_1S_1$ class in red.

Multimers are non-covalently bound and their formation is dependent on the sample concentration. Therefore, the introduction of a suitable in-source CID voltage will dissociate multimers back to their monomeric species. Figure 45 showed that the assigned $N_1O_1S_1$ multimers intensities and formations are not dependent on the sample solvent composition or toluene:methanol ratios. Thus, Figure 46 shows only 0.3 mg/mL crude oil-2 mass spectra analysed using toluene:methanol ratio of 6:4 with 0.1% formic acid. The analysis was undertaken at in-source CID 0, 30 and 40 V. In Figure 46 multimers were observed when no in-source was used in the top crude oil-2 mass spectrum. These multimers were previously assigned as $N_1O_1S_1$. An in-source CID at 30 and 40 V in the middle and bottom crude oil-2 mass spectra in Figure 46 were introduced. At in-source CID 30 V the intensity of $N_1O_1S_1$ multimers were reduced *via* dissociation of these non-covalently bound complexes. The dissociation of assigned $N_1O_1S_1$ multimers was even further observed at higher in-source CID, 40 V. Another observation in Figure 46 is that the use of in-source CID has resulted in a gain in signal intensity of crude oil-2 mass spectra for the non multimer region, predominantly N_1 containing compounds. In Figure 46 when no in-source CID is used the intensity is at approximately 1.5×10^8. The intensity has increased to 3×10^8 and 5×10^8 for in-source CID 30 and 40 V respectively. $N_1O_1S_1$ multimers are heterogeneous and can be resulted from the aggregation of N_1S_1 class with O_1 class or O_1S_1 class with N_1 class.

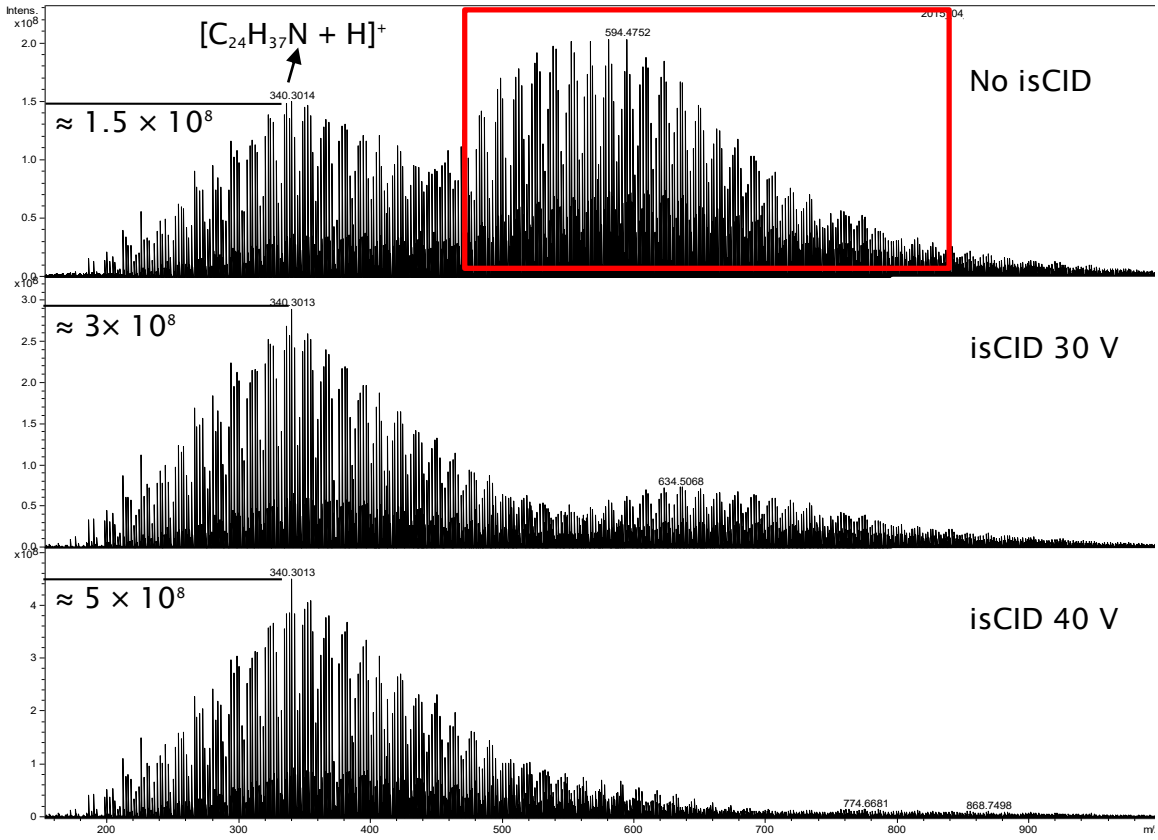

Figure 46 0.3 mg/mL solution of crude oil-2 in toluene:methanol ratio of 6:4 was analysed using positive ion ESI FT-ICR MS. 0.1% formic acid was added. In-source CID at 30 V and 40 V.

In Figure 43 and Figure 44 multimers were observed for crude oil-2 at 0.1 and 0.3 mg/mL respectively. These multimers were assigned as $N_1O_1S_1$ and dissociated using in-source CID in Figure 46. The use of in-source CID has proved that these are non-covalently bound molecules. However, the assignment of these multimers as $N_1O_1S_1$ needs further checking using the crude oil-2 mass spectrum. Therefore, the use of isCID is needed because of the formation of multimers. Further, it is critical that inter laboratory comparisons are undertaken with identical solvent compositions and with source conditions that break up any possible multimers.

Figure 47 shows an expanded *m/z* region for 0.3 mg/mL crude oil-2 mass spectra. The top mass spectrum in Figure 47 shows the analysis without the use of in-source CID. *m/z* 496.3609 in top mass spectrum of Figure 47 has two possible elemental formulae assignments, $[C_{32}H_{49}NOS + H]^+$ with 0.8 ppm error or $[C_{35}H_{45}NO + H]^+$ with 5.9 ppm error. The difference in theoretical *m/z* between $[C_{32}H_{49}NOS + H]^+$ and $[C_{35}H_{45}NO + H]^+$ is 3.4 m*m/z* units which corresponds to a common isobar found in crude oil. Thus, at high *m/z* if the two ions are present there will be insufficient resolution to resolve them. The assignment of crude oil-

2 multimers can be either $N_1O_1S_1$ or N_1O_1 containing compounds. (See Figure 47 top and middle mass spectrum)

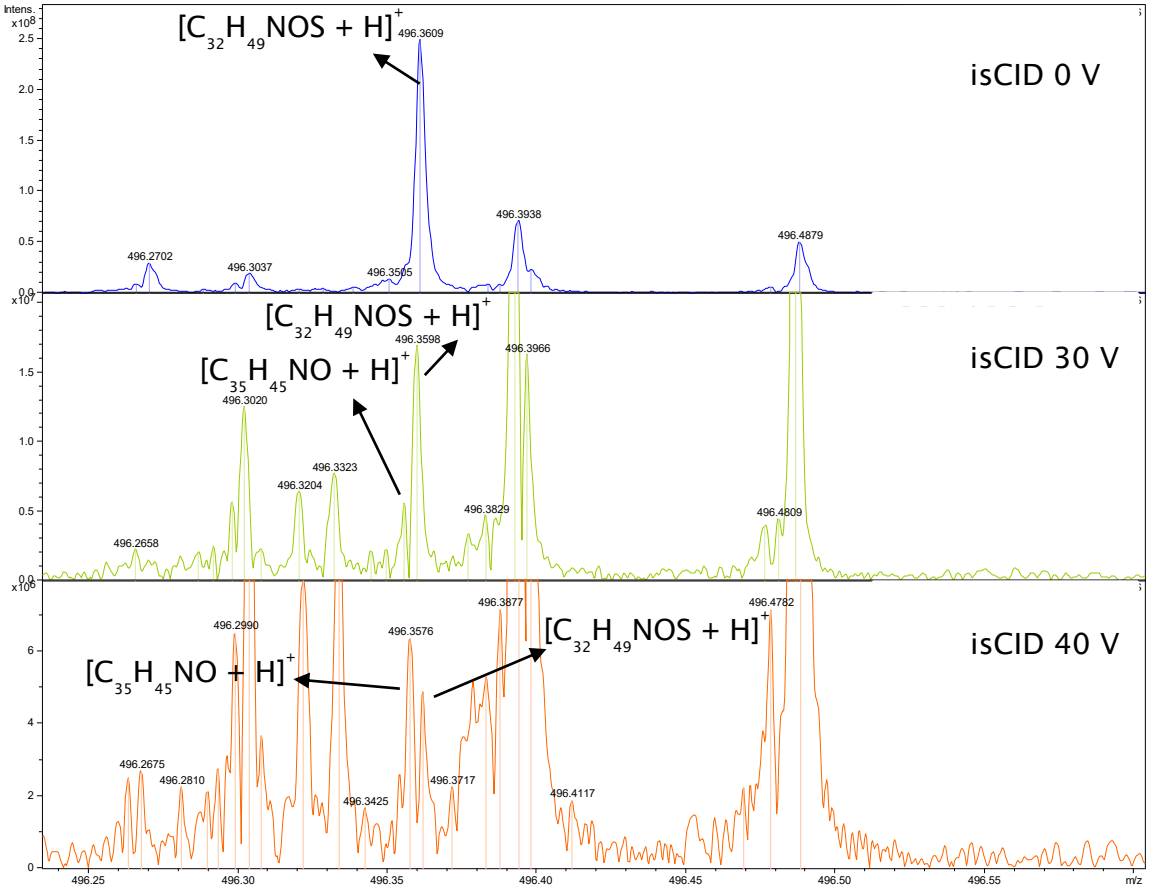

Figure 47 0.3 mg/mL solution of crude oil-2 was analysed using positive ion ESI FT-ICR MS at toluene:metanol ratio of 6:4 with 0.1% formic acid. The mass spectrum is expanded at *m/z* 496. In-source CID were used at 30 V and 40 V.

The analysis in the middle mass spectrum in Figure 47 was undertaken using in-source CID at 30 V. The reduction in ion intensity from approximately 2.5×10^8 for *m/z* 496.36 in top mass spectrum in Figure 47 to 1.5×10^8 in the middle mass spectrum is observed at in-source CID 30 V. This observed reduction in ion intensity further proves that *m/z* 496.3609 in the top mass spectrum in Figure 47 is a multimer. The use of in-source CID in the middle mass spectrum in Figure 47 has resulted in the decrease in the ion intensity of the multimer identified in the top mass spectrum at *m/z* 496.3609. This reduction in ion intensity has revealed two peaks in the middle mass spectrum, $[C_{32}H_{49}NOS + H]^+$ and $[C_{35}H_{45}NO + H]^+$, that were not resolved in the top mass spectrum. Thus, the multimer at *m/z* 496.3609 in the top mass spectrum in Figure 47 could be assigned as $[C_{32}H_{49}NOS + H]^+$ or $[C_{35}H_{45}NO + H]^+$. The analysis in the bottom mass spectrum of Figure 47 is undertaken using in-source CID at 40 V.

The multimer ion intensity of $[C_{32}H_{49}NOS + H]^+$ is further reduced from the middle mass spectrum at in-source CID 30 V in Figure 47 to the bottom mass spectrum at in-source CID 40 V. This suggests that the multimer elemental formula assignment of *m/z* 496.3609 as $[C_{32}H_{49}NOS + H]^+$ and not as $[C_{35}H_{45}NO + H]^+$ in Figure 47 top mass spectrum is correct. Figure 48 is similar to Figure 47 but the expanded *m/z* region for crude oil-2 is at *m/z* 426 instead of *m/z* 496.

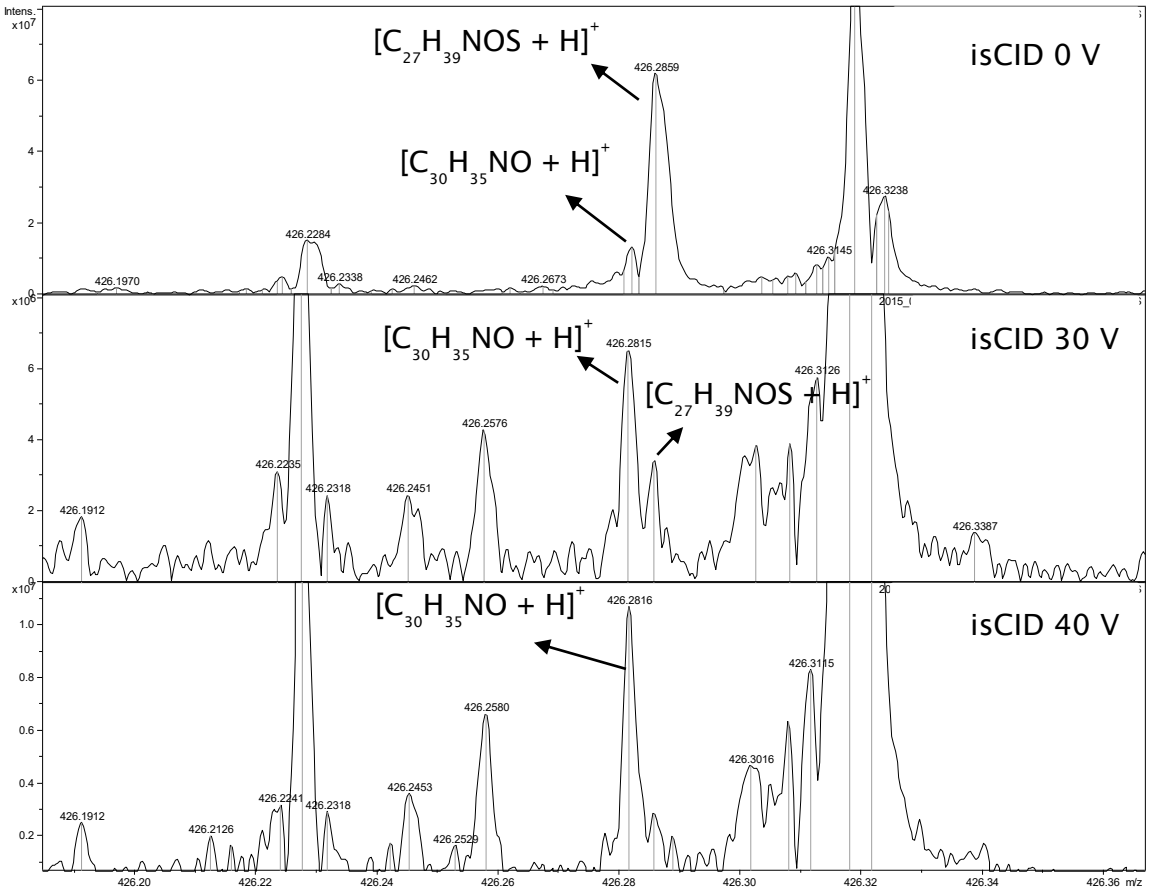

Figure 48 0.3 mg/mL solution of crude oil-2 was analysed using positive ion ESI FT-ICR MS at toluene:metanol ratio of 6:4 with 0.1% formic acid. The mass spectrum is expanded at *m/z* 426. In-source CID were used at 30 V and 40 V.

The difference between ions in the expanded *m/z* 496 in Figure 47 and *m/z* 426 in Figure 48 is in the degree of alkylation, $(-CH_2)_5$. Figure 48 top mass spectrum shows that $[C_{27}H_{39}NOS + H]^+$ and $[C_{30}H_{35}NO + H]^+$ are resolved. However, ions that are related to the same class and DBE but different degree of alkylation, $[C_{32}H_{49}NOS + H]^+$ and $[C_{35}H_{45}NO + H]^+$, in Figure 47 top mass spectrum were not resolved. N_1O_1 and $N_1O_1S_1$ ions were resolved in Figure 48 top mass spectrum which have the same class and DBE value as N_1O_1 and $N_1O_1S_1$ in Figure 47. This is because the resolving power of FT-ICR MS is more at *m/z* 426 in Figure 48

compared to *m/z* 496 in Figure 47. Further, the ion intensity of the $N_1O_1S_1$ multimer is reduced at *m/z* 426.2859 to approximately 6×10^7 in Figure 48 top mass spectrum compared to the $N_1O_1S_1$ multimer at *m/z* 496.3609 with intensity at 2.5×10^8 in Figure 47 top mass spectrum. The discussion of Figure 47 and Figure 48 suggest that multimers assignment for crude oil-2 as $N_1O_1S_1$ that were made using PetroOrg in Figure 45 is correct. This extends to multimers identified at 0.1 and 0.3 mg/mL crude oil-2 mass spectra at different toluene:methanol ratios in Figure 43 and Figure 44 respectively.

Regardless of the use of in-source CID in Figure 48 at expanded *m/z* 426 $N_1O_1S_1$ multimer and N_1O_1 class ions were resolved. However, at higher *m/z* 496 the N_1O_1 class was not resolved from the $N_1O_1S_1$ multimer in the top no in-source CID mass spectrum in Figure 47. The use of in-source CID in Figure 47 middle and bottom mass spectra reduced the $N_1O_1S_1$ multimer intensity and therefore N_1O_1 was resolved. Building on this the DBE *versus* carbon number plots for N_1O_1 class or $N_1O_1S_1$ multimers should have gaps in the assignments when no in-source CID is used.

Figure 49 shows DBE *versus* carbon number plots for crude oil-2 N_1O_1 and $N_1O_1S_1$ at in-source CID 0 and 40 V. Gaps, highlighted using black circles, in the assignment of $N_1O_1S_1$ multimer and N_1O_1 class are observed in their DBE *versus* carbon number plots when no in-source CID is used. This is in accordance with the discussion of Figure 47 top mass spectrum when no in-source CID is used. It showed that at *m/z* 496 the N_1O_1 class is not resolved from the $N_1O_1S_1$ multimer. However, N_1O_1 was resolved from $N_1O_1S_1$ when in-source CID is used in Figure 47 middle and bottom crude oil-2 mass spectra. This is reflected in Figure 49 DBE *versus* carbon number plots of N_1O_1 and $N_1O_1S_1$ with in-source CID at 40 V. The use of in-source CID at 40 V dissociated the $N_1O_1S_1$ multimers and revealed the $N_1O_1S_1$ class DBE *versus* carbon number distribution. This distribution is different from the $N_1O_1S_1$ plot when no in-source CID is used. Further, no gaps were observed in the assignment of the N_1O_1 class DBE *versus* carbon number plot with in-source CID at 40 V.

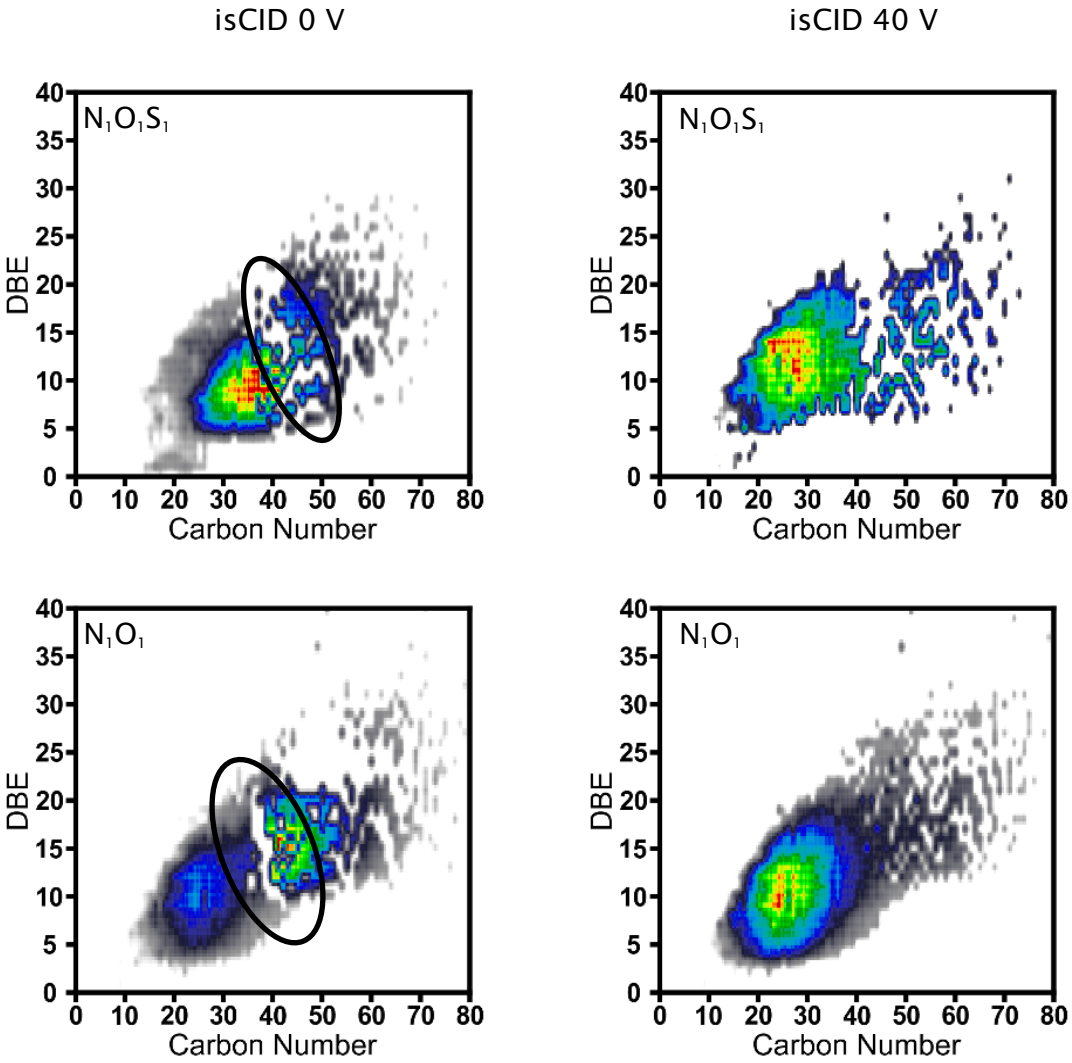

Figure 49 DBE *versus* carbon number plots are shown for N_1O_1 and $N_1O_1S_1$ at isCID 0 and 40 V. 0.1 mg/mL crude oil-2 was analysed using positive ion ESI FT-ICR MS at toluene:methanol ratio of 1:9 with 0.1% formic acid.

$N_1O_1S_1$ multimers were observed for crude oil-2 at 0.1 and 0.3 mg/mL in Figure 43 and Figure 44 respectively. In Figure 43 and Figure 44 crude oil-2 mass spectra the $N_1O_1S_1$ multimer region was highlighted using red box. Figure 43 and Figure 44 showed that the variation in the sample solvent composition of toluene:methanol ratios did not affect the $N_1O_1S_1$ multimer formation. This was the opposite for multimer observed in the N_1 DBE *versus* carbon number plots for crude oil-2 at 0.1 mg and 0.3 mg/mL in Figure 33 and Figure 35 respectively. The addition of formic acid and the analysis undertaken at toluene:methanol ratio of 1:9 resulted in dissociation of multimer observed in N_1 DBE *versus* carbon number plots for crude oil-2. The formation of $N_1O_1S_1$ multimers are not dependent on the sample solvent composition and these multimers were dissociated using in-source CID at 40 V.

The crude oil-2 $N_1O_1S_1$ multimers in Figure 43 and Figure 44 mass spectra suggest that their formation depends solely on the concentration of crude oil-2. Thus, reducing the concentration of crude oil-2 below the concentration required for $N_1O_1S_1$ multimer formation can be used as an alternate method to the use of in-source CID for multimer dissociation. Figure 50 shows crude oil-2 mass spectrum analysed using positive ion ESI FT-ICR MS at 0.05 mg/mL. The $N_1O_1S_1$ multimers that were observed in Figure 43 and Figure 44 crude oil-2 mass spectra at 0.1 and 0.3 mg/mL respectively were not observed at 0.05 mg/mL crude oil-2 mass spectrum in Figure 50. This is because at 0.05 mg/mL of crude oil-2 the concentration is not enough to form non-covalently bound complexes. However, the use of less concentrated crude oil sample has the disadvantage of reducing the ion intensities of the monomeric ions in crude oil-2 mass spectrum. This can be compensated through averaging more spectra to increase the signal-to-noise ratio but at the expense of increasing the analysis time.

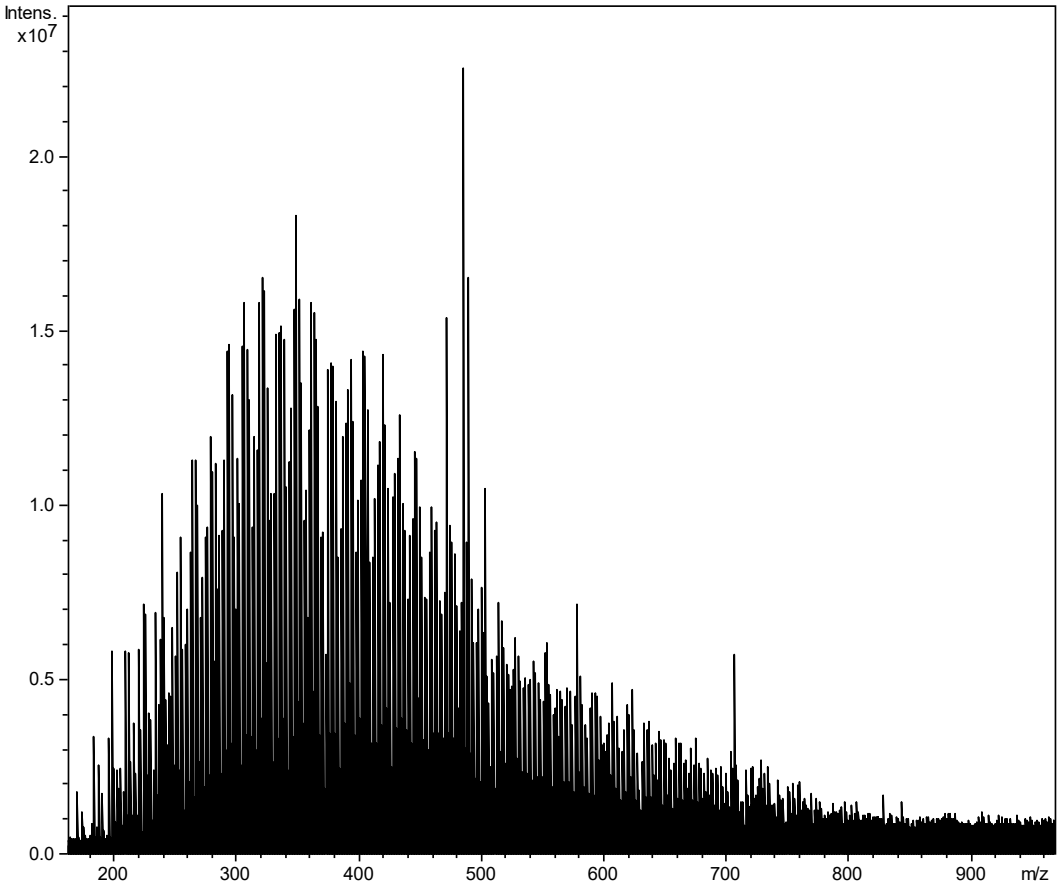

Figure 50 0.05 mg/mL solution of crude oil-2 analysed using positive ion ESI FT-ICR MS in toluene:methanol ratio of 6:4 t:m with 0.1% FA.

4.2 Characterisation of HC and S_1 class in crude oil-1, 2 and 3 using positive ion APPI FT-ICR MS

Polycyclic aromatic compounds (PACs) contain two or more benzenoid rings and various functional groups. Polycyclic aromatic hydrocarbons (PAHs) [56], also known as polynuclear aromatic hydrocarbons or poly-aromatic hydrocarbons are subsets of PACs. However, the difference is that PAHs contain two or fused benzenoid rings but with no other elements than carbon and hydrogen.[143] Thus, PACs are considered as a broader group of compounds that include heterocyclic compounds in which one or more of the carbon atoms in the PAH ring system is replaced by nitrogen, oxygen or sulfur atoms.

Polycyclic aromatic hydrocarbons can be found in a variety of different environmental samples such as coal, soil, water, and petrochemicals. PAHs are found in crude oil in significant amounts, with some exceeding 2000 μg per kg.

The introduction of PAHs into the environment can be through incomplete combustion such as forest fires and pyrolysis of fossil fuels.[144] PAHs are formed through the production of free radicals by pyrolysis at 500-800 °C of fuel hydrocarbons in the reducing zone of flame with insufficient supply of oxygen.

PAHs can be formed as well by Diels-Alder reactions of alkenes to form cyclic alkenes. Dehydrogenation of these cyclic alkenes leads to the formation of stable aromatic compounds, leading to the formation of PAHs.[145]

PAHs are considered to be neutral stable molecules. Their lipohilicity is high as indicated by their high water-octanol partition coefficients (K_{ow}). Hence solubility of PAHs in water decreases with increasing molecular weight. In geological environments PAHs exhibit prolonged half-lives. As mentioned earlier, most PAHs originate from high temperature anthropogenic process and human activities. Thus, these PAHs can be found in higher concentration in young shallow sediments of lakes.[146] However, the PAH perylene is an exception where it has been found in both marine and fresh water sediments. Perylene concentration in surface sediment is low whereas its concentration in sediment tends to increase with depth.[147] Perylene can be used as a geochemical indicator as it resists degradation and alteration. Perylene has been used as an indicator to reliably identify the maturity of crude oil reserve by measuring the ratio of perylene to its methylated derivatives.[148]

PAHs are classified as persistent organic pollutants (POPs). The level of persistence is increased with increasing ring number.[143] These compounds are of great concern to the environmental protection agency (EPA) due to their carcinogenic and mutagenic properties. There are currently 16 PAHs, which are monitored by the EPA in the environment. (See Figure 51). PAHs have been analysed using different analytical methods including high performance liquid chromatography (HPLC)[149,150], supercritical fluid chromatography (SFC)[151], gas chromatography (GC)[152] and HPLC hyphenated to dopant-assisted atmospheric-pressure photoionisation mass spectrometry.[153]

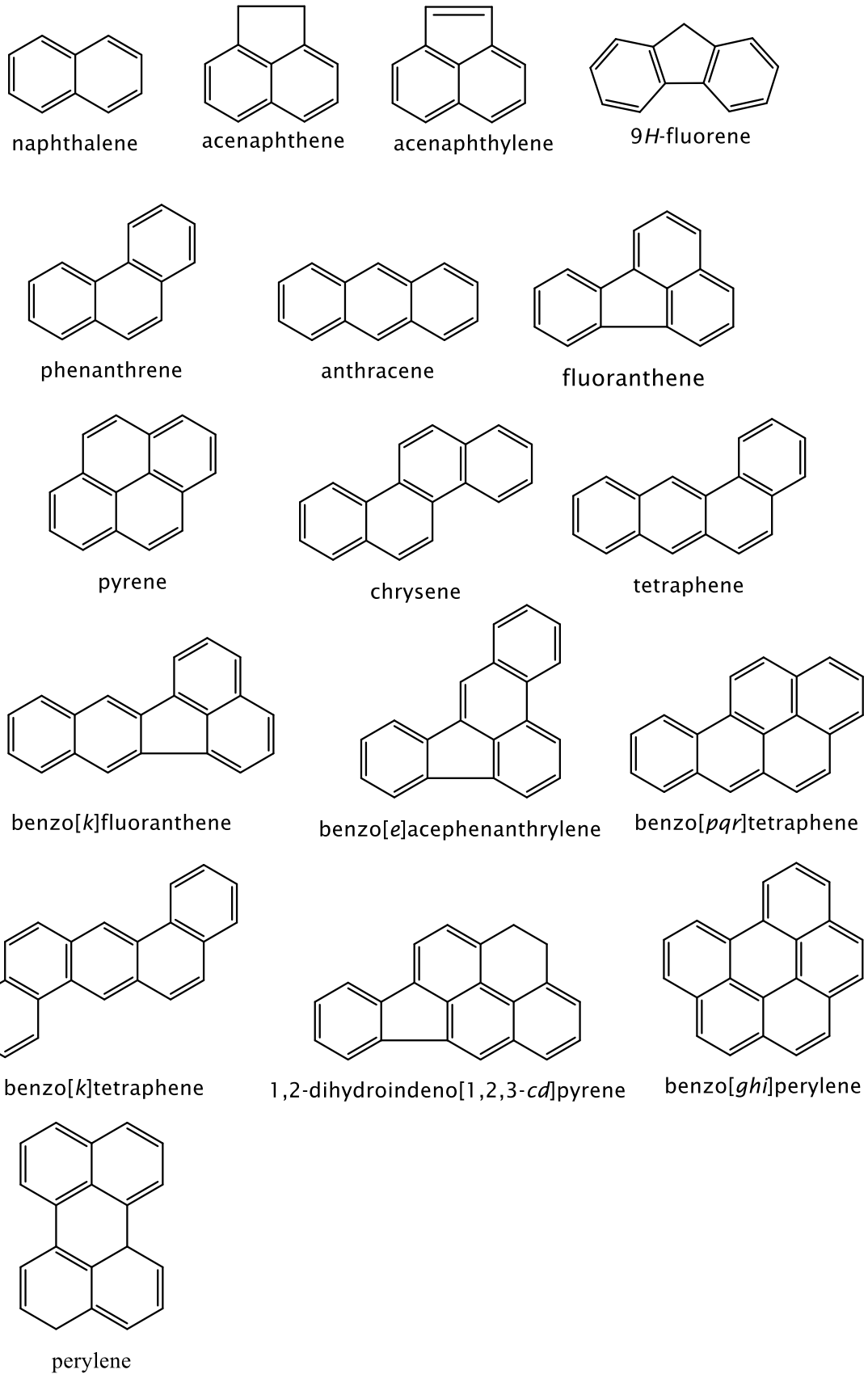

Figure 51 Molecular structures for 16 PAHs, monitored by EPA.[154]

In this study the analysis of crude oils is undertaken using positive ion APPI FT-ICR MS. If the analysis was undertaken using field desorption ionisation it can

take few minutes. This is because the current applied to the FD emitter is slowly increased to volatise and ionise molecules according to their boiling point. A mass spectrum using APPI can be acquired in couple of seconds. Therefore, signal averaging of hundreds of scans can be undertaken. In the positive ion APPI FT-ICR MS analysis of crude oil-1 ,2 and 3 the signal of 200 scans were averaged. High mass resolving power mass spectrometer is essential in the analysis of crude oil mass spectrum acquired using positive ion APPI. This is because the crude oil mass spectrum contains approximately five times the number of ions compared to the compounds ionised by positive ion ESI crude oil mass spectrum. Further, in positive ion APPI radical cations $M^{+\cdot}$ and protonated molecules $[M + H]^+$ are observed in the crude oil mass spectrum for the same molecule. This complicates the mass spectrum and the need also to resolve $^{13}C\ M^{+\cdot}$ from $^{12}C\ [M + H]^+$, differing by m*m/z* 4.5 units. (See Figure 52).

Commonly found nominal isobars in petroleum analysis are illustrated in Table 20. The need for high resolution is even more when the analysis is undertaken using APPI as the ionisation source. For example, $C_4/^{13}CH_3S$ has a difference of 1.1 m*m/z* units.

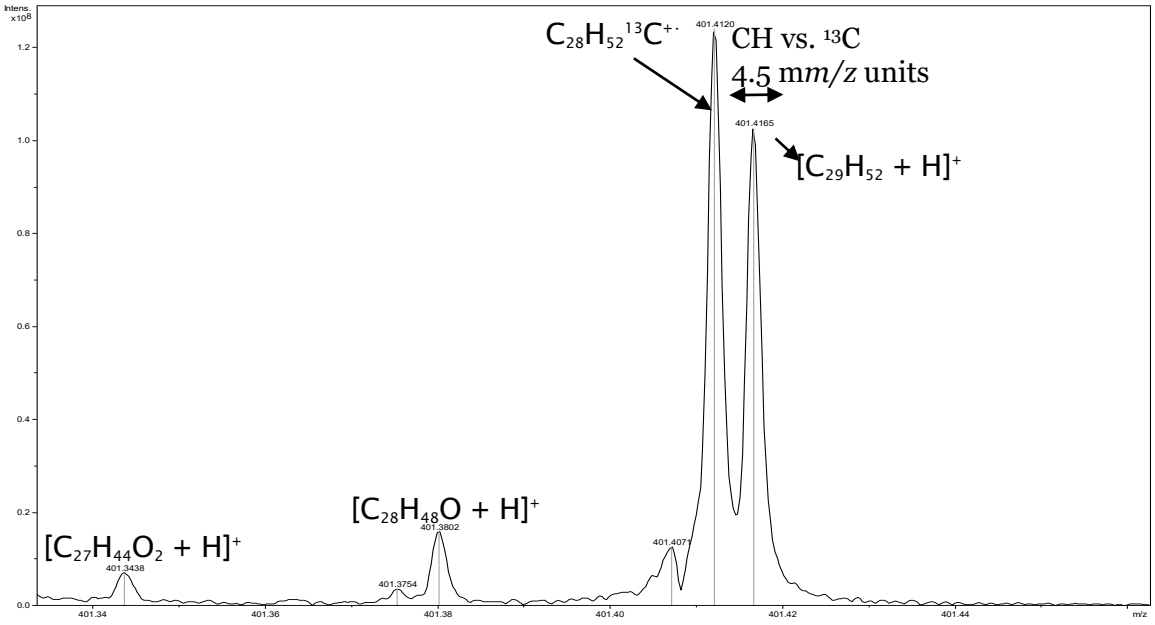

Figure 52 Positive ion APPI FT-ICR MS of 0. 5 mg/mL solution of crude oil-3 dissolved in 100% toluene. Expanded *m/z* from 401.32 to 401.45.

Table 20 Isobars observed when positive ion APPI is used for crude oil analysis.

Isobars	Mass difference in m*m/z* units	Minimum RP at *m/z* 400
C_4 &$^{13}CH_3S$	1.1	364,000*
$C_2H^{34}S$ & $NS^{13}C$	2.8	143,000
H_4S & C_3	3.4	118,000
$^{13}C_2$ & CN	3.6	112,000*
C_2N & $^{34}SH_4$	3.9	103,000*
CH & ^{13}C	4.5	89,000*
H_3NS & $C_3{}^{13}C$	4.7	86,000
^{13}CH & N	8.1	50,000
C_2H_2 & $^{13}C_2$	8.9	45,000
N_2 & CO	11.2	36,000
CH_2 & N	12.6	32,000*
O_2 & S	17.8	23,000

*Isobars due to the presence of odd- and even-electron ions species.

Figure 53 shows crude oil-1, 2 and 3 mass spectra acquired using positive ion APPI FT-ICR MS. The most abundant class observed in the crude oil-1,2 and 3 mass spectra are radical cations of the HC-R class at even *m/z* values. The most abundant odd *m/z* values in crude oil-1, 2 and 3 mass spectra correspond to the ^{13}C of the HC-R class.

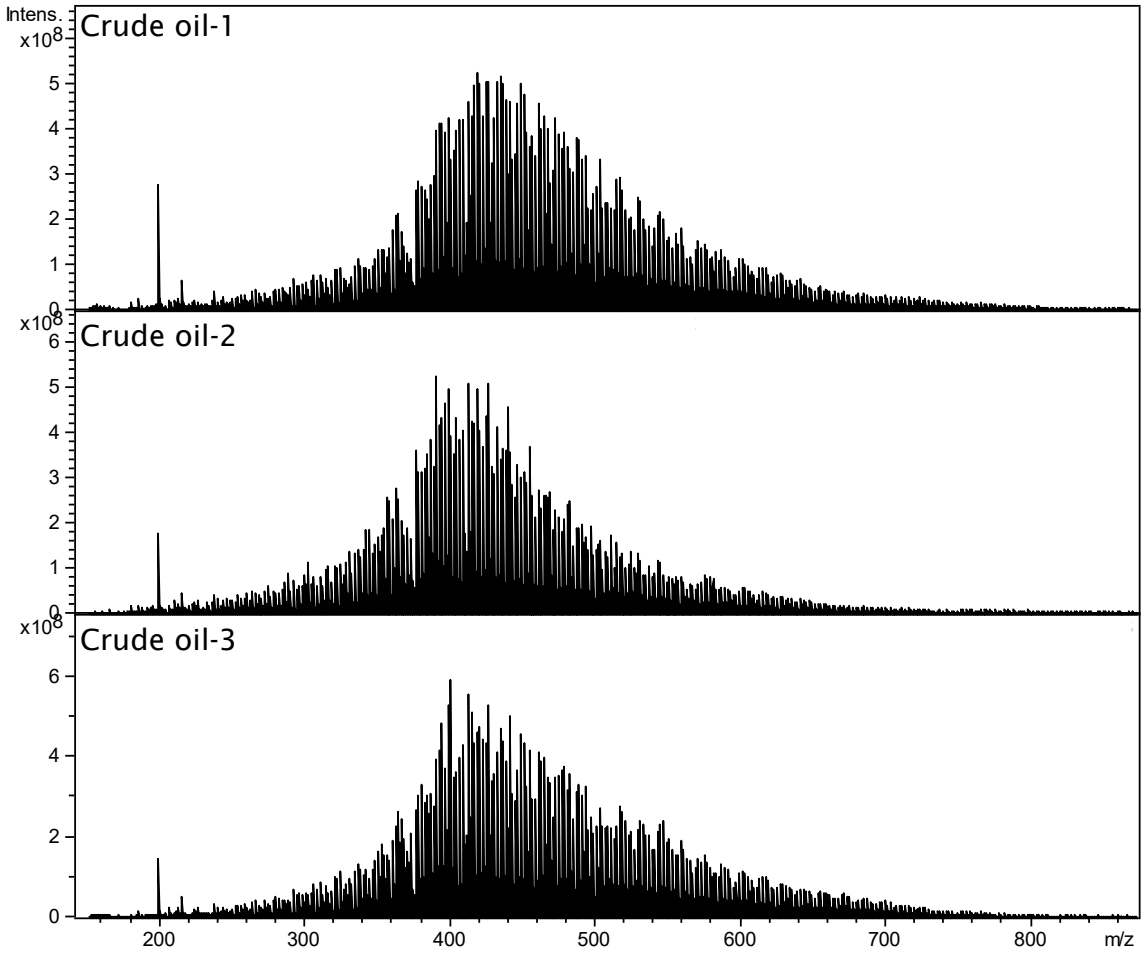

Figure 53 Positive ion APPI FT-ICR MS of 0.5 mg/mL solutions of crude oils in toluene.

There were no significant differences in the observed signal intensities for crude oil-1, 2 and 3 mass spectra for hydrocarbon containing compounds, HC-R and HC. This observation is extended to the HC-R and HC DBE *versus* carbon number plots for crude oil-1, 2 and 3. (See Figure 54). The DBE distribution for crude oil-1, 2 and 3 start from DBE 1 to approximately DBE 27. The protonated molecules for the HC plots for crude oil-1, 2 and 3 show similar ion intensities distribution within the HC class. However, the radical cations of HC-R class show slight differences in ions intensities distribution for crude oil-1, 2 and 3 in their DBE *versus* carbon number plots, regarding the most intense ions. (See Figure 54)

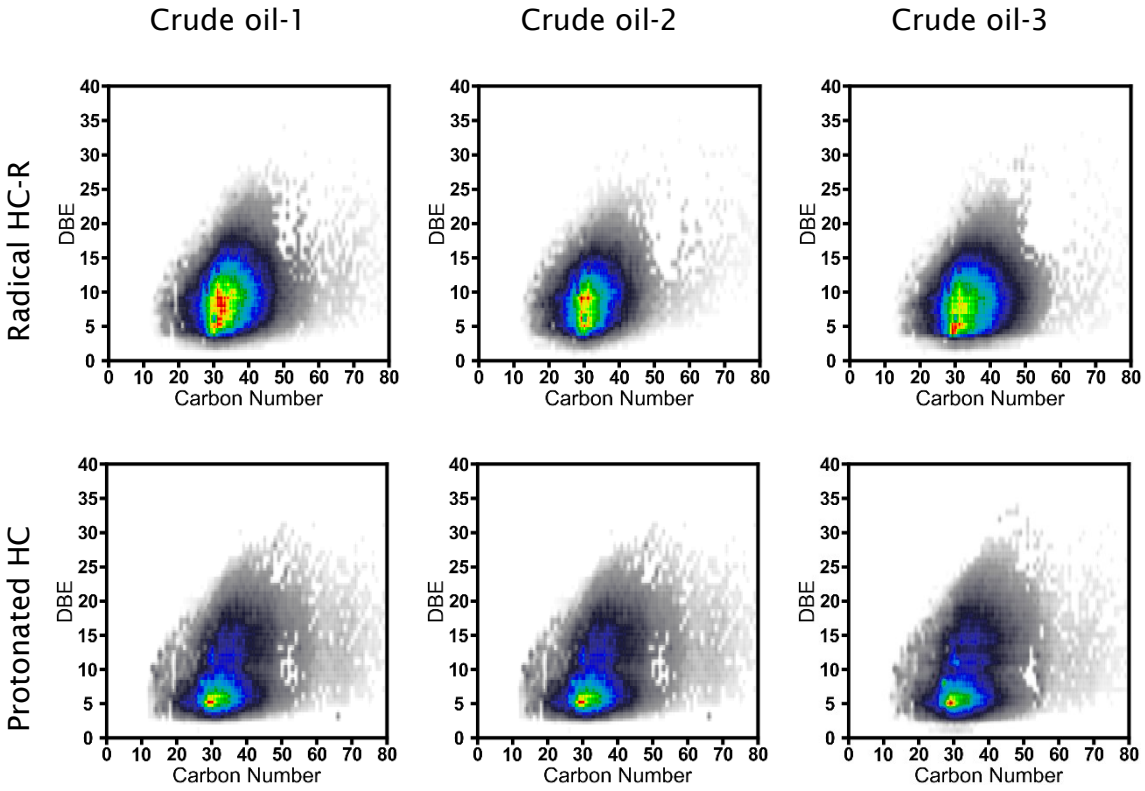

Figure 54 HC-R and HC DBE *versus* carbon number plots for crude oil-1, 2 and 3 are shown. The analysis was undertaken using positive ion APPI FT-ICR MS.

The second most abundant class observed in crude oil-1, 2 and 3 mass spectra in Figure 53 are ions containing one sulfur in their structures. S_1-R radical cations and S_1 protonated molecules DBE *versus* carbon number plots are shown in Figure 55 for crude oil-1, 2 and 3. Sulfur in crude oil is probably present in a thiophene containing compounds with a DBE value of 3 for a thiophene ring. Crude oil-1 and 2 show similar ions intensities distribution in their S_1 and S_1-R DBE *versus* carbon number plots. However, crude oil-3 S_1 class plot shows different DBE *versus* carbon number distribution compared to S_1 of crude oil-1 and 2. The intensity distribution is higher at lower DBE values for S_1 of crude oil-3. Further, this is probably related to the type of crude oil-3, classified as a sour crude oil.

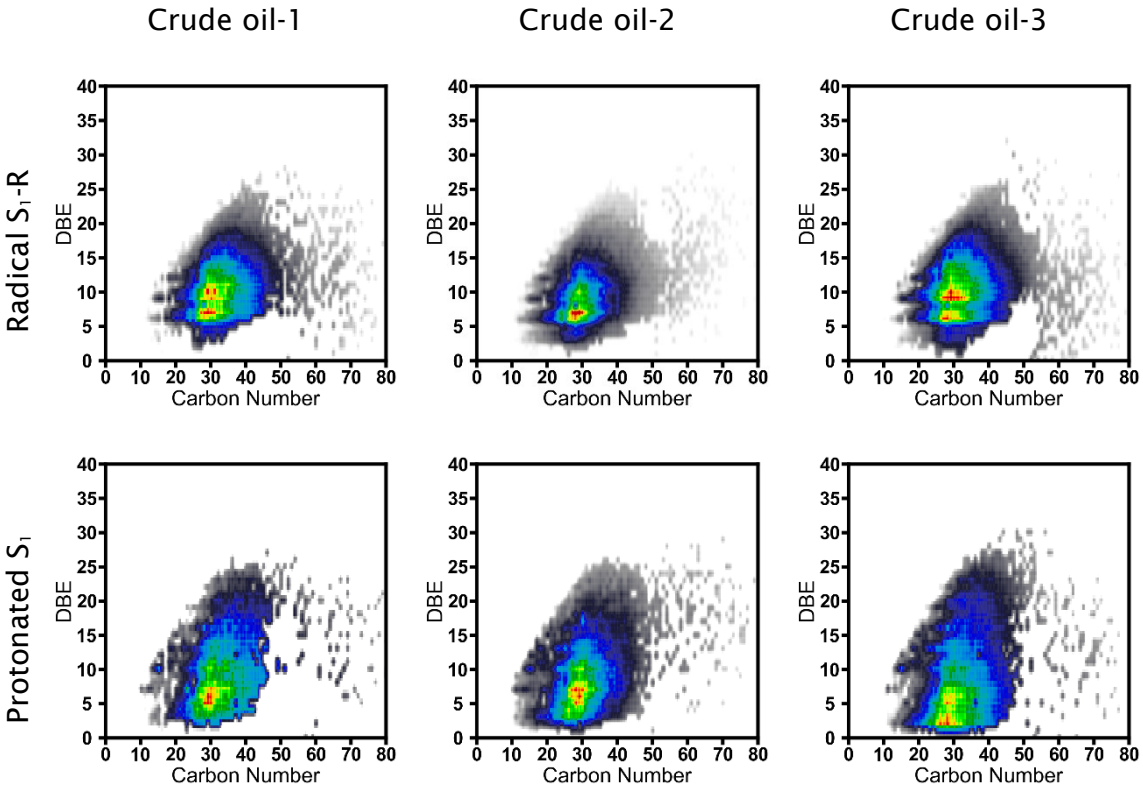

Figure 55 S_1-R and S_1 DBE *versus* carbon number plots for crude oil-1, 2 and 3 are shown. The analysis was undertaken using positive ion APPI FT-ICR MS.

Hydrocarbon containing compounds and sulfur containing compounds are ionised using atmospheric pressure photoionisation through direct photon ionisation[155] or proton transfer[58,63]. Further compounds ionisable using APPI include polar molecules. However, thiophene and hydrocarbon containing compounds are not efficiently ionised using ESI. One possible method to ionise sulfur using ESI is through derivatisation process. The process involves the conversion of sulfur containing compounds in crude oil to sulfonium salts in solution prior to ESI. The derivatisation is undertaken using a strong alkylating reagent.[54,156] However, the use of derivatisation step has only enabled the ionisation of sulfur containing compounds but not hydrocarbon species in crude oil. Another method for ionising sulfur containing compounds using ESI are through spraying a $PdCl_2$ solution with diluted crude oil solution.[157]. The sulfur containing compounds are observed in the positive ion ESI mass spectrum as molecular ions. The complexation process of sulfur heterocycles with Pd^{+2} depends on many parameters such as sample flow rate and sample to Pd^{+2} ratio.

Other complexing reagents have been reported in the literature to improve the ionisation efficiency for sulfur containing compounds in crude oil by ESI. Complexation using silver was found to be the best.[158,159] Silver complexation with

ESI as the ionisation source was applied to the analysis of alkenes, arenes and polystyrenes.[160,161] Recently, silver trifluoromethanesulfonate has been used as complexing reagent for the analysis of heavy crude oils using positive ion ESI FT-ICR MS.[162] The cationisation process involves the reaction of silver cation Ag^+ with π or σ electrons that can be shared. Thus, aromatics of the HC class can be ionised through the complexation with Ag^+. Further nucleophilic atoms such as sulfur can donate its lone pairs of electrons to form complexes with the silver cation. This process is not as time consuming as using a strong alkylating reagent for derivatisation.

In positive ion ESI the use of toluene:methanol ratio of 1:9 with 0.1% formic acid for crude oil analysis showed a significant increase in ions intensities of nitrogen containing compounds and reduced multimer formation compared with toluene:methanol ratios of 3:7 and 6:4 with 0.1% formic acid. Further, sulfur and hydrocarbon containing compounds were observed in positive ion ESI FT-ICR MS crude oil mass spectrum using toluene:methanol ratio of 1:9 with 0.1% formic acid. These compounds are not usually observed using ESI. One possible explanation that the ionisation efficiencies of S_1 and HC compounds are increased at toluene:methanol ratio of 1:9, in similar way to N_1. Thus, the intensity of these ions are above the noise level in the mass spectrum and their elemental formulae can be assigned. Whereas at toluene:methanol ratios of 3:7 and 6:4 the ions intensities of S_1 and HC compounds are at the noise level in their positive ion ESI mass spectrum. Figure 56 shows expanded nominal *m/z* 303 for crude oil-3 mass spectra. The analysis was undertaken in positive ion ESI FT-ICR MS using toluene:methanol ratios of 1:9, 3:7 and 6:4 with 0.1% formic acid. Two protonated molecules are observed in crude oil-3 mass spectrum analysed using toluene:methanol ratio of 1:9 with 0.1% formic acid, $[C_{23}H_{26} + H]^+$ and $[C_{20}H_{30}S + H]^+$. However, these protonated molecules are not observed in Figure 56 crude oil-3 mass spectra that were analysed using toluene:methanol ratios of 3:7 and 6:4 with 0.1% formic acid. Further, the ion intensity of *m/z* 303.214 is significantly reduced from toluene:methanol ratios of 1:9 to 3:7 with 0.1% formic acid. Actually, at toluene:methanol ratio of 3:7 with 0.1% formic acid *m/z* 303.214 is just above the noise level. This information is revealed by comparing the two mass spectra, at toluene:methanol ratios of 1:9 and 3:7 with 0.1% formic acid. (See Figure 56). This information will be missed If the mass spectrum was only inspected at toluene:methanol ratio of 3:7 without comparing it to the mass spectrum at toluene:methanol ratio of 1:9.

This is because *m/z* 303.214 signal will be probably interpreted as part of the noise level of crude oil-3 mass spectrum, acquired at toluene:methanol ratio of 3:7. This observation may support the earlier suggestion that S_1 class, represented in this case by *m/z* 303.214, is ionised at toluene:methanol ratio of 3:7 and 6:4 but with at very low ionisation efficiency. However at toluene:methanol ratio of 1:9 the ionisation efficiency is significantly increased for S_1, observed for *m/z* 303.214 in Figure 56. These observation made regarding S_1 with *m/z* value of 303.214 might be applicable to the HC containing compounds such as $[C_{23}H_{26} + H]^+$ at *m/z* 303.211 in Figure 56.

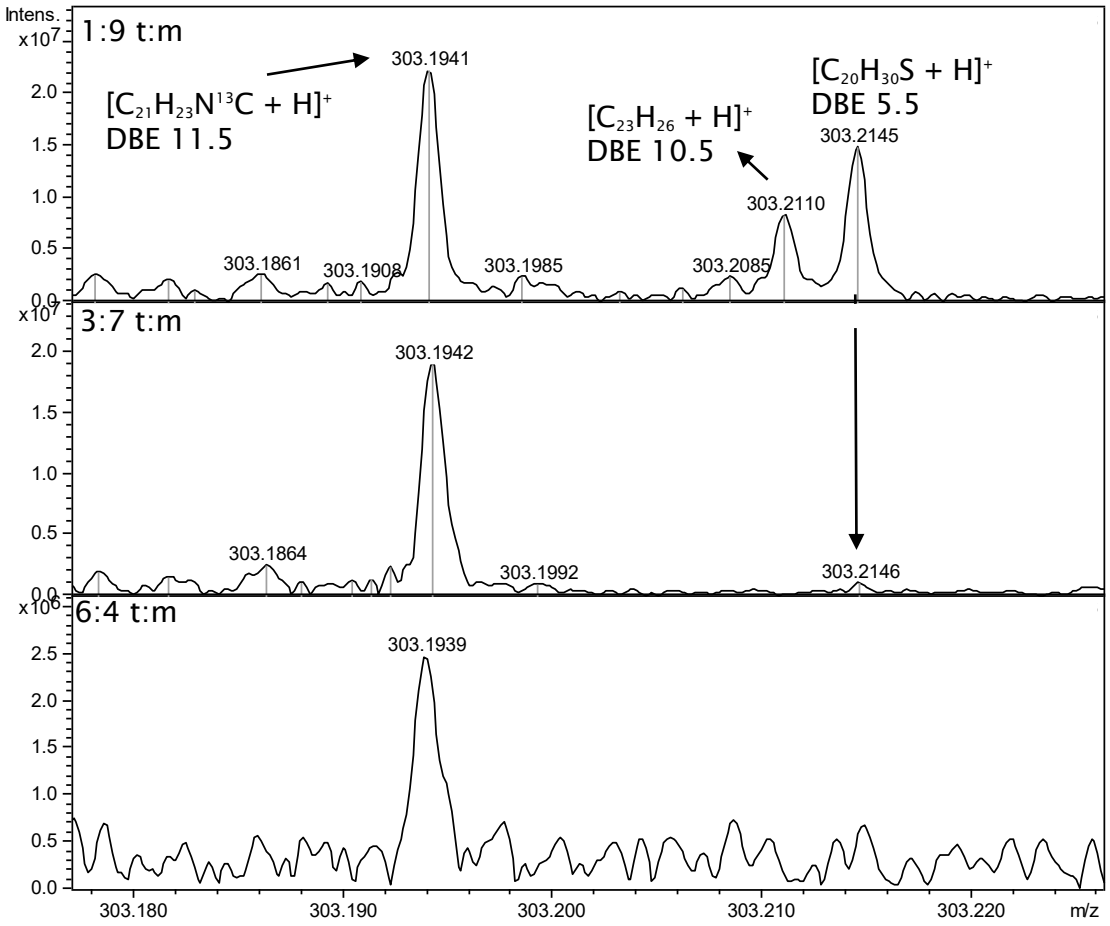

Figure 56 0.1 mg/mL solution of crude oil-3 was analysed using positive ion ESI FT-ICR MS using different toluene:methanol ratios with 0.1% formic acid. *m/z* of crude oil-3 mass spectra are expanded at 303.

Figure 57 shows HC and S_1 DBE *versus* carbon number plots for crude oil-3. Only the most intense ions that were observed in the positive ion APPI HC class plot were observed in the positive ion ESI HC plot. The same was observed for the S_1 DBE *versus* carbon number plot where only the most ions are observed in the positive ion ESI plot. This might be that average spectra at 300 is not enough to detect all the ions of S_1 and HC class in positive ion ESI. Or S_1 and HC molecules with higher carbon numbers and DBE values are either not ionisable or not soluble in toluene:methanol ratio of 1:9.

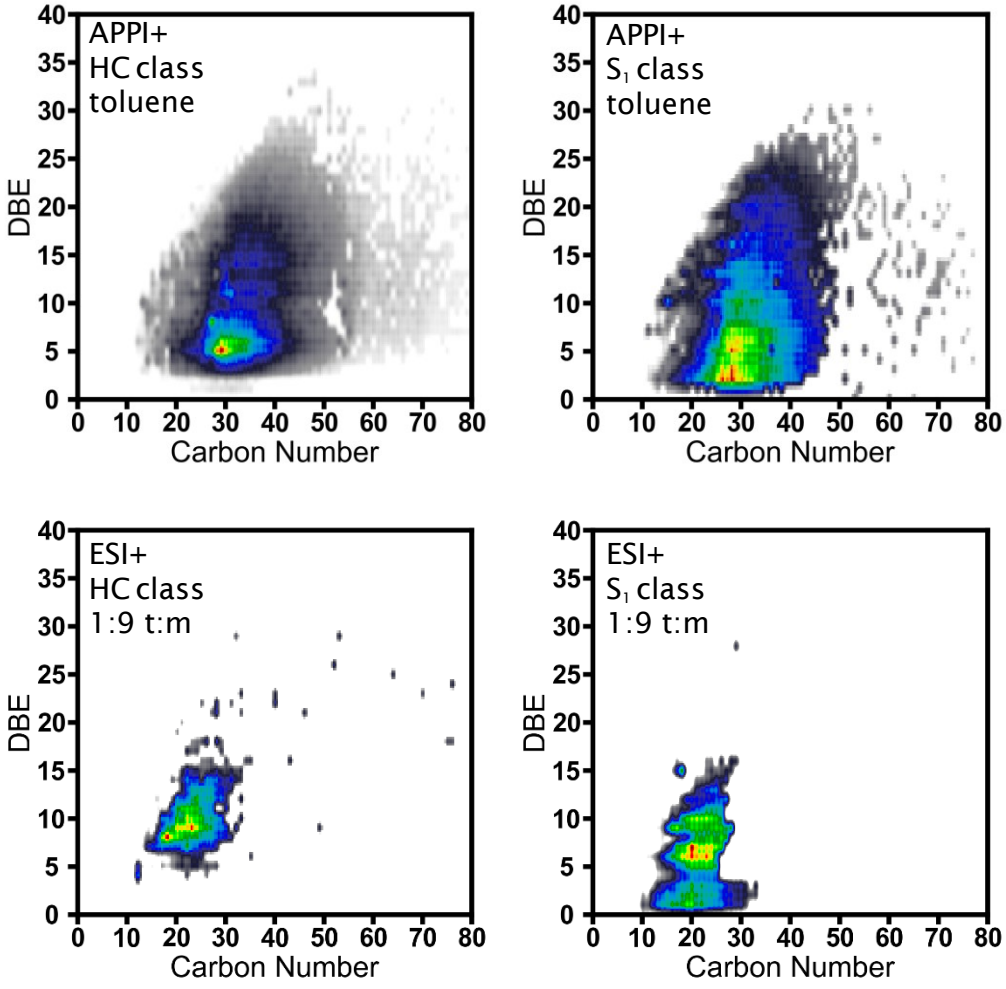

Figure 57 Crude oil-3 HC and S_1 DBE *versus* carbon number plots. The data were acquired using positive ion APPI and ESI FT-ICR MS.

4.3 Characterisation of crude oils using negative ion ESI and APPI

Most crude oils contain a small amount of polar molecules that cause variety of production problems.[87] Crude oil acids can cause liquid-phase corrosion at elevated temperature between 220 and 400 ºC.[163] However, crude oil acids such as naphthenic acids (NAs) can provide useful geochemical information about the crude oil source rock and the degree of maturation of the crude oil.[164,165] Further, high amount of acids in crude oil might indicate biodegradation.[166-168]

The presence of NAs in crude oil is of concern to the crude oil refining industry because of NAs induced corrosion in the refinery. NAs are defined as molecules containing carboxylic acid functional group attached to the sidechain of a saturated ring. The general formula for naphthenic acids (NAs) is $C_nH_{2n+z}O_2$ where n is the number of carbon atoms and Z is a negative even integer representing the hydrogen deficiency number.[122,169,170] A further oxidation of NAs might be referred to as oxy-naphthenic acids (ONAs) with the general formula of $C_nH_{2n+z}O_x$. However, the term NAs might be used to refer to oxy-naphthenic acids (ONAs) and even to other heteroatom containing molecules that are extractable in the acid fraction of crude oil. In this work, classic naphthenic acids with the formula $C_nH_{2n+z}O_2$ are referred to as NAs. (See Figure 58)

Crude oil acidity is measured using the total acid number (TAN) method, *i.e.* the milligrams of potassium hydroxide required to neutralise one gram of crude oil. However, measurement of TAN cannot be reliably used as an indicator of NAs induced corrosion. This is because crude oils with high TAN have shown similar corrosiveness compared to crude oils with low TAN.[41] However, generally crude oil with a TAN of more than 0.5 shows a high level of corrosion. Thus, a better method of analysis is required to understand the relationship between corrosion and naphthenic acids content in crude oils.

Canada has an unconventional source of crude oil, the Athabasca oil sand. It is composed of water, sand, clay and bitumen. It is estimated that there are 174 billion barrels of extractable bitumen.[171] The bitumen is extracted from the oil sands using the Clark hot water extraction method. However, the extraction process of bitumen is heavily dependent on the use of water, approximately three barrels of water are required for each barrel of bitumen produced. The oil sands process water (OSPW) is recycled before discharging into the tailing ponds. These ponds are estimated to cover more than 170 km^2 in northern Alberta.[172] The main

component of OSPW is naphthenic acids at approximately 100 mg/mL which are toxic to the aquatic environment and can enter ground and river waters.[15,173,174] The characterisation of naphthenic acids in OSPW and crude oils are required because of corrosion and toxicity. This is because the current production rate of bitumen from oil sands is at approximately 1.4 million barrels per day. The problem of OSPW is further aggravated as the production of bitumen is expected to be at 5-6 million barrels per day by year 2030.

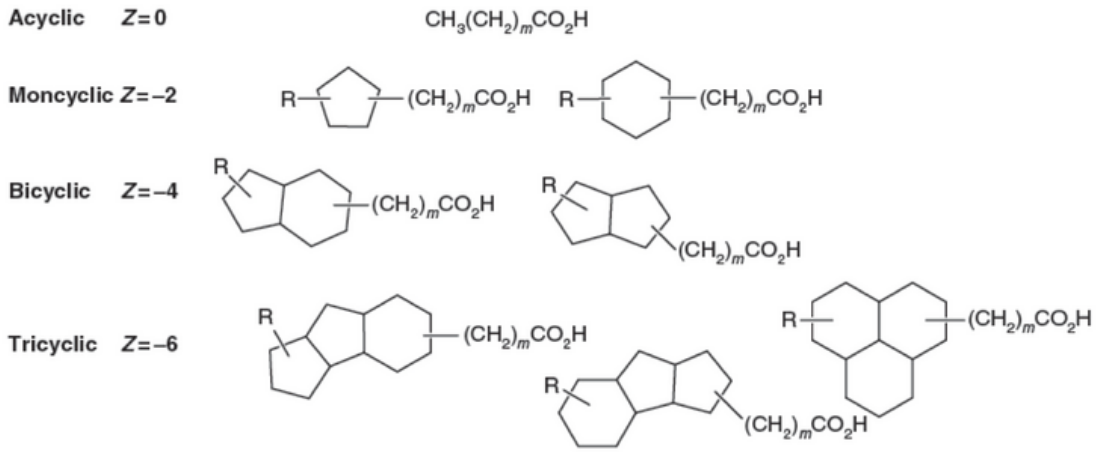

Figure 58 Naphthenic acids (NAs) are complex mixtures of monocarboxylic acids containing one or more alkyl-substituted alicyclic rings (naphthenes). Modification of Figure 1 from Water Research, 2001, 35, pp. 2595-2606.

The advent of electrospray ionisation (ESI) was an important development in the field of crude oil analysis as it was possible to ionise the most polar species in crude oil, Zhan and Fenn.[52] Negative ion electrospray ionisation can ionise the most acidic species in the crude of which pyrrolic nitrogen and naphthenic acids constitute a large part.[115] Other ionisation techniques coupled to mass spectrometry have been used to characterise organic acids such as fast atom bombardment (FAB)[175], chemical ionisation[176], atmospheric pressure negative ion chemical ionisation (APCI)[176] and negative ion atmospheric pressure photoionisation (APPI).[138] Further, crude oils organic acids have been characterised by variety of analytical techniques such as GC×GC[177], GC-MS[178,179], FT-IR spectroscopy[180] and ^{13}C NMR spectroscopy[181].

4.3.1 Comparison between crude oils N_1, HC and S_1 classes analysed using negative ion APPI Orbitrap MS

In negative ion atmospheric pressure photoionisation ions can be formed through electron capture, charge exchange, proton transfer or substitution reaction.[62] Compounds that have gas phase acidity such as naphthenic acids form mostly deprotonated molecules $[M - H]^-$ through proton transfer. Negative molecular ions $M^{-\cdot}$ can be formed for compounds with positive electron affinity through electron capture or charge exchange.[182] Figure 59 shows crude oil-1, 2 and 3 mass spectra acquired by negative ion APPI MS using a Q Exactive™ Plus Orbitrap MS .

The most intense ions identified in the mass spectra of crude oil-1 and 3 in Figure 59 are homologues series, labelled using * symbol, of deprotonated hydrocarbons with DBE value of 9.5. The labelled homologous series starts at *m/z* 179.0860 with elemental formula of $[C_{14}H_{12} - H]^-$. Then subsequent identified ion peaks in the mass spectra of crude oil-1 and 3 are further addition of CH_2. (See Table 21). The deprotonated hydrocarbons homologous series are identified as well in crude oil-2 mass spectrum and labelled using * symbol. However, this homologous series are not the most intense ions in the crude oil-2 mass spectrum. The most intense ions are related to different DBEs of the N_1 class, probably pyrrolic compounds. The first labelled N_1 class ion in crude oil-2 mass spectrum using # symbol is *m/z* 222.1287 with elemental formula of $[C_{16}H_{17}N - H]^-$ with DBE value of 9.5. The subsequent ions, labelled using # symbol, in crude oil-2 mass spectrum are *m/z* 236.1445 and *m/z* 250.1603 with elemental formulae of $[C_{17}H_{19}N - H]^-$ and $[C_{18}H_{21}N - H]^-$ respectively. The other identified N_1 class homologous series in crude oil-2 mass spectrum is labelled using the · symbol with DBE value of 12.5. The first labelled ion using · symbol in crude oil-2 mass spectrum is at *m/z* 244.1133 with elemental formula $[C_{18}H_{15}N - H]$- and DBE value of 12.5. Then, the following three ions in crude oil-2 mass spectrum labelled using · symbol are *m/z* 258.1292, *m/z* 272.1450 and *m/z* 286.1606 with elemental formulae of $[C_{19}H_{17}N - H]$-, $[C_{20}H_{19}N - H]$- and $[C_{21}H_{21}N - H]$- respectively. It should be noted that the two identified N_1 class homologous series using # and · symbols are the most intense ions in crude oil-2 mass spectrum at DBE value of 9.5 and 12.5 respectively. The difference between DBE 12.5 and 9.5 is 3 which suggests an addition of an aromatic ring to the suggested N_1 pyrrolic structure.

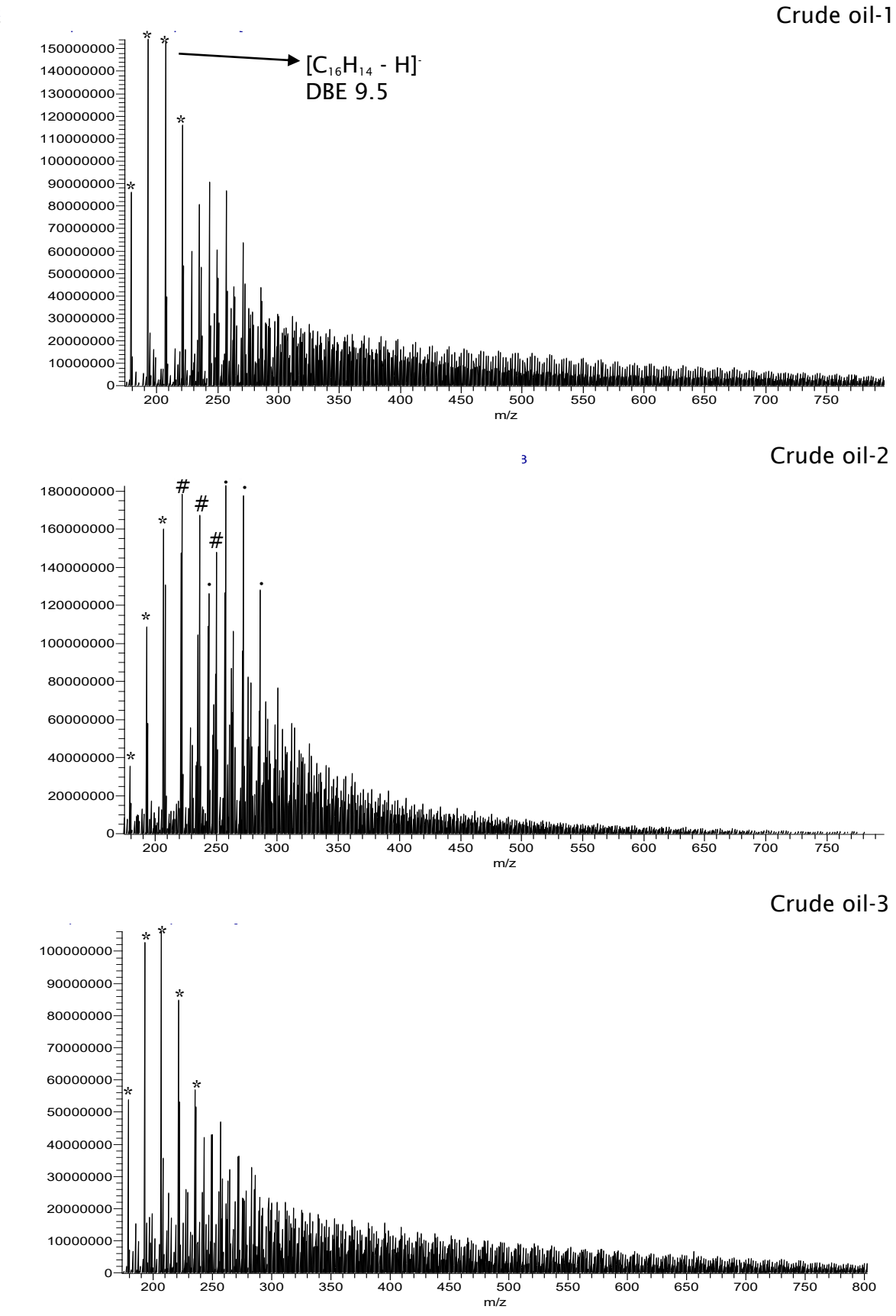

Figure 59 Crude oil 1, 2 and 3 mass spectra acquired using negative ion APPI Orbitrap MS. See Table 21 for labelling of peaks using *, #, and · symbols.

Table 21 Lists the first *m/z* values identified in crude oil mass spectra of Figure 59. The subsequent labelled *m/z* values in the mass spectra are addition of CH_2.

m/z	Labelled	Elemental formula	Class	DBE
179.0860	*	$[C_{14}H_{12} - H]^-$	HC	9.5
222.1287	#	$[C_{16}H_{17}N - H]^-$	N_1	9.5
244.1133	·	$[C_{18}H_{15}N - H]$-	N_1	12.5

Figure 60 shows DBE *versus* carbon number plots for HC class for crude oil-1, 2 and 3. Crude oil-1 and 2 show similar distribution of DBE and carbon number. The DBE distribution for crude oil-1 and 3 start from approximately DBE 9 to 33. However, crude oil-2 has a lower starting DBE values compared to crude oil-1 and 3, from DBE 6. These compounds that represent different DBEs and degree of alkylation are highlighted in Figure 60 for crude oil-2 using a black circle.

Figure 61 shows an expanded *m/z* at 197 for crude oil-1, 2 and 3 mass spectra acquired using negative ion APPI Orbitrap MS. The deprotonated hydrocarbon $[C_{15}H_{18} - H]^-$ with DBE value of 7.5 at *m/z* 197.133 is shown. The shown mass spectra in Figure 61 for crude oil-1, 2 and 3 further confirm the conclusion of Figure 60 HC DBE *versus* carbon number plots. Figure 61 shows that the relative abundance of $[C_{15}H_{18} - H]^-$ with DBE value of 7.5 in crude oil-2 mass spectrum is significantly greater compared to $[C_{15}H_{18} - H]^-$ in crude oil-1 and 3 mass spectra. This conclusion extends to DBE values that were highlighted in crude oil-2 HC DBE *versus* carbon number plots in Figure 61, from DBE 6 to 8. It should be noted that when mass spectra are shown the DBE value is referenced to the ion. However, in DBE *versus* carbon number plots the DBE value is shown for the neutral molecule. In Figure 61 crude oil 1, 2 and 3 mass spectra other deprotonated molecules than $[C_{15}H_{18} - H]^-$ are observed. *m/z* 197.154 with $[C_{12}H_{22}O_2 - H]$- and DBE value of 2.5 is observed in crude oil-1, 2 and 3 mass spectra. This ion is related to the O_2 class and is only observed as deprotonated molecule. The negative ion APPI Orbitrap MS data for the O_2 class is with accordance with the negative ion ESI Orbitrap MS data and it will be discussed later in this section (4.3.1).

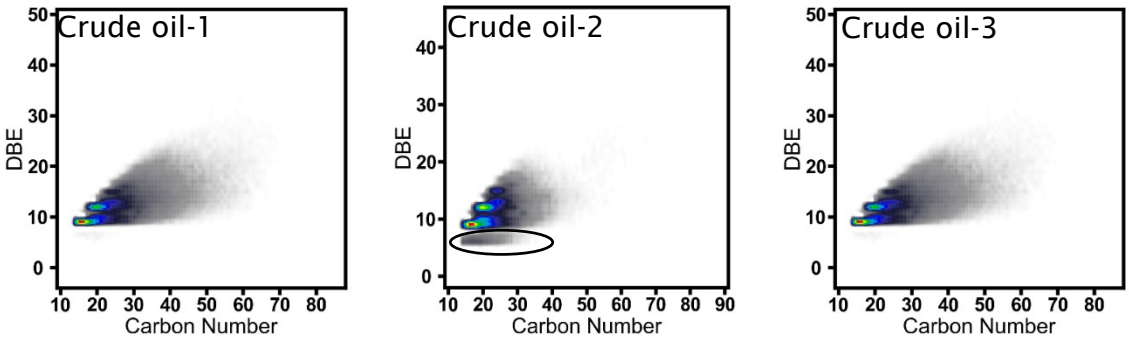

Figure 60 DBE *versus* carbon number plots for negative ion APPI-Orbitrap MS for deprotonated HC class molecules. A circle is used to highlight the difference in DBE distribution.

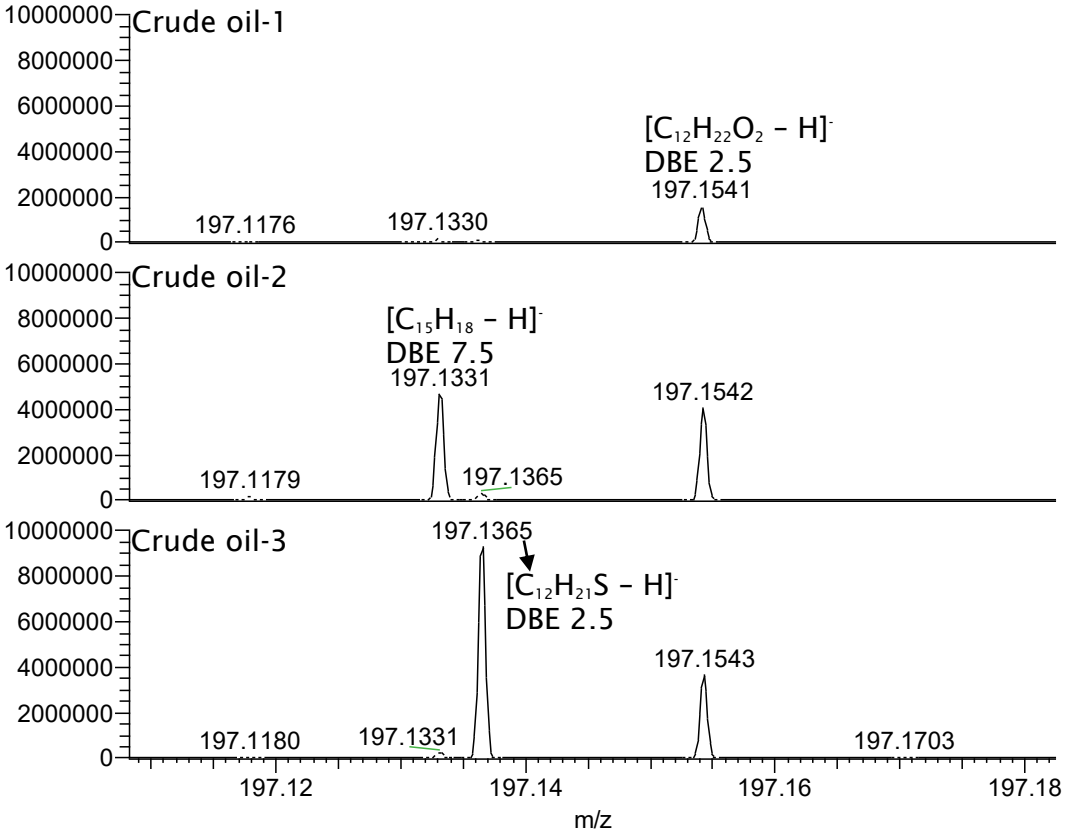

Figure 61 Expanded *m/z* at 197 for crude oil-1, 2 and 3 mass spectra acquired using negative ion APPI Orbitrap MS.

The negative ion APPI data of crude oil-2 mass spectrum in Figure 61 showed an important observation, the high signal intensity of the HC class ion with DBE value of 7.5. Similar observation can be made about the mass spectrum for crude oil-3 but for the S_1 class. Crude oil-3 mass spectrum in Figure 61 shows a

significant relative abundance of *m/z* 197.1365 which cannot be observed in crude oil-1 and 2 mass spectra. *m/z* 197.1365 in crude oil-3 mass spectrum is assigned as $[C_{12}H_{21}S - H]^-$ with DBE value of 2.5. The discussion about S_1 class will be presented later in this section. However, for preliminary observation the high relative abundance observed for $[C_{12}H_{21}S - H]^-$ in crude oil-3 mass spectrum is probably attributed to the unique property of this crude oil, classified as sour crude oil and therefore high sulfur containing.

The discussion for the HC class in Figure 60 and Figure 61 for crude oil-1, 2 and 3 was about deprotonated molecules. However, radical anions, $M^{-\cdot}$, for the HC class are observed in crude oil-1, 2 and 3 mass spectra. Figure 62 shows an expanded *m/z* at 192 for crude oil-1, 2 and 3 mass spectra acquired using negative ion APPI Orbitrap MS. *m/z* 192.093 is observed in crude oil-1, 2 and 3 mass spectra with similar relative abundances. *m/z* 192.093 in crude oil-1, 2 and 3 mass spectra is assigned as $C_{15}H_{12}^{-\cdot}$, negative molecular ion with DBE value of 10. Other than HC-R class ion is observed at *m/z* 192 in the mass spectra of crude oils in Figure 62, N_1 containing compound. *m/z* 192.0813 in crude oil-1, 2 and 3 mass spectra of Figure 62 is assigned as deprotonated molecule $[C_{14}H_{11}N - H]^-$ with DBE value of 10.5. A possible structure for *m/z* 192.0813 is a pyrrolic containing compound. The ion intensity of $[C_{14}H_{11}N - H]^-$ is the highest abundance in crude oil-2 mass spectrum followed by crude oil-1 and 3 mass spectra. This matches the observation made about crude oil-2 mass spectrum in Figure 59 compared to crude oil-1 and 3 mass spectra which shows that the most intense ions in the mass spectrum of crude oil-2 are related to the N_1 class with DBE value of 9.5 and 12.5.

The negative ion APPI Orbitrap MS data showed that the relative abundance of N_1 class with DBE value of 9.5 and 12.5, possibly pyrrolic containing compounds, in crude oil-2 mass spectrum is significantly greater compared to N_1 class in crude oil-1 and 3 mass spectra. It should be noted that the nitrogen containing compounds in crude oils are divided into basic (pyridinic) and neutral compounds (pyrrolic). The basic containing compounds are ionised using positive ion ESI producing protonated molecules, $[M + H]^+$. See section 4.1.2 for positive ion ESI FT-ICR MS data for crude oil-1, 2 and 3 analysed using toluene:methanol ratio of 1:9 with 0.1% formic acid. The data showed that the combined ion intensities of the N_1 class, possibly pyridinic containing compounds, are the most intense for crude oil-2 compared to the N_1 class of crude oil-1 and 3. The neutral part of the nitrogen containing compounds, possibly pyrrolic containing compounds, in

crude oils can be ionised using negative ion ESI or APPI. However, during hydroprocessing nonbasic N-containing compounds are hydrogenated to basic compounds.[36]

The presence of basic nitrogen containing compounds in the feedstock (< 50 ppm) causes catalysts deactivation. The data of crude oil-2 in positive ion ESI suggests that basic pyridinic containing compounds are the most abundant in crude oil-2 compared to crude oil-1 and 3. Thus, it is expected that the problem of catalyst deactivation will be the most with crude oil-2 refining process.

Further, the negative ion APPI data of crude oil-2 suggested that neutral pyrrolic containing compounds are significantly more abundant in crude oil-2 compared to crude oil-1 and 3, specifically for N_1 with DBE 9.5 and 12.5. These compounds are hydrogenated to basic compounds during hydroprocessing possibly aggravating the problem of catalyst deactivation caused by crude oil-2 refining process.

The solution of this problem is the removal of nitrogen containing compounds through hydrodenitrogenation (HDN) process. However, conventional HDN catalysts might not be adequately effective for heavy crude oils such as the analysed crude oil-2. Thus, the interpretation of crude oil mass spectral data could be used by scientists working in the field of catalysis to design more specific catalysts for HDN. Further, nitrogen containing compounds are not just catalyst deactivator for hydrodesulfurisation (HDS) but causes environmental problems and affects fuel stability during storage.[35]

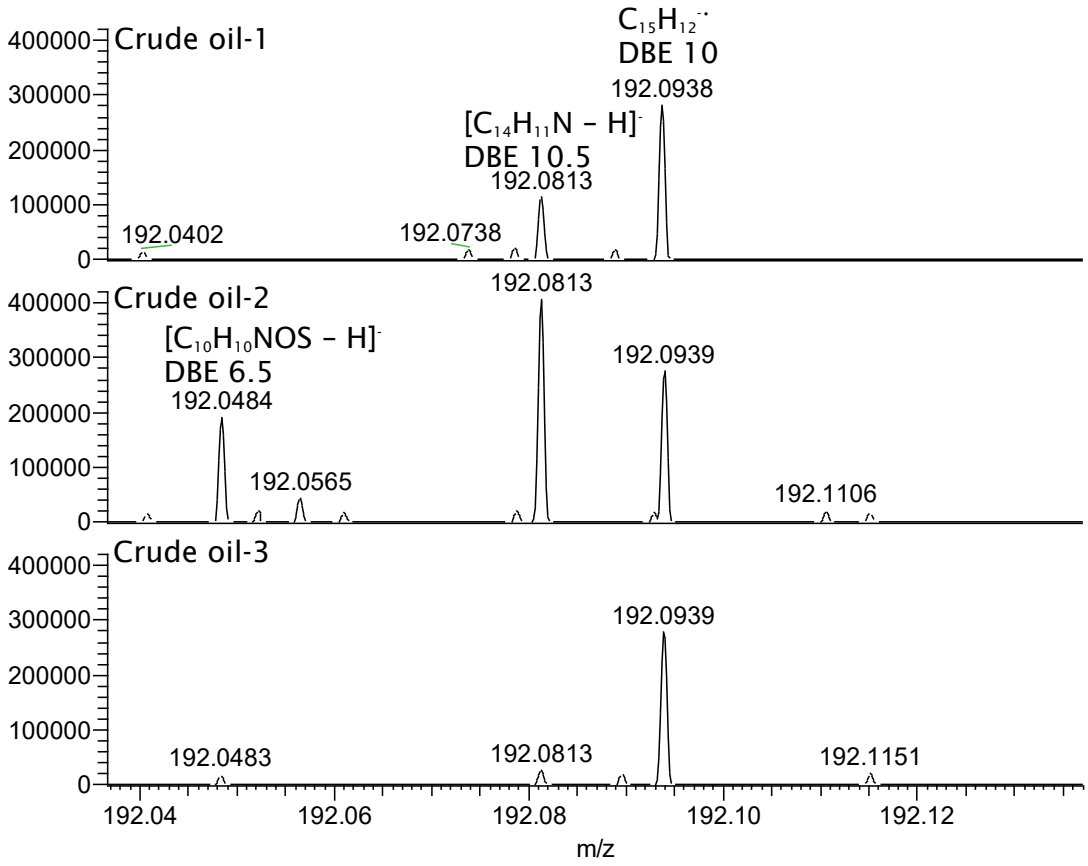

Figure 62 Expanded *m/z* at 192 for crude oil-1, 2 and 3 mass spectra acquired using negative ion APPI Orbitrap MS.

The deprotonated molecules of the HC class for crude oil-1, 2 and 3 were discussed in Figure 60 DBE *versus* carbon number plots. It revealed some differences regarding crude oil-2 DBE distribution of the deprotonated HC class, from DBE 6 to 8 compared to crude oil-1 and 3. (See Figure 61 *m/z* 197.133 $[C_{15}H_{18} - H]^-$ with DBE value of 7.5). The HC class is not just observed as deprotonated molecule in crude oil-1, 2 and 3 mass spectra but as well as negative molecular ion. (See Figure 62 *m/z* 192.094 $C_{15}H_{12}^{-\cdot}$ with DBE value of 10). There was no significant differences in the ion intensity of $C_{15}H_{12}^{-\cdot}$ in Figure 62 across crude oil-1, 2 and 3 mass spectra. However, the DBE *versus* carbon number plots for negative molecular ion of the HC-R class in Figure 63 revealed major differences for crude oil-3, highlighted using a black box. Figure 63 shows that from DBE 10 and upward crude oil 1, 2 and 3 have similar HC-R plots.

The DBE *versus* carbon number plots of negative molecular ions of HC-R plots from DBE 10 and upward in Figure 63 are similar to the deprotonated molecules of the HC class in Figure 60 for crude oil-1, 2 and 3. Thus, hydrocarbon containing compounds from DBE 10 and upward have negative molecular ion and

deprotonated molecule for the same neutral molecule and are observed in mass spectra of crude oil-1, 2 and 3. However, crude oil-3 HC-R DBE *versus* carbon number plots in Figure 63 showed another distribution of DBE values, starting from DBE 5 to 9, which is not observed in crude oil-1 and 2 HC-R plots. Further, these molecules are only observed in crude oil-3 mass spectrum as negative molecule ions and not as deprotonated molecules.

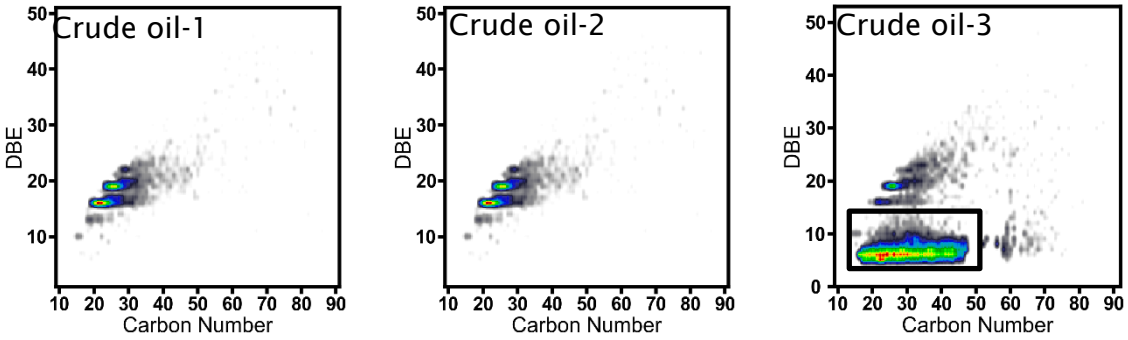

Figure 63 DBE *versus* carbon number plots for negative ion APPI-Orbitrap MS for radical anions HC-R class. A square is used to highlight the difference in DBE distribution.

Figure 64 shows expanded *m/z* at 426 for crude oil-1, 2 and 3 mass spectra acquired using negative ion APPI Orbitrap MS. *m/z* 426.4230 with elemental formula of $C_{31}H_{54}^{\cdot\cdot}$ and DBE value of 5 is only observed in crude oil-3 mass spectrum. Figure 64 crude oil mass spectra further confirm the observation made regarding Figure 63 HC-R DBE *versus* carbon number plots. The lower DBE value distribution, from DBE 5 to 9, that is observed for crude oil-3 in Figure 63 is probably associated with the fact that crude oil-3 is a light crude oil. Light crude oils have a higher proportion of light hydrocarbons compared to heavy crude oils. However, the data for crude oil-3 suggests that straight or branched chain hydrocarbons are not ionised under the used negative ion APPI conditions. An aromatic ring such as benzene is required for the ionisation process to take place through charge exchange or electron capture producing a negative molecular ion $M^{\cdot\cdot}$. This is probably related to the fact that molecules with an aromatic ring are more stable compared to alkanes. Further, deprotonated molecules were not observed in crude oil-3 mass spectra for ions with DBE value from 5 to 9.

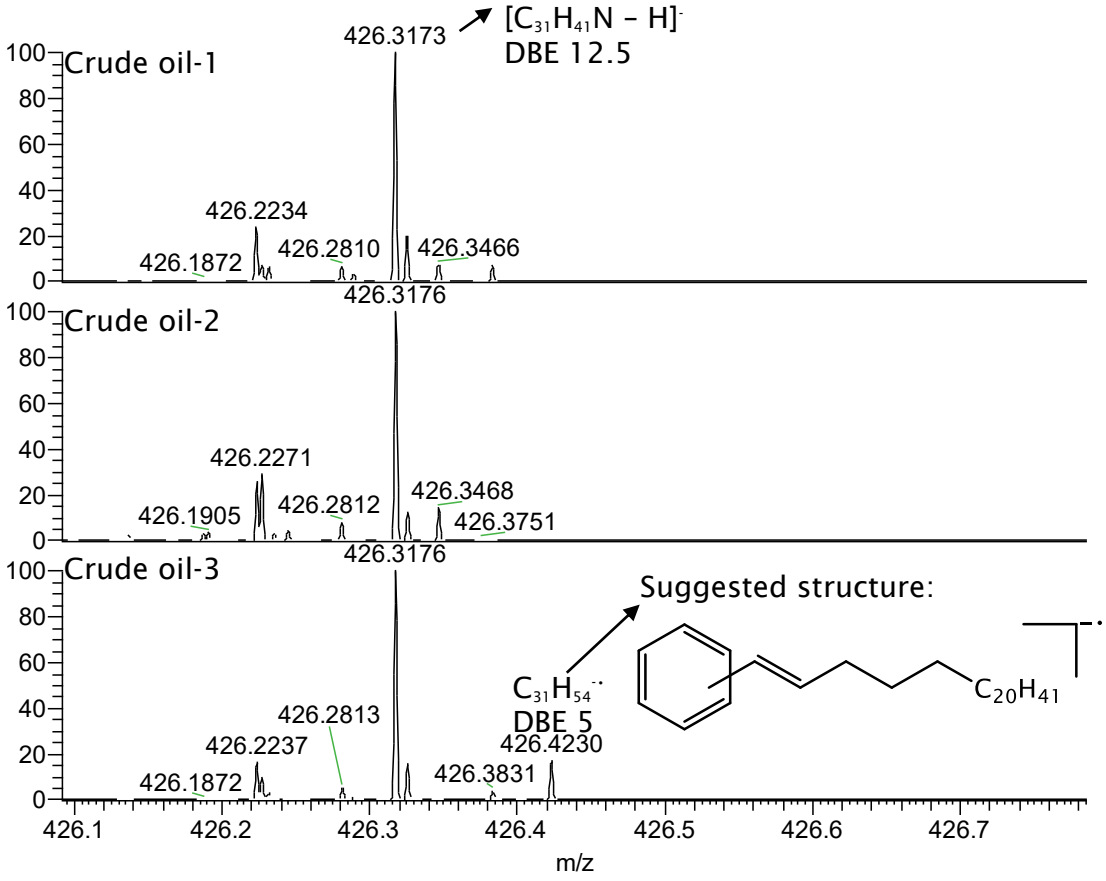

Figure 64 Expanded negative ion APPI Orbitrap MS for *m/z* 426 for crude oil-1, 2 and 3 .

The negative molecular ion series that were identified in crude oil-3 HC-R DBE *versus* carbon number plots in Figure 63 started from DBE 5. However, no negative molecular ion with a DBE value of 4 was observed in crude oil-3 mass spectrum. DBE value of 4 represents a molecule containing benzene. This can be due to many reasons such as the stability of the ion at DBE 4 and/or its abundance in crude oil-3. Further, the effect of toluene should not be excluded as factor in the ionisation process. It was suggested that the electron affinity plays a role in the ionisation of low polarity compounds *via* electron capture mechanism.[183] It should be noted that the electron affinity of toluene is -1.11 eV.[184] Thus, it is not expected for toluene as a sample solvent to capture thermal electrons. However, the reverse is true for sample solvents with positive electron affinity.[182] The effect of changing the sample solvent and concentration in negative ion APPI should be further investigated in future work.

It can be argued that the starting DBE value of crude oil-3 HC-R class is at 5 rather than 4 is because negative molecular ions at DBE 5 are more stable ions. (See Figure 63 for HC-R DBE *versus* carbon number plots). The difference between DBE

5 and 4 is one DBE which corresponds to an addition of a double bond or a ring. Figure 64 shows expanded *m/z* for crude oil-1, 2 and 3 mass spectra. *m/z* 426.4230 in crude oil-3 mass spectrum is assigned as $C_{31}H_{54}^{\cdot\cdot}$ with a DBE value of 5. One of the possible structure is having a benzene ring with a double bond being on the alkyl chain. Another possible structure is having a saturated six membered ring in addition to the aromatic ring. (See Figure 65) The alky chain can be substituted at any position on the ring structure. The alkyl chain can be as well straight or branched. Different isomers of $C_{31}H_{54}^{\cdot\cdot}$ should as well be considered.

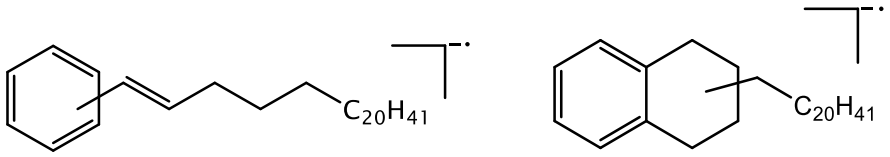

Figure 65 Suggested structures for *m/z* 426.4230, $C_{31}H_{54}^{\cdot\cdot}$, shown in Figure 64.

Previously in Figure 61 the discussion was about deprotonated molecules from negative ion APPI of HC class for crude oil-1, 2 and 3 mass spectra acquired using Orbitrap MS. In Figure 61 another observation was made about the deprotonated molecule of S_1 class for crude oil-3. In Figure 61 the negative ion APPI mass spectrum of crude oil-3 showed a significant ion intensity of *m/z* 197.1365 with respect to crude oil-1 and 2. This *m/z* value is related to the S_1 class with elemental formula of $[C_{12}H_{21}S - H]^-$ and DBE value of 2.5. The significant intensity extends to all the homologous series of S_1 with DBE value of 2.5 with respect to crude oil-3. (See Figure 66 for crude oil-3 S_1 DBE *versus* carbon number plot).

Figure 66 shows DBE *versus* carbon number plots for the deprotonated molecules of the S_1 class for crude oil-1, 2 and 3. Crude oil-1 and 2 have similar DBE *versus* carbon number distribution and ion intensities colour coding for the S_1 class. The DBE distribution for crude oil-1 and 2 starts from DBE 1 to 26. Each DBE value has a different degree of alkylation, the carbon number in the S_1 plots. The observed ion intensities at lower DBE values, below DBE 10, for crude oil-1 and 2 are less compared to ion intensities from DBE 10 and upward. However, the S_1 DBE *versus* carbon number plot for crude oil-3 has a different distribution of ion intensities. Ions with lower DBE values starting from DBE 1 are most intense compared to ions with high DBE values in the S_1 plot of crude oil-3. Further, the S_1 plot of crude oil-3 in Figure 66 shows another difference from crude oil-1 and 2 that is related to the deprotonated molecules with a DBE value of 0.5 for the ion.

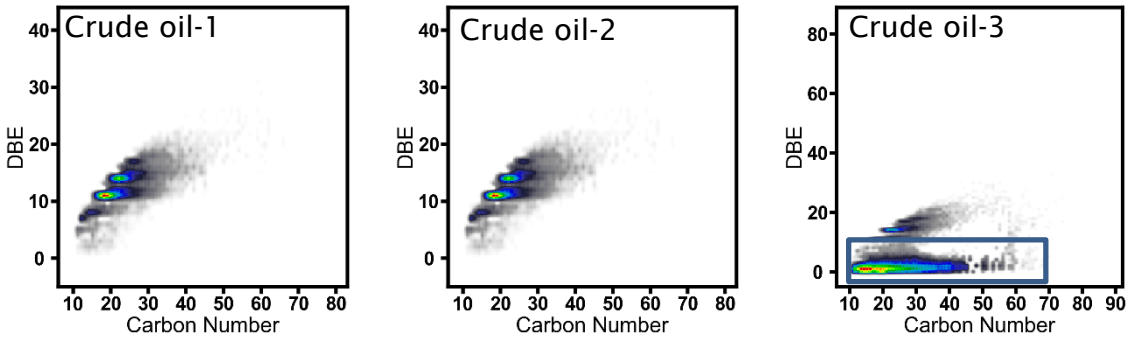

Figure 66 DBE *versus* carbon number plots for negative ion APPI-Orbitrap MS for deprotonated S_1 class molecules. A square is used to highlight the difference in DBE distribution.

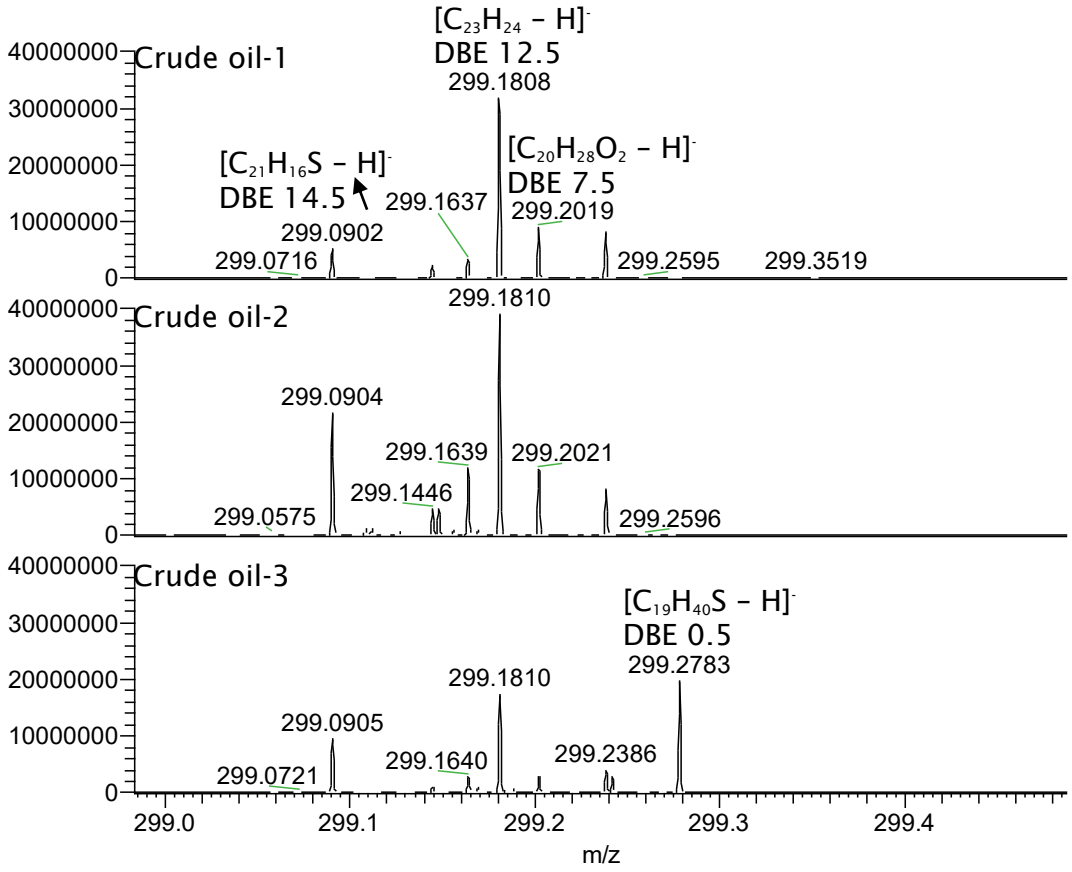

Figure 67 Crude oil-1, 2 and 3 mass spectra were acquired using negative ion APPI-Orbitrap MS. *m/z* is expanded at nominal 299.

Figure 67 shows expanded *m/z* at 299 for crude oil-1, 2 and 3 mass spectra acquired using negative ion APPI Orbitrap MS. *m/z* 299.2783 is observed in crude oil-3 mass spectrum but it is not observed in crude oil-1 and 2 mass spectra.

m/z 299.2783 is assigned as deprotonated molecule of $[C_{19}H_{40}S - H]^-$ with a DBE value of 0.5 for the ion and 0 for the neutral molecule, $C_{19}H_{40}S$. The mass spectral data in Figure 67 further confirms the observation made using the S_1 DBE *versus* carbon number plots in Figure 66 for crude oil-1, 2 and 3. A DBE value of 0 indicates that there is no double bond or a ring in the structure of S_1 class molecules with a DBE value of 0. The observation made using the crude oil mass spectra in Figure 67 and the S_1 plots in Figure 66 are reflecting the type of the analysed crude oils. Sour crude oil such as crude oil-3 is rich with compounds containing sulfur. The data of Figure 66 suggest that the intensity distribution of S_1 class ions within each crude oil is different. This is because crude oil-3 showed more intense ions at lower DBE value of S_1 in Figure 66 compared to crude oil-1 and 2. This is probably because crude oil-3 is a sour crude oil.

However, the colour coding in DBE *versus* carbon number plots is assigned based on the ions intensities distribution within each assigned class in a crude oil mass spectrum. Thus, DBE *versus* carbon number plots can be used to show the ion distribution differences for a certain class but cannot be used to compare ion intensities across different crude oils. To compare ion intensities, the crude oil mass spectrum is used. For example, in Figure 61 expanded *m/z* mass spectra of crude oil-1, 2 and 3 suggested that the signal intensity of S_1 containing ion with DBE value of 2.5 is significantly more intense in crude oil-3 mass spectrum compared with crude oil-1 and 2 mass spectra. Figure 68 shows the combined ions intestines for the deprotonated molecules of the S_1 class for crude oil-1, 2 and 3. The data was acquired in triplicates using negative ion APPI Orbitrap MS and the associated error bar with each crude oil sample is shown. The data in Figure 68 shows that the combined ions intensities of S_1 in crude oil-2 is more than S_1 of crude oil-1. This further proves the idea that DBE *versus* carbon number plots cannot be used to compare ions intensities. This is because S_1 plots of crude oil-1 and 2 in Figure 66 are similar. The S_1 combined ions intensities of crude oil-3 in Figure 68 is significantly more abundant compared to crude oil-1 and 2. However, Figure 68 plot cannot be used to judge on the individual DBE contribution to S_1 combined ions intensities.

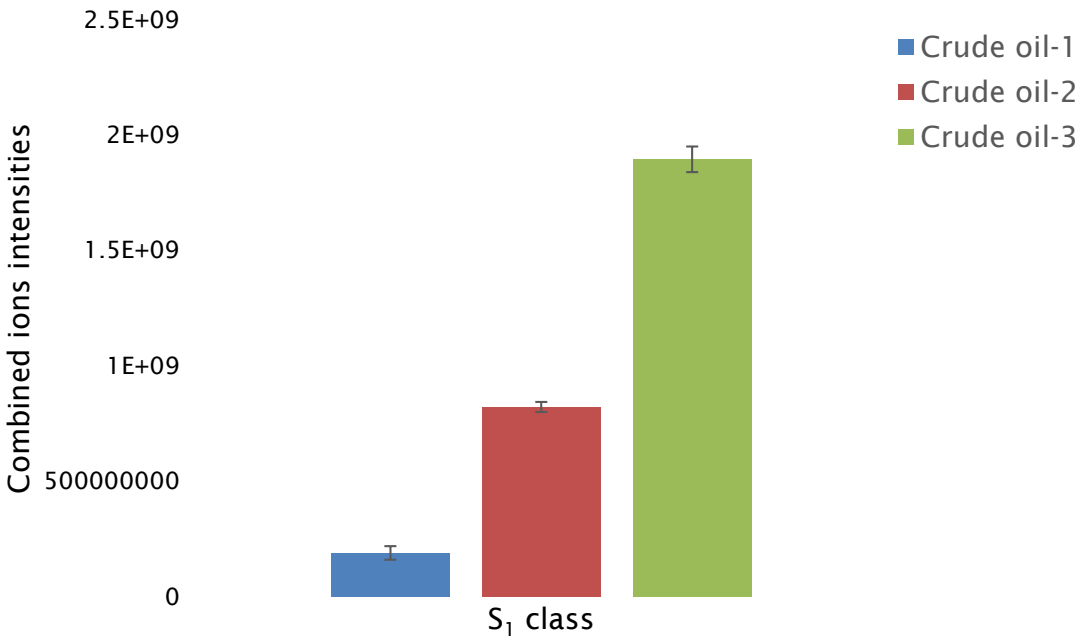

Figure 68 Combined ions intensities in negative ion APPI Orbitrap MS for the deprotonated molecules of the S_1 class for crude oil-1, 2 and 3.

The data presented in Figure 68 can be broken to show the contribution of each DBE to the combined ions intensities of the S_1 class. Figure 69 shows DBE contribution from 0 to 20 to the combined ions intensities of S_1 deprotonated molecules for crude oil-1, 2 and 3. Crude oil-1 has the lowest combined ions intensities from DBE 1 to 20 compared with crude oil-2. However, this trend is not the same when comparing crude-1 and 3 DBE combined ions intensities of S_1. DBE value of 10 and 13 in crude oil-1 have a higher combined ions intensities compared with crude oil-3. The DBE combined ions intensities for crude oil-1start to increase form DBE 10 to 19 compared with lower DBE combined ions intensities for crude oil-1 from 9 to 1.

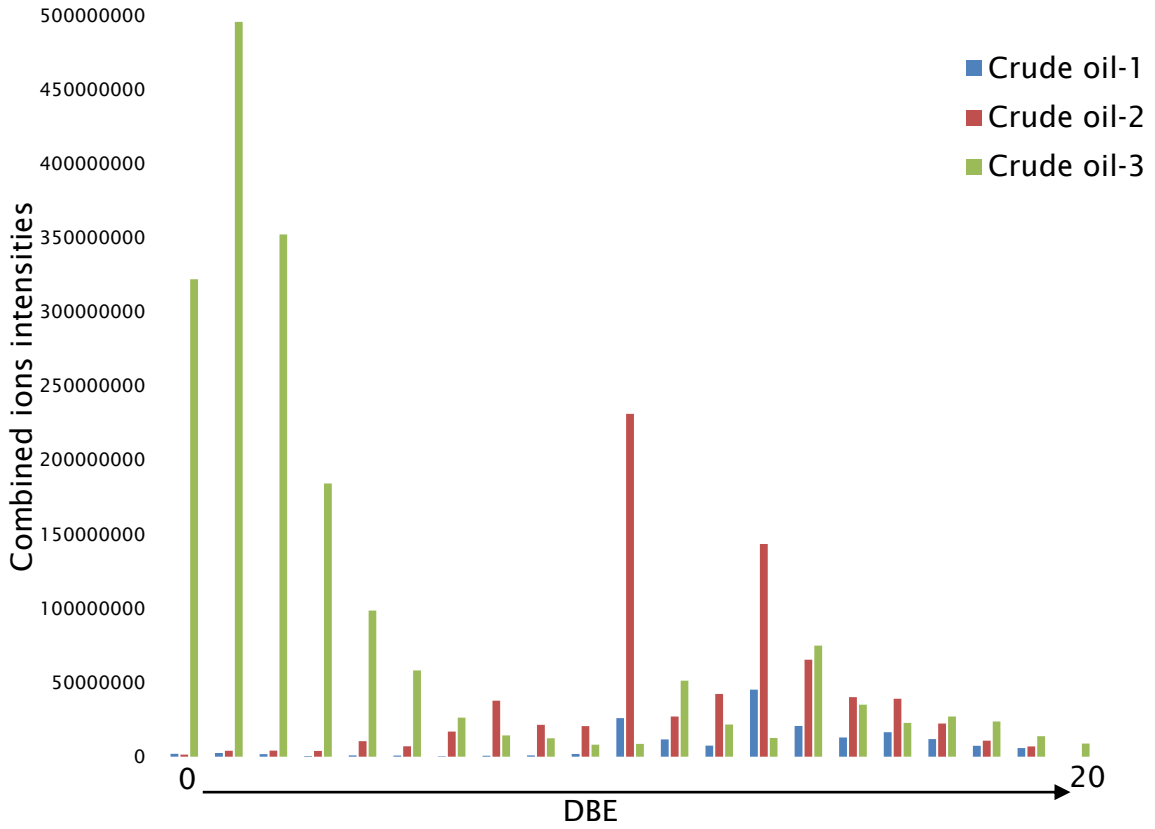

Figure 69 Combined ions intensities in negative ion APPI Orbitrap MS for the different DBEs of the S_1 class for crude oil-1, 2 and 3.

Crude oil-2 DBE combined ions intensities from 1 to 20 have higher intensities compared to crude oil-1. (See Figure 69). Thus, the data presented in Figure 68 about S_1 class combined ions intensities for crude oil-2 compared to crude oil-1 are reflected in the DBE combined ions intensities of S_1 in Figure 69.

Crude oil-2 high DBEs, from 7 to 19, are more intense compared to crude oil-2 low DBE values, from 7 to 1. Crude oil-2 most intense DBEs are at 11 and 13. The combined ions intensities of these DBEs are significantly higher compared to crude oil-1 and 3. This means that the most contributing DBEs for S_1 combined ions intensities in Figure 68 for crude oil-2 are DBE 10 and 13. Further, the difference between DBE 13 and 10 is 3 which corresponds to the addition of an aromatic ring.

In Figure 69 crude oil-3 shows a combined ions intensities at DBE 0 for S_1 that is not observed for crude oil-1 and 2. The DBE combined ions intensities of S_1 for crude oil-3 is significantly higher from DBE 0 to 5 compared with crude oil-3 higher DBE values, from 6 to 20. This shows that the most contributing DBEs to the combined ions intensities of S_1 for crude oil-3 in Figure 68 are from DBE 0 to 5. It can be noted in Figure 69 that crude oil-3 have an overall lower DBE

combined ions intensities of S_1 compared to crude oil-2 at high DBE values. This is observed for DBE values of 7, 8, 9, 10, 12 and 16. Further, crude oil-1 which has the lowest S_1 class combined ions intensities, shown in Figure 68, have a higher DBE combined ions intensities of S_1 in Figure 69 at DBE 10 and 13 compared to crude oil-3.

Crude oil-3 is a light and sour crude oil with a severe odour of sulfur. This property of severe odour is probably related to its high content of S_1 containing compounds from DBE 0 to 5. (See Figure 69). The odour can be probably linked specifically to S_1 containing compounds with a DBE value of 0 that are not observed in crude oil-1 and 2. These compounds are probably thiol containing compounds. Table 22 shows that the thiols containing compounds have low odour detection threshold compared to other commonly used solvents such as methanol.

Table 22 Odour detection threshold of thiols.[185]

Compound	Odour detection threshold (ppm)	Compound	Odour detection threshold (ppm)
Hydrogen sulfide	0.0047	Carbon disulfide	0.21
Methanethiol	0.0021	Methanol	100
Ethanethiol	0.001	Kerosene	1
Propanethiol	0.00075	Ammonia	46.8
Butanethiol	0.001	Sulfur dioxide	3

The combined ions intensities of S_1 for crude oil-3 in Figure 69 at DBE 0 is composed of the combination of the ions intensities of S_1 DBE 0 homologous series. Table 23 lists some of these ions with the highest ions intensities in the homologous series. The corresponding neutral molecule is shown for each *m/z* value. The relative abundance in Table 23 is related to the S_1 deprotonated molecule at specific *m/z* value. The calculated DBE for the neutral molecule is 0 and for the deprotonated molecule is 0.5. Each molecule is different from the subsequent molecule by 14.0156 Da, equivalent to the addition of $-CH_2$. In Table 23 the first ion in the homologous series is at *m/z* 187.1525.

Table 23 Lists the most intense ions of S_1 DBE 0 homologous series for crude oil-3

Recalibrated *m/z*	**Theoretical *m/z***	**ppm mass error**	**Relative abundance**	**DBE - ion**	**DBE - neutral**	**Molecular formula**
187.1525	187.1526	0.25	9707167	0.5	0	$C_{11}H_{24}S$
201.1683	201.1682	0.19	10496786	0.5	0	$C_{12}H_{26}S$
215.1839	215.1839	0.003	17021384	0.5	0	$C_{13}H_{28}S$
229.1995	229.1995	0.17	18733384	0.5	0	$C_{14}H_{30}S$
243.2152	243.2152	0.18	18627144	0.5	0	$C_{15}H_{32}S$
257.2308	257.2308	0.08	17342692	0.5	0	$C_{16}H_{34}S$
271.2465	271.2465	0.16	13811705	0.5	0	$C_{17}H_{36}S$
285.2621	285.2621	0.33	16544870	0.5	0	$C_{18}H_{38}S$
299.2778	299.2778	0.003	19958772	0.5	0	$C_{19}H_{40}S$
313.2934	313.2934	0.06	18892040	0.5	0	$C_{20}H_{42}S$
327.3091	327.3091	0.01	13047287	0.5	0	$C_{21}H_{44}S$
341.3247	341.3247	0.18	11100671	0.5	0	$C_{22}H_{46}S$
355.3404	355.3404	0.12	11484693	0.5	0	$C_{23}H_{48}S$

In Figure 70 a thiol structure is suggested for the deprotonated and neutral molecule of $[C_{11}H_{24}S - H]^-$ and $C_{11}H_{24}S$ respectively. The deprotonated molecule is observed at *m/z* 187.1525 in crude oil-3 mass spectrum. (See Table 23). However, the suggested structure in Figure 70 can have isomers that cannot be distinguished using mass spectrometry.

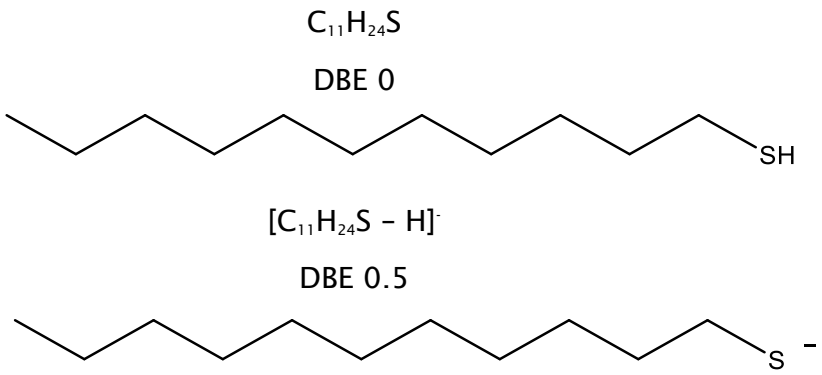

Figure 70 Structure is suggested for the deprotonated molecule at *m/z* 187.1525. A suggested structure for the corresponding neutral is shown.

In conclusion, the analysis using negative ion APPI Orbitrap MS showed major differences in the molecular composition of crude oil-1, 2 and 3 regarding HC, HC-R, N_1, S_1 and S_1-R classes. For example, the HC class for crude oil-2 from DBE 6 to 8 showed a significant abundance compared to crude oil-1 and 3. Further N_1, possibly pyrrolic containing compounds, are more abundant in crude oil-2 mass spectrum. The HC-R DBE *versus* carbon number plots showed that crude oil-3 had molecules with DBE value from 5 to 9 that are not observed for crude oil-1 and 2.

4.3.2 Comparison between crude oil-1, 2 and 3 O_2 classes analysed using negative ion APPI and ESI Orbitrap MS

The analysis of crude oil-1, 2 and 3 revealed that hydrocarbon containing compounds are observed in the mass spectra as negative molecular ion and deprotonated molecules. However, molecules with high gas phase acidity such as the O_2 class showed only deprotonated molecules in crude oil-1, 2 and 3 mass spectra.[182] Crude oil-1, 2 and 3 were analysed using negative ion ESI and APPI Orbitrap MS. The analysis was undertaken in triplicates for each crude oil sample. The negative ion ESI-MS DBE *versus* carbon number plots for the O_2 class of crude oil-1, 2 and 3 are shown in Figure 71. The data in Figure 71 was acquired using negative ion ESI Orbitrap MS. Crude oil-1, 2 and 3 have similar DBE and carbon number distribution for the O_2 class. Further, similar DBE *versus* carbon number plots for the O_2 class was observed for crude oil-1,2 and 3 in negative ion ESI and APPI Orbitrap MS.

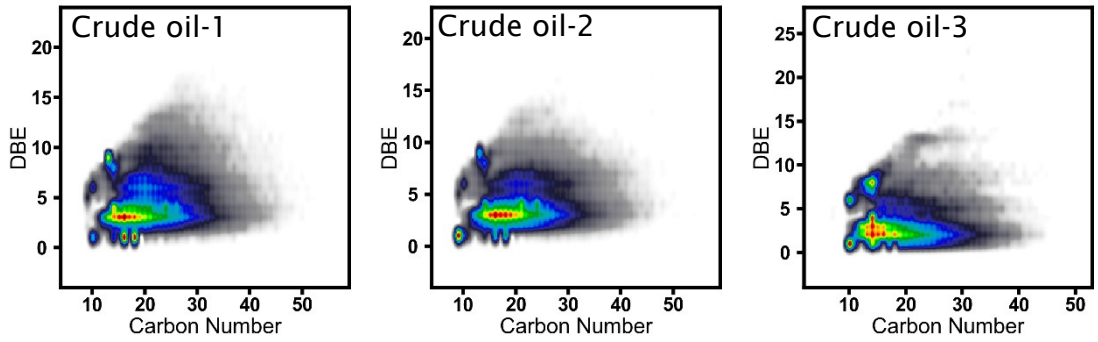

Figure 71 DBE *versus* carbon number plots for negative ion ESI-Orbitrap MS for O_2 class.

Figure 72 shows the combined ions intensities for all the ions in the mass spectrum for crude oil-1, 2 and 3 that their elemental formulae have O_2. The analysis was undertaken using negative ion APPI Orbitrap MS. It shows that crude oil-2 has higher abundance of O_2 compared to crude oil-1 and 3. Crude oil-3 has the lowest abundance of O_2 compared to the other analysed crude oils. Further, the data for the O_2 class for crude oil-1, 2 and 3 using negative ion APPI in Figure 72 is with accordance with the O_2 class data obtained using negative ion ESI Orbitrap MS in Figure 73.

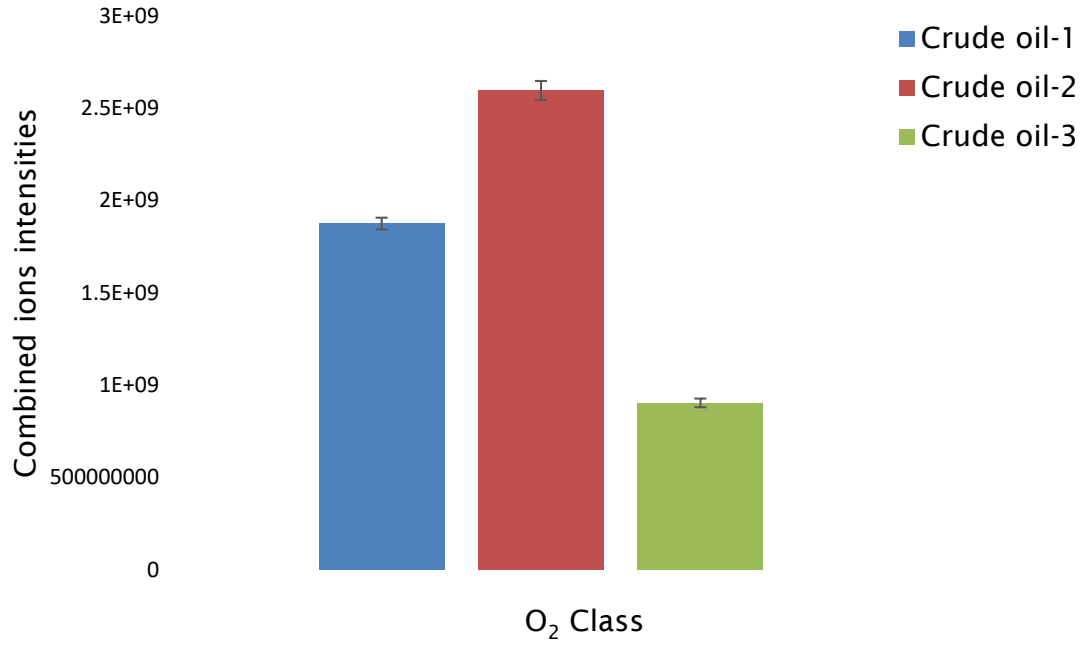

Figure 72 Combined ions intensities in negative ion APPI Orbitrap MS for crude oil-1, 2 and 3.

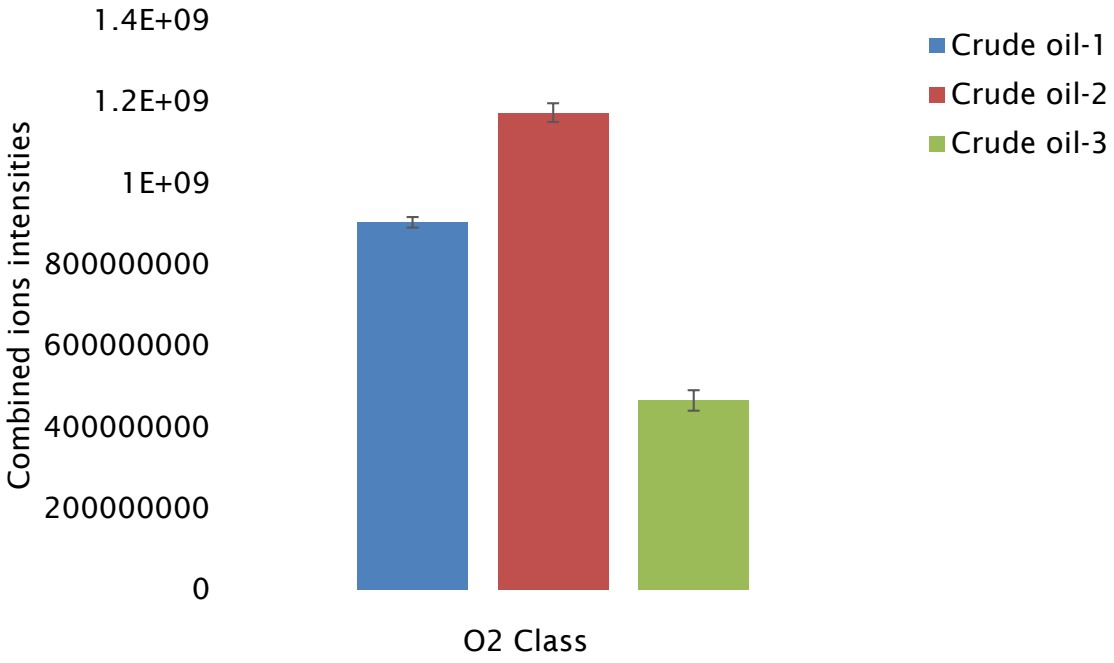

Figure 73 Combined ions intensities in negative ion ESI Orbitrap MS for O_2 class for crude oil-1, 2 and 3.

Figure 72 and Figure 73 showed the combined ions intensities for the O_2 class, combining the different DBEs for the O_2 class for each crude oil. This plot can be broken down to show the combined ions intensities contribution for each DBE value for crude oil-1, 2 and 3. Figure 74 shows the combined ions intensities for each individual DBE value from 1 to 17 for crude oil-1, 2 and 3. The data in Figure 74 is acquired using negative ion ESI Orbitrap MS and is with accordance with the data acquired using negative ion APPI Orbitrap MS. DBE 1 for crude oil-1, 2 and 3 has similar combined ions intensities values. DBE 1 structure represents saturated fatty acids. For DBE 2 the lowest combined ions intensities are observed for crude oil-1 rather than crude oil-3. Except for DBE 2 crude oil-3 has the lowest combined ions intensities across all DBE values compared to crude oil-1 and 2. Further, for crude oil-1 and 2 the most intense combined ions intensities are for DBE 3 compared to other DBE values of crude oil-1 and 2. Whereas for crude oil-3 DBE 2 has the most intense combined ions intensities compared to the other DBE values of crude oil-3. The data in Figure 74 suggest that crude oil-2 DBE 2, 3 and 4 are the most intense compared with crude oil-1 and 3. For crude oil-2 the DBE from 5 to 10 has similar combined ions intensities in comparison to crude oil-1. However, for crude oil-3 DBE 4 to 10 is significantly less compared to crude oil-1 and 2. This suggests that the most contributing DBE for crude oil-2 O_2 class combined ions intensities in Figure 72 are DBE 2, 3 and 4 (being the most intense).

It has been argued that biodegradation process for crude oil significantly decreases the relative abundance of DBE 1, saturated fatty acids. This process of crude oil biodegradation is accompanied with increasing the contribution of O_2 compounds with high DBE values, specifically from DBE 2 to 4 with one to three ring cyclic naphthenic acids.[186] Model structures are suggested in Figure 74 for naphthenic acids with DBEs value from 1 to 4. According to this conclusion crude oil-2 is the most biodegraded compared to crude oil 1 and 3. This is because the data in Figure 74 suggest that DBE 3 is significantly more intense for crude oil-2 compared to crude oil-1 and 3. The data in Figure 74 as well suggest that crude oil-3 is slightly biodegraded to non-degraded because the difference in combined ion intensity between DBE 1 and 2 is the least compared to crude oil-1 and 2. Further the DBE 3 combined ions intensities for crude oil-3 is lowest compared to crude oil-1 and 2.

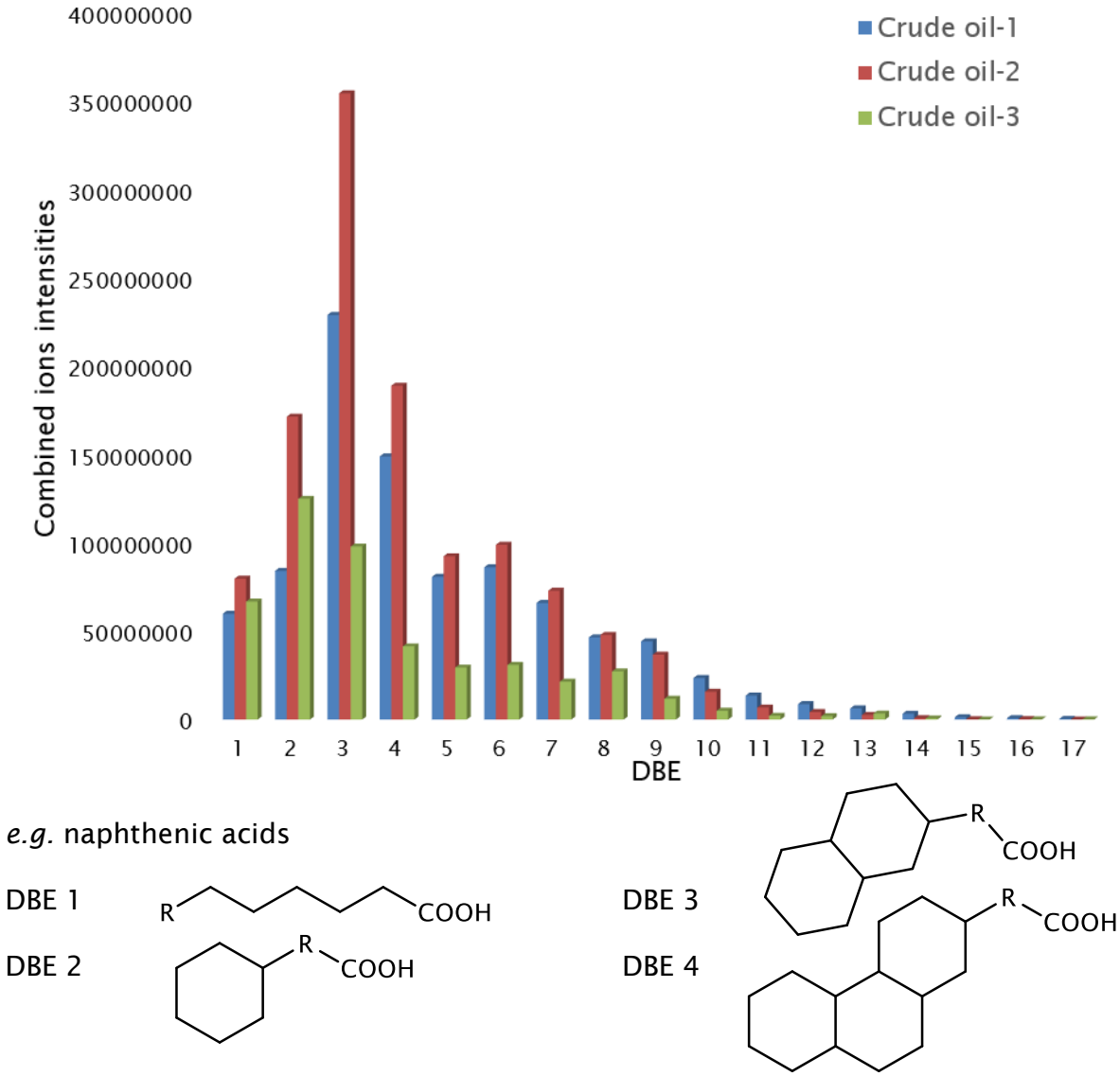

Figure 74 DBE combined ions intensities for crude oil-1, 2 and 3 are shown for O_2 class from DBE 1 to 17. Data was acquired using negative ion ESI Orbitrap MS

4.4 Summary

Crude oil-1, 2 and 3 were analysed using ESI and APPI. In positive ion ESI FT-ICR MS the importance of different sample solvent composition of toluene:methanol was illustrated on the ionisation and multimer formation. Crude oil-1, 2 and 3 were dissolved in toluene:methanol ratios of 1:9, 3:7 and 6:4 with and without the addition of 0.1% formic acid. The ionisation of N_1 containing compounds in crude oil-1, 2 and 3 were the highest at toluene:methanol ratio of 1:9 with 0.1% formic acid. The ionisation of N_1 compounds in crude oil-1,2 and 3 were decreased according to the toluene increase in the sample solvent, from toluene:methanol ratio of 3:7 to 6:4 even with the addition of 0.1% formic acid. However, the rate of decrease in the ionisation of N_1 when the toluene content was increased in the sample solvent was different among different crude oils. The decrease in the ionisation of N_1 containing compounds was less for crude oil-3 compared to crude oil-1 and 2. This further complicates the comparison of N_1 containing compounds in different crude oils. Thus, the solvent composition that showed the highest ionisation of N_1 containing compounds should be used to compare different crude oils, toluene:methanol ratio of 1:9 with 0.1% formic acid. Further, multimers observed in N_1 DBE *versus* carbon number plots for crude oil-1 and 2 were not only concertation driven but also sample solvent composition dependent. The use of toluene:methanol ratio of 1:9 decreased multimer formation. The addition of 0.1% formic acid to toluene:methanol ratios of 1:9, 3:7 and 6:4 reduced multimer formation in N_1 DBE *versus* carbon number plots for crude oil-1 and 2.

The analysis of crude oil-1, 2 and 3 using positive ion ESI ionised basic molecules. To ionises hydrocarbon and thiophene containing compounds positive ion APPI is employed. The analysis using positive ion APPI FT-ICR MS showed that the most abundant ions in the mass spectra of crude oil-1,2 and 3 were related to the radical cations of HC-R and S_1-R classes of compounds. However, no significant differences in the ions intensities were observed for S1-R and HC-R classes in crude oil-1, 2 and 3. However, the use of negative ion APPI showed significant differences in crude oil-1, 2 and 3 regarding the HC, HC-R, N_1, S_1 and S_1-R classes. For example, the HC-R plot of crude oil-3 showed ions series from DBE 5 to 9 which are not observed in the HC-R plots of crude oil-1 and 2. This is probably attributed to the type of crude oil-3, classified as light crude oil. Further, the S_1 class of crude oil-3 is more abundant at lower DBE values compared to crude oil-1 and 2.

The O_2 class for crude oil-1, 2 and 3 were compared using negative ion ESI and APPI Orbitrap MS. Similar DBE *versus* carbon number plots for the O_2 class was observed for crude oil-1,2 and 3 in negative ion ESI and APPI Orbitrap MS. The combined ion intensities for the O_2 class for crude oil-1, 2 and 3 using negative ion APPI is with accordance with the O_2 class data obtained using negative ion ESI Orbitrap MS. The combined ion intensities data show that crude oil-2 has higher abundance of O_2 compared to crude oil-1 and 3. Crude oil-3 has the lowest abundance of O_2 compared to the other analysed crude oils.

Chapter 5: Structure elucidation of N_1 containing compounds in crude oil-2 using positive ion ESI FT-ICR MS/MS

Crude oil contains different heteroatom compounds, which can be ionised using a variety of ionisation techniques. For example polar molecules containing nitrogen atoms, probably pyridinic containing compounds, are ionised using positive ion ESI producing protonated molecules, $[M + H]^+$. In positive ion ESI of crude oil, ions containing N_1 are typically the most abundant in the mass spectrum. Figure 75 shows examples of compounds that are probably contained in crude oil, can be ionised *via* positive ion ESI. Nitrogen containing compounds in crude oils are catalyst deactivators for different processes such as hydroprocessing. (See Chapter 1- polar molecule in crude oil). Structural elucidation of nitrogen containing compounds in crude oil might help in designing more effective catalysts for HDN process. Crude oil-2 was chosen for all tandem MS experiment because of its rich content of N_1 containing compounds. The product ion mass spectra were acquired using positive ion ESI FT-ICR MS/MS.

Acridine

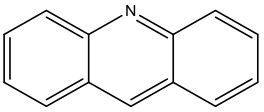

Pyrido[4,3-g]quinoline

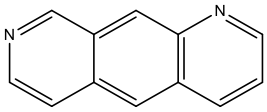

Benzo[4,5]thieno[2,3-b]pyridine

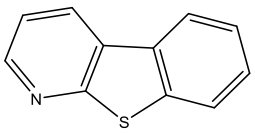

Figure 75 N containing compounds that are ionised by positive ion ESI.

Figure 76 shows an FT-ICR MS instrument where ions can be isolated up to an isolation window of $m/z \pm 0.5$ unit in the quadrupole mass analyser. Subsequent fragmentation of the precursor ion is undertaken in the hexapole collision cell. Image current detection of the product ions are subsequently undertaken in the ICR cell. It should be noted that distonic ions are suggested throughout the discussion of this chapter for radical cation fragments for the fragmentation of pyridine containing compounds. This is because the proton is presumed to be on the nitrogen of the pyridine ring and subsequent CH_2 fragmentation is derived from the alkyl chain. Thus, the suggested structure of some fragment ions are illustrated as distonic ions where the proton is on the nitrogen and the radical is on the alkyl chain.

Collision-induced dissociation (CID) experiments will be discussed in this chapter for crude oil-2 product ion mass spectra of N_1 precursor ions. CID is the most widely used ion activation method in tandem MS.[187] CID was previously compared to 50 eV EI process.[188] The fragmentation is suggested to be affected by the amount of the transferred energy to the ion. In CID, ions are collided with neutral molecules. Under the collision process, the translational energy is converted to internal energy causing the fragmentation of the ions. The time scale of this process is identical to the electron ionisation process, 10^{-15} s.[71,134]

In CID, two mechanisms are proposed for the formation of product ions. The first mechanism is a two-step process where the ion is first activated through collision with gas molecules and then followed by unimolecular dissociation of the activated ion.[189] The second mechanism is proposed to be a one-step process, called a stripping mechanism. This process is difficult to prove because of structure rearrangement when CID is used.[189]

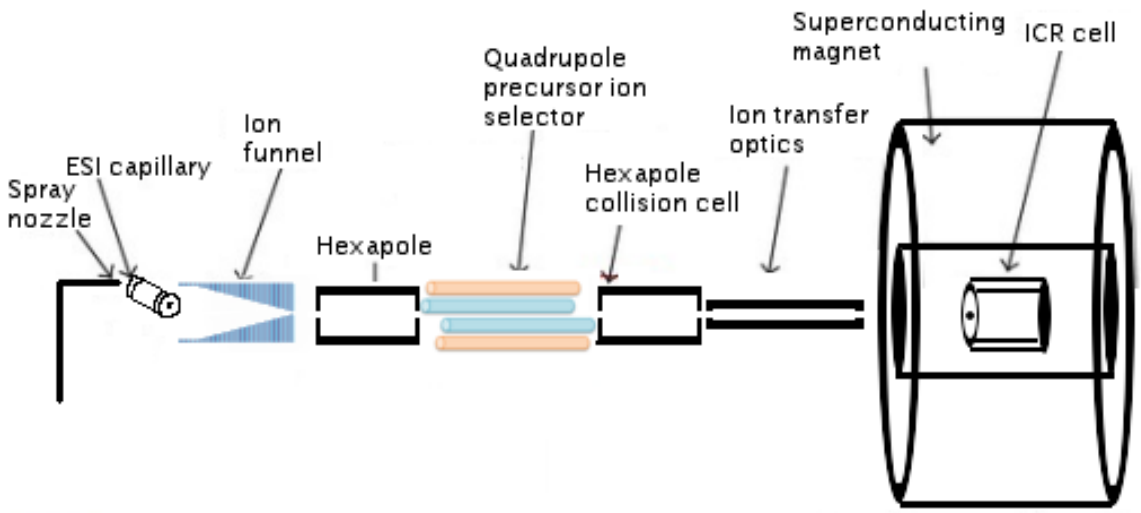

Figure 76 Schematic of an FT-ICR MS.

5.1 Method development: increasing the number of average spectra (AS)

Crude oil-2 was chosen for method development of tandem MS experiment because of its rich content of heterocycles. Despite multimer formation for crude oil-2 at 0.3 mg/mL, a high concentration is needed for tandem MS experiment as higher signal intensity is obtained for the precursor ion. Multimers were dissociated through using in-source CID at 40 V. The use of in-source CID also resulted in increasing the ion intensity of the precursor ion. (See Figure 77)

An expanded *m/z* at 340 of crude oil-2 shows the range of precursor ions that can pass through an isolation window of *m/z* ± 0.5. (See Figure 78). The base peak ion is the protonated molecule $[C_{24}H_{37}N + H]^+$ at DBE 6.5 for the ion (DBE 7 for the neutral molecule ($C_{24}H_{37}N$)).

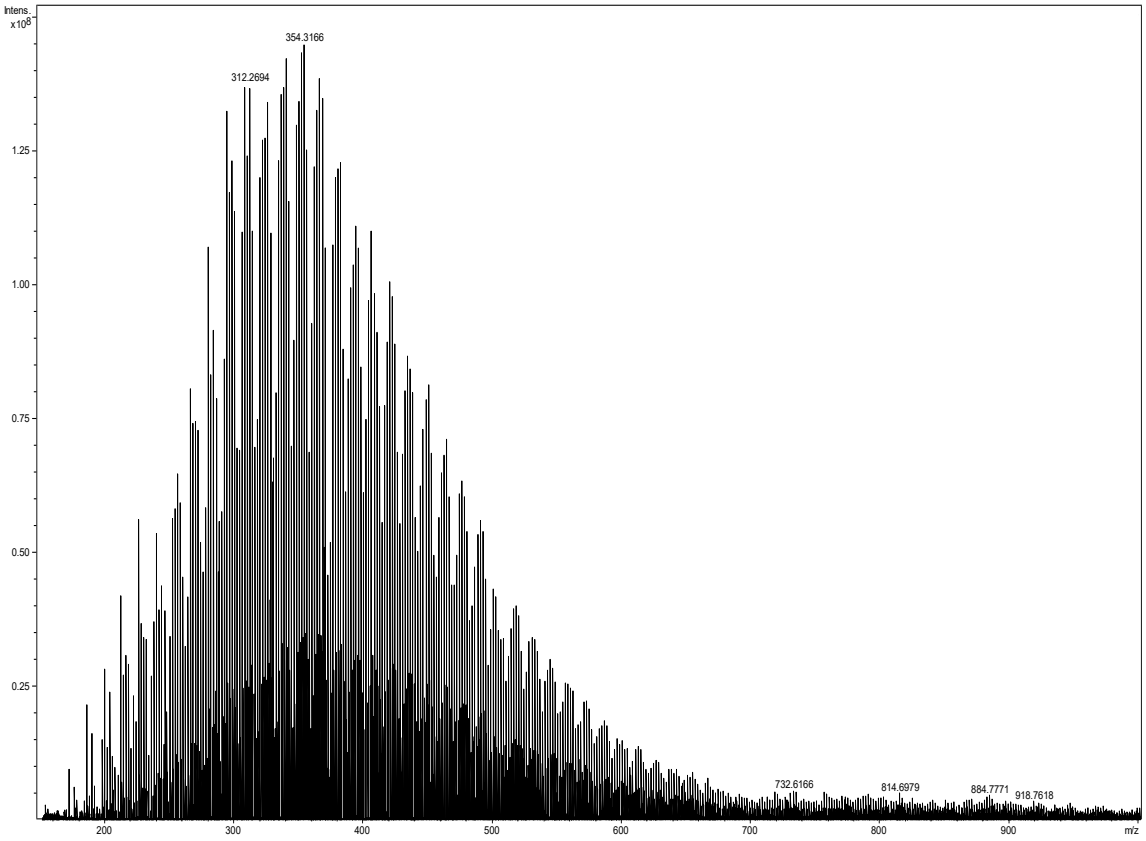

Figure 77 0.3 mg/mL crude oil-2 analysed using positive ion ESI FT-ICR MS with isCID 40 V.

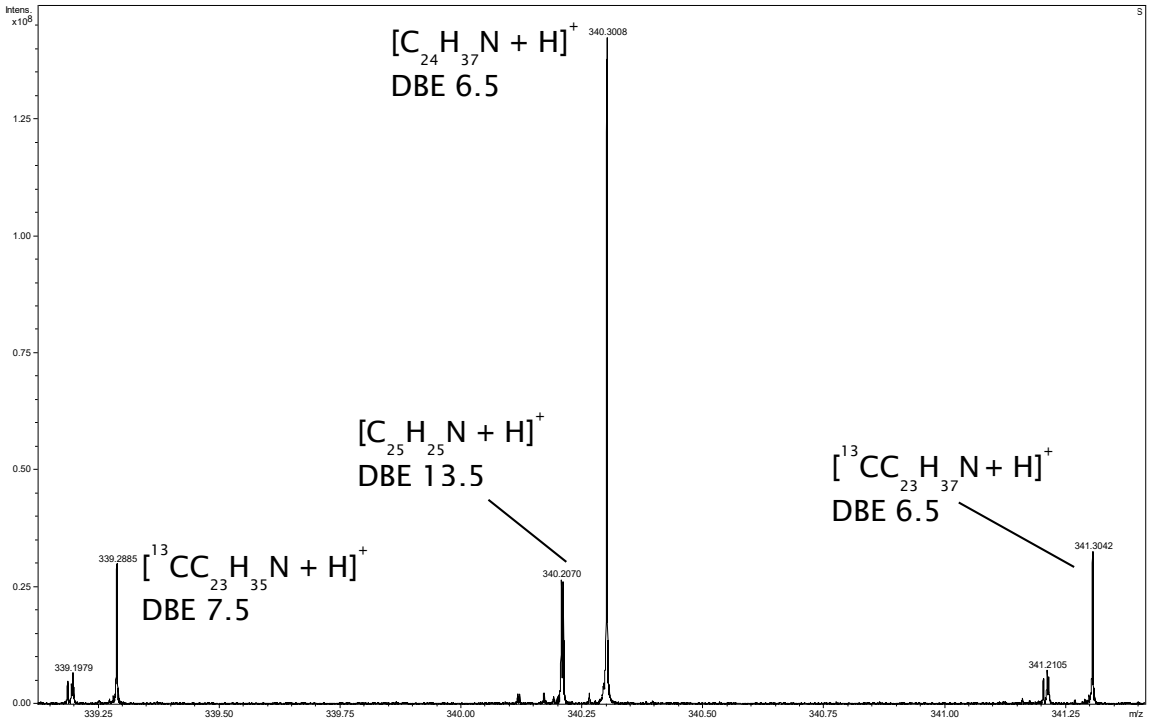

Figure 78 Expanded view at *m/z* 340 for 0.3 mg/mL crude oil-2 showing the range of precursor ions. isCID 40 V.

In Figure 79 the quadrupole was set to filter *m/z* 340 in crude oil-2 mass spectrum with an isolation window at *m/z* ± 0.5. The product ion mass spectra were obtained using collision energy at 40 V. (See Figure 79). The difference between the two mass spectra in Figure 79 is the number of average spectra (AS). At AS 300 the intensity of fragment ions is at approximately at 4×10^6. The mass spectrum acquired at AS 300 shows fragment ions for precursor ions $[C_{24}H_{37}N + H]^+$ and $[C_{25}H_{25}N + H]^+$ at DBE value of 6.5 and 13.5 respectively. These precursor ions were observed in Figure 78 mass spectrum at isolation of *m/z* 340 ± 0.5. The fragment ions observed in Figure 79 AS 300 product ion mass spectrum are different from their precursor ions in the number of CH_2 and DBE value. Fragment ion $C_{24}H_{22}N^+$ has DBE value of 14.5 which is different from its precursor ion, $[C_{25}H_{25}N + H]^+$ with a DBE value of 13.5, by one. This suggests that a double bond was formed in the fragment ion. Further, a loss of CH_2 is observed as well. Another fragment ion was observed at $C_{23}H_{20}N^+$ with a DBE value of 14.5 which is different from the previous fragment ion, $C_{24}H_{22}N^+$ by CH_2. This suggests that the observed fragmentation mechanism in AS 300 product ion mass spectrum are mainly formation of double bond through loss of 2H and losses of CH_2. Another fragment ion at DBE value of 7.5 is observed in the AS 300 product ion mass spectrum, $C_{20}H_{28}N^+$. This fragment ion is related to precursor ion $[C_{24}H_{37}N + H]^+$

with a DBE value of 6.5. Again similar fragmentation mechanism is observed for precursor ion with a DBE value of 6.5 to the one with a DBE value of 13.5, losses of 2H and $(CH_2)_n$. The fragment ion $C_{20}H_{28}N^+$ has lost 2H and $(CH_2)_4$ compared to its precursor ion at $[C_{24}H_{37}N + H]^+$. All fragment ions discussed in AS 300 product ion mass spectrum in Figure 79 were even electron fragment ions. Improvement in S/N of fragment ions can be made through increasing the number of AS above 300. This was observed in Figure 79 for product ion mass spectrum that was acquired at AS 800 instead of AS 300. The increase in ion intensity for fragment ions are significant from approximately 4×10^6 to 0.5×10^8 for product ion mass spectrum at AS 300 and 800 respectively. Further fragment ions that were not detected in AS 300 product ion mass spectrum were observed in AS 800 product ion mass spectrum. However, this improvement in S/N of fragment ions in the bottom product ion mass spectrum in Figure 79 comes with an increase in the analysis time from 15 min. for AS 300 to 40 min. for AS 800.

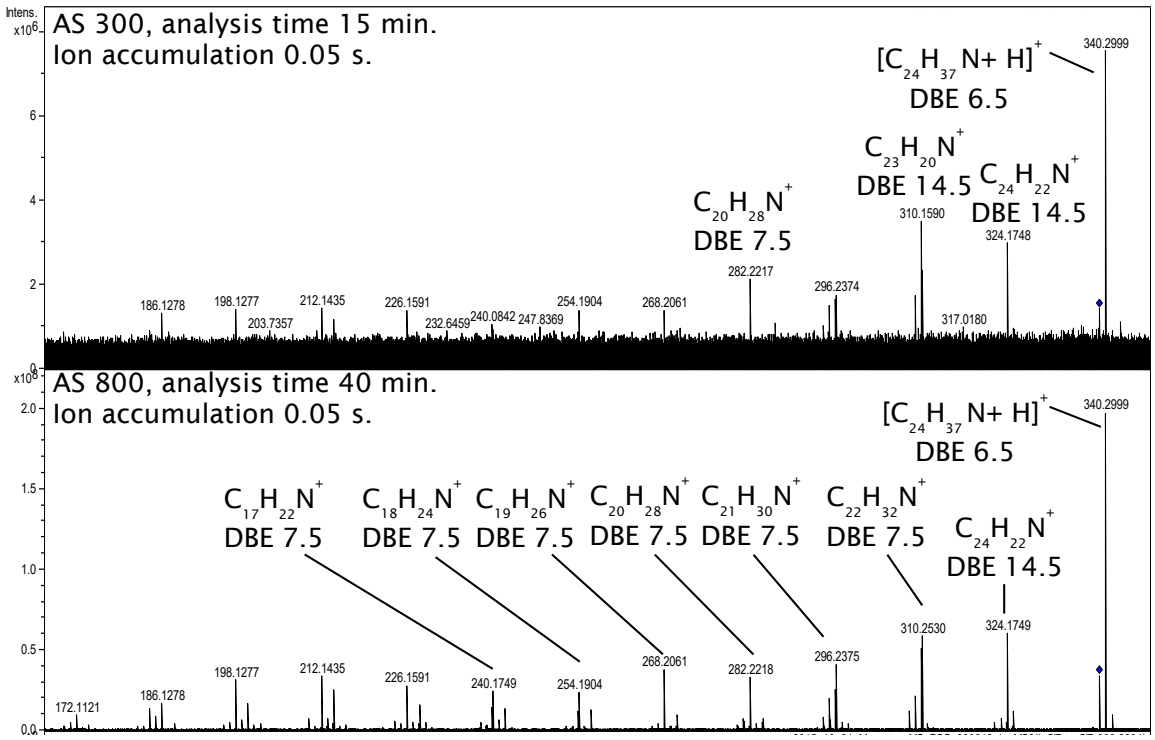

Figure 79 Two product ion mass spectra of crude oil-2 *m/z* 340 ± 0.5 acquired at different AS using CE at 40 V. isCID 40 V.

Only even electron ion fragments are observed in Figure 79 product ion mass spectrum acquired at AS 300 for precursor ions $[C_{24}H_{37}N + H]^+$ and $[C_{25}H_{25}N + H]^+$ respectively. This is because the used averaged spectra detected only the most intense fragment ions, at DBE value of 7.5 and 14.5. Even electron ion fragments at DBE value of 14.5 and 7.5 are the most intense in product ion mass spectra acquired at AS 300 and 800. However, at AS 800 odd electron ion fragments are observed but at much lower intensity compared to even electron ion fragments. Other even electron ion fragments are observed in AS 800 product ion mass spectrum at DBE value of 8.5 and 15.5. However, the ion intensity of these fragment ions are lower compared to fragment ions with DBE value of 7.5 and 14.5. Even electron ion fragments with DBE value of 8.5 is related to the precursor ions $[C_{24}H_{37}N + H]^+$ with a DBE value of 6.5. Thus, a formation of two double bonds is suggested. Similarly, even electron ion fragments with DBE value of 15.5 is related to the precursor ions $[C_{25}H_{25}N + H]^+$ with a DBE value of 13.5.

The range of fragment ions that are observed in Figure 79 AS 300 product ion mass spectrum can be easily labelled and visualised. Increasing the AS from 300 to 800 in Figure 79 has significantly increased the number of fragment ions that are observed in the bottom product ion mass spectrum. Thus, only the most intense fragment ions could be labelled on AS 800 product ion mass spectrum.

Since the majority of fragments that are observed in the product ion mass spectrum are losses of $H^{\cdot}$ or 2H or $(CH_2)_n$. Therefore, a DBE *versus* carbon number plot could be employed to aid data visualisation of even and odd electron fragment ions. N_1 even and odd electron ion fragments in bottom product ion mass spectrum at AS 800 in Figure 79 are plotted using DBE *versus* carbon number plot in Figure 80. The bubble size in Figure 80 corresponds to ion intensity. Thus the most intense ion in the plot is precursor ion $[C_{24}H_{37}N + H]^+$. The bubble size of all ions are scaled according to the intensity of the most intense ion in the plot, $[C_{24}H_{37}N + H]^+$ in Figure 80.

Two N_1 precursor ions are observed in Figure 80, $[C_{24}H_{37}N + H]^+$ and $[C_{25}H_{25}N + H]^+$ at DBE value of 6.5 and 13.5 respectively. For precursor ion $[C_{24}H_{37}N + H]^+$ even electron ion fragment series at DBE 6.5 is observed which corresponds to only losses of CH_2. Loss of $H^{\cdot}$ is observed as odd electron ion fragments series at DBE 7. The most abundant ion series is even electron ion fragments at DBE 7.5 which matched the observation made using the AS 800 product ion mass spectrum in Figure 79. The last observed CH_2 loss for DBE 6.5, 7 and 7.5 are at carbon

number value of 12. However, for DBE 8 and 8.5 are at carbon number values of 13 and 14 respectively.

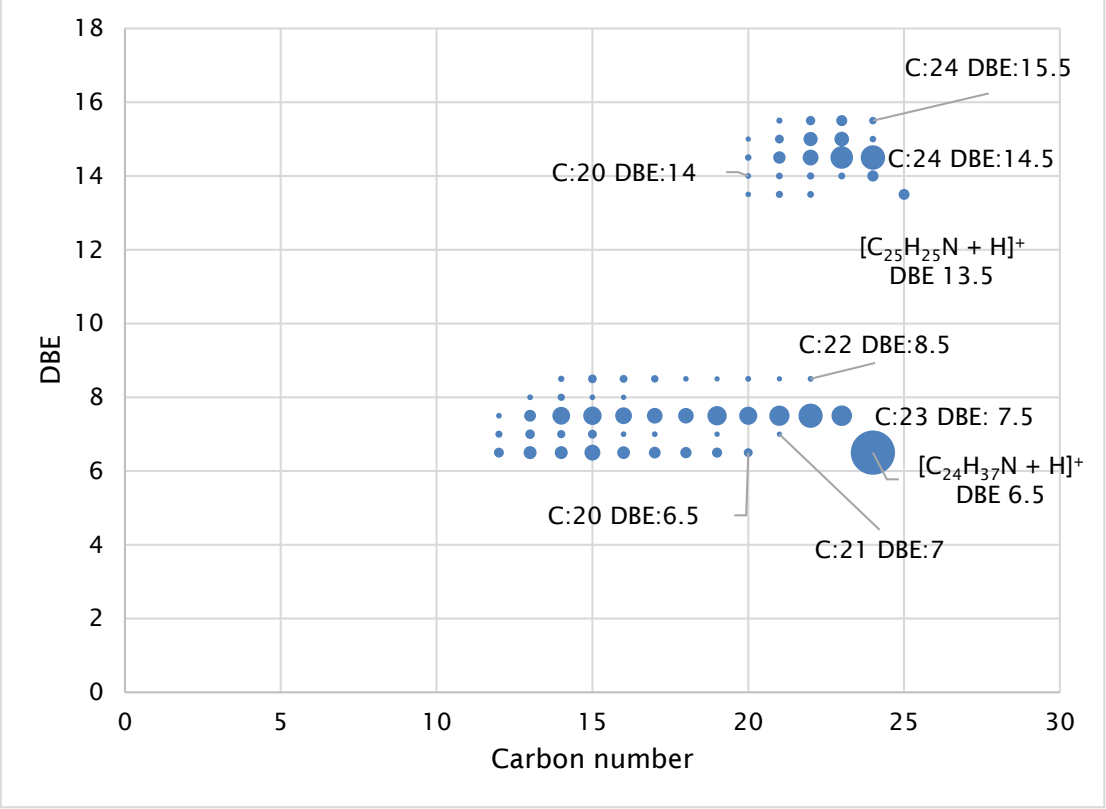

Figure 80 Fragment ions for precursor ions, $[C_{24}H_{37}N + H]^+$ and $[C_{25}H_{25}N + H]^+$, at *m/z* 340 ± 0.5. Data was taken from Figure 79 AS 800.

The other precursor ion in Figure 80 plot is $[C_{25}H_{25}N + H]^+$ with a DBE value of 13.5. The higher DBE value means that the aromaticity of this ion is higher compared to precursor ion $[C_{24}H_{37}N + H]^+$ with a DBE value of 6.5. Similar fragmentation that was observed for precursor ion $[C_{24}H_{37}N + H]^+$ was observed for $[C_{25}H_{25}N + H]^+$ in terms of $H^{\cdot}$, 2H and CH_2 losses. Thus fragment ion series which correspond to only losses of CH_2 are observed at DBE 13.5, at the same DBE value as the precursor ion $[C_{25}H_{25}N + H]^+$. The lowest *m/z* fragment ion that corresponds to CH_2 loss could be used to suggest the core aromatic structure of the precursor ion. Further, odd electron ion fragments series are observed at DBE values of 14 and 15. Even electron ion fragments are observed at DBE value of 14.5 and 15.5. For precursor ions $[C_{24}H_{37}N + H]^+$ and $[C_{25}H_{25}N + H]^+$ the most intense fragment ions are even electron ions with DBE value of 7.5 and 14.5 respectively. This is probably because these fragment ions are the most energetically stable compared to fragment ions at other DBE values. The lowest *m/z* fragment ions that are observed for precursor ion $[C_{25}H_{25}N + H]^+$ is at carbon number value of 20 for fragment ions series with a DBE value of 13.5, 14, 14.5, and 15. This indicates

that precursor ion with high DBE value such as $[C_{25}H_{25}N + H]^+$ is less alkylated compared to precursor ion $[C_{24}H_{37}N + H]^+$.

5.2 Method development: increasing the ion accumulation time

The significant increase in S/N of fragment ions in Figure 79 was achieved through increasing the number of average spectra from 300 to 800. However, this has resulted in increasing the analysis time from 15 min. for AS 300 to 40 min. for AS 800. In this study the increase in ion accumulation time will be explored as an alternative method to increasing the average spectra for improving the S/N of fragment ions. However, increasing the ion accumulation time could cause space charge effect within the ICR cell affecting peak shape, resolution and mass accuracy of fragment ions. Figure 81 shows quadrupole isolation of *m/z* 340 ± 0.5 without using CE. The mass spectra that are shown are expanded at *m/z* at 340.2-340.3. The protonated molecule $[C_{24}H_{37}N + H]^+$ with DBE value of 6.5 is shown. Fragments of this precursor ion were shown earlier in Figure 79 and Figure 80.

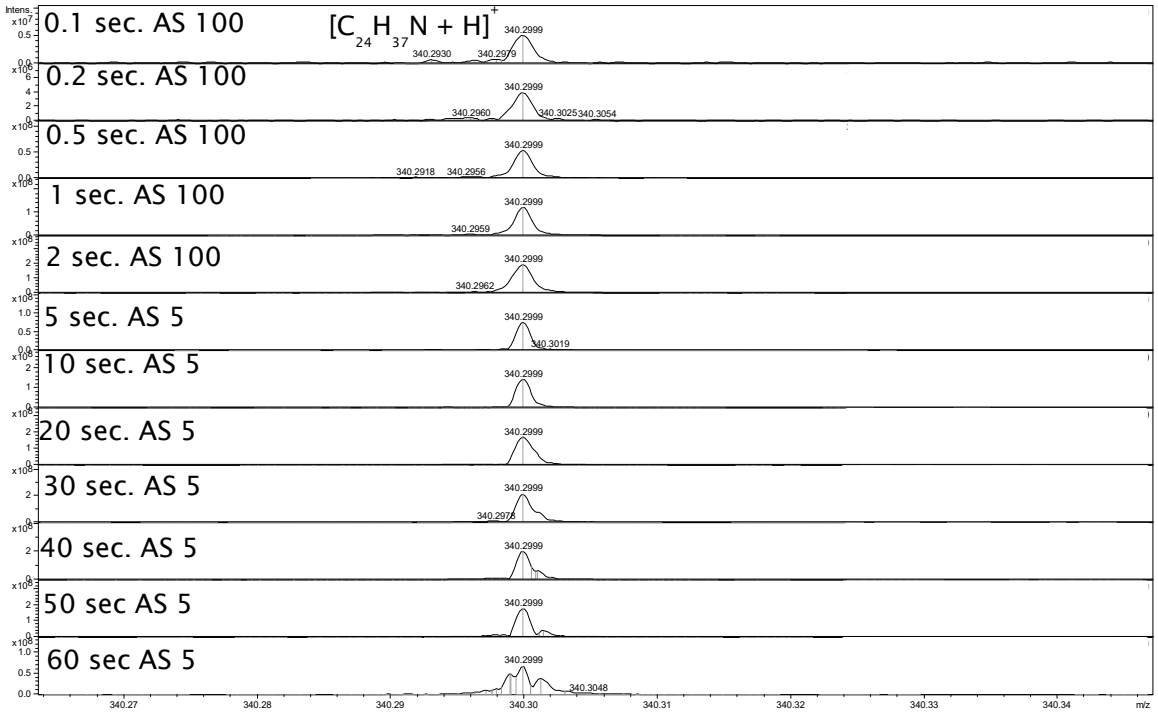

Figure 81 Quadrupole isolation of *m/z* 340 ± 0.5 in crude oil-2 mass spectrum. *m/z* expanded to focus on *m/z* 340.2999. isCID 40 V.

In Figure 81 the mass spectrum at ion accumulation time of 0.1 s and AS 100 has an intensity scale of 10^7. The increase of intensity from 10^7 to 10^8 is achieved through increasing the ion accumulation time from 0.1 s to 0.5 s, 1 s and 2 s with maintaining the number of AS at 100. Further, mass spectra acquired at ion accumulation time of 5 s, 10 s, 20 s, 30 s, 40 s, 50 s and 60 s were all acquired at AS 5 instead of 100 compared to the ion accumulation times of previous mass spectra. From ion accumulation time at 5 s and above there is no need for AS 100 to achieve an intensity of 10^8. AS 5 was enough to achieve an intensity of 10^8 in mass spectra acquired using ion accumulation times above 5 s. While AS 100 was required for mass spectra acquired at ion accumulation time of 0.2 s, 0.5 s, 1 s and 2 s to achieve an intensity of 10^8. Thus there is no need to increase the ion accumulation time above 5 s as there is no significant gain in intensity for the precursor ion at *m/z* 340.2999. Further, the peak shape of *m/z* 340.2999 in mass spectrum at ion accumulation time of 5 s is the least broad compared to *m/z* 340.2999 in other mass spectra with different ion accumulation times. It can be noted that at high ion accumulation time in Figure 81 such as the 60 s ion accumulation time peak splitting is observed at *m/z* 340.2999 in the mass spectrum. This is probably caused by the space charge effect in the ICR cell due to the increase of the ion population. In Figure 82, the *m/z* values for $[C_{25}H_{25}N$ +

$H]^+$ and $[C_{22}H_{29}NS + H]^+$ alter due to the change in ion accumulation times and no internal calibration was used.

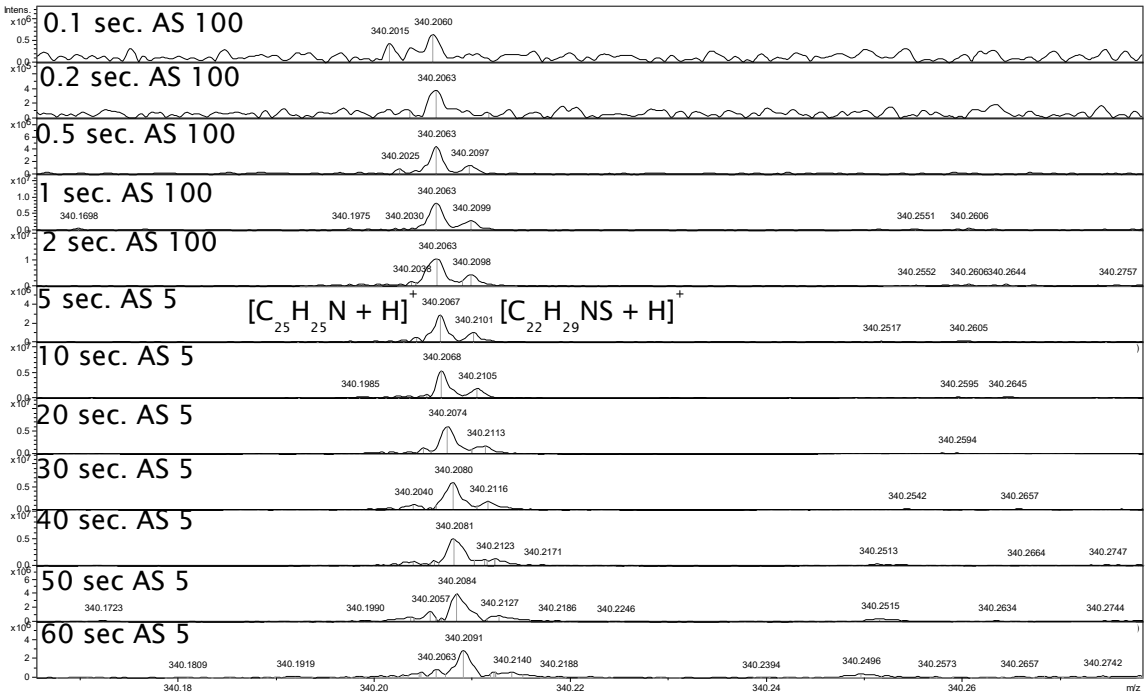

Figure 82 Quadrupole isolation of *m/z* 340 ± 0.5 in crude oil-2 mass spectrum. *m/z* expanded to focus on *m/z* 340.206. isCID 40 V.

Quadruple isolation of *m/z* 340 ± 0.5 in crude oil-2 mass spectrum isolated other precursor ions than *m/z* 340.2999 with elemental formula of $[C_{24}H_{37}N + H]^+$ and DBE value of 6.5, observed in Figure 81 mass spectra. These other precursor ions are $[C_{25}H_{25}N + H]^+$ and $[C_{22}H_{29}NS + H]^+$ with DBE value of 13.5 and 8.5. The *m/z* different between the two precursor ions are at m*m/z* of 3.4. Therefore, increasing the ion accumulation time might affect the resolution of these two isobaric precursor ions. As a result, fragment ions could be miss-assigned. $[C_{25}H_{25}N + H]^+$ and $[C_{22}H_{29}NS + H]^+$ were resolved in quadrupole isolation of *m/z* 340 ± 0.5 in Figure 78 for mass spectrum acquired with ion accumulation time of 50 ms. Fragment ions of these precursor ions were resolved as well in AS 800 product ion mass spectrum in Figure 79. Figure 82 is similar to Figure 81 but the expanded *m/z* is from 340.16 to 340.27. Figure 82 shows that $[C_{25}H_{25}N + H]^+$ and $[C_{22}H_{29}NS + H]^+$ were resolved in mass spectrum acquired at AS 5 with ion accumulation time of 5 s. Ion accumulation time of 5 s could be used to acquire crude oil product ion mass spectra.

In conclusion, an advantage was observed for quadrupole isolation of *m/z* 340 ± 0.5 with ion accumulation time at 5 s. (See Figure 81). The advantage is that the ion intensity of $[C_{24}H_{37}N + H]^+$ in the mass spectrum is at the scale of 10^8 with

average spectra (AS) of 5 and ion accumulation time of 5 s. (See Figure 81). However, an AS of 100 was required to achieve an intensity of 10^8 for $[C_{24}H_{37}N + H]^+$ using ion accumulation times less than 5 s. Further, enough resolution was achieved to distinguish precursor ions that are different by 3.4 m*m/z* units at ion accumulation time of 5 s. Therefore, acquiring product ion mass spectra with ion accumulation time of 5 s should be used. Taking these conclusions into account the ion intensity of fragment ions can be increased significantly through acquiring at ion accumulation time of 5 s with fewer average spectra, significantly decreasing the analysis time.

Figure 79 shows that improvement in S/N for fragment ions were observed in product ion mass spectrum at AS 800 instead of AS 300 but at the expense of increasing the analysis time to 40 min. These product ion mass spectra at AS 300 and 800 were acquired using ion accumulation time of 0.05 s. Figure 83 shows 6 different product ion mass spectra of crude oil-2 at *m/z* 340 ± 0.5 with CE 40 V. In Figure 83 the product ion mass spectrum at AS 800 with ion accumulation time of 0.05 s is shown. The intensity scale of AS 800 product ion mass spectrum is at approximately 2×10^8 (intens.), labelled on the product ion mass spectrum in Figure 83. The aim is to achieve the same level of intensity but at reduced analysis time. Figure 83 shows product ion mass spectra acquired using ion accumulation time at 5 s with AS 10, 15, 20, 30 and 40. The product ion mass spectrum at AS 40 with ion accumulation time of 5 s has an intensity of 3×10^8. This intensity is comparable to the product ion mass spectrum at AS 800 with ion accumulation time of 0.05 s, 2×10^8. However, the analysis time was reduced from 40 min. to 4.5 min. for product ion mass spectrum AS 800 with ion accumulation time of 0.05 s to AS 40 with ion accumulation time of 5 s respectively. (See Figure 83).

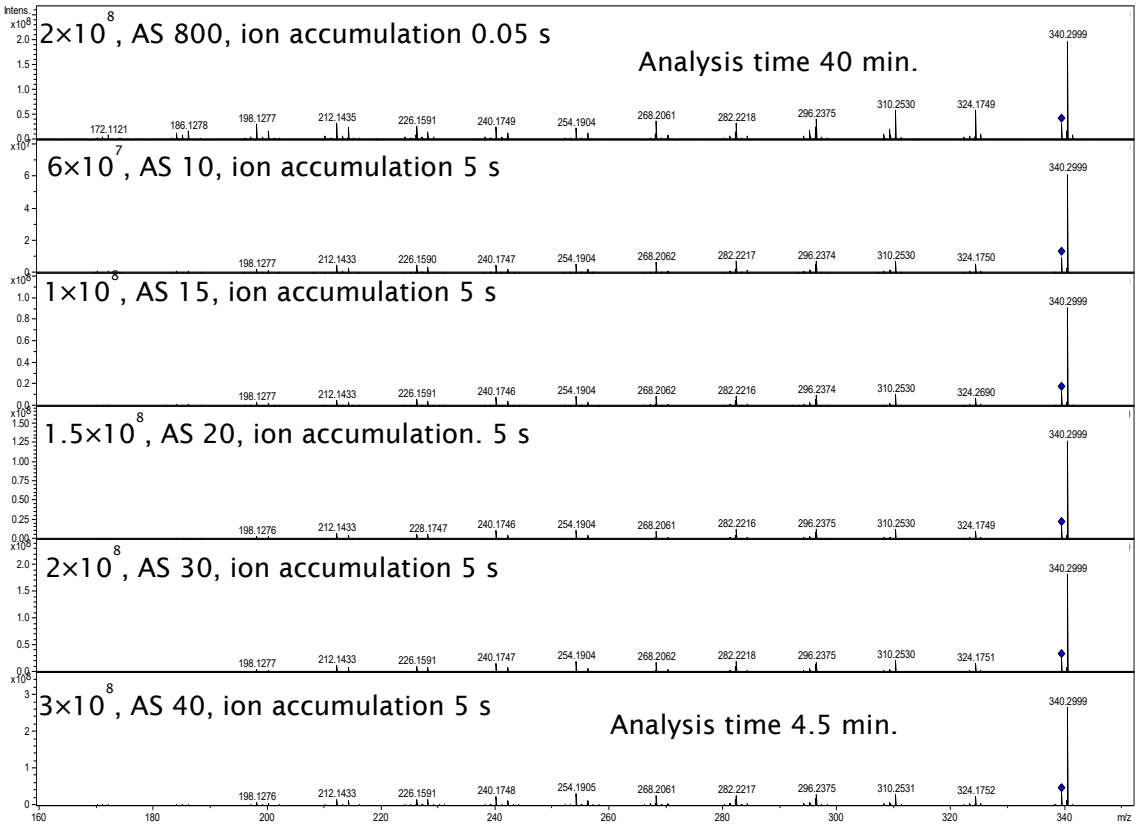

Figure 83 0.5 mg/mL crude oil-2 product ion mass spectra at *m/z* 340 ± 0.5 with CE 40 V. isCID 40 V.

The conclusion around Figure 83 is that ion accumulation time of 5 s and AS 40 should be used for crude oil product ion mass spectra acquisition of CID experiments in positive ion ESI FT-ICR MS/MS. The product ion mass spectra in Figure 83 of AS 800 ion accumulation 0.05 and AS 40 ion accumulation 5 s are at expanded *m/z* from 201.8-229.9 in Figure 84. $C_{15}H_{10}N^+$ fragment ion is observed in product ion mass spectrum at AS 40 with ion accumulation 5 s but are not observed in product ion mass spectrum at AS 800 with ion accumulation 5 s. This provides an additional reason to use ion accumulation time at 5 s with AS 40. This is because not just the analysis was significantly reduced but additionally low intensity fragment ions can be observed in the product ion mass spectrum. The detection of low *m/z* fragment ions which probably have low intensities could be useful in aiding the structure elucidation of the core aromatic molecule of nitrogen containing compounds in crude oils.

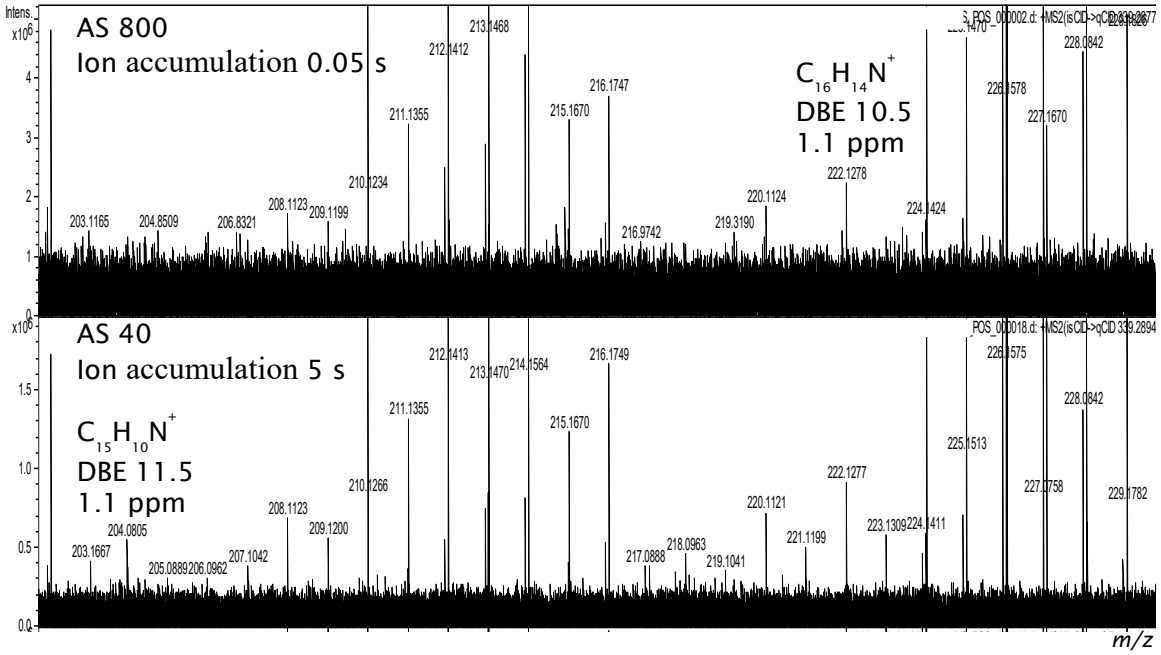

Figure 84 0.5 mg/mL crude oil-2 product ion mass spectra at *m/z* 340 ± 0.5 with CE 40 V. isCID 40 V. Expanded *m/z* 201.8-229.9.

Figure 85 shows two DBE *versus* carbon plots for N_1 fragment ions at quadrupole isolation of *m/z* 340 ± 0.5 with CE 40 V. These plots are used to compare even electron ion fragments for the same precursor ions but for product ion mass spectra acquired using different ion accumulation times and average spectra. The top plot is for product ion mass spectrum acquired using AS 800 with ion accumulation 0.05 s. The bottom plot is for product ion mass spectrum acquired using AS 40 with ion accumulation 5 s. (See Figure 83 for the corresponding product ion mass spectra). The discussion of Figure 84 suggested that low intensity low *m/z* ions could be detected using ion accumulation time at 5 s. This could be useful in aiding the elucidation of the aromatic structure of N_1 containing compounds. In Figure 85 losses of CH_2 for the precursor ion, $[C_{24}H_{37}N + H]^+$, are detected down to carbon number 11 in the plot with ion accumulation 5 s but to carbon number 12 in the plot with ion accumulation at 0.05 s. The fragment ion at carbon 12 has the elemental formula of $C_{12}H_{14}N^+$, different from the precursor ion $[C_{24}H_{37}N + H]^+$ by $(CH_2)_{12}$. Losses of CH_2, having the same DBE value as the precursor ion, are useful because they can be viewed as a delakylation of the precursor ion without introducing a double bond. This will aid in defining the core aromatic structure of the precursor ion.

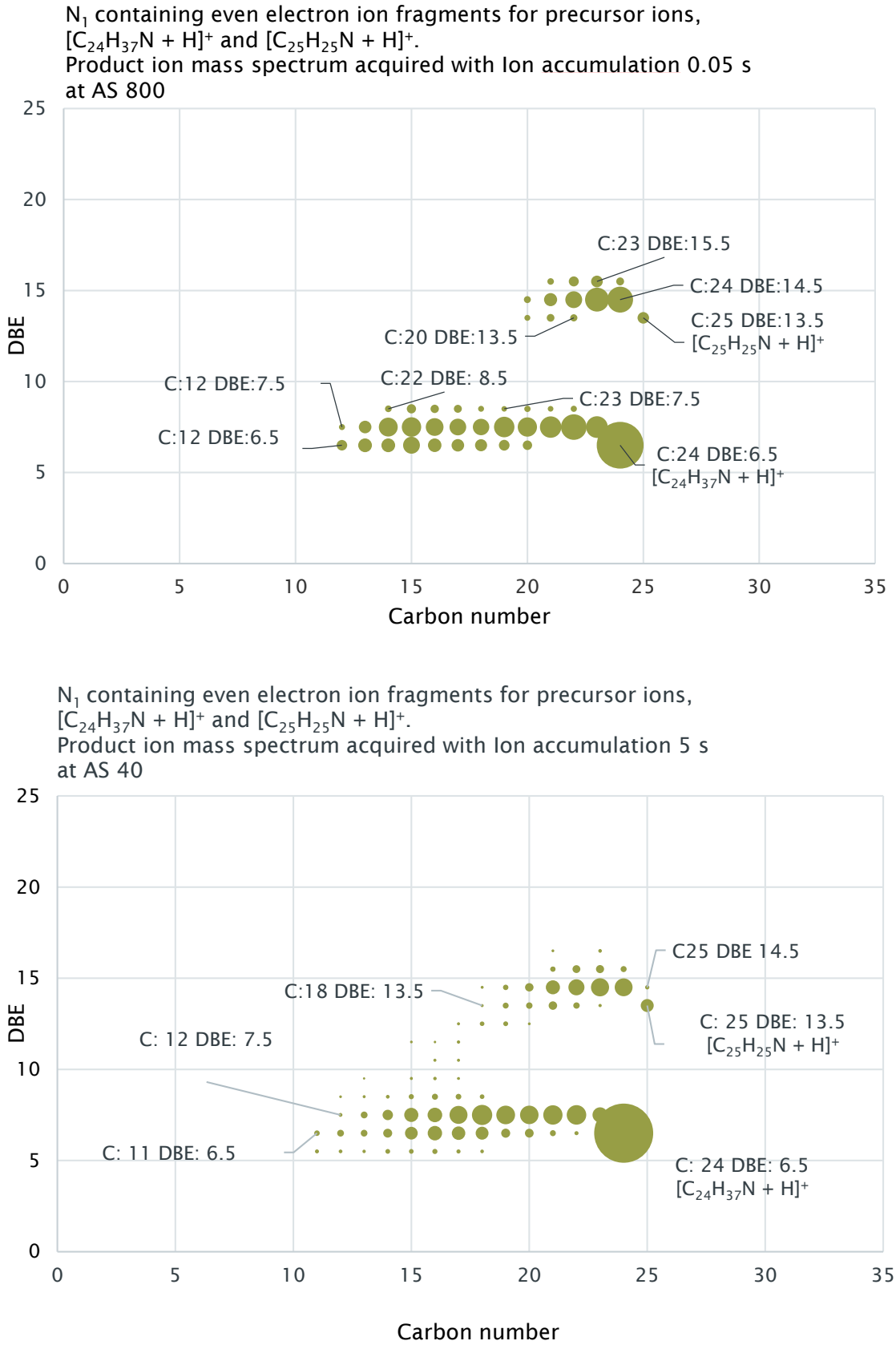

Figure 85 DBE *versus* carbon number plots showing N_1 even electron ion fragments for precursor ions that pass through quadrupole isolation of *m/z* 340 ± 0.5 for crude oil-2 at CE 40 V.

The other N_1 precursor ion in Figure 85 plots, $[C_{25}H_{25}N + H]^+$ at DBE 13.5. The same observation that was made regarding precursor ion $[C_{24}H_{37}N + H]^+$ in Figure 85 is true for precursor ion $[C_{25}H_{25}N + H]^+$. In ion accumulation 0.05 s AS 800 plot CH_2 losses are observed for precursor ion $[C_{25}H_{25}N + H]^+$ down to carbon number 20. (See Figure 85 DBE 13.5). However, for ion accumulation 5 s AS 40 plot CH_2 losses are observed down to carbon number 18. Again these losses of CH_2 can be used to define the core aromatic structure of the precursor ion. The elucidation of the core structure of precursor ions $[C_{24}H_{37}N + H]^+$ and $[C_{25}H_{25}N + H]^+$ at DBE 6.5 and 13.5 respectively will be undertaken in the following sections. Further, structure of different DBEs of N_1 containing compounds will be elucidated using the conclusions made around Figure 85 in the following sections.

5.3 The need for different collision energies for structure elucidation of N_1 precursor ions

Figure 86 shows product ion mass spectra acquired using ion accumulation time 5 s at AS 40 with different CEs. The intensity of the precursor ion $[C_{24}H_{37}N + H]^+$, is observed in product ion mass spectrum at CE 40 V, is significantly reduced at CE 50 V and completely fragmented at CE 60 V. The use of higher collision energy with the optimised positive ion ESI FT-ICR MS/MS method can be useful in revealing structural information. This is specifically true for N_1 containing compounds with higher DBE value such as the precursor ion $[C_{25}H_{25}N + H]^+$ with DBE value of 13.5. This precursor ion passes through the used quadrupole isolation at *m/z* 340 ± 0.5 in Figure 86. The rational for using high CE, at 50 and 60 V, is that precursor ions with high DBE value are more aromatic and hence more stable. Thus, the use of high CE in the collision cell should result in low *m/z* fragment ions in the product ion mass spectrum. These low *m/z* fragments can be in the elucidation of structure of N_1 containing compounds.

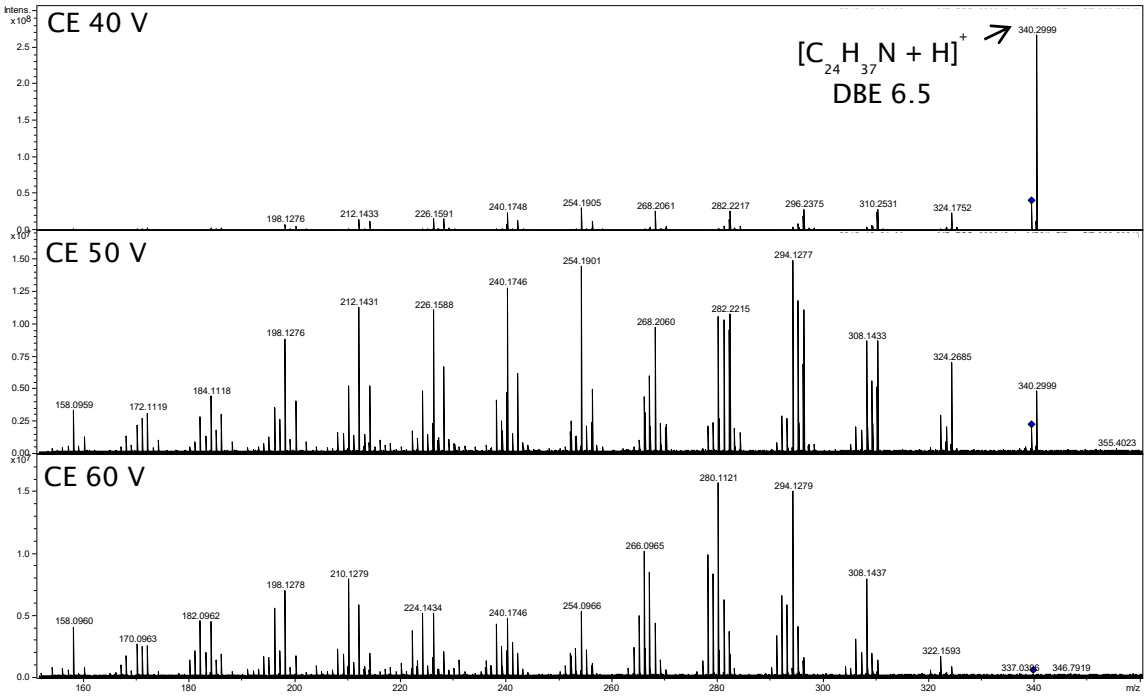

Figure 86 Product ion mass spectra at different CEs for *m/z* 340 ± 0.5 of crude oil-2. Ion accumulation 5 s. AS 40.

N_1 even and odd electron ion fragments that are observed in Figure 86 product ion mass spectra at CE 40 V, 50 V and 60 V, related to precursor ions $[C_{24}H_{37}N + H]^+$ and $[C_{25}H_{25}N + H]^+$, can be plotted using DBE *versus* carbon number plots. Figure 87 shows 3 DBE *versus* carbon number plots at CE 40 V, 50 V and 60 V. In CE 40 V plot even and odd electron ion fragments for two N_1 precursor ions are observed, $[C_{24}H_{37}N + H]^+$ and $[C_{25}H_{25}N + H]^+$. In CE 50 V plot these precursor ions are still observed but at much lower intensity compared to the fragment ions. In CE 60 V precursor ions, $[C_{24}H_{37}N + H]^+$ and $[C_{25}H_{25}N + H]^+$, are completely fragmented due to the use of high CE. In Figure 86 losses of CH_2, $H^{\cdot}$, and 2H are observed for precursor ions $[C_{24}H_{37}N + H]^+$ and $[C_{25}H_{25}N + H]^+$ at DBE value of 6.5 and 13.5 respectively. For precursor ion $[C_{24}H_{37}N + H]^+$ with a DBE value of 6.5 losses of CH_2 are observed at DBE 6.5, the same DBE value as the precursor ion. The lowest CH_2 loss *m/z* fragment is observed in CE 40 V, 50 V and 60 V plots at carbon number 11, different from the precursor ion $[C_{24}H_{37}N + H]^+$ by $(CH_2)_{13}$. Therefore, increasing the CE energy for precursor ion $[C_{24}H_{37}N + H]^+$ with DBE value of 6.5 is not needed. This is because it did not result in observing lower *m/z* fragments. However, the other precursor ion, $[C_{25}H_{25}N + H]^+$ with DBE value of 13.5, the use of high CE at 50 V and 60 V resulted in observing lower *m/z* fragments that are not observed at CE 40 V. In Figure 87 CE 40 V plot the lowest *m/z* fragment for precursor ion $[C_{25}H_{25}N + H]^+$, corresponds to CH_2 losses, is at carbon number 18 which is different from the precursor ion by $(CH_2)_7$. However, at CE 50 and 60 V plots the lowest *m/z* fragment for precursor ion $[C_{25}H_{25}N + H]^+$ is at carbon number 17. This is one less CH_2 loss at DBE 13.5 for precursor ion $[C_{25}H_{25}N + H]^+$ at CE 50 V and 60 V plot compared to CH_2 loss observed in CE 40 V plot. Thus, the identified carbon 17 fragment ion at DBE 13.5, even electron ion fragment of $C_{17}H_{10}N^+$, is closer to the core structure of the precursor ion with a DBE value of 13.5 in CE 50 V and 60 V plots. CH_2 losses form the precursor ion can be viewed as a delakylation of the precursor ion because there is no change in its DBE value.

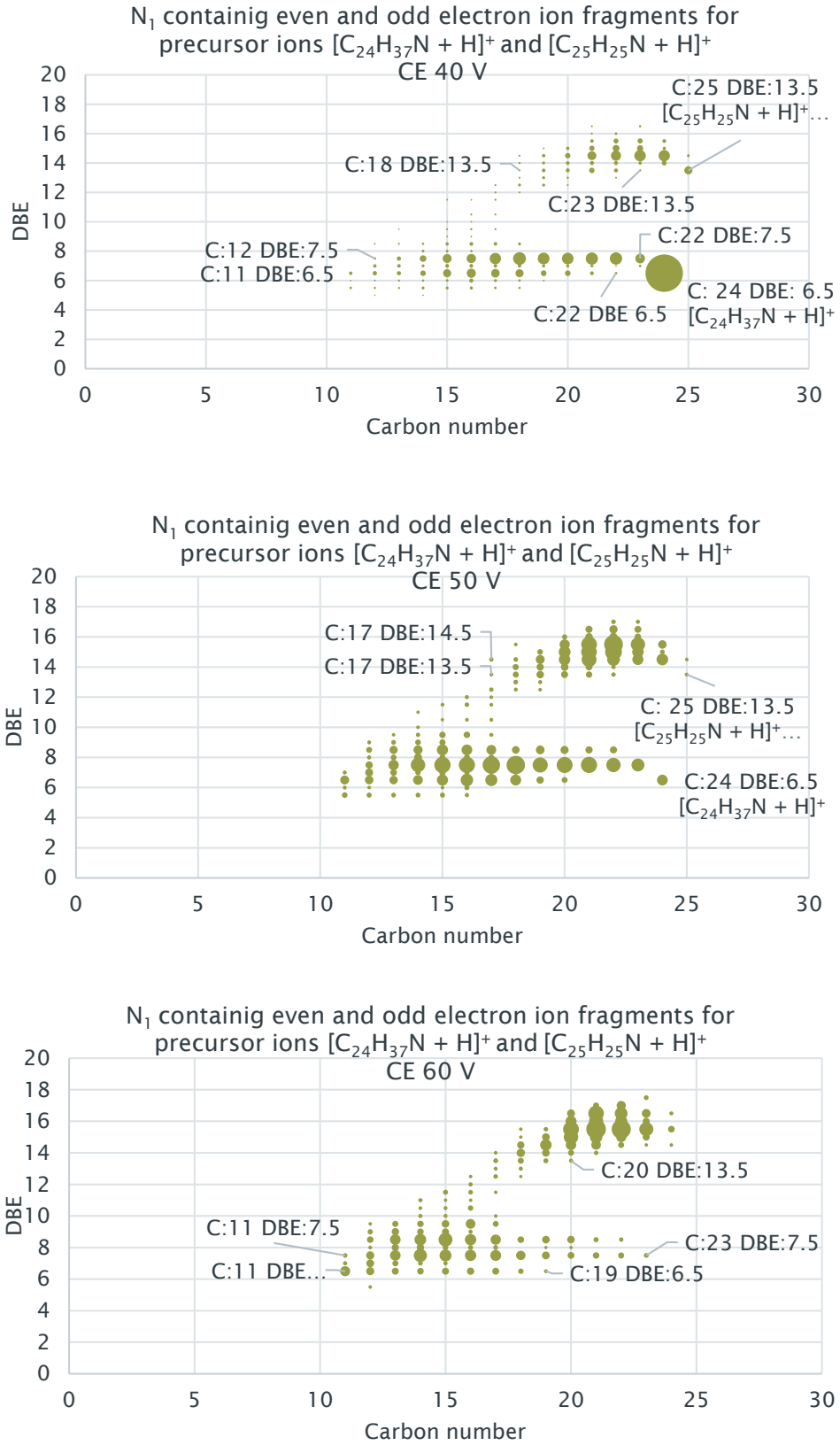

Figure 87 DBE *versus* carbon number plots showing N_1 even and odd electron ion fragments for precursor ions that pass through quadrupole isolation of *m/z* 340 ± 0.5 for crude oil-2.

Figure 87 showed the DBE *versus* carbon number plots for N_1 even and odd electron ion fragments at *m/z* 340 ± 0.5. However, the product ion mass spectra should be presented for fragment ions with low *m/z* values. This is because low *m/z* fragment ions can be used to suggest the core structure of the precursor ion. Figure 88 shows expanded *m/z* for crude oil-2 product ion mass spectra at CE 40 V, 50 V and 60 V. The even electron ion fragment at *m/z* 242.0961 is assigned an elemental formula of $C_{18}H_{12}N^+$ with DBE value of 13.5. This fragment ion is the result of only CH_2 losses from the precursor ion of $[C_{25}H_{25}N + H]^+$ with DBE value of 13.5. The product ion mass spectra show that the intensity of this fragment is higher at increased CE of 50 V and 60 V.

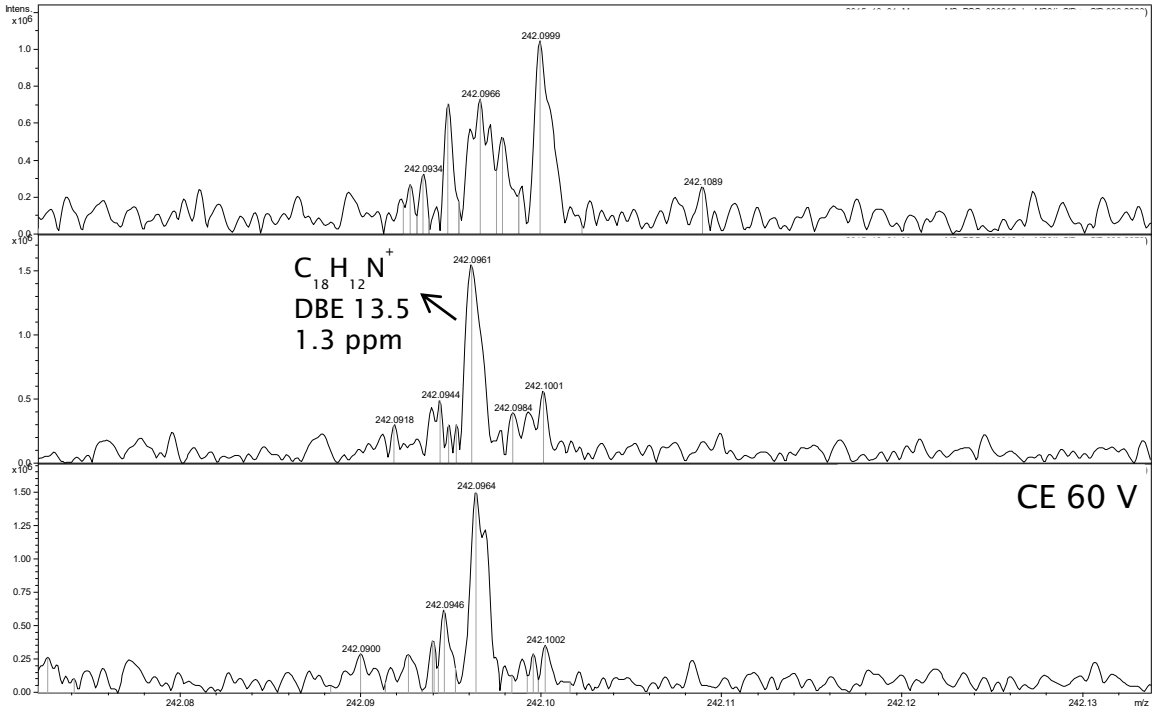

Figure 88 Expanded *m/z* for crude oil-2 product ion mass spectra at different CEs for *m/z* 340 ± 0.5. Ion accumulation 5 s. AS 40.

However, the fragment ion in Figure 88 is not the lowest observed *m/z* fragment in the product ion mass spectra that corresponds to CH_2 losses from precursor ion $[C_{25}H_{25}N + H]^+$. Figure 89 shows even electron ion fragment, $C_{17}H_{10}N^+$, that is probably losses of $(CH_2)_8$ from the precursor ion of $[C_{25}H_{25}N + H]^+$. This fragment ion is only observed in Figure 89 product ion mass spectra at CE 50 V and 60 V. No further CH_2 losses from the precursor ion of $[C_{25}H_{25}N + H]^+$ were observed beyond fragment ion of $C_{17}H_{10}N^+$ in product ion mass spectra of CE 40 V, 50 V and 60 V. This suggests that fragment ion $C_{17}H_{10}N^+$ might corresponds to the dealkylated core aromatic structure of precursor ion $[C_{25}H_{25}N + H]^+$. Two core

structures for this precursor ion are suggested in Figure 89. The alkyl chain, $(CH_2)_8$, for the molecule can be substituted on any position of the aromatic rings.

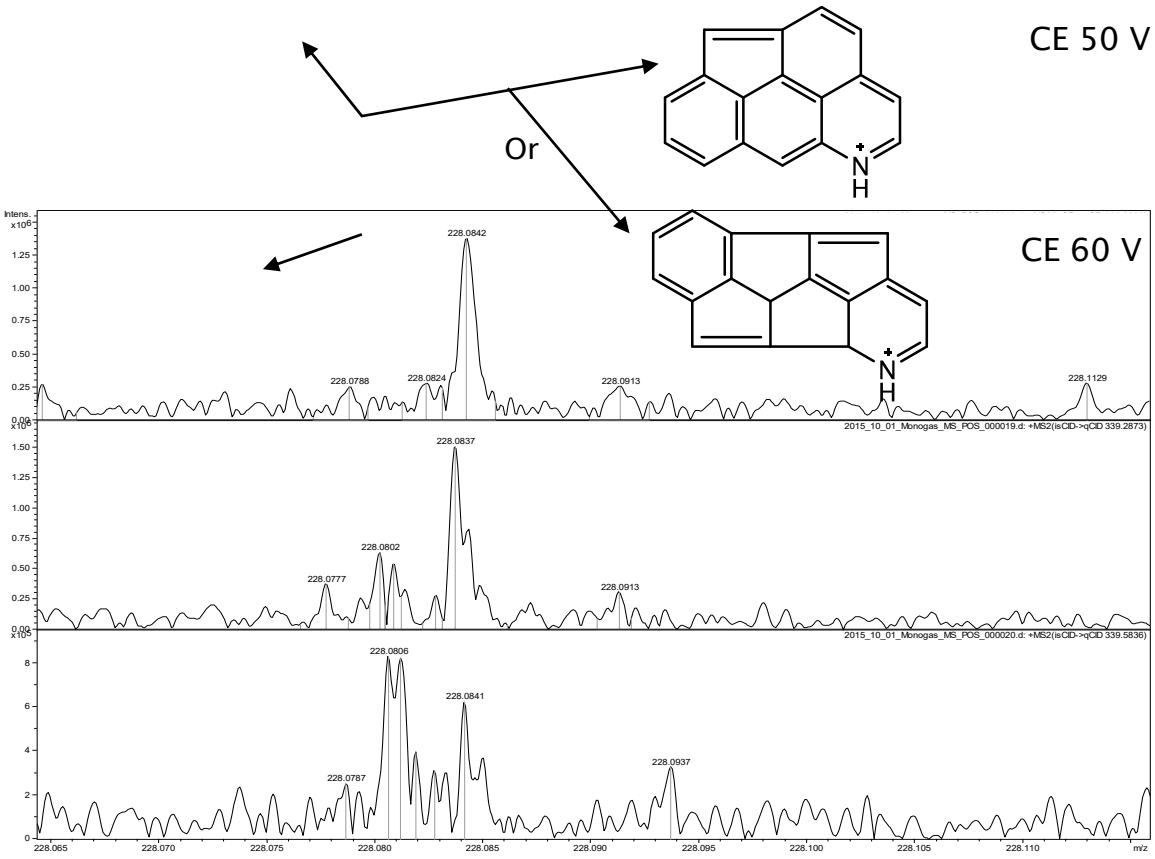

Figure 89 Expanded *m/z* between 228.06 – 228.11 for crude oil-2 product ion mass spectra at different CEs for precursor ion *m/z* 340 ± 0.5. Ion accumulation 5 s. AS 40.

Figure 87 showed even and odd electron ion fragments that are related to precursor ions $[C_{24}H_{37}N + H]^+$ and $[C_{25}H_{25}N + H]^+$. All fragments retained the nitrogen in the structure. The fragments were divided into 3 main categories, loss of CH_2, loss of $H^·$ and loss of 2H. Each change in DBE value which corresponds to $H^·$ and 2H losses are accompanied by horizontal losses of $(CH_2)_n$. However, other losses are observed for precursor ion $[C_{25}H_{25}N + H]^+$ in Figure 86 product ion mass spectra when *m/z* is expanded at certain *m/z* values. Figure 90 shows expanded *m/z* at 254 for crude oil-2 product ion mass spectra at CE of 40 V, 50 V and 60 V. The intensity scale is at 6×10^6 for all product ion mass spectra. The intensity of the even electron ion fragment $C_{19}H_{12}N^+$ with DBE value of 14.5 is significantly

increased in product ion mass spectrum at CE 60 V. The structure of $C_{19}H_{12}N^+$ with DBE value of 14.5 is suggested in Figure 90. This fragment ion is related to the precursor ion $[C_{25}H_{25}N + H]^+$ with a DBE value of 13.5. This means that this fragment ion, $C_{19}H_{12}N^+$, has lost $(CH_2)_6$ and 2H compared to its precursor ion $[C_{25}H_{25}N + H]^+$. The suggested structure for $C_{19}H_{12}N^+$ in Figure 90 has a double bond in the alkyl chain to reflect the loss of 2H from the precursor ion.

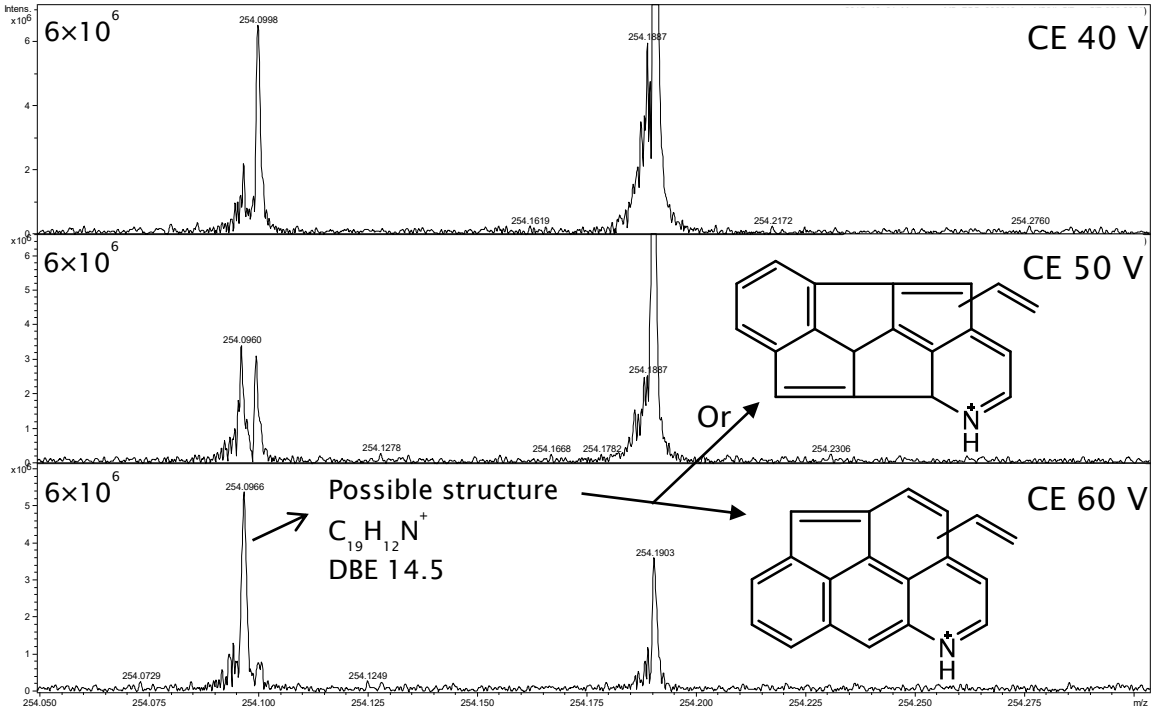

Figure 90 Expanded *m/z* between 254.05 – 254.27 for crude oil-2 product ion mass spectra at CEs 40, 50 and 60 V for precursor ion *m/z* 340 ± 0.5.

Figure 91 shows expanded *m/z* at 227 for crude oil-2 product ion mass spectra, acquired using positive ion ESI FT-ICR MS/MS at *m/z* 340 ± 0.5 with CE 40 V, 50 V and 60 V. *m/z* 227.0858 is only observed at CE 60 V with elemental formula of $C_{18}H_{11}^+$ and DBE value of 13.5. The first observation is that this fragment ion has lost the nitrogen. The hypothesis is that this process of N-expulsion from the aromatic ring is through loss of HCN from fragment ion $C_{19}H_{12}N^+$ in Figure 90 to give fragment ion $C_{18}H_{11}^+$ at CE 60 V. It should be noted that N-expulsion fragment ion, $C_{18}H_{11}^+$, in Figure 91 is only observed in CE 60 V product ion mass spectrum. This is because this fragment ion is related to the precursor ion $[C_{25}H_{25}N + H]^+$

with a DBE value of 13.5. The core structure was suggested for this precursor ion in Figure 89, has 4 six membered aromatic ring and one 5 membered aromatic ring. Thus, a high CE at 60 V was required to observed N-expulsion from the aromatic ring at $C_{18}H_{11}^+$ for precursor ion $[C_{25}H_{25}N + H]^+$. One of the six membered aromatic ring of precursor ion $[C_{25}H_{25}N + H]^+$ was suggested to be pyridine in Figure 89. The suggested N-expulsion from the aromatic ring from $C_{19}H_{12}N^+$ in Figure 90 to $C_{18}H_{11}^+$ in Figure 91 through loss of HCN supports this suggestion.

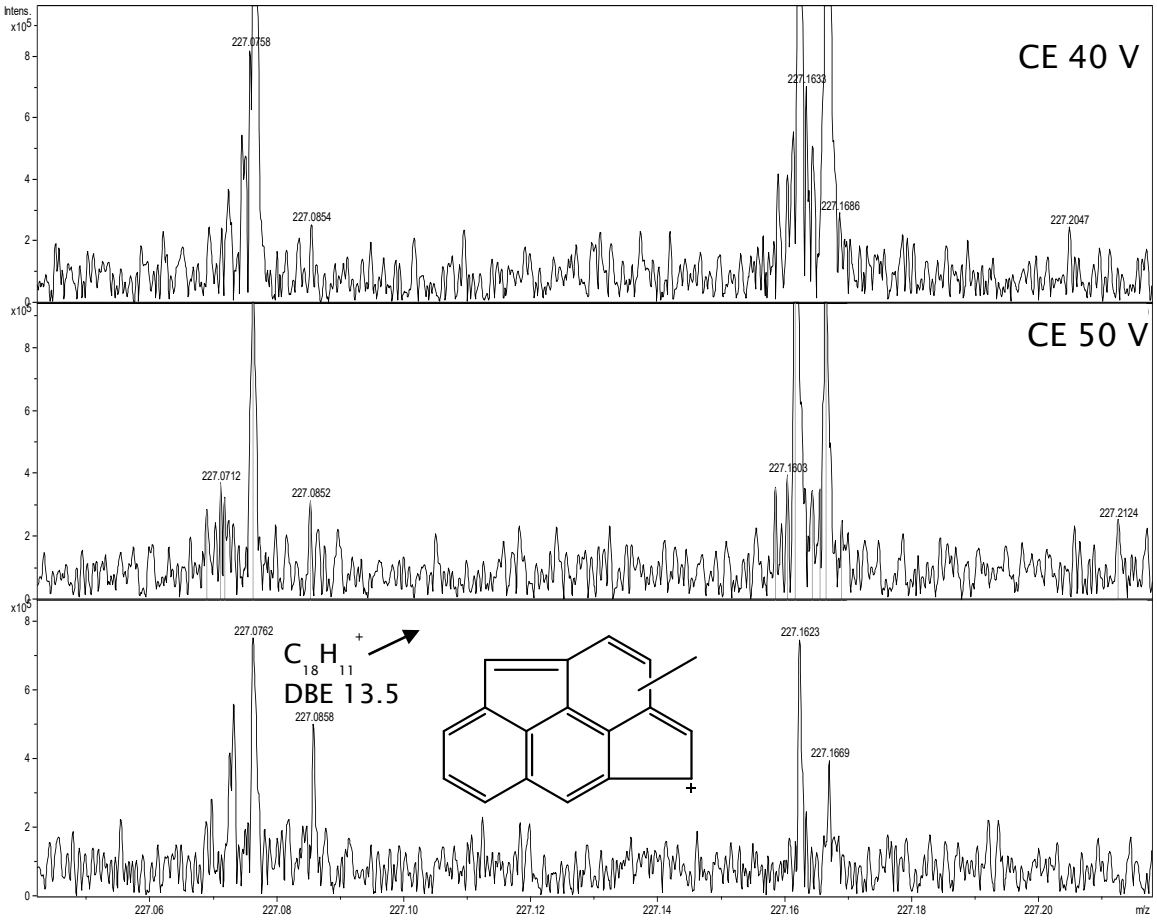

Figure 91 Expanded *m/z* between 227.06 – 227.20 for crude oil-2 product ion mass spectra at different CEs for *m/z* 340 ± 0.5. Ion accumulation 5 s. AS 40.

Not only N-expulsion from the aromatic ring through loss of HCN from $C_{19}H_{12}N^+$ in Figure 90 to $C_{18}H_{11}^+$ in Figure 91 is suggested in product ion mass spectra of precursor ion $[C_{25}H_{25}N + H]^+$. The loss of CH_3CN from $C_{21}H_{14}N^+$ in Figure 92 to give $C_{19}H_{11}^+$ in Figure 93 is as well suggested. The intensity of the fragment ion $C_{21}H_{14}N^+$ is increased with increasing the collision energy from CE 40 V to 60 V. At CE 60 V the fragment ion $C_{21}H_{14}N^+$ is the base peak ion in its product ion mass spectrum. (See Figure 86 product ion mass spectrum at CE 60 V). The structure of fragment

ion $C_{21}H_{14}N^+$ is suggested in Figure 92, related to its precursor ion $[C_{25}H_{25}N + H]^+$. The differences from the precursor ion are losses of CH_2 and the formation of two double bonds through loss of 4H.

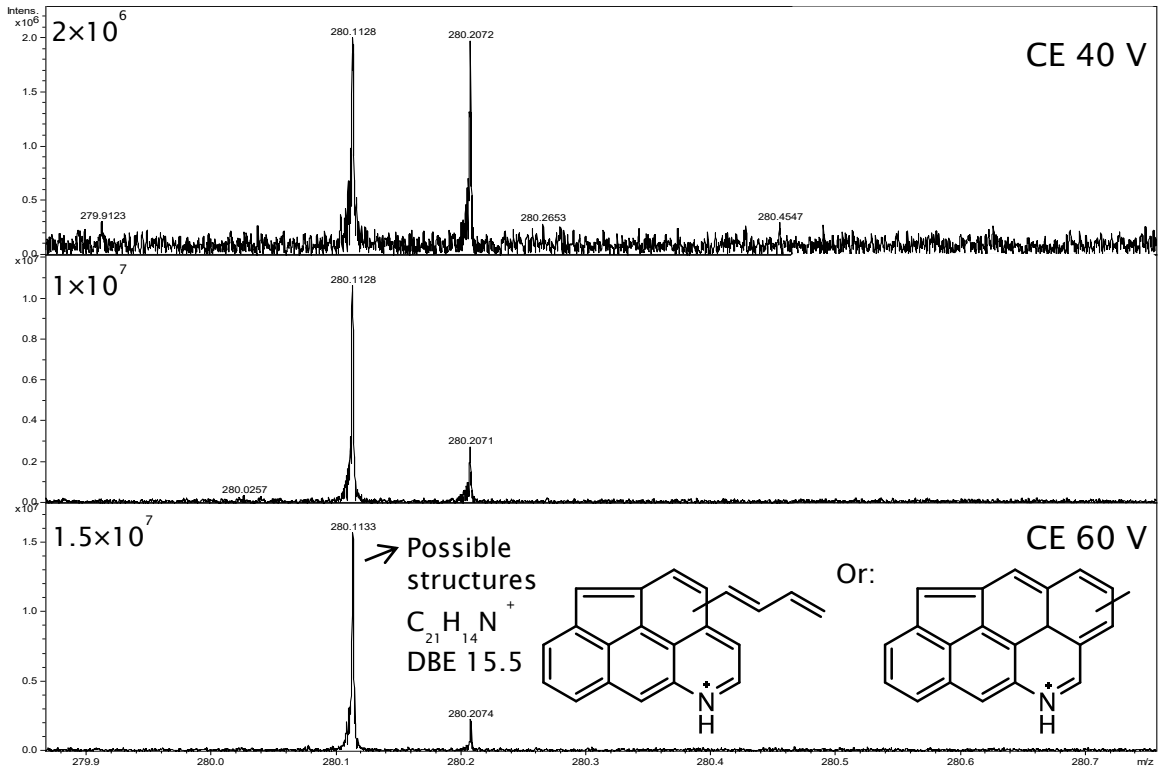

Figure 92 Expanded *m/z* between 279.9 – 280.7 for crude oil-2 product ion mass spectra at different CEs showing $C_{21}H_{14}N^+$ fragment for precursor *m/z* 340 ± 0.5.

The intensity scale of fragment ion $C_{18}H_{11}^+$ in Figure 91 is at ~ 5 × 10^5 and it is only observed in CE 60 V product ion mass spectrum. However, the other N-expulsion fragment ion from the aromatic ring is $C_{19}H_{11}^+$ in Figure 93 with intensity of ~ 1 × 10^6 and ~ 2.5 × 10^6 for CE 50 V and 60 V respectively. The differences in intensity between the two fragment ions, $C_{18}H_{11}^+$ and $C_{19}H_{11}^+$, might be due to the stability of these fragment ions. This suggests that fragment ion $C_{19}H_{11}^+$ with DBE value of 14.5 is more stable compared to fragment ion $C_{18}H_{11}^+$ with a DBE value of 13.5, shown in Figure 93 and Figure 91 respectively. Another reason for differences in ion intensities of $C_{18}H_{11}^+$ and $C_{19}H_{11}^+$ might be related to the intensity of the fragment ion from which the N-expulsion was hypothesised. $C_{18}H_{11}^+$ with intensity of ~ 5 × 10^5 in Figure 91 CE 60 V was suggested to be resulted from loss of HCN from $C_{19}H_{12}N^+$ with intensity of ~ 5 × 10^6 in Figure 90 CE 60 V. However, for $C_{19}H_{11}^+$ with intensity of ~ 2.5 × 10^6 in Figure 93 CE 60 V was suggested to be resulted from loss of CH_3CN from $C_{21}H_{14}N^+$ with intensity of ~ 1.5 × 10^7 in Figure 92 CE 60 V. Thus, the reason behind $C_{19}H_{11}^+$ being more intense

than $C_{18}H_{11}^{+}$ in Figure 91 might be related to the intensity from which the loss of nitrogen had occurred.

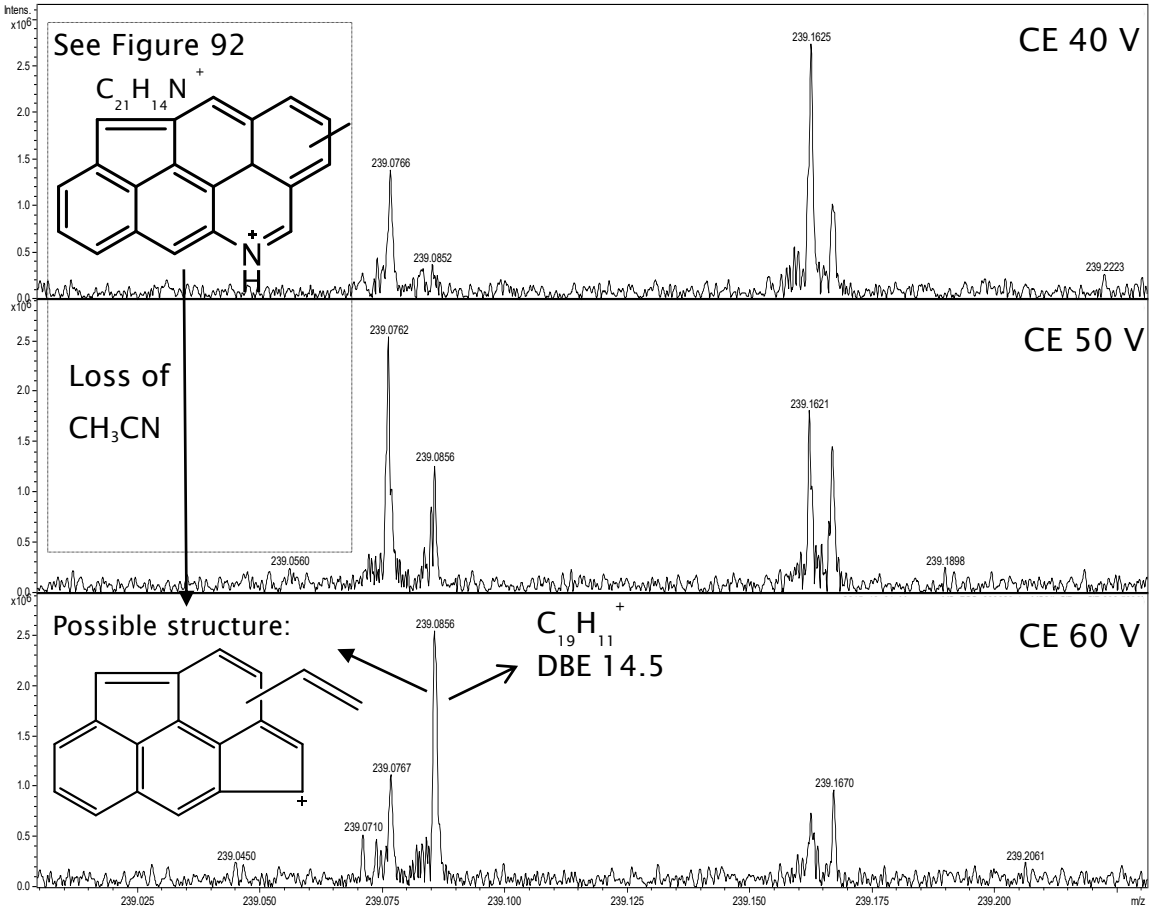

Figure 93 Expanded *m/z* 239.02 – 239.20 for crude oil-2 product ion mass spectra at different CEs for precursor *m/z* 340 ± 0.5 showing N explusion fragment ion, $C_{19}H_{11}^{+}$.

In conclusion, two precursor ions, $[C_{24}H_{37}N + H]^{+}$ and $[C_{25}H_{25}N + H]^{+}$ were isolated at *m/z* 340 ± 0.5 with DBE value of 6.5 and 13.5 respectively. Fragments of precursor ion with DBE of value 6.5 were mentioned but not discussed in details. The discussion of N_1 DBE 6.5 fragments ions is undertaken in the following section at different isolation windows of the homologous series. For the other precursor ion, $[C_{25}H_{25}N + H]^{+}$ with DBE value of 13.5 many conclusions were suggested. First precursor ion with high DBE such as N_1 precursor ion with DBE value of 13.5 value required a high CE at 50 V and 60 V to observe low *m/z* fragments that are used to suggest the core aromatic structure. Further, fragment ions, related to N-expulsion from the aromatic ring were observed at CE 50 V and 60 V but not at CE 40 V for precursor ion $[C_{25}H_{25}N + H]^{+}$ with DBE value of 13.5.

5.4 Homologous series experiment for N_1 precursor ion at DBE 6.5 and 13.5

A tandem MS method in positive ion ESI FT-ICR MS/MS was developed using ion accumulation time of 5 s with AS 40 at an analysis time of 4.5 min. The developed method was used for the purpose of structure elucidation of precursor ions of crude oil-2 at *m/z* 340 ± 0.5. Two precursor ions that are related to the N_1 class were isolated at *m/z* 340 ± 0.5, $[C_{24}H_{37}N + H]^+$ and $[C_{25}H_{25}N + H]^+$ at DBE value of 6.5 and 13.5 respectively. The elucidation of structure for N_1 precursor ion at DBE value of 13.5 and the need for high CE were shown. The structure elucidation of N_1 precursor ion which passes through *m/z* 340 ± 0.5, $[C_{24}H_{37}N + H]^+$ with DBE value of 6.5 will be undertaken in this part.

Each DBE value for the N_1 class has a homologues series. For example, the previously discussed N_1 class precursor ion with DBE of 6.5 that passes through the quadrupole isolation at *m/z* 340 ± 0.5 have a homologous series. In the homologous series each precursor ion is different from the other precursor ion by the exact mass of CH_2. However, it is not clear that these differences in CH_2 in a homologous series are sequential addition of CH_2 on the same alkyl chain or branching of the alkyl chain is occurring. The use of Tandem MS might be useful and offer further clarification on how CH_2 is added in a homologous series. In this study the homologous series of N_1 class of DBE value of 6.5 and 13.5 were investigated from *m/z* 172 to 354. Figure 94 shows 14 overlaid mass spectra of crude oil-2 using quadrupole isolation in positive ion ESI FT-ICR MS. The most intense homologous series of precursor ions identified in the overlaid mass spectra are N_1 precursor ions with DBE of 6.5. The N_1 precursor ions with DBE value of 13.5 are as well isolated but their intensities are less compared to N_1 precursor ions with DBE value of 6.5. Thus, not all precursor ions can be visualised in Figure 94 overlaid mass spectra. However, the homologous series of N_1 precursor ions with DBE value of 13.5 will be discussed as well. Further, the core aromatic structure of N_1 precursor ion with DBE value of 6.5 will be suggested. Please note that the core aromatic structure of N_1 precursor ion with DBE value of 13.5 was suggested in the previous section. In this section all tandem MS experiments were undertaken at only CE 40 V. This is because the purpose of this section is to follow a homologous series. Further there is no need

for high CE with N_1 precursor ion with DBE value of 6.5 to observed low *m/z* fragments.

However, high CE was needed for more aromatic precursor N_1 precursor ion at DBE value of 13.5 where its structure was suggested in the previous section. This is because more aromatic structure is more stable.

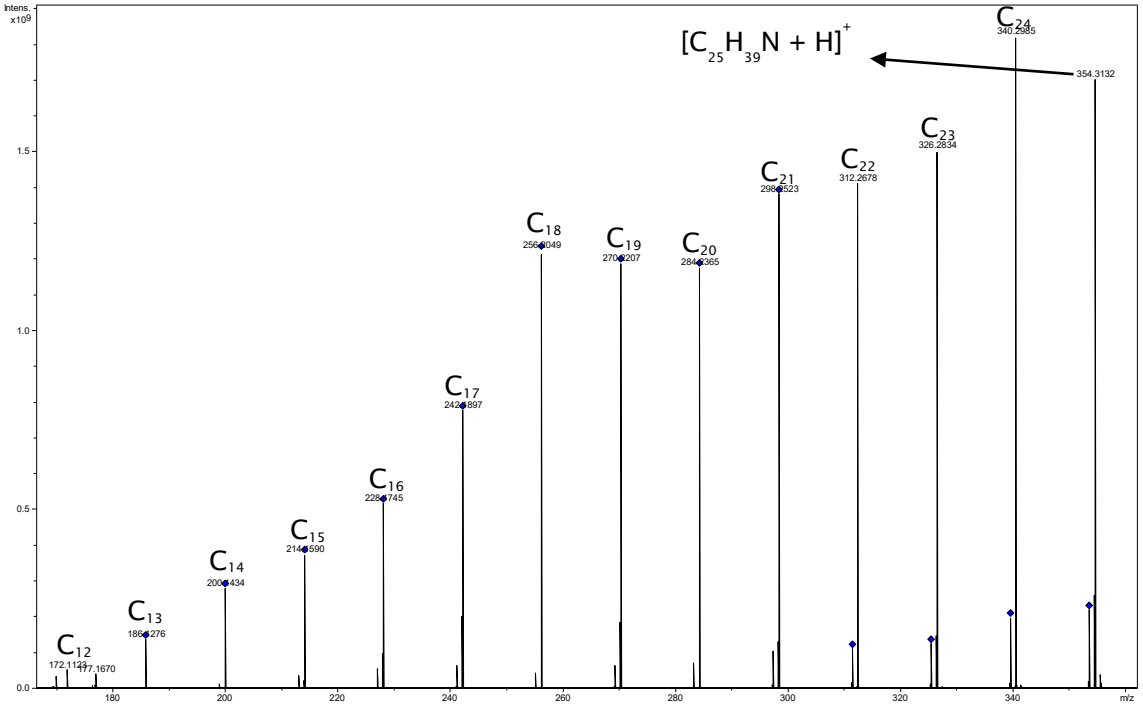

Figure 94 14 mass spectra are overlaid for crude oil-2 using quadrupole isolation at different *m/z* values at isolation window of *m/z* ± 0.5. AS 5, ion accumulation time 5 s, CE 0 V.

In Figure 94 the labelling of homologous series of N_1 precursor ions with DBE value of 6.5 is undertaken as following; at *m/z* 354.3132 the elemental formula is written as protonated molecule $[C_{25}H_{39}N + H]^+$; then the labelling is undertaken using the carbon number for each CH_2 reduction. Thus, at *m/z* 172.1123 labelled as C_{12} corresponds to $[C_{12}H_{13}N + H]^+$ with DBE value of 6.5. For each quadrupole isolation in Figure 94 a product ion mass spectrum was acquired at CE 40 V using CID in positive ion ESI FT-ICR MS/MS.

Figure 95 shows 7 product ion mass spectra from precursor ions isolation at *m/z* 354 to 270. The product ion mass spectra were acquired using CE 40 V in the collision cell. Similar fragment ions were observed at different *m/z* values. The data interpretation will be undertaken using DBE *versus* carbon number plots.

However, first some key observation can be made using the product ion mass spectra at *m/z* expanded of Figure 95 product ion mass spectra.

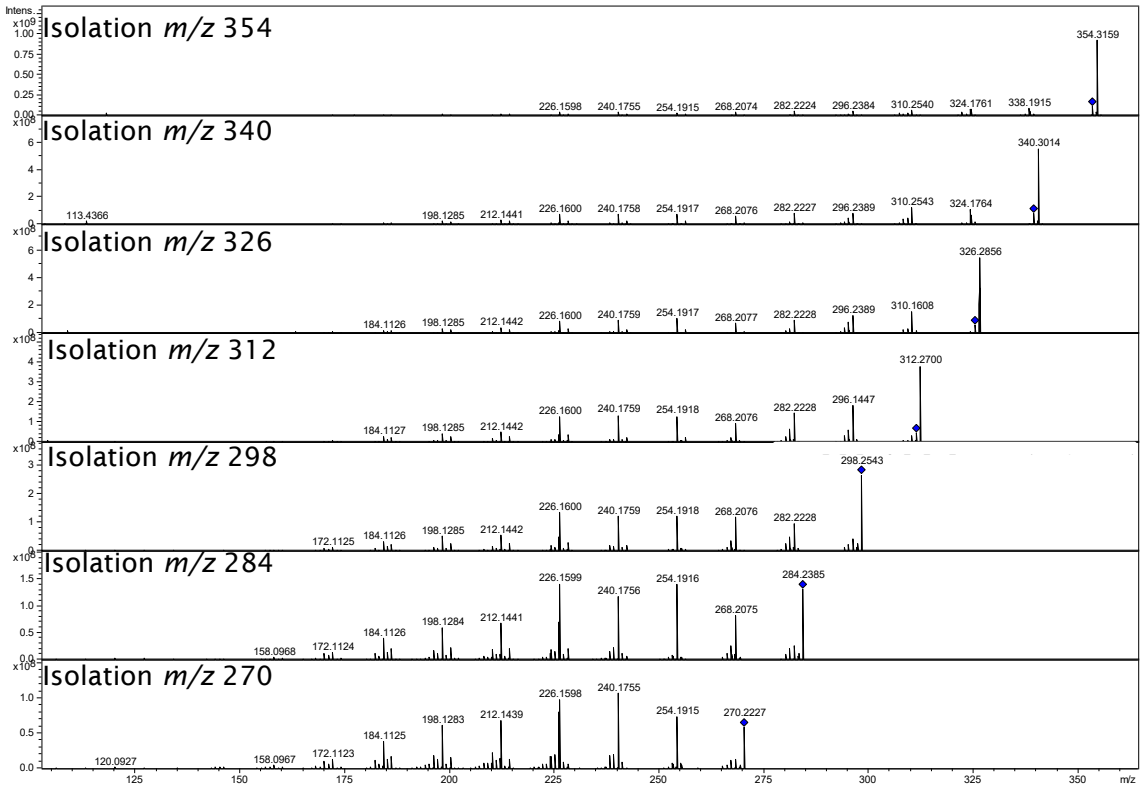

Figure 95 Product ion mass spectra of crude oil-2 at different *m/z* ± 0.5 isolation of precursor ion, CE 40 V, AS 40, ion accumulation time 5 s, isCID 40 V.

Figure 96 is expanded *m/z* of Figure 95 from *m/z* 156.04 - 156.11. Figure 96 shows even electron ion fragment of $C_{11}H_{10}N^+$ at DBE value of 7.5, is different by one DBE from the corresponding precursor ion at DBE 6.5. This suggests the formation of a double bond in the fragment ion at DBE value of 7.5. It should be noted that the fragment ion of $C_{11}H_{10}N^+$ in Figure 96 is the result of losses of different numbers of CH_2 as each precursor ion is different in each product ion mass spectrum by only the number of CH_2. In Figure 96 $C_{11}H_{10}N^+$ has a different intensity in each product ion mass spectrum. $C_{11}H_{10}N^+$ intensity is at ~ 10^5 in product ion mass spectra at isolation of *m/z* 354 and *m/z* 340. This is despite the fact that at this isolation window the intensity of the corresponding precursor ions, $[C_{25}H_{39}N + H]^+$ and $[C_{24}H_{37}N + H]^+$ are the highest compared to other isolated precursor ions in the homologous series. (See Figure 94). The reason can be viewed that to reach fragment ion $C_{11}H_{10}N^+$ the intensity of the precursor ion with more alkylation is consumed with more losses of CH_2, $H^\cdot$ and 2H. But for

precursor ions with less alkylation these losses are less till reaching $C_{11}H_{10}N^+$. This is probably why in Figure 96 $C_{11}H_{10}N^+$ has intensity of ~ 10^6 for *m/z* 326 to 270 product ion mass spectra but intensity of ~ 10^5 for *m/z* 354 and 340. The interest in $C_{11}H_{10}N^+$ is that this fragment ion could lose HCN through N-expulsion from the aromatic ring to give $C_{10}H_9^+$. However, this fragment ion is not observed when *m/z* is expanded at 128.45 – 129.65 for N_1 precursor ions homologous series isolated from *m/z* 354 to 270.

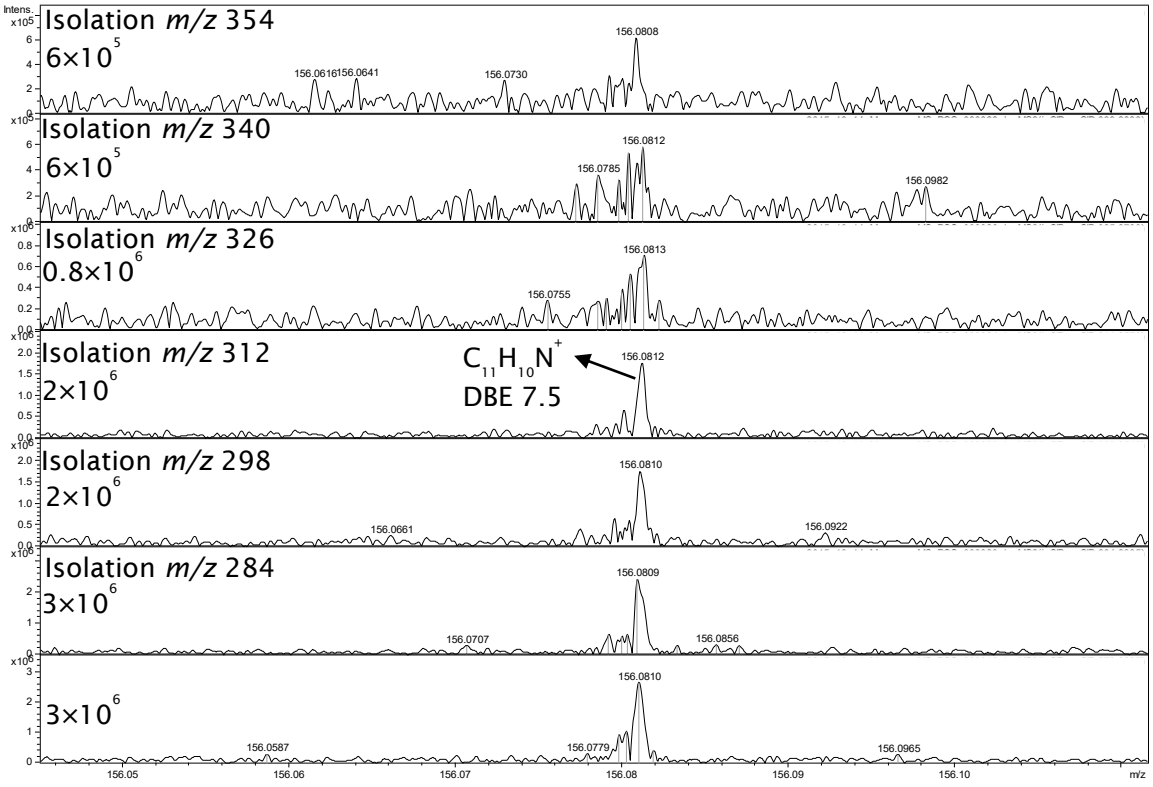

Figure 96 *m/z* is expanded from 156.04 - 156.11 of Figure 95.

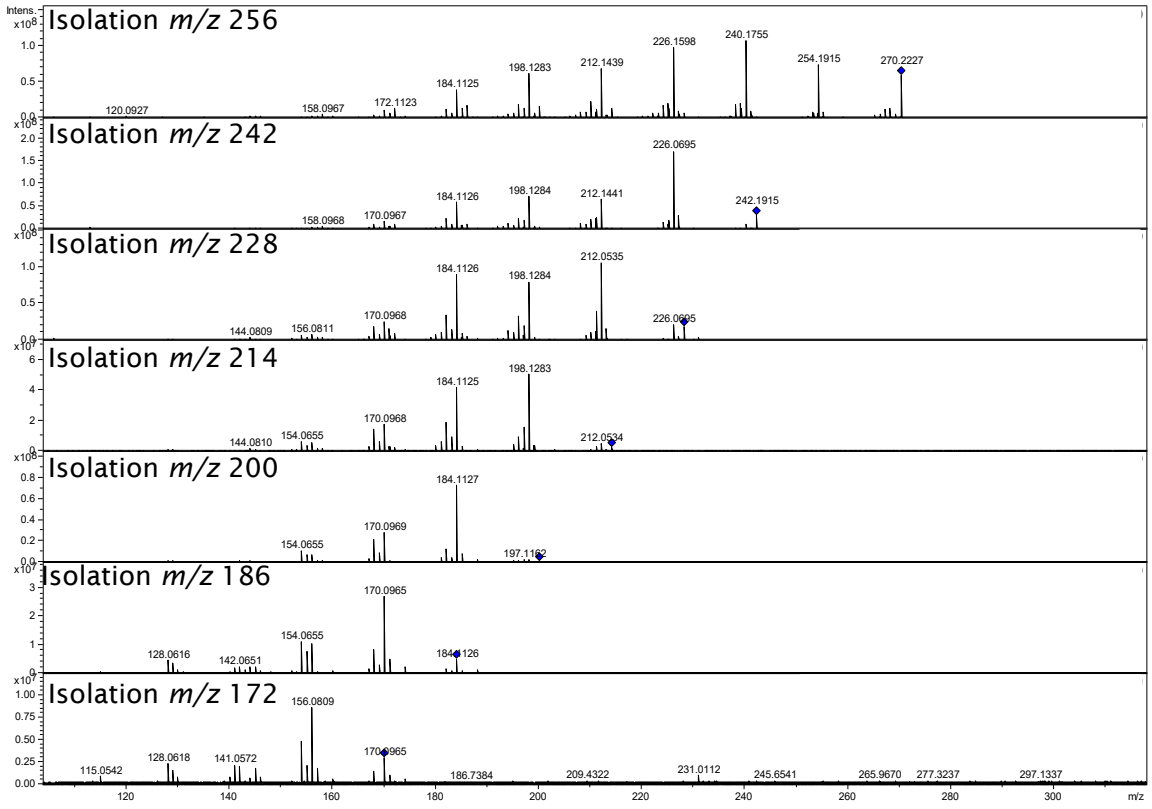

Figure 97 Product ion mass spectra of crude oil-2 from precursor ion *m/z* 256 to 172 in decrement of *m/z* 14 at CE 40 V, AS 40, ion accumulation time 5 s, isCID 40 V.

Figure 97 shows 7 product ion mass spectra from precursor ions isolation at *m/z* 256 to 172. The product ion mass spectra were acquired using CE 40 V in the collision cell. The data interpretation will be undertaken using DBE *versus* carbon number plots at later stage. The discussion around Figure 95 and Figure 96 can be applied to Figure 97, Figure 98 and Figure 99. Even electron ion fragment $C_{11}H_{10}N^+$ is observed in Figure 98 product ion mass spectra and its intensity is increased for precursor ion with less alkylation. This means that the intensity of $C_{11}H_{10}N^+$ is more for precursor ions that pass through the isolation window at *m/z* 200, 186 and 172, has an intensity of ~ 10^7. This despites that these precursor ions which are labelled as C_{14}, C_{13} and C_{12} in Figure 94 are the least intense in the N_1 homologous series at DBE 6.5. As mentioned previously that more alkylated precursor ions have less intense characteristic low *m/z* fragments because the intensity of the precursor ion is consumed with losses of CH_2. The conclusions made using Figure 96 matches those made using Figure 98.

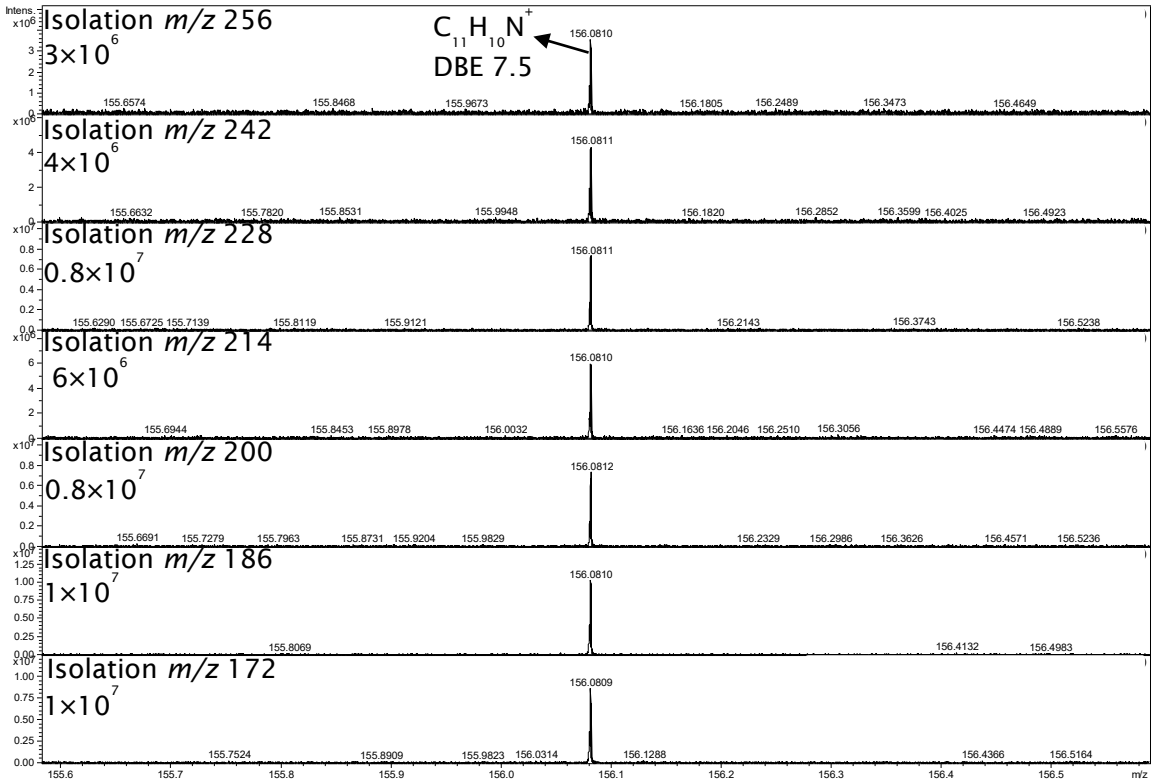

Figure 98 *m/z* is expanded from 155.6 - 156.6 of Figure 97.

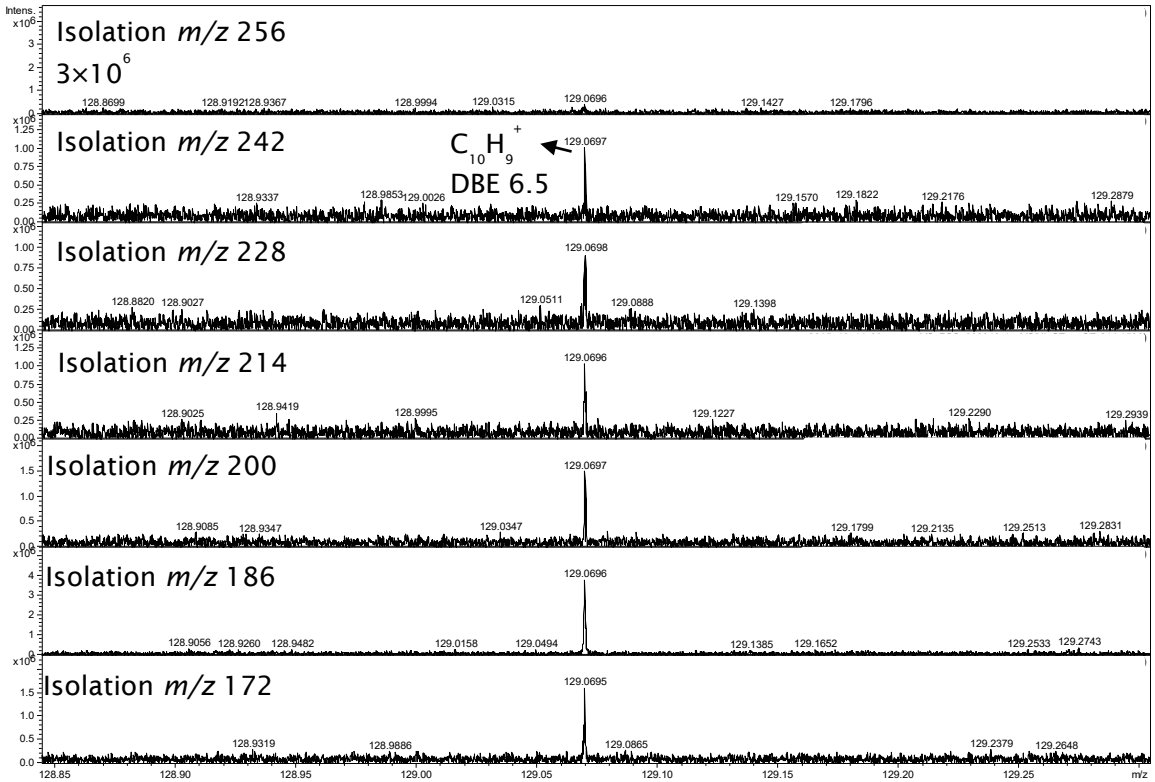

Figure 99 *m/z* is expanded from 128.84 – 129.30 of Figure 97.

The process of N-expulsion from the aromatic ring is suggested through loss of HCN from $C_{11}H_{10}N^+$ in Figure 98 to $C_{10}H_9^+$ in Figure 99. It should be noted that the intensity of $C_{10}H_9^+$ is significantly increased for *m/z* 242 to 172 product ion mass spectra compared to *m/z* 256. (See Figure 99). The increase in intensity of $C_{10}H_9^+$ could be related to the intensity from which HCN loss is suggested, $C_{11}H_{10}N^+$ in Figure 98. $C_{11}H_{10}N^+$ has a higher intensity for precursor ions with less alkylation. $C_{10}H_9^+$ fragment could be as well coming directly from the precursor ion. In CID experiment fragment ions could be from the precursor ion and/or fragments of fragments. In this case the data is suggesting that the main route for N-expulsion is through fragments of fragments. This is because $C_{10}H_9^+$ was not observed for N_1 DBE 6.5 precursor ions of homologous series isolated from *m/z* 354 to 270. This is despite that the corresponding precursor ions are the most intense in the N_1 homologous series of precursor ions with DBE value of 6.5. (See Figure 94). Further, the intensity of $C_{11}H_{10}N^+$ in Figure 96 is on the scale of 10^6 but in Figure 98 is on the scale of 10^7 for corresponding precursor ions with less alkylation. Thus, $C_{10}H_9^+$ was only observed in Figure 99 where $C_{11}H_{10}N^+$ had higher intensity of 10^7 in Figure 98 for precursors ions from C_{12} to C_{17}. C_{12} precursor ion corresponds to $[C_{12}H_{13}N + H]^+$ with DBE value of 6.5.

In conclusion, the approach used to observe low *m/z* characteristic fragments for N_1 precursor ion with DBE value of 6.5 was different from N_1 precursor ion with DBE value of 13.5. To clarify, at quadrupole isolation of *m/z* 340 ± 0.5 both N_1 precursor ions at DBE 6.5 and 13.5 were isolated. However, at quadrupole isolation of *m/z* 340 ± 0.5, N_1 precursor ion at DBE 13.5 is less alkylated and more aromatic compared to N_1 precursor ion at DBE 6.5. Thus, there are fewer CH_2 losses to reach the core aromatic structure for N_1 precursor ion at DBE 13.5 compared to N_1 precursor ion with DBE value of 6.5.

Low *m/z* fragment ions such as N-expulsion were not observed for N_1 DBE 6.5 precursor ion isolated at *m/z* 340 ± 0.5 with CE at 40 V. This is probably because the isolated precursor ion has a long alkyl where many CH_2 losses are occurring until reaching the fragment ion from where N is expulsed from the ring. However, low *m/z* fragment ions such as N expulsion can be observed for N_1 DBE 6.5 precursor ion if the isolation of the precursor ion was undertaken at low *m/z* value in the homologous series which has reduced number of alkyl chains such as *m/z* 172 ± 0.5 instead of *m/z* 340 ± 0.5.

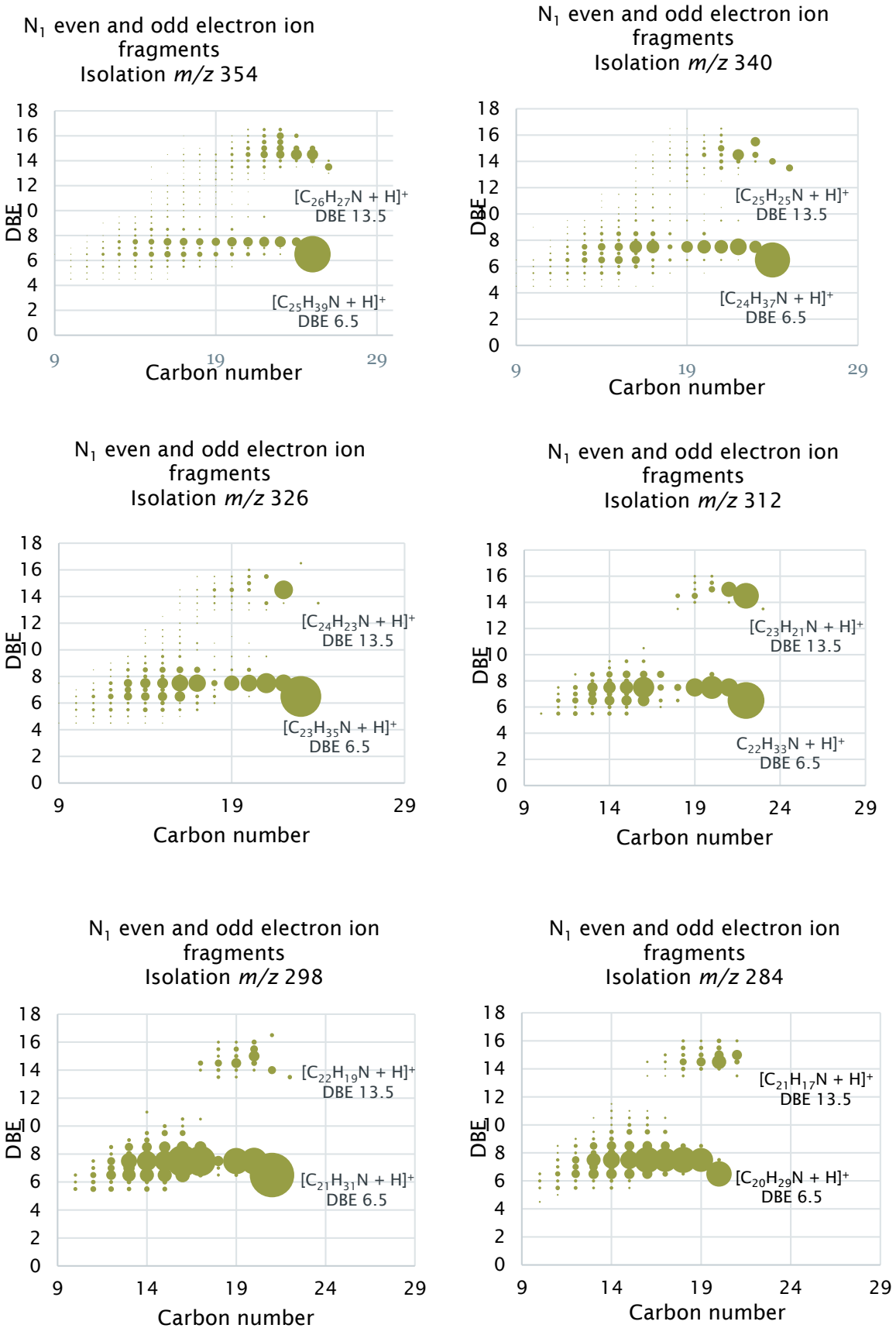

Figure 100 Fragment ions for N_1 precursor ions at DBE 6.5 and 13.5 are plotted for crude oil-2 at CE 40 V using DBE *versus* carbon number plots.

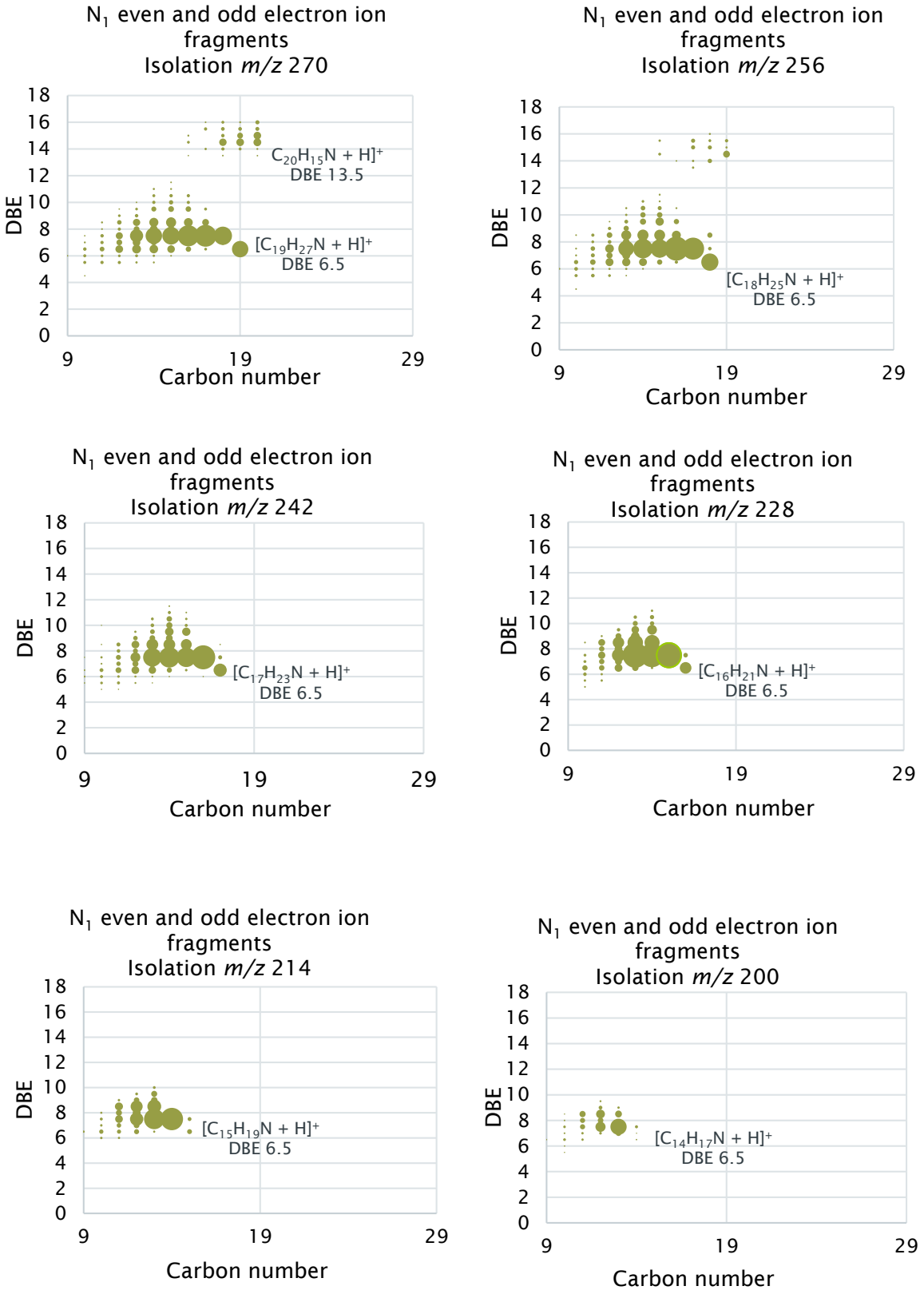

Figure 101 Fragment ions for N_1 precursor ions at DBE 6.5 and 13.5 from *m/z* 270 to 200 in decrement of CH_2, *m/z* 14 are plotted for crude oil-2 at CE 40 V using DBE *versus* carbon number plots.

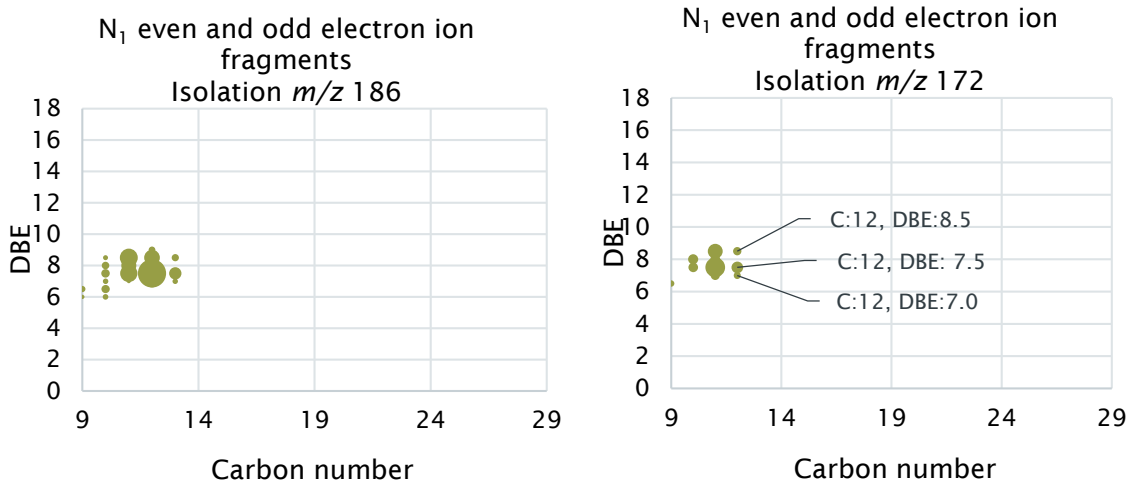

Figure 102 Fragment ions for N_1 precursor ion at DBE 6.5 is plotted for crude oil-2 at CE 40 V using DBE *versus* carbon number plots.

N_1 even and odd electron ion fragments in product ion mass spectra of Figure 95 and Figure 97 are plotted using DBE *versus* carbon number plots in Figure 100, Figure 101 and Figure 102. Two N_1 precursor ions of the same nominal mass are observed in Figure 100 DBE *versus* carbon number plot at quadrupole isolation of *m/z* 354, $[C_{25}H_{39}N + H]^+$ at DBE 6.5 and $[C_{26}H_{27}N + H]^+$ at DBE 13.5. Fragment ions that are related to these precursor ions were previously discussed in details. However, these fragment ions are mainly CH_2, $H^\cdot$ and 2H losses. In Figure 100, the next plot is DBE *versus* carbon number of *m/z* 340 which is different from the previous plot *m/z* 354 plot by CH_2. Thus, the N_1 precursor ions that are observed in *m/z* 340 plot are one CH_2 less compared with N_1 precursor ions in *m/z* 354 plot. Further, the fragment ions that are observed for N_1 precursor ions in *m/z* 340 plot are different from *m/z* 354 plot by one CH_2. This observation extends to all plots in Figure 100 where the difference between plots are in the number of CH_2 of the isolated precursor ions. The data in Figure 100, Figure 101 and Figure 102 suggest that the CH_2 is added to N_1 DBE 6.5 and 13.5 precursor ions sequentially on the alkyl chain. However, in Figure 100 uneven intensities are observed within the homologous series of CH_2 fragment ions and these could be attributed of multiple R groups on the aromatic structure. N_1 even and odd electron ion fragments for N_1 precursor ion at DBE 13.5 is observed till isolation *m/z* 256 DBE *versus* carbon number plot. (See Figure 101). In *m/z* 242 plot no fragment ions are observed for N_1 precursor ion at DBE value for 13.5. From *m/z* 242 plot and onward fragment ions are only observed for N_1 precursor ion with DBE value of 6.5. (See Figure 101). In the quadrupole isolation at *m/z* 242 ± 0.5

no N_1 precursor ion at DBE of 13.5 was observed. (See Figure 94). This can be due to that the starting point of N_1 homologous series with DBE of 13.5 is at *m/z* 256. Further, it could be that there is N_1 precursor ion with DBE 13.5 at *m/z* 242 but its signal intensity is below S/N ratio of 3:1. Regardless of the reason the resulted product ions mass spectra from quadrupole isolation at *m/z* 242 ± 0.5 and onward is simpler due to the presence of N_1 fragment ions that is related to one N_1 precursor ion, N_1 precursor ion with DBE value of 6.5. Thus, the confidence in the assignment of fragment ions that is related to N_1 precursor ion with DBE value of 6.5 is increased.

The MS/MS data in Figure 100, Figure 101 and Figure 102 suggest that the alkyl chain for the different N_1 precursor ions with DBE value of 6.5 and 13.5 could be straight chains. This is because fragment ions that corresponds to CH_2 losses are sequential. Further, the presence of isomers should be considered. The fragmentation of N_1 precursor ions involve the loss of CH_2, $H^{\cdot}$ and 2H. (See Figure 100). Thus, isolating the precursor ion with the same DBE value but at lower degree of alkylation results in simpler product ion mass spectra as there are fewer losses of CH_2, $H^{\cdot}$ and 2H. (See Figure 102 for N_1 fragment ions for N_1 precursor ion at DBE 6.5). Further, characteristic fragment ions such as N expulsion and the dealkylated molecule were observed for N_1 precursor ion with DBE value of 6.5 with less degree of alkylation such as at quadrupole isolation *m/z* 172 ± 0.5.

Figure 103 shows quadrupole isolation at *m/z* 172 ± 0.5 of crude oil-2 using positive ion ESI FT-ICR MS. Only one N_1 precursor ion at DBE 6.5 is isolated at *m/z* 172 ± 0.5, $[C_{12}H_{13}N + H]^+$. This will result in a simpler product ion mass spectrum as can be observed in Figure 104. This is because at isolation of *m/z* 172 ± 0.5 the N_1 precursor ion with a DBE value of 6.5 has an alkyl chain length of $CH_3(CH_2)_2$ which results in fewer CH_2 losses across the different DBE losses of 2H and $H^{\cdot}$. This can be clearly observed when comparing fragment ions of N_1 precursor ion at DBE 6.5 in *m/z* 172 DBE *versus* carbon number plot in Figure 102 against *m/z* 354 plot in Figure 100.

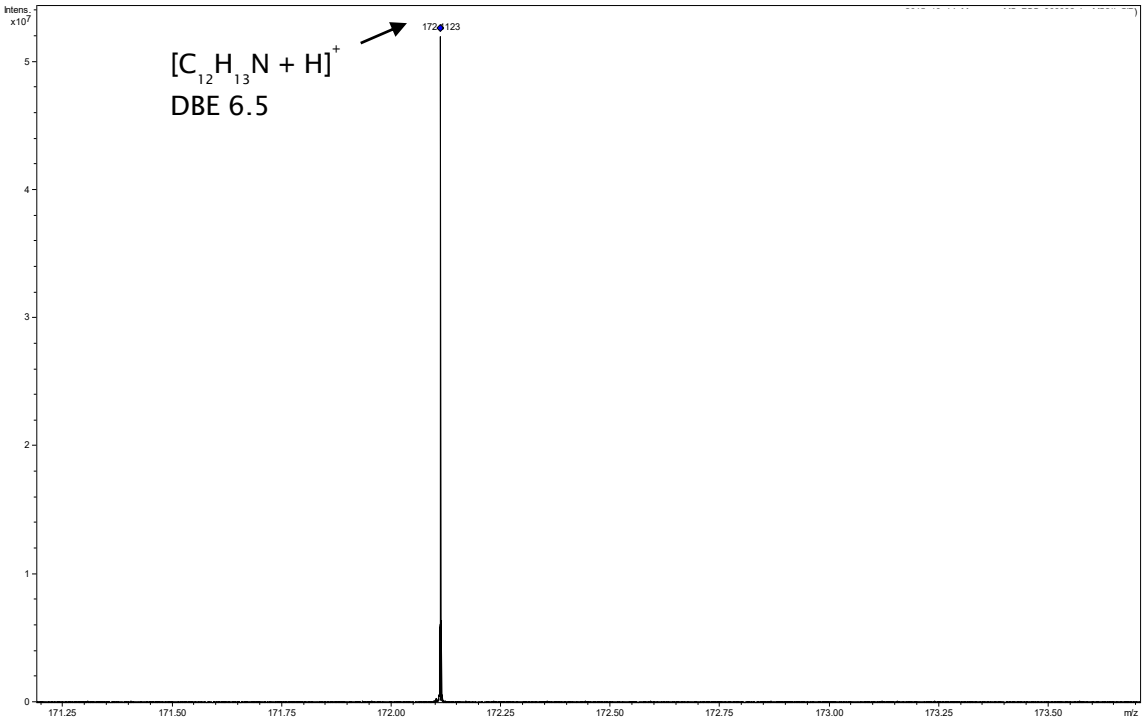

Figure 103 Quadrupole isolation of precursor ion nominal *m/z* 172 ± 0.5 for 0.5 mg/mL crude oil-2. AS 5, CE 0 V. Expanded *m/z* 171.2-173.6.

Figure 104 shows the product ion mass spectrum for quadrupole isolation at nominal *m/z* 172 ± 0.5 with CE at 40 V. The precursor ion that was observed at this isolation window in Figure 103 at *m/z* 172.1123 with elemental formula of $[C_{12}H_{13}N + H]^+$ is completely fragmented in the product ion mass spectrum at CE 40 V in Figure 104. The first observed fragment ion in the product ion mass spectrum in Figure 104 is an odd electron ion fragment with elemental formula of $C_{12}H_{13}N^{+\cdot}$. This fragment ion is the result of loss of $H^{\cdot}$ from the precursor ion which makes its DBE value at 7. Subsequent loss of CH_2 is observed in the product ion mass spectrum at the same DBE value of 7. This fragment ion is observed at $C_{11}H_{11}N^{+\cdot}$ which is the result of CH_2 loss from fragment ion $C_{12}H_{13}N^{+\cdot}$ and/or results directly from the precursor ion, $[C_{12}H_{13}N + H]^+$. Loss of 2H from precursor ion $[C_{12}H_{13}N + H]^+$ is observed in the product ion mass spectrum in Figure 104 at $C_{12}H_{12}N^+$ with DBE value of 7.5. $C_{12}H_{12}N^+$ can be as well originate from loss of $H^{\cdot}$ from $C_{12}H_{13}N^{+\cdot}$ fragment ion. $C_{12}H_{12}N^+$ has a DBE value of 7.5, different from precursor ion $[C_{12}H_{13}N + H]^+$ with DBE value of 6.5 by one DBE. This indicates that in $C_{12}H_{12}N^+$ a double bond was formed which is probably on the alkyl chain or a ring. (See the suggested structure for $C_{12}H_{12}N^+$ in Figure 104). $C_{12}H_{12}N^+$ could lose CH_2 to give $C_{11}H_{10}N^+$, the base peak ion in the product ion mass spectrum. $C_{11}H_{10}N^+$ fragment ion could as well originate directly from the precursor ion $[C_{12}H_{13}N + H]^+$

or from $C_{12}H_{13}N^{+\cdot}$ fragment ion by loss of $H^{\cdot}$ and CH_2. (See Figure 105 for schematic representation of fragment ions for precursor ion $[C_{12}H_{13}N + H]^+$)

The discussion around N_1 fragment ions with DBE value of 7 and 7.5 can be extended to other fragment ions that are observed in the product ion mass spectrum in Figure 104, fragment ions with DBE value of 8 and 8.5. Further, the discussion can be extended to fragment ions for other precursor ions such as N_1 with DBE of 13.5 that its fragment ions are observed in Figure 100 and Figure 101. This is because similar losses are observed which are losses of CH_2 which have the same DBE value as the precursor ion, losses of $H^{\cdot}$ and losses of 2H. For each loss that results in change of DBE value, loss of $H^{\cdot}$ or 2H, of the fragment ions there are losses of CH_2 for this DBE value. Not all fragment ions that are observed in Figure 104 are characteristic fragment ions. Characteristic fragment ions can be used to suggest the core aromatic structure of the molecule as the remainder is the alkyl chain, attached to the aromatic ring. It could be as well that these fragments are formed through ring and double bond formation as part of the fragmentation.

In Figure 104 $C_9H_8N^+$ with DBE value of 6.5 is a characteristic even electron ion fragment which has the same DBE value as the precursor ion, $[C_{12}H_{13}N + H]^+$ with DBE value of 6.5. This suggests that $C_9H_8N^+$ is the result of only losses of CH_2. $C_9H_8N^+$ is suggested to be the core aromatic structure of precursor $[C_{12}H_{13}N + H]^+$ as a quinoline type structure and/or could be isoquinoline. (See Figure 104 for $C_9H_8N^+$ proposed structure which is then used to propose the precursor ion structure $[C_{12}H_{13}N + H]^+$).

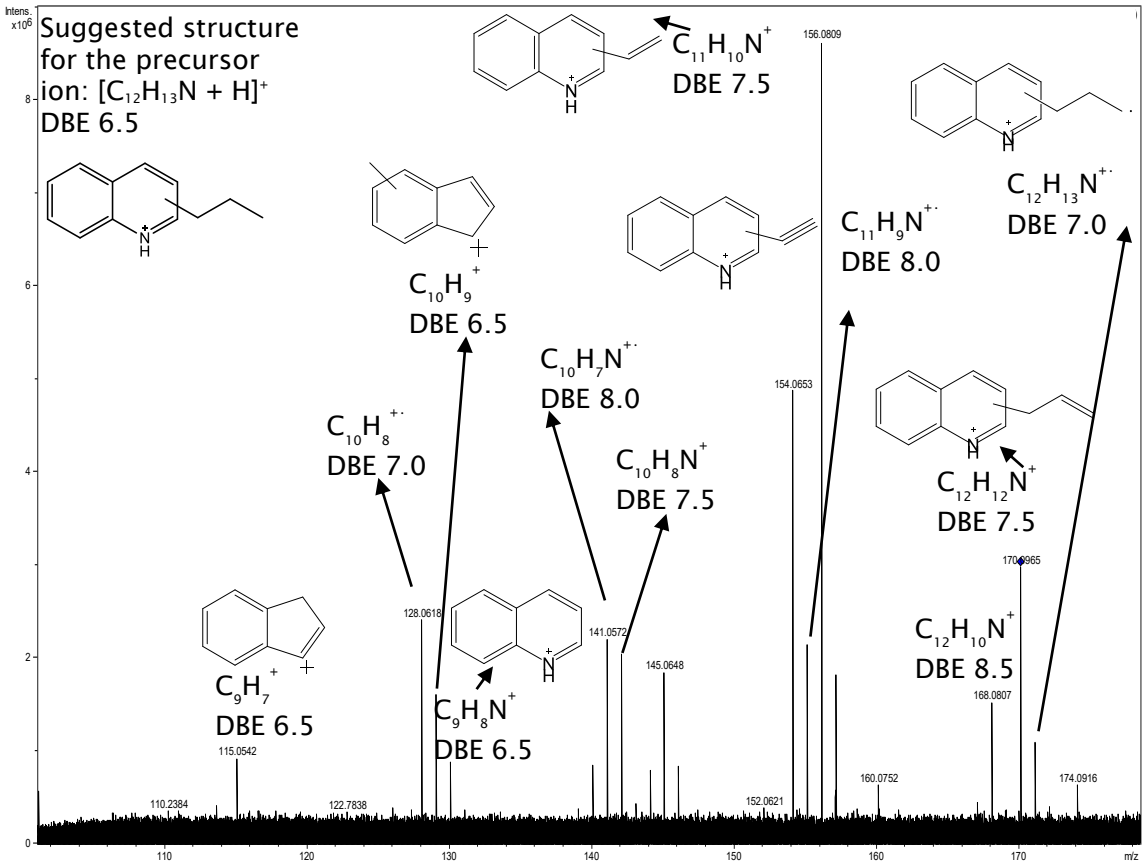

Figure 104 Quadrupole isolation of precursor ion at *m/z* 172 ± 0.5 for 0.5 mg/mL crude oil-2. AS 40, CE 40 V. isCID 40 V. Structures shown are suggested based on MS/MS data and oil industry knowledge.

The further confirmation of quinoline type structure for the precursor ion in Figure 104 is the observation of fragment ions that are related to N expulsion from the aromatic ring through losses of HCN and CH_3CN. For example, $C_{10}H_9^+$ and $C_9H_7^+$ could result through loss of HCN and CH_3CN respectively from $C_{11}H_{10}N^+$. $C_{10}H_9^+$ and $C_9H_7^+$ fragment ions could as well originate directly from the precursor ion.

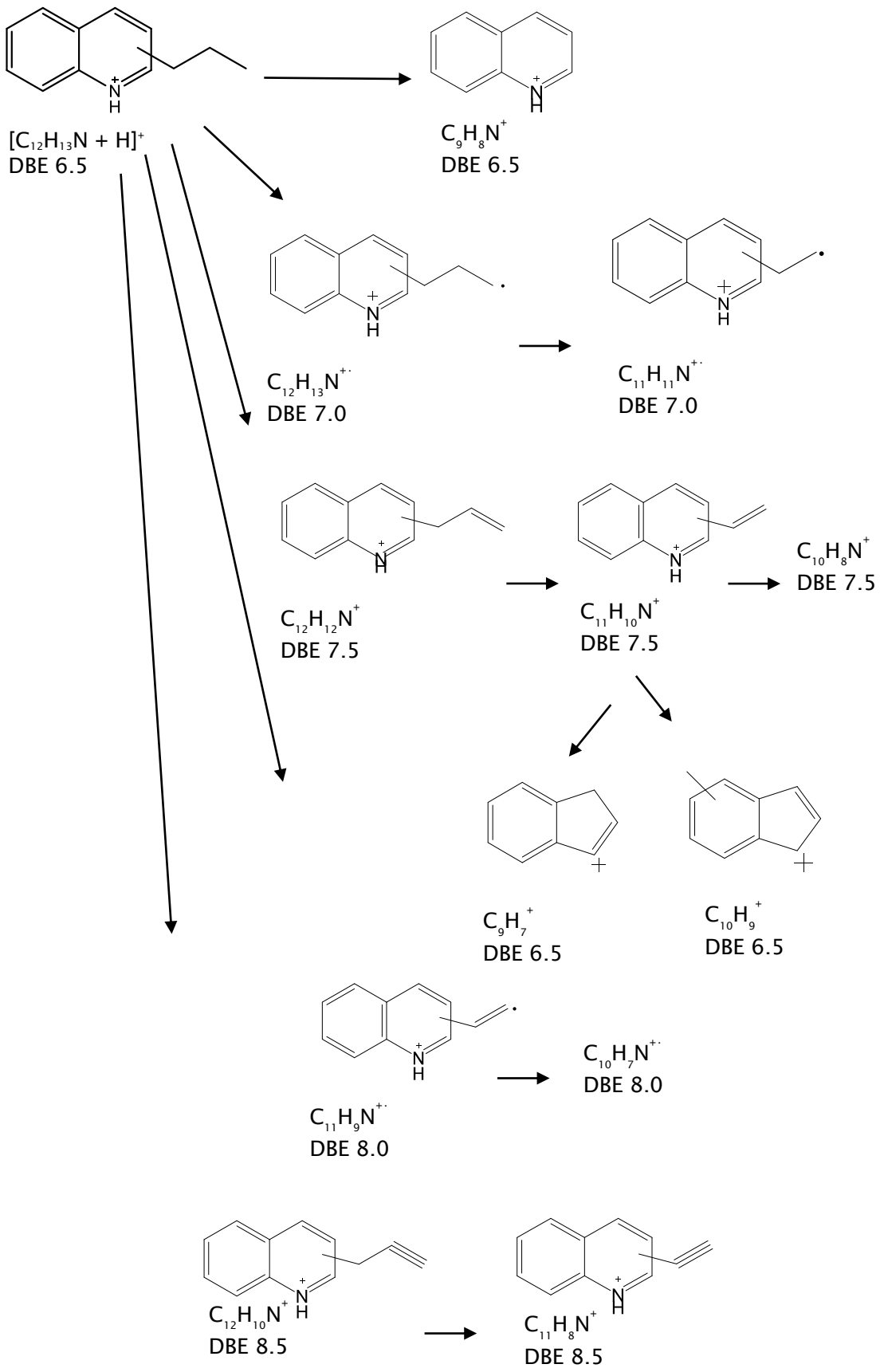

Figure 105 Schematic of fragment ions of precursor ion $[C_{12}H_{13}N + H]^+$ with suggested structures. Odd electron ion fragments were proposed to be distonic ions.

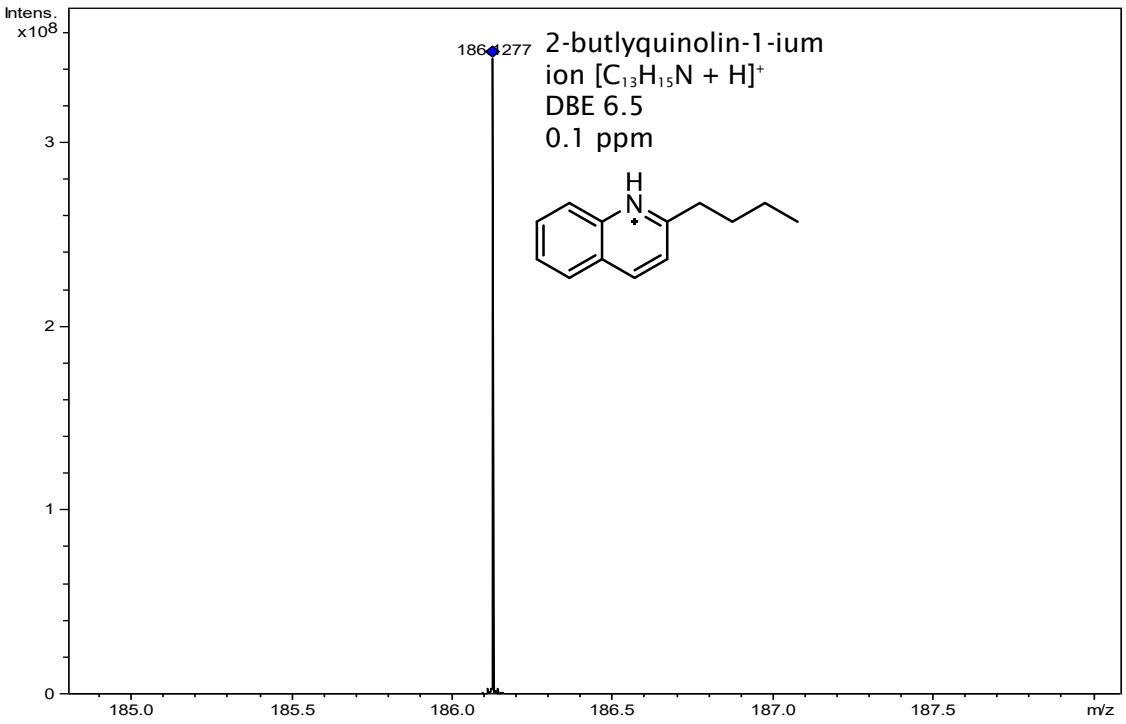

Figure 106 Quadrupole isolation of 50 ng/mL solution (6:4 toluene:methanol) of 2-butylquinolin-1-ium ion at *m/z* 186 ± 0.5 using positive ion ESI FT-ICR MS. CE 0 V. AS 5.

In Figure 106 shows the positive ion ESI FT-ICR mass spectrum of a model compound, 2-butylquinoline. In Figure 106 the precursor ion is isolated using quadrupole isolation at *m/z* 186 ± 0.5. *m/z* 186.1277 is the protonated molecule of $[C_{13}H_{15}N + H]^+$ at DBE value of 6.5 and its product ion mass spectrum is shown in Figure 107 (A) at CE 40 V. Previously, in Figure 104 product ion mass spectrum fragment ions were observed for precursor ion $[C_{12}H_{13}N + H]^+$ with DBE value of 6.5. $[C_{12}H_{13}N + H]^+$ precursor ion is different from 2-butlyquinolin-1-ium, $[C_{13}H_{15}N + H]^+$, by one CH_2. However, since N_1 DBE 6.5 in crude oil-2 is present as homologous series the quadrupole isolation for the precursor ion could be undertaken at *m/z* 186 ± 0.5 instead of *m/z* 172 ± 0.5. The product ion mass spectrum at quadrupole isolation of *m/z* 186 ± 0.5 for crude oil-2 is different from product ion mass spectrum at *m/z* 172 ± 0.5 by one CH_2 different for all fragment ions. (See Figure 102 for N_1 even and odd electron ion fragments for *m/z* 172 and 186 plots respectively). Thus, the same discussion about *m/z* 172 ± 0.5 product ion mass spectrum in Figure 104 could be applied to *m/z* 186 ± 0.5 product ion mass spectrum in Figure 107 (B).

The N expulsion from the aromatic ring that was proposed for fragment ion $C_9H_7^+$ in Figure 104 is observed in Figure 107 A & B product ion mass spectra. The A

product ion mass spectrum shows fragment ions of 2-butlyquinolin-1-ium. The observed fragment ion at *m/z* 115.0542 in A product ion mass spectrum is characteristic of quinoline structure where the N is expulsed from the pyridine ring. The loss of N through expulsion could be directly from the precursor ion and/or from a fragment ion such as loss of HCN from $C_{10}H_8N^+$. Regardless of the origin of fragment ion $C_9H_7^+$ its observation in the mass spectrum supports the suggestion made in Figure 104 that the nitrogen in the precursor ion $[C_{12}H_{13}N + H]^+$ is pyridinic. This suggestion extends to all the N_1 homologous series precursor ions with DBE value of 6.5.

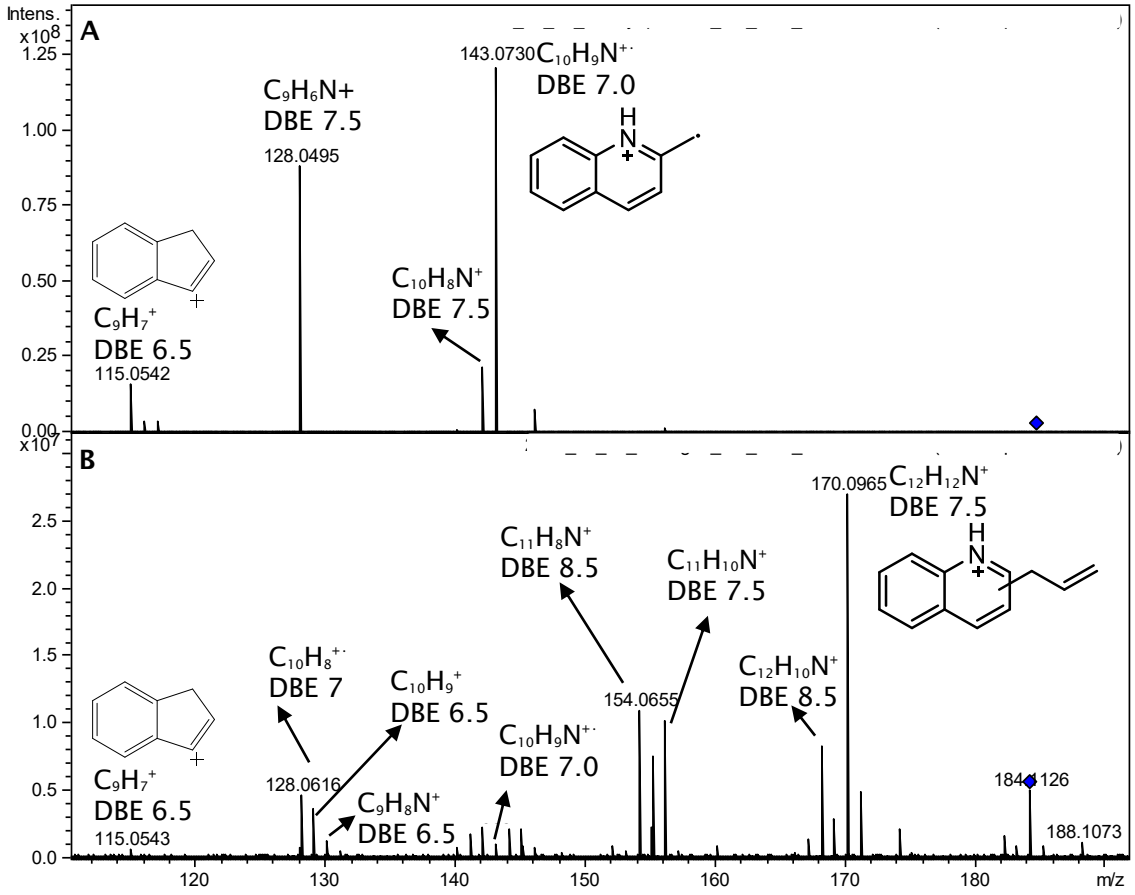

Figure 107 (A) product ion mass spectrum of 50 ng/mL of 2-butlyquinolin-1-ium at *m/z* 186 ± 0.5. (B) product ion mass spectrum of 0.5 mg/mL crude oil-2 at *m/z* 186 ± 0.5. In A and B CE is 40 V, AS 40 and ion accumulation time 5 s.

Other important information than N expulsion can be deduced from product (A) ion mass spectrum of 2-butlyquinolin-1-ium in Figure 107. The base peak fragment ion in product (A) ion mass spectrum is $C_{10}H_9N^{+\cdot}$ with DBE value of 7.0. Further no C_{11} or C_{12} fragment ions are observed in product (A) ion mass spectrum at DBE value of 6.5, 7 and 7.5 from the precursor ion, $[C_{13}H_{15}N + H]^+$. The first

observed fragment ion corresponds to C_{10}, the base peak fragment ion at $C_{10}H_9N^{+\cdot}$. On the contrary for B product ion mass spectrum in Figure 107 C_{12} and C_{11} fragment ions are observed such as $C_{12}H_{12}N^+$ and $C_{11}H_{10}N^+$ with DBE value of 7.5. This shows that precursor ion with the same elemental formula, $[C_{13}H_{15}N + H]^+$, are isolated in A and B in Figure 107 but different product ion mass spectra are observed. This is because in (A) the product ion mass spectrum of 2-butlyquinolin-1-ium, $[C_{13}H_{15}N + H]^+$ is observed. However, B product ion mass spectrum is probably the result of different isomers of $[C_{13}H_{15}N + H]^+$, isolated from crude oil-2 at *m/z* 186 ± 0.5.

The base peak ion in A product ion mass spectrum is odd electron ion at DBE value of 7.0 while in B product ion mass spectrum is an even electron ion at DBE value of 7.5. The base peak fragment ion in A product ion mass spectrum, $C_{10}H_9N^{+\cdot}$, is observed in B product ion mass spectrum but at much lower abundance. The observation of $C_{10}H_9N^{+\cdot}$ in B product ion mass spectrum might indicate that 2-butlyquinoline is one of the isomer for precursor ion $[C_{13}H_{15}N + H]^+$ in crude oil-2. The abundance of $C_{10}H_9N^{+\cdot}$ in B product ion mass spectrum suggest as well that the contribution of 2-butlyquinolin-1-ium to the isomeric mix is low compared to the other possible isomers of $[C_{13}H_{15}N + H]^+$. Another possible explanation that $C_{10}H_9N^{+\cdot}$ fragment in B product ion mass spectrum could be the result from losses of another isomeric form of precursor ion $[C_{13}H_{15}N + H]^+$ than 2-butlyquinolin-1-ium. Regardless of the reason the data of Figure 107 (A) suggest that if 2-butlyquinolin-1-ium is present in crude oil-2 as a one form of isomers for $[C_{13}H_{15}N + H]^+$ is going to be at lower abundance compared to the other possible isomers of $[C_{13}H_{15}N + H]^+$.

The difference observed in fragment ions between A and B product ion mass spectra suggest that the position of the alkyl chain on the aromatic ring affects the fragmentation. In B product ion mass spectrum C_{12} and C_{11} fragment ions at different DBEs were observed. These fragments were not observed in A product ion mass spectrum for the model compound, 2-butlyquinolin-1-ium. Thus for 2-butlyquinolin-1-ium with elemental formula of $[C_{13}H_{15}N + H]^+$ the first observed fragment in A product ion mass spectrum is $C_{10}H_9N^{+\cdot}$. Fragment ions for 2-butlyquinolin-1-ium at $C_{11}H_{11}N^{+\cdot}$ and $C_{12}H_{13}N^{+\cdot}$ are not observed in A product ion mass spectrum which is probably linked to the position of the alkyl chain on the pyridinium ring. However, in B product ion mass spectrum C_{11} and C_{12} fragment ions are observed at different DBEs, fragments related to precursor ion of $[C_{13}H_{15}N + H]^+$. These losses of CH_2 at C_{11} and C_{12} are probably linked to the

position of the alkyl chain on the suggested quinoline structure of precursor ion $[C_{13}H_{15}N + H]^+$ with DBE value of 6.5. Losses of CH_2 are not only observed at *m/z* 186 ± 0.5 for precursor ion $[C_{13}H_{15}N + H]^+$ in Figure 107 B product ion mass spectrum but as well for all the homologous series for N_1 precursor ions with DBE value of 6.5. (See Figure 100, Figure 101 and Figure 102). Further, the most abundant fragment ions series for N_1 precursor ions with DBE 6.5 are even electron ions at DBE value of 7.5, the formation of a double bond. (See Figure 100, Figure 101 and Figure 102). However, for 2-butlyquinolin-1-ium the most abundant fragment ion was odd electron ion fragment at 7.0. (See Figure 107 A product ion mass spectrum). Thus, the data suggest that the position of the alkyl chain might affect whether the base peak fragment ion is odd or even electron ion in the product ion mass spectrum.

In conclusion, the comparison between A and B product ion mass spectra in Figure 107 at quadrupole isolation of *m/z* 186 ± 0.5 for the model compound and crude oil-2 have pointed many observations. The first observation regarding 2-butlyquinolin-1-ium in Figure 107 A product ion mass spectrum was about *m/z* 115.0542 fragment ion with elemental formula of $C_9H_7^+$. $C_9H_7^+$ fragment ion is suggested to be the result of N expulsion and hence is characteristic of quinoline containing compounds. $C_9H_7^+$ was observed in crude oil-2 product ion mass spectra in Figure 107 (B) and Figure 104. This supports the suggestion that the N_1 precursor ions with DBE value of 6.5 are quinoline containing compounds. The second observation is related to the effect of the position of the alkyl chain on the aromatic ring to the observed fragment ions in the product ion mass spectrum. (See Figure 107 A and B). Thus, if different isomers of $[C_{13}H_{15}N + H]^+$ were commercially available it can offer an understanding about the position of the alkyl chain on the ring.

In addition, simpler MS/MS spectra of low *m/z* precursor ion species are observed such as for the isolation of precursor ion at *m/z* 186 ± 0.5 in Figure 107 B product ion mass spectrum. This is because the isolation windows will contain fewer species. Fewer possible combinations of elements, leading to fewer peaks, fragments, per nominal Da

5.5 Structure elucidation of N_1 precursor ions with different DBE values

Many conclusions were made about tandem MS experiments in positive ion ESI FT-ICR MS/MS. The increase of AS from 300 to 800 showed significant increase in the detection of fragment ions but at the expense of increasing the analysis time from 15 minutes to 40 minutes. The increase of ion accumulation time from 50 ms to 5 s at AS 40 offered the advantage of significantly decreasing the analysis time to 4.5 minutes without sacrificing the S/N of fragment ions. Further, low *m/z* low intensity fragment ions were observed in the product ion mass spectrum that can be used to suggest the core aromatic structure of the precursor ion. The developed positive ion ESI FT-ICR MS/MS method was used in the structure elucidation of N_1 precursor ions at DBE value of 6.5 and 13.5. A CE of 60 V was required to observe N expulsion fragment ions and the dealkylated molecule for N_1 precursor ion with DBE value of 13.5. Whereas a CE of 40 V was enough to observe N expulsion fragment ions and the dealkylated molecule for N_1 precursor ion with DBE value of 6.5. A precursor ion with a higher DBE value is more stable and thus requires more CE to observe low *m/z* fragment ions. It should be noted that quadrupole isolation of N_1 precursor ion with DBE value of 6.5 is better undertaken at low *m/z* value such as *m/z* 172 ± 0.5 instead of *m/z* 340 ± 0.5. This is because a simpler product ion mass spectrum is observed because of the short alkyl chain that is attached to the aromatic structure of the precursor ion resulting in fewer losses of CH_2. Further, characteristic fragment ions such as N expulsion were not observed in the product ion mass spectrum for N_1 precursor ion with DBE 6.5 at isolation of *m/z* 340 ± 0.5 but was observed at *m/z* 172 ± 0.5. This is because N_1 precursor ion with DBE 6.5 isolated at *m/z* 340 ± 0.5 has long alkyl chain compared to N_1 precursor ion with DBE 6.5 at *m/z* 172 ± 0.5. Thus, majority of fragment ions observed in the product ion mass spectrum at *m/z* 340 ± 0.5 are subsequent losses of CH_2.

In the following study quadrupole isolation for N_1 precursor ions at different DBE values was undertaken. The isolation of the precursor ions was undertaken at low *m/z* values for reasons that were previously discussed such as obtaining simpler product ion mass spectra. Product ion mass spectra were obtained using positive ion ESI FT-ICR MS/MS at CE 40 V. Table 24 shows the list of N_1 precursor ions that were isolated at different DBEs from 3.5 to 10.5 in crude oil-2. A product ion mass spectrum was obtained for each precursor ion. Note that N_1 precursor ions at DBE value of 3.5 and 10.5 are both isolated at *m/z* 192 ± 0.5.

Table 24 N_1 precursor ions from DBE 3.5 to 10.5.

DBE value	Precursor ion	Quadrupole isolation *m/z* ± 0.5
3.5	$[C_{13}H_{21}N + H]^+$	192
4.5	$[C_{13}H_{19}N + H]^+$	190
5.5	$[C_{14}H_{19}N + H]^+$	202
6.5	$[C_{14}H_{17}N + H]^+$	200
7.5	$[C_{14}H_{15}N + H]^+$	198
8.5	$[C_{14}H_{13}N + H]^+$	196
9.5	$[C_{14}H_{11}N + H]^+$	194
10.5	$[C_{14}H_9N + H]^+$	192

The product ion mass spectra for N_1 precursor ions at DBE value of 7.5, 8.5 and 9.5 are shown in Figure 108 at CE 40 V. For precursor ion $[C_{14}H_{15}N + H]^+$ at DBE value of 7.5 the most intense fragment is an odd electron ion fragment, $C_{13}H_{11}N^{+\cdot}$ at DBE 9.0. The second most intense fragment ion in the product ion mass spectrum is $C_{12}H_9N^{+\cdot}$ at DBE 9.0. Thus, one of the most intense fragment ion series for precursor ion $[C_{14}H_{15}N + H]^+$ at DBE value of 7.5 are odd electron ion fragments with DBE value of 9.0. DBE 9.0 fragment ions are the result of losses of $H^{\cdot}$ and 2H from the precursor ion. However, in the previous section (5.4) the most intense fragment ion series for N_1 precursor ions at DBE value of 6.5 and 13.5 were even electron ion fragments at DBE value of 7.5 and 14.5 respectively. Further, the base peak ion for the protonated 2-butylquinoline precursor ion at DBE 6.5 was an odd electron ion fragment at DBE 7.0. Thus, the alkyl chain position on the pyridinium ring have probably affected the fragmentation and hence the base peak ion is an odd electron ion. This conclusion might be expandable to the product ion mass spectrum of precursor ion $[C_{14}H_{15}N + H]^+$ in Figure 108. This is because the most intense fragment ion series are odd electron ions at DBE 9.0.

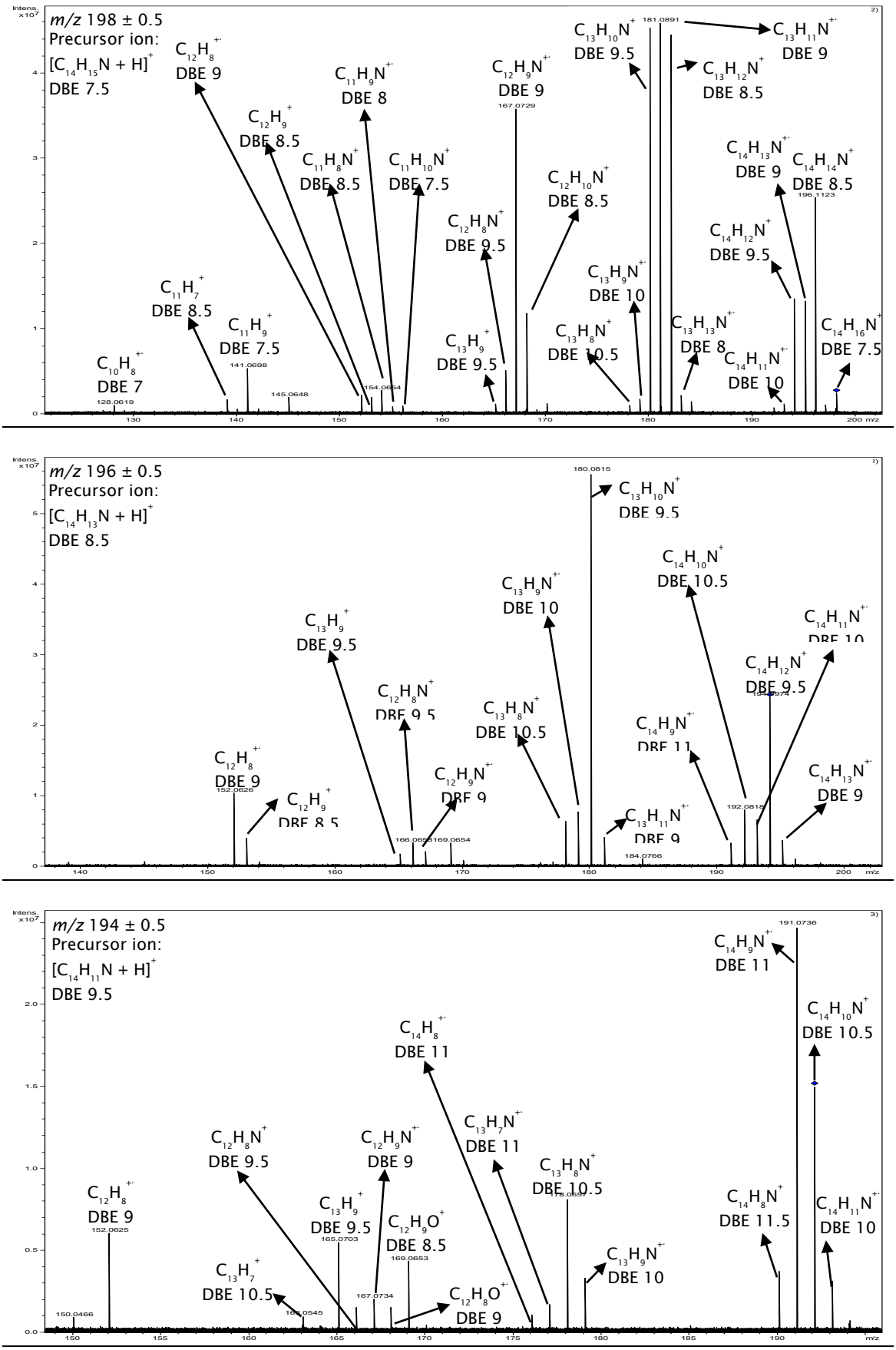

Figure 108 Product ion mass spectra for N_1 precursor ions of crude oil-2 at DBE value of 7.5, 8.5 and 9.5. Data was acquired in positive ion ESI FT-ICR MS/MS. CE 40 V, AS 40 and ion accumulation time 5 s.

Different isomers of precursor ion $[C_{14}H_{15}N + H]^+$ should be considered. However, the ratio of different isomers might be different. Even electron ion fragments, $C_{13}H_{12}N^+$ and $C_{13}H_{10}N^+$ at DBE 8.5 and 9.5 respectively have similar intensity to the base peak ion fragment, $C_{13}H_{11}N^{+\cdot}$ at DBE 9.0. (See Figure 108 *m/z* 198 ± 0.5 product ion mass spectrum). This trend in intensity for fragments ions with C_{13} at DBE values of 8.5, 9.0 and 9.5 was not observed in product ion mass spectra of precursor ions $[C_{14}H_{13}N + H]^+$ and $[C_{14}H_{11}N + H]^+$ respectively. This trend in intensity, fragment ions having similar intensity to base peak fragment ion, could be related to different isomers of precursor ion $[C_{14}H_{15}N + H]^+$ having similar ratios. (See Figure 108 *m/z* 198 ± 0.5 product ion mass spectrum)

A schematic of fragment ions for product ion mass spectrum of precursor ion $[C_{14}H_{15}N + H]^+$ in Figure 108 was suggested in Figure 109. The dealkylated ion is suggested to be $C_{11}H_{10}N^+$ with DBE value 7.5 which has the same DBE value as the precursor ion, $[C_{14}H_{15}N + H]^+$, indicating that only losses of CH_2 have occurred. (See Figure 109). $C_{11}H_{10}N^+$ was used to suggest the core aromatic structure of the precursor ion. Different DBE fragment ions are observed with their CH_2 losses at DBE 8.5, 9.0, 9.5, 10.0 and 10.5. The nitrogen in the suggested structure of the precursor ion is within a pyridine ring. This is supported by the observation of fragment ion $C_{11}H_9^+$ at DBE 7.5. $C_{11}H_9^+$ could be the result of N expulsion from the pyridinium ring through the loss of HCN from fragment ion $C_{12}H_{10}N^+$ at DBE 8.5. (See Figure 109). The product ion mass spectrum of precursor ion $[C_{14}H_{13}N + H]^+$ at DBE value of 8.5 is observed in Figure 108 at quadrupole isolation of *m/z* 196 ± 0.5 with CE 40 V. The base peak fragment ion is even electron ion at *m/z* 180.0815 with elemental formula of $C_{13}H_{10}N^+$ at DBE value of 9.5. This indicates the formation of a double bond through loss of 2H in the fragment ion of $C_{13}H_{10}N^+$ as the precursor ion has a DBE value of 8.5. Similarly, the base peak fragment ion for N_1 precursor ions at DBE value of 6.5 was even electron ion fragment at DBE value of 7.5. Base peak even fragment ion might be indicative of the position of the alkyl chain on the proposed quinoline ring structure. A schematic was proposed in Figure 110 for precursor ion $[C_{14}H_{13}N + H]^+$ at DBE value of 8.5. The dealkylated ion was not observed for this precursor ion. Instead the fragment ion at $C_{12}H_9N^{+\cdot}$ at DBE value of 9.0 was used to suggest the core structure of the precursor ion. N expulsion from the ring structure was observed and could be through loss of HCN from $C_{13}H_{10}N^+$ to form $C_{12}H_9^+$ at DBE value of 9.5 and 8.5 respectively. (See Figure 110). Distonic ions were proposed for odd electron ion fragment because they are more stable. (See Figure 110).

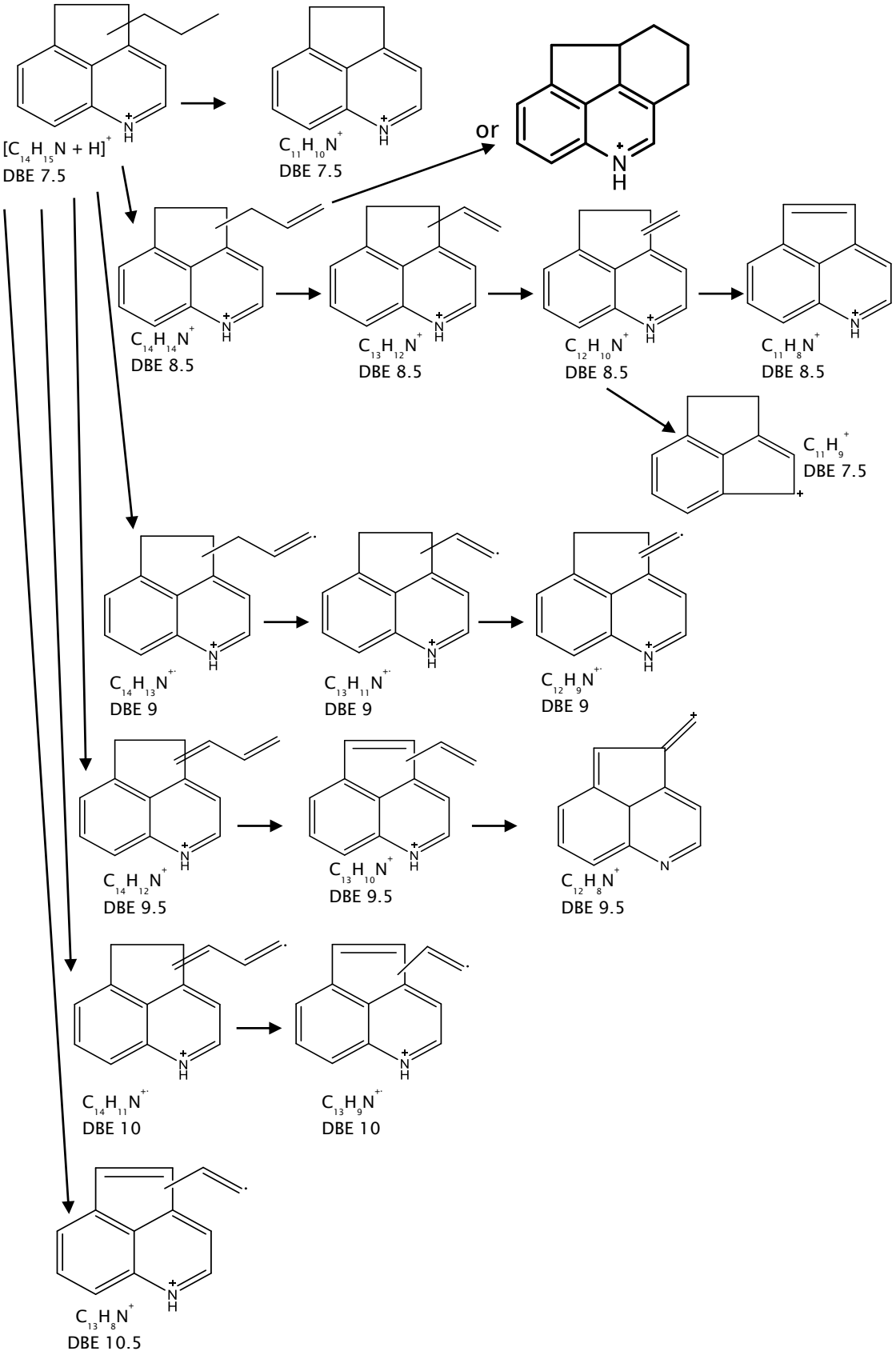

Figure 109 Schematic of fragment ions of precursor ion $[C_{14}H_{15}N + H]^+$ with suggested structures. Fragments with alkene side chains could be illustrated as well as rings. E.g. $C_{14}H_{14}N^+$, $C_{13}H_{12}N^+$, $C_{14}H_{13}N^{+\cdot}$, etc.

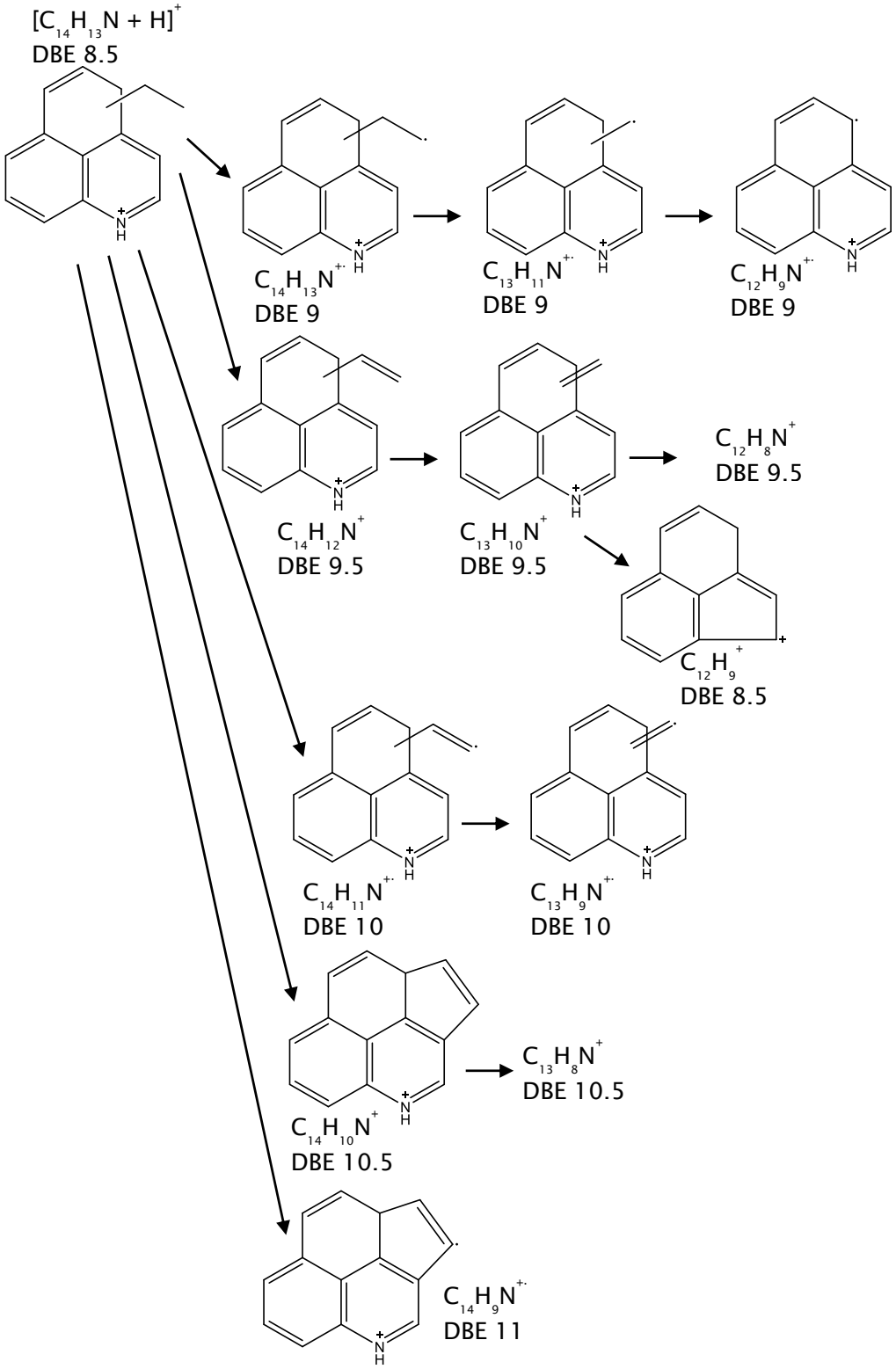

Figure 110 Schematic of fragment ions of precursor ion $[C_{14}H_{13}N + H]^+$ with suggested structures. Odd electron ion fragments were proposed to be distonic ions.

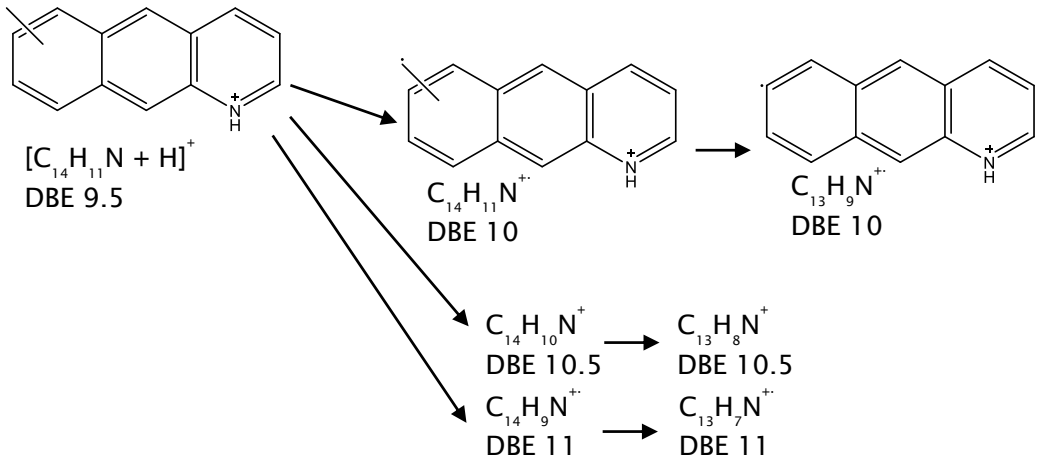

Figure 111 Schematic of fragment ions of precursor ion $[C_{14}H_{11}N + H]^+$ with suggested structures.

Fragments ions of precursor ion $[C_{14}H_{11}N + H]^+$ at DBE value of 9.5 was observed in Figure 108 at quadrupole isolation of *m/z* 194 ± 0.5. The base peak fragment ion is odd electron ion fragment, $C_{14}H_9N^{+\cdot}$ at DBE value of 11.0. N expulsion from the ring is observed in the product ion mass spectrum at $C_{14}H_8^{+\cdot}$, $C_{13}H_9^+$, $C_{13}H_7^+$, $C_{12}H_8^{+\cdot}$ and $C_{12}H_6^{+\cdot}$. The most characteristic fragment ions that were observed in the product ion mass spectrum of precursor ion $[C_{14}H_{11}N + H]^+$ in Figure 108 were illustrated in Figure 111. The dealkylated ion which represent only losses of CH_2 from the precursor ion was not observed in the product ion mass spectrum. Thus the, suggestion of the core aromatic structure of the precursor ion was based on $C_{13}H_9N^{+\cdot}$ at DBE value of 10.0. (See Figure 111). The nitrogen of precursor ion $[C_{14}H_{11}N + H]^+$ is suggested to be pyridinic because N expulsion fragment ions were observed such as $C_{13}H_9^+$ at DBE value of 9.5. $C_{13}H_9^+$ at DBE 9.5 fragment ion could be formed through the loss of HCN from $C_{14}H_{10}N^+$ at DBE 10.5.

The proposed N expulsion fragment ions were observed in product ion mass spectra for N_1 precursor ions with DBE values of 6.5, 7.5, 8.5 and 9.5. (See Figure 107 and Figure 108). In Figure 107 quadrupole isolation at *m/z* 186 ± 0.5 was used to isolate precursor ion of 2-butlyquinolin-1-ium and the precursor ion in crude oil-2. *m/z* 115 with elemental formula of $C_9H_7^+$ and DBE value of 6.5 was observed in the product ion mass spectra of 2-butlyquinolin-1-ium and crude oil-2. The proposed fragmentation pathway is through loss of HCN from $C_{10}H_8N^+$ to form $C_9H_7^+$. (See Table 25). The same proposed fragmentation pathway can be observed for N_1 precursor ions at DBE values of 7.5, 8.5 and 9.5. In theory, if the observed N expulsion ions in Table 25 for precursor ions with DBE values of 7.5,

8.5, 9.5 would be reduced to DBE value of 6.5 a fragment ion at *m/z* 115 with elemental formula of $C_9H_7^+$ would be observed. Thus, a further confirmation can be deduced that N in precursor ion with DBE values of 7.5, 8.5 and 9.5 is in a pyridine ring. This is because the use of 2-butlyquinolin-1-ium ion with DBE 6.5, suggested that *m/z* 115 $C_9H_7^+$ is characteristic of quinoline structure. Further, the N expulsion fragment ions in Table 25 have the same carbon number value as the dealkylated ion for a given N_1 precursor ion. For example, $C_{11}H_{10}N^+$ with DBE value of 7.5 is suggested to be the dealkylated fragment ion of precursor ion $[C_{14}H_{15}N + H]^+$ with DBE value of 7.5. (See Figure 109). $C_{11}H_9^+$ is suggested to be formed through loss of HCN from $C_{12}H_{10}N^+$. (See Figure 109). $C_{11}H_9^+$ has the same carbon number as the suggested dealkylated fragment ion, $C_{11}H_{10}N^+$, at carbon number of 11. The same observation is true for the model compound and crude oil-2 N_1 precursor ions at DBE values of 6.5, 7.5, 8.5 and 9.5.

Table 25 Proposed N expulsion fragment ions through loss of HCN for different N_1 precursor ions.

Precursor ion	DBE	Fragment ion	DBE	N expulsion fragment ion	DBE
$[C_{13}H_{15}N + H]^+$	6.5	$C_{10}H_8N^+$	7.5	$C_9H_7^+$	6.5
$[C_{14}H_{15}N + H]^+$	7.5	$C_{12}H_{10}N^+$	8.5	$C_{11}H_9^+$	7.5
$[C_{14}H_{13}N + H]^+$	8.5	$C_{13}H_{10}N^+$	9.5	$C_{12}H_9^+$	8.5
$[C_{14}H_{11}N + H]^+$	9.5	$C_{14}H_{10}N^+$	10.5	$C_{13}H_9^+$	9.5

In the book of Mass Spectrometry of Heterocyclic compounds[190] the EI fragmentation of 1- and 3-methylisoquinoline Figure 112 a and b was discussed. The decomposing sequence is $M^{+\cdot}$ $-H^{\cdot}$ – HCN. The loss of HCN is suggested to be from the benzazatropylium cation at *m/z* 142 to give *m/z* 115. The fragment ion at *m/z* 115 was observed in the positive ion ESI product ion mass spectrum of 2-butlyquinolin-1-ium. (See Figure 107 A). Further *m/z* 115 was observed for N_1 precursor ion with DBE value of 6.5 for crude oil-2 product ion mass spectra in Figure 107 B and Figure 104. This suggests that *m/z* 115 $C_9H_7^+$ for N_1 precursor ion at DBE 6.5 is formed through loss of HCN of benzazatropylium cation, $C_{10}H_8N^+$. The formation of benzazatropylium cation could be extended to fragment ion of $C_{12}H_{10}N^+$, $C_{13}H_{10}N^+$ and $C_{14}H_{10}N^+$ in Table 25.

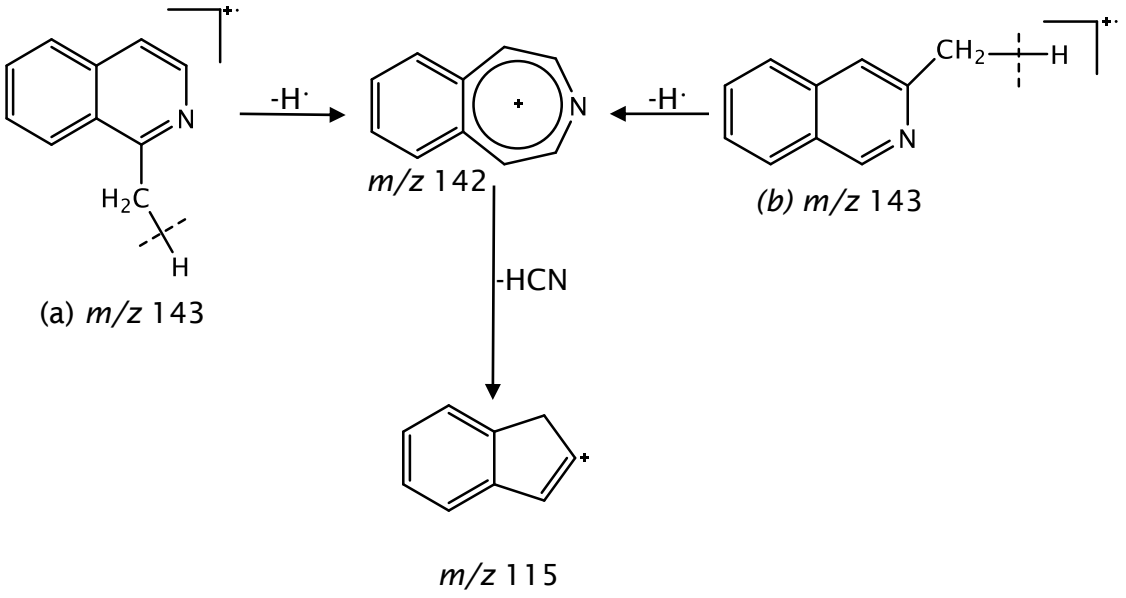

Figure 112 Fragmentation of 1- and 3-methylisoquinoline.[190]

The core aromatic structure was previously proposed for N_1 precursor ions with DBE values of 6.5, 7.5, 8.5 and 9.5. The core structure was proposed either using the dealkylated ion or low *m/z* fragments in the product ion mass spectra. In Table 26 the core aromatic structure is proposed for N_1 precursor ions from DBE value of 3.5 to 10.5. The structure was proposed for each N_1 precursor ion using the dealkylated ion or low *m/z* fragments in the product ion mass spectra. Further, Table 26 lists the most intense fragment ion observed in the product ion mass spectrum for a particular precursor ion. The most intense fragment ion can be either an even or odd electron ion fragment. The most intense fragment ion was even electron ion fragment for N_1 precursor ions with DBE values of 3.5, 5.5, 6.5, 8.5 and 10.5. Whereas odd electron ion fragments were the most intense for N_1 precursor ions with DBE values of 4.5, 7.5 and 9.5. The observation of most intense odd or even electron ion was suggested to be linked to the position of the alkyl chain on the ring structure. This is because odd electron ion fragment, $C_{10}H_9N^{+\cdot}$ at DBE 7, was the most intense fragment ion in the product ion mass spectrum of 2-butlyquinolin-1-ium which has the elemental formula of $[C_{14}H_{17}N + H]^+$ at DBE 6.5. (See Figure 107 A). Whereas in Figure 107 B , the same elemental formula was isolated in crude oil-2 at *m/z* 186 ± 0.5, $[C_{14}H_{17}N + H]^+$, but the most intense fragment ion was even electron ion, $C_{13}H_{14}N^+$ at DBE 7.5. (See Table 26).

Table 26 Possible N_1 core structures at different DBE values for crude oil-2.

Precursor ion	Core aromatic structure	DBE	Most intense fragment ion	DBE
$[C_{13}H_{21}N + H]^+$	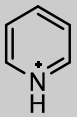	3.5	$C_{10}H_{14}N^+$	4.5
$[C_{13}H_{19}N + H]^+$	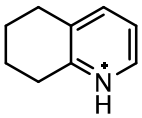	4.5	$C_{10}H_{11}N^{+\cdot}$	6.0
$[C_{14}H_{19}N + H]^+$	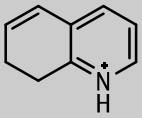	5.5	$C_{13}H_{16}N^+$	6.5
$[C_{14}H_{17}N + H]^+$	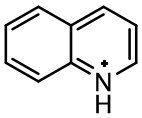	6.5	$C_{13}H_{14}N^+$	7.5
$[C_{14}H_{15}N + H]^+$	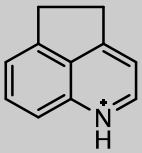	7.5	$C_{13}H_{11}N^{+\cdot}$	9.0
$[C_{14}H_{13}N + H]^+$	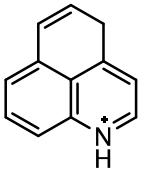	8.5	$C_{13}H_{10}N^+$	9.5
$[C_{14}H_{11}N + H]^+$	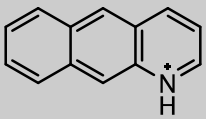	9.5	$C_{14}H_9N^{+\cdot}$	11.0
$[C_{14}H_9N + H]^+$	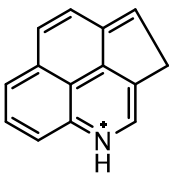	10.5	$C_{14}H_8N^+$	11.5

Chapter 6: Conclusions

The solvent composition study in positive ion ESI FT-ICR MS of crude oil-1, 2 and 3 revealed important findings in relation to ionisation response and multimer formation. Different petroleomics labs use different ratios of toluene:methanol to dissolve crude oil samples. Further, within the same lab different sample solvent compositions of toluene:methanol were used to dissolve crude oil samples. The sample solvent composition has a significant effect on the resultant data. Therefore, there is a need to standardise sample solvent composition in order to compare data across different labs. Three different ratios of toluene:methanol at 1:9, 3:7 and 6:4 with and without the addition of 0.1% formic acid were used to dissolve crude oil-1, 2 and 3. The mass spectra acquired for crude oil-1, 2 and 3 using different toluene:methanol solvent ratios showed different ionisation responses for N_1 containing compounds even with the addition of formic acid. For example, *m/z* 404.332 with elemental formula $[C_{29}H_{41}N + H]^+$ in crude oil-1, 2 and 3 mass spectra is most intense using toluene:methanol solvent ratio of 1:9 with 0.1% formic acid. However, the ion intensity of *m/z* 404.332 was affected by different rates when the toluene content was increased in the sample solvent in different crude oils. When the toluene content was increased in the sample solvent, the decrease in ion intensity of *m/z* 404.332 was less for crude oil-3 compared to crude oil-1 and 2. This effect was not only observed for one ion, *m/z* 404.332, but as well in the combined N_1 ion intensity plot for crude oil-1, 2 and 3. Thus, the solvent composition at toluene:methanol solvent ratio of 1:9 with 0.1% formic acid should be used to compare the N_1 class in different crude oils. If the 1:9 toluene:methanol solvent ratio is not used false comparison could be resulted due to different ionisation responses for N_1 in different crude oils.

One of the other findings regarding the solvent composition study is the multimer formation. Multimer formation in N_1 DBE *versus* carbon number plots were not only concentration driven but also solvent composition dependent. The increase of methanol in the sample solvent reduced multimer formation. Further, the addition of 0.1% formic acid reduced multimer formation in different solvent ratios of toluene:methanol. Therefore, using toluene:methanol solvent ratio of 1:9 with 0.1% formic acid has two main advantages. The first is increasing the ionisation of nitrogen containing compounds allowing their comparison in different crude oils. The second is reducing multimer formation, probably due to the increase in the acidity of the sample solvent.

Nitrogen containing compounds were the most abundant ions in positive ion ESI mass spectra of crude oil-1, 2 and 3. For ionising other compounds classes in crude oil such as sulfur and hydrocarbon containing compounds positive ion APPI FT-ICR MS is used. Similar ion intensities distribution in S_1 DBE *versus* carbon number plots were observed for crude oil-1 and 2. However, for crude oil-3, the intensity distribution is higher at lower DBE values for the S_1 class. This could be related to the type of crude oil-3, classified as a sour crude oil. Further, sulfur and hydrocarbon containing compounds were observed in positive ion ESI FT-ICR MS crude oil mass spectrum using toluene:methanol solvent ratio of 1:9 with 0.1% formic acid. These compounds are not usually observed using ESI. One possible explanation that the ionisation efficiencies of S_1 and HC compounds are increased at toluene:methanol solvent ratio of 1:9, in similar way to the N_1 containing compounds. However, only the most intense ions that were observed in the positive ion APPI HC and S_1 DBE *versus* carbon number plots were observed in the positive ion ESI HC and S_1 DBE *versus* carbon number plots.

Crude oil-1, 2 and 3 were analysed using negative ion APPI. The data showed similar DBE and carbon number distributions for the HC class for crude oil-1 and 3. Whereas crude oil-2 had ion series starting from DBE 6 that were not observed in crude oil-1 and 3. The negative molecular ion HC-R plot showed major differences regarding crude oil-3 from DBE 5 to 9 compared to crude oil-1 and 2, probably related to the fact that crude oil-3 is a light crude oil. Further, crude oil-3 S_1 class is significantly more abundant at lower DBE values compared to crude oil-1 and 2. This is probably related to crude oil-3 being classified as a sour crude oil. The suitability of using negative ion APPI instead of negative ion ESI was assessed based on the O_2 class. The O_2 class for crude oil-1, 2 and 3 were compared using negative ion APPI and ESI. The O_2 combined ions intensities data were comparable between the two ionisation techniques for crude oil-1, 2 and 3. This demonstrates that negative ion APPI could be used for the analysis of crude oil instead of using negative ion ESI.

The previous conclusions were focussed on characterising the different compound classes for crude oil-1, 2 and 3. Crude oil-2 had the most abundant N_1 containing compounds compared to crude oil-1 and 3. Therefore, it is expected that catalyst deactivation due to nitrogen containing compounds would be more significant for crude oil-2. The elucidation of structure of nitrogen containing compounds might help in designing more effective catalysts for HDN process. In this work a positive ion ESI FT-ICR MS/MS method was developed for the purpose of structural elucidation of different N_1 containing compounds in crude oil-2. In this method, the analysis time of the positive ion ESI FT-ICR MS/MS experiment was reduced from 40 min to 4.5 min. This was achieved through increasing the ion accumulation time from 0.05 s to 5 s while decreasing the average spectra from AS 800 to 40. Not just the analysis was significantly reduced but additionally low intensity fragment ions can be observed in the product ion mass spectrum. The detection of low *m/z* fragment ions which have low intensities could be useful in aiding the structural elucidation of the core aromatic structure of nitrogen containing compounds in crude oil-2.

Another important parameter to consider for structural elucidation is the collision energy (CE). A CE of 60 V instead of 40 V was needed for precursor ion with high DBE value such as precursor ion $[C_{25}H_{25}N + H]^+$ with DBE value of 13.5. A CE of 60 V resulted in observing lower *m/z* fragments in the product ion mass spectrum of precursor ion $[C_{25}H_{25}N + H]^+$ that is not observed when CE 40 V is used. For example, at CE 60 V fragment ion $C_{17}H_{10}N^+$ is observed in the product ion mass spectrum of precursor ion $[C_{25}H_{25}N + H]^+$ which might correspond to the dealkylated core aromatic structure. Further at CE 60 V, N expulsion fragment ions from the aromatic ring are observed in the product ion mass spectrum of precursor ion $[C_{25}H_{25}N + H]^+$. For example, N expulsion fragment ion $C_{18}H_{11}^+$ is suggested through loss of HCN from fragment ion $C_{19}H_{12}N^+$.

However, a CE of 40 V was enough to observe the dealkylated molecule and N expulsion from the aromatic ring for N_1 precursor ion with DBE value of 6.5. This is because N_1 precursor ion with DBE value of 6.5 is less aromatic compared to N_1 precursor ion with DBE value of 13.5 and therefore a CE of 40 V is used. However, the data showed that isolating the N_1 precursor ion with DBE value of 6.5 is best undertaken at lower degree of alkylation in the homologous series. For example, N expulsion fragment ions were not observed for precursor ion $[C_{24}H_{37}N + H]^+$ with DBE value of 6.5. However, N expulsion fragment ions were observed for the less alkylated precursor ion, $[C_{12}H_{13}N + H]^+$ with DBE value of 6.5. In the product ion

mass spectrum of precursor ion $[C_{12}H_{13}N + H]^+$ fragment ion $C_9H_7^+$ at *m/z* 115 is observed, probably through loss of HCN from $C_{10}H_8N^+$. This same fragment ion at *m/z* 115 is observed in the product ion mass spectrum of 2-butlyquinolin-1-ium. This suggests that *m/z* 115, $C_9H_7^+$, is characteristic of quinoline structure. Therefore, the nitrogen in crude oil-2 $[C_{12}H_{13}N + H]^+$ is probably in a pyridine ring. Similar N expulsion fragment ion from the aromatic ring is observed for precursor ions in crude oil-2 at DBE values of 7.5, 8.5 and 9.5. Thus, the nitrogen in precursor ion with DBE values of 7.5, 8.5 and 9.5 is suggested to be in a pyridine ring.

Further, the core aromatic structure was not only proposed for N_1 precursor ions at DBE values of 6.5 and 13.5 but as well from DBE value of 3.5 to 10.5. The structure was proposed for each N_1 precursor ion from DBE value of 3.5 to 10.5 using the dealkylated ion or low *m/z* fragments and further validated using N expulsion fragment ions in the corresponding product ion mass spectra.

Appendix

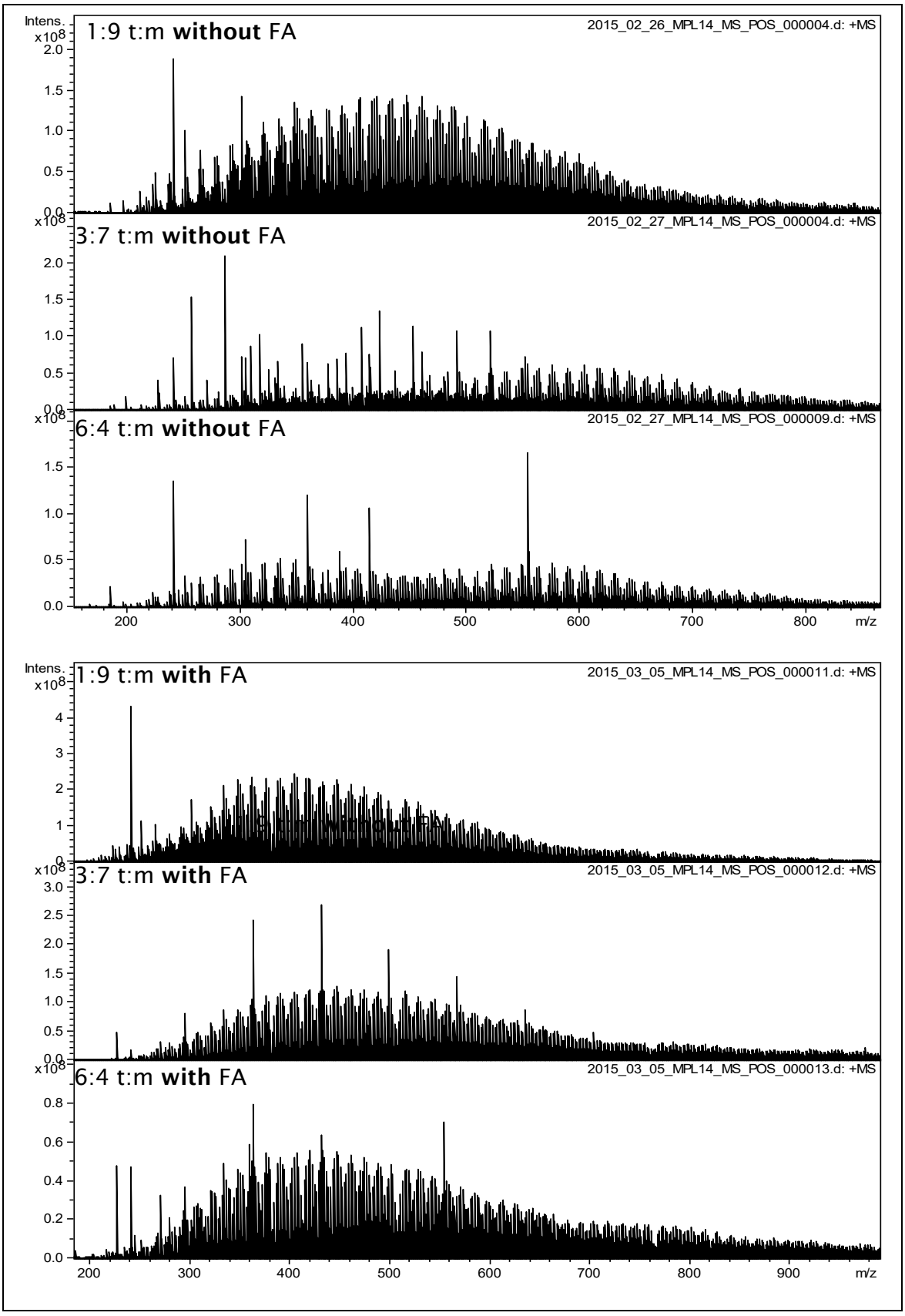

Figure 113 Mass spectra for Figure 29 and Figure 30.

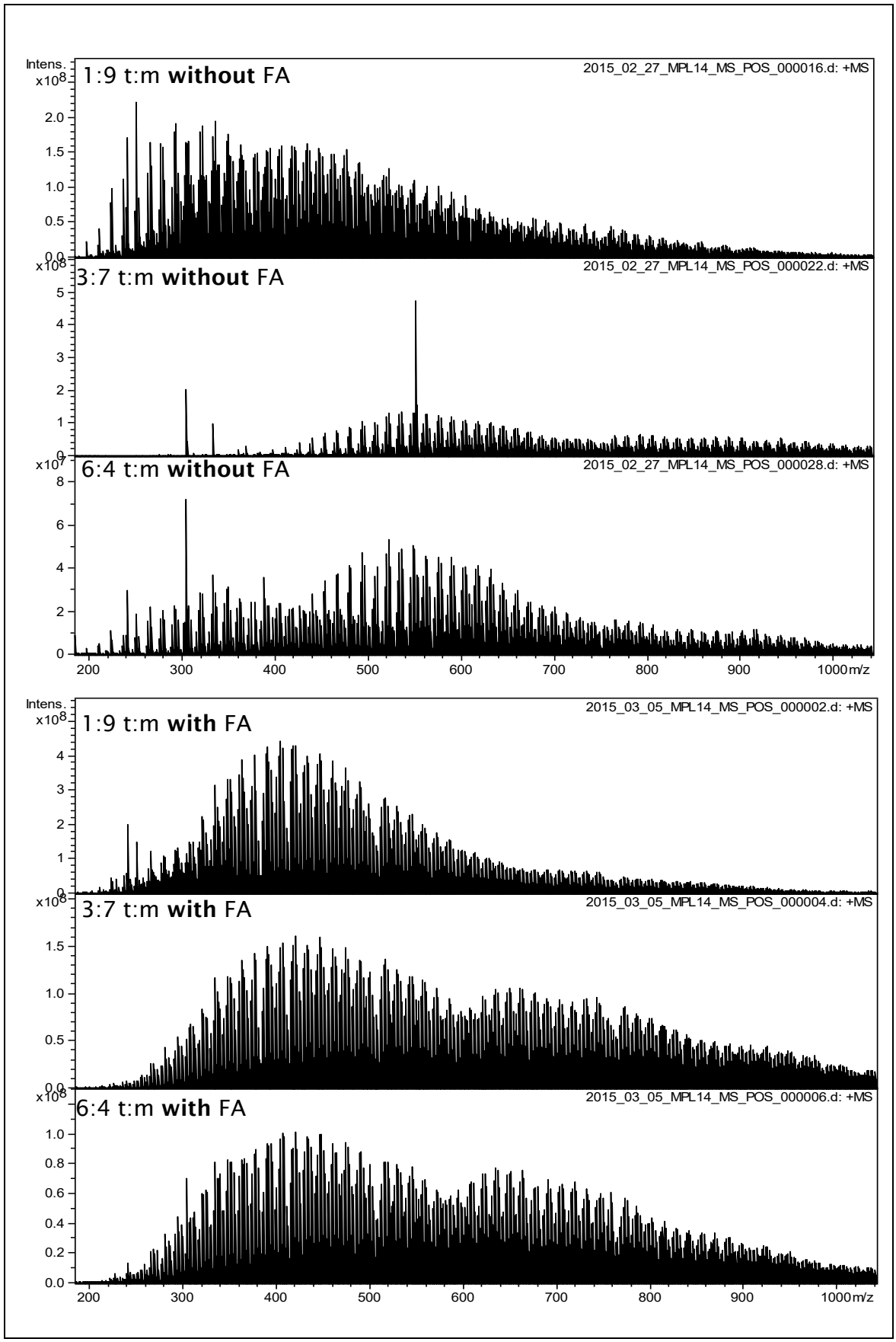

Figure 114 mass spectra for Figure 31 and Figure 32

Appendix

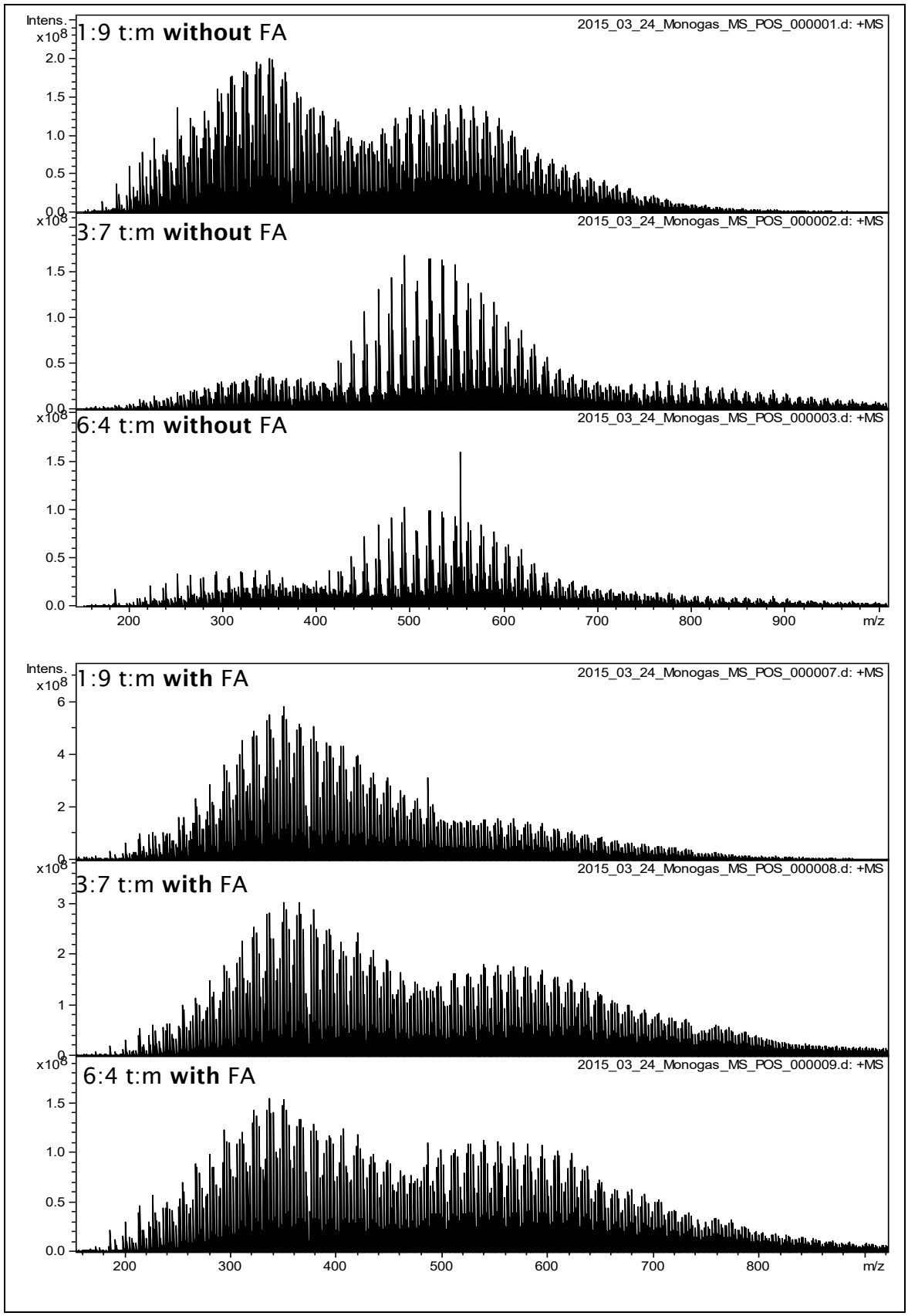

Figure 115 mass spectra for Figure 33 and Figure 34.

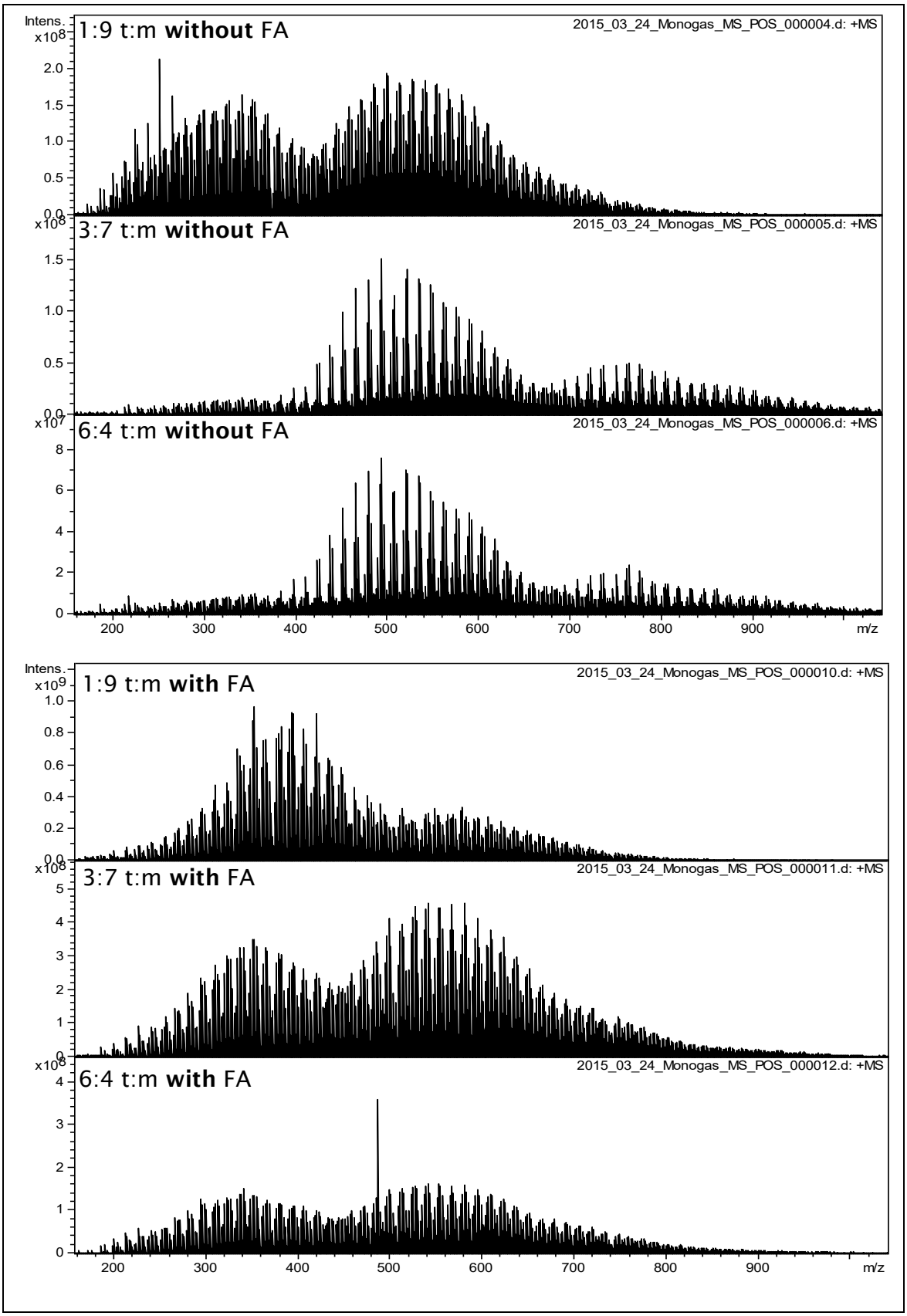

Figure 116 mass spectra for Figure 35 and Figure 36.

Appendix

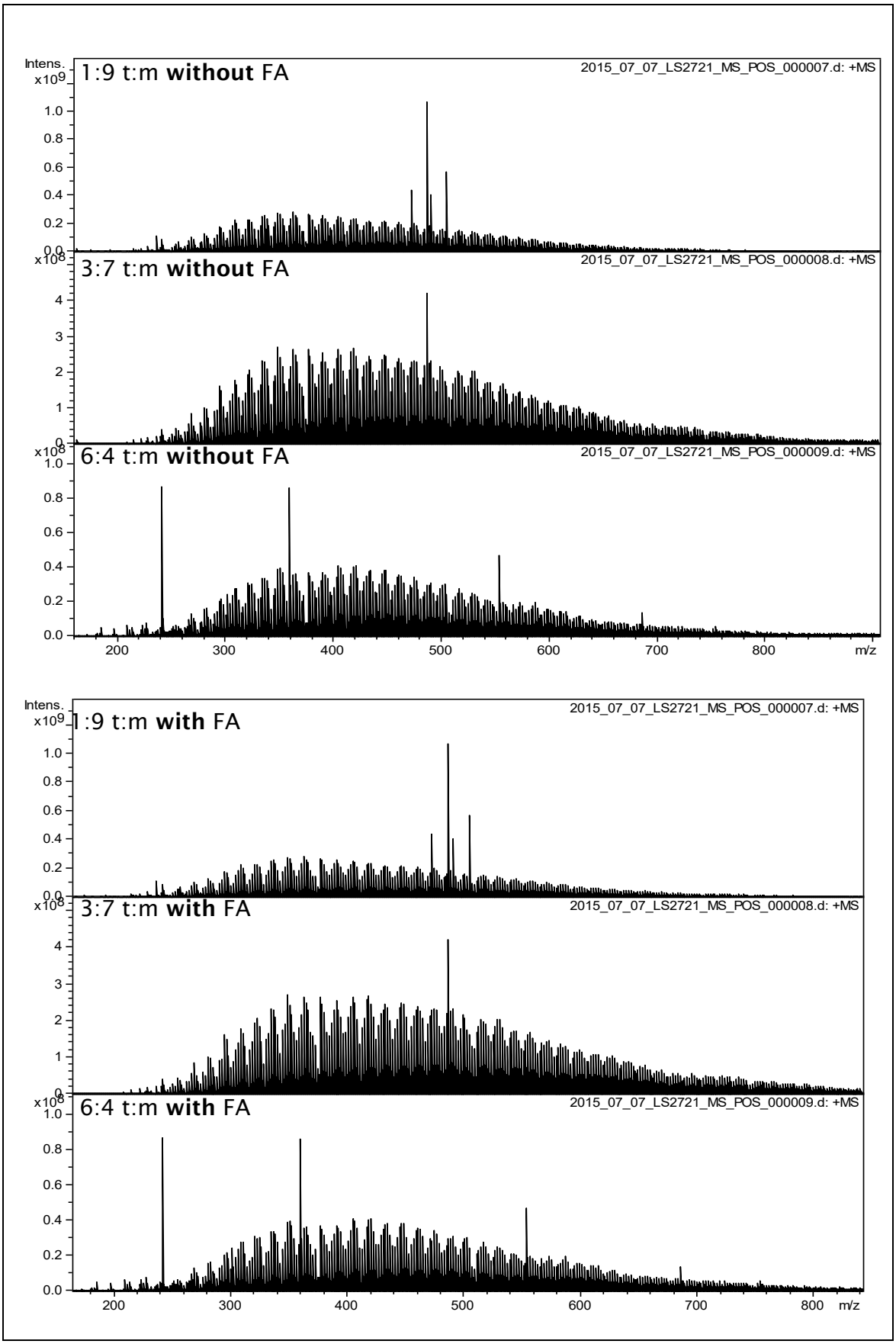

Figure 117 mass spectra for Figure 37 and Figure 38.

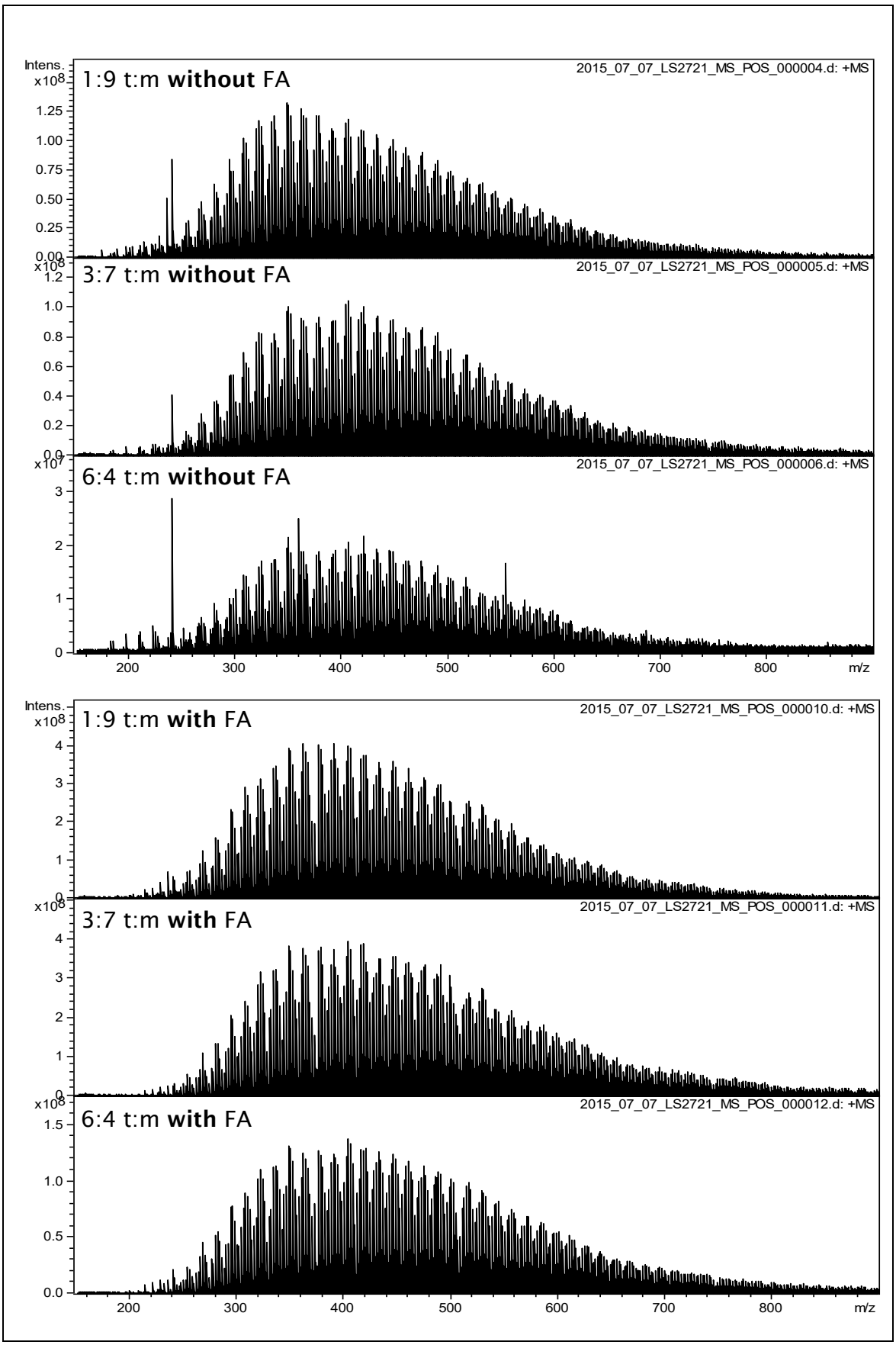

Figure 118 mass spectra for Figure 39 and Figure 40.

Appendix

References

References

(1) Speight, J. G.: *Handbook of petroleum product analysis*; John Wiley & Sons, 2015.

(2) Speight, J. G.; Ozum, B.: *Petroleum refining processes*; CRC Press, 2001.

(3) World Energy Outlook Special Report *International Energy Agency* **2015** 36 - 38.

(4) Nashawi, I. S.; Malallah, A.; Al-Bisharah, M. Forecasting World Crude Oil Production Using Multicyclic Hubbert Model. *Energy & Fuels* **2010**, *24*, 1788-1800.

(5) 2015 World Oil Outlook *Organisation of the Petroleum Exporting Countries* **2015**.

(6) Braun, R. L.; Rothman, A. J. Oil-Shale Pyrolysis - Kinetics and Mechanism of Oil Production. *Fuel* **1975**, *54*, 129-131.

(7) Smith, G. E. Fluid flow and sand production in heavy-oil reservoirs under solution-gas drive. *SPE Production Engineering* **1988**, *3*, 169-180.

(8) Acevedo, S.; Escobar, G.; Gutierrez, L. B.; Rivas, H.; Gutierrez, X. Interfacial Rheological Studies of Extra-Heavy Crude Oils and Asphaltenes - Role of the Dispersion Effect of Resins in the Adsorption of Asphaltenes at the Interface of Water-in-Crude Oil-Emulsions. *Colloid Surface A* **1993**, *71*, 65-71.

(9) Martinez-Palou, R.; Mosqueira, M. D.; Zapata-Rendon, B.; Mar-Juarez, E.; Bernal-Huicochea, C.; Clavel-Lopez, J. D.; Aburto, J. Transportation of heavy and extra-heavy crude oil by pipeline: A review. *Journal of Petroleum Science and Engineering* **2011**, *75*, 274-282.

(10) Slavcheva, E.; Shone, B.; Turnbull, A. Review of naphthenic acid corrosion in oilrefining. *British Corrosion Journal* **1999**, *34*, 125-131.

(11) Furimsky, E.; Massoth, F. E. Deactivation of hydroprocessing catalysts. *Catalysis Today* **1999**, *52*, 381-495.

(12) Dorbon, M.; Ignatiadis, I.; Schmitter, J. M.; Arpino, P.; Guiochon, G.; Toulhoat, H.; Huc, A. Identification of Carbazoles and Benzocarbazoles in a Coker Gas Oil and Influence of Catalytic Hydrotreatment on Their Distribution. *Fuel* **1984**, *63*, 565-570.

(13) Gallup, D. L.; Curiale, J. A.; Smith, P. C. Characterization of sodium emulsion soaps formed from production fluids of Kutei Basin, Indonesia. *Energy & Fuels* **2007**, *21*, 1741-1759.

(14) Brocart, B.; Hurtevent, C. Flow Assurance Issues and Control with Naphthenic Oils. *Journal of Dispersion Science and Technology* **2008**, *29*, 1496-1504.

(15) Barrow, M. P.; Peru, K. M.; Fahlman, B.; Hewitt, L. M.; Frank, R. A.; Headley, J. V. Beyond Naphthenic Acids: Environmental Screening of Water from Natural Sources and the Athabasca Oil Sands Industry Using Atmospheric Pressure Photoionization Fourier Transform Ion Cyclotron Resonance Mass Spectrometry. *J. Am. Soc. Mass Spectrom.* **2015**, *26*, 1508-1521.

References

(16) Tissot, B.; Welte, D. H. Petroleum occurrence and formation. *Springer-Verlag, Berlin* **1984**, *699*, 249.

(17) Behar, F.; Pelet, R.; Roucache, J. Geochemistry of asphaltenes. *Org. Geochem.* **1984**, *6*, 587-595.

(18) Sinninghe Damsté, J. S.; Eglinton, T. I.; De Leeuw, J. W.; Schenck, P. A. Organic sulphur in macromolecular sedimentary organic matter: I. Structure and origin of sulphur-containing moieties in kerogen, asphaltenes and coal as revealed by flash pyrolysis. *Geochimica et Cosmochimica Acta* **1989**, *53*, 873-889.

(19) Orr, W. L. Kerogen Asphaltene Sulfur Relationships in Sulfur-Rich Monterey Oils. *Org. Geochem.* **1986**, *10*, 499-516.

(20) McGrath, H. G.; Charles, M. E.: *Origin and Refining of Petroleum*; American Chemical Society, 1971; Vol. 103.

(21) Ho, T. Y.; Rogers, M. A.; Drushel, H. V.; Koons, C. B. Evolution of Sulfur-Compounds in Crude Oils. *Aapg Bulletin-American Association of Petroleum Geologists* **1974**, *58*, 2338-2348.

(22) Hunt, J. M. Chemical composition of a crude oil. *Petroleum Geochemistry and Geology, 2nd edition.* **1996**, p. 39.

(23) K. Rajagopal, S. M. C. S. An Experimental Study of Asphaltene Particle Sizes in n-Heptane-Toluene Mixtures by Light Scattering. . *Brazilian Journal of Chemical Engineering* **2004**, *21*, 601- 609.

(24) Mullins, O.; Sheu, E.; Hammami, A.; Marshall, A. G. Asphaltenes, Heavy Oils and Petroleomics *Springer* **2007**,

(25) Pfeiffer, J. P.; Saal, R. N. J. Asphaltic Bitumen as Colloid System. *Laboratorium N. V. de Bataafsche Petroleum Maatschappij, Amsterdam, Holland* **1939**.

(26) Twu, C. H. An Internally Consistent Correlation for Predicting the Critical Properties and Molecular-Weights of Petroleum and Coal-Tar Liquids. *Fluid Phase Equilibria* **1984**, *16*, 137-150.

(27) Philippi, G. T. Time and Mechanism of Origin of the Heavy to Medium-Gravity Naphthenic Crude Oils. *Geochimica et Cosmochlmlca Acta* **1977**, *41*, 33-52.

(28) Klein, G. C.; Angstrom, A.; Rodgers, R. P.; Marshall, A. G. Use of saturates/aromatics/resins/asphaltenes (SARA) fractionation to determine matrix effects in crude oil analysis by electrospray ionization Fourier transform ion cyclotron resonance mass spectrometry. *Energy & Fuels* **2006**, *20*, 668-672.

(29) Suatoni, J. C.; Swab, R. E. Rapid Hydrocarbon Group-Type Analysis by High-Performance Liquid-Chromatography. *Journal of Chromatographic Science* **1975**, *13*, 361-366.

(30) Gary, J. H.; Handwerk, G. E.; Kaiser, M. J.: *Petroleum Refining: Technology and Economics*; CRC press, 2007.

(31) Hsu, C.; Robinson, P.: Practical advances in petroleum processing, vol 1, Chapter 7: hydrotreating and hydrocracking: fundamentals. Springer, New York, 2006.

References

(32) Speight, J. G.; Özüm, B.: *Petroleum Refining Processes: Feedstock terminology, availability, and evaluation*; Marcel Dekker, 2002.

(33) Hughey, C. A.; Rodgers, R. P.; Marshall, A. G.; Walters, C. C.; Qian, K. N.; Mankiewicz, P. Acidic and neutral polar NSO compounds in Smackover oils of different thermal maturity revealed by electrospray high field Fourier transform ion cyclotron resonance mass spectrometry. *Org. Geochem.* **2004**, *35*, 863-880.

(34) Dufresne, P. Hydroprocessing catalysts regeneration and recycling. *Applied Catalysis A General* **2007**, *322*, 67-75.

(35) Van Looij, F.; Van der Laan, P.; Stork, W.; DiCamillo, D.; Swain, J. Key parameters in deep hydrodesulfurization of diesel fuel. *Applied Catalysis A: General* **1998**, *170*, 1-12.

(36) Furimsky, E. Hydrodenitrogenation of petroleum. *Catalysis Reviews-Science and Engineering* **2005**, *47*, 297-489.

(37) Czogalla, C.-D.; Boberg, F. Sulfur compounds in fossil fuels I. *Sulfur Reports* **1983**, *3*, 121-161.

(38) Sheu, E. Y. Petroleum asphaltene-properties, characterization, and issues. *Energy & Fuels* **2002**, *16*, 74-82.

(39) Groenzin, H.; Mullins, O. C. Molecular size and structure of asphaltenes from various sources. *Energy & Fuels* **2000**, *14*, 677-684.

(40) Laredo, G. C.; Lopez, C. R.; Alvarez, R. E.; Cano, J. L. Naphthenic acids, total acid number and sulfur content profile characterization in Isthmus and Maya crude oils. *Fuel* **2004**, *83*, 1689-1695.

(41) Laredo, G. C.; Lopez, C. R.; Alvarez, R. E.; Castillo, J. J.; Cano, J. L. Identification of naphthenic acids and other corrosivity-related characteristics in crude oil and vacuum gas oils from a Mexican refinery. *Energy & Fuels* **2004**, *18*, 1687-1694.

(42) Turnbull, A.; Slavcheva, E.; Shone, B. Factors controlling naphthenic acid corrosion. *Corrosion* **1998**, *54*, 922-930.

(43) McNaught, A. D.; Wilkinson, A. IUPAC. Compendium of Chemical Terminology, 2nd ed. (the "Gold Book"). . **1997**, http://goldbook.iupac.org/.

(44) Fenn, J. B.; Mann, M.; Meng, C. K.; Wong, S. F.; Whitehouse, C. M. Electrospray Ionization-Principles and Practice. *Mass Spectrometry Reviews* **1990**, *9*, 37-70.

(45) Mora, J. F.; Van Berkel, G. J.; Enke, C. G.; Cole, R. B.; Martinez-Sanchez, M.; Fenn, J. B. Electrochemical processes in electrospray ionization mass spectrometry. *J. Mass Spectrom.* **2000**, *35*, 939-952.

(46) Wilm, M. S.; Mann, M. Electrospray and Taylor-Cone theory, Dole's beam of macromolecules at last? *International Journal of Mass Spectrometry and Ion Processes* **1994**, *136*, 167-180.

(47) La Mora, D.; Fernandez, J. The current emitted by highly conducting Taylor cones. *Journal of fluid mechanics* **1994**, *260*, 155-184.

(48) Iribarne, J. V.; Thomson, B. A. On the evaporation of small ions from charged droplets. *Journal of Chemical Physics* **1976**, *64*, 2287-2294.

References

(49) Dole, M.; Mack, L.; Hines, R.; Mobley, R.; Ferguson, L.; Alice, M. d. Molecular beams of macroions. *The Journal of Chemical Physics* **1968**, *49*, 2240-2249.

(50) Fenn, J. B.; Mann, M.; Meng, C. K.; Wong, S. F.; Whitehouse, C. M. Electrospray ionization for mass spectrometry of large biomolecules. *Science* **1989**, *246*, 64-71.

(51) Annesley, T. M. Ion suppression in mass spectrometry. *Clin. Chem.* **2003**, *49*, 1041-1044.

(52) Zhan, D. L.; Fenn, J. B. Electrospray mass spectrometry of fossil fuels. *International Journal of Mass Spectrometry* **2000**, *194*, 197-208.

(53) Marshall, A. G.; Rodgers, R. P. Petroleomics: chemistry of the underworld. *Proc. Natl. Acad. Sci. U S A* **2008**, *105*, 18090-18095.

(54) Purcell, J. M.; Juyal, P.; Kim, D. G.; Rodgers, R. P.; Hendrickson, C. L.; Marshall, A. G. Sulfur speciation in petroleum: Atmospheric pressure photoionization or chemical derivatization and electrospray ionization fourier transform ion cyclotron resonance mass spectrometry. *Energy & Fuels* **2007**, *21*, 2869-2874.

(55) Muller, H.; Andersson, J. T.; Schrader, W. Characterization of high-molecular-weight sulfur-containing aromatics in vacuum residues using Fourier transform ion cyclotron resonance mass spectrometry. *Anal. Chem.* **2005**, *77*, 2536-2543.

(56) Marshall, A. G.; Rodgers, R. P. Petroleomics: the next grand challenge for chemical analysis. *Acc. Chem. Res.* **2004**, *37*, 53-59.

(57) Hsu, C. S.; Hendrickson, C. L.; Rodgers, R. P.; McKenna, A. M.; Marshall, A. G. Petroleomics: advanced molecular probe for petroleum heavy ends. *J. Mass Spectrom.* **2011**, *46*, 337-343.

(58) Robb, D. B.; Covey, T. R.; Bruins, A. P. Atmospheric Pressure Photoionization: An Ionization Method for Liquid Chromatography−Mass Spectrometry. *Anal. Chem.* **2000**, *72*, 3653-3659.

(59) Raffaelli, A.; Saba, A. Atmospheric pressure photoionization mass spectrometry. *Mass Spectrom. Rev.* **2003**, *22*, 318-331.

(60) Robb, D. B.; Blades, M. W. Effects of solvent flow, dopant flow, and lamp current on dopant-assisted atmospheric pressure photoionization (DA-APPI) for LC-MS. Ionizationvia proton transfer. *Journal of the American Society for Mass Spectrometry* **2005**, *16*, 1275-1290.

(61) Robb, D. B.; Blades, M. W. Factors affecting primary ionization in dopant-assisted atmospheric pressure photoionization (DA-APPI) for LC/MS. *J. Am. Soc. Mass Spectrom.* **2006**, *17*, 130-138.

(62) Kauppila, T. J.; Kuuranne, T.; Meurer, E. C.; Eberlin, M. N.; Kotiaho, T.; Kostiainen, R. Atmospheric pressure photoionization mass spectrometry. Ionization mechanism and the effect of solvent on the ionization of naphthalenes. *Anal. Chem.* **2002**, *74*, 5470-5479.

(63) Purcell, J. M.; Hendrickson, C. L.; Rodgers, R. P.; Marshall, A. G. Atmospheric pressure photoionization fourier transform ion cyclotron resonance

mass spectrometry for complex mixture analysis. *Anal. Chem.* **2006**, *78*, 5906-5912.

(64) Schaub, T. M.; Hendrickson, C. L.; Quinn, J. P.; Rodgers, R. P.; Marshall, A. G. Instrumentation and method for ultrahigh resolution field desorption ionization fourier transform ion cyclotron resonance mass spectrometry of nonpolar species. *Anal. Chem.* **2005**, *77*, 1317-1324.

(65) Comisarov, M. B.; Marshall, A. G. *Chem. Phys. Lett.* **1974**, *25*, 282.

(66) Marshall, A. G.; Hendrickson, C. L.; Jackson, G. S. Fourier transform ion cyclotron resonance mass spectrometry: a primer. *Mass Spectrom. Rev.* **1998**, *17*, 1-35.

(67) Marshall, A. G.; Hendrickson, C. L. Fourier transform ion cyclotron resonance detection: principles and experimental configurations. *International Journal of Mass Spectrometry* **2002**, *215*, 59-75.

(68) Dehmelt, H. Ion traps. *Rev. Mod. Phys.* **1990**, *62*, 525-530.

(69) Shi, S. D. H.; Drader, J. J.; Freitas, M. A.; Hendrickson, C. L.; Marshall, A. G. Comparison and interconversion of the two most common frequency-to-mass calibration functions for Fourier transform ion cyclotron resonance mass spectrometry. *International Journal of Mass Spectrometry* **2000**, *195*, 591-598.

(70) Amster, I. J. Fourier transform mass spectrometry. *Journal of Mass Spectrometry* **1996**, *31*, 1325-1337.

(71) Gross, J. H.: Mass Spectrometry: a text book. In *Mass Spectrometry: a text book*; Springer-Velang, 2004.

(72) Marshall, A. G.; Comisarow, M. B.; Parisod, G. Theory of Fourier-Transform Ion-Cyclotron Resonance Mass Spectroscopy-Iii .1. Relaxation and Spectral-Line Shape in Fourier-Transform Ion Resonance Spectroscopy. *Journal of Chemical Physics* **1979**, *71*, 4434-4444.

(73) Batey, J. H. The physics and technology of quadrupole mass spectrometers. *Vacuum* **2014**, *101*, 410-415.

(74) Miller, P. E.; Denton, M. B. The Quadrupole Mass Filter - Basic Operating Concepts. *Journal of Chemical Education* **1986**, *63*, 617-622.

(75) de Hoffmann, E. Tandem mass spectrometry: a primer. *Journal of Mass Spectrometry* **1996**, *31*, 129-137.

(76) Hardman, M.; Makarov, A. A. Interfacing the orbitrap mass analyzer to an electrospray ion source. *Anal. Chem.* **2003**, *75*, 1699-1705.

(77) Makarov, A. Electrostatic axially harmonic orbital trapping: a high-performance technique of mass analysis. *Anal. Chem.* **2000**, *72*, 1156-1162.

(78) Makarov, A.; Denisov, E.; Kholomeev, A.; Balschun, W.; Lange, O.; Strupat, K.; Horning, S. Performance evaluation of a hybrid linear ion trap/orbitrap mass spectrometer. *Anal. Chem.* **2006**, *78*, 2113-2120.

(79) Makarov, A.; Denisov, E.; Lange, O.; Horning, S. Dynamic range of mass accuracy in LTQ Orbitrap hybrid mass spectrometer. *J. Am. Soc. Mass Spectrom.* **2006**, *17*, 977-982.

References

(80) Kingdon, K. A method for the neutralization of electron space charge by positive ionization at very low gas pressures. *Physical Review* **1923**, *21*, 408.

(81) Knight, R. Storage of ions from laser – produced plasmas. *Applied Physics Letters* **1981**, *38*, 221-223.

(82) Hu, Q.; Noll, R. J.; Li, H.; Makarov, A.; Hardman, M.; Graham Cooks, R. The Orbitrap: a new mass spectrometer. *J. Mass Spectrom.* **2005**, *40*, 430-443.

(83) Perry, R. H.; Cooks, R. G.; Noll, R. J. Orbitrap mass spectrometry: instrumentation, ion motion and applications. *Mass Spectrom. Rev.* **2008**, *27*, 661-699.

(84) Makarov, A.; Denisov, E.; Lange, O.; Horning, S. Dynamic range of mass accuracy in LTQ Orbitrap hybrid mass spectrometer. *Journal of the American Society for Mass Spectrometry* **2006**, *17*, 977-982.

(85) Henry, K. D.; McLafferty, F. W. Electrospray ionization with Fourier – transform mass spectrometry. Charge state assignment from resolved isotopic peaks. *Organic Mass Spectrometry* **1990**, *25*, 490-492.

(86) Senko, M. W.; Beu, S. C.; McLafferty, F. W. Automated assignment of charge states from resolved isotopic peaks for multiply charged ions. *J. Am. Soc. Mass Spectrom.* **1995**, *6*, 52-56.

(87) Altgelt, K. H.: *Composition and analysis of heavy petroleum fractions*; CRC Press, 1993.

(88) Chmielowiec, J.; George, A. E. Polar Bonded-Phase Sorbents for High-Performance Liquid-Chromatographic Separations of Polycyclic Aromatic-Hydrocarbons. *Anal.l Chem.* **1980**, *52*, 1154-1157.

(89) Abd-El Hamid, N. A.; El-Gizawy, S. M. Chemically bonded cyclodextrin stationary phase for the high-performance liquid chromatographic separation and determination of sulphonamides. *Analyst* **1989**, *114*, 571-573.

(90) Wise, S.; Chesler, S.; Hertz, H.; Hilpert, L.; May, W. Chemically-bonded aminosilane stationary phase for the high-performance liquid chromatographic separation of polynuclear aromatic compounds. *Anal. Chem.* **1977**, *49*, 2306-2310.

(91) Boduszynski, M. M.; Altgelt, K. H. Composition of Heavy Petroleums .4. Significance of the Extended Atmospheric Equivalent Boiling-Point (Aebp) Scale. *Energy & Fuels* **1992**, *6*, 72-76.

(92) Altgelt, K. H.; Boduszynski, M. M. Composition of Heavy Petroleums .3. An Improved Boiling-Point Molecular-Weight Relation. *Energy & Fuels* **1992**, *6*, 68-72.

(93) Tong, J.; Han, X.; Wang, S.; Jiang, X. Evaluation of structural characteristics of Huadian oil shale kerogen using direct techniques (solid-state 13C NMR, XPS, FT-IR, and XRD). *Energy & Fuels* **2011**, *25*, 4006-4013.

(94) Albert, D. K. Determination of Nitrogen Compound Distribution in Petroleum by Gas-Chromatography with a Thermionic Detector. *Anal. Chem.* **1978**, *50*, 1822-1829.

References

(95) Richardson, J. S.; Miiller, D. E. Identification of Dicyclic and Tricyclic Hydrocarbons in the Saturate Fraction of a Crude-Oil by Gas-Chromatography Mass-Spectrometry. *Anal. Chem.* **1982**, *54*, 765-768.

(96) Wang, Z. D.; Fingas, M. Differentiation of the Source of Spilled Oil and Monitoring of the Oil Weathering Process Using Gas Chromatography-Mass Spectrometry. *Journal of Chromatography A* **1995**, *712*, 321-343.

(97) Venkatramani, C. J.; Phillips, J. B. Comprehensive two - dimensional gas chromatography applied to the analysis of complex mixtures. *Journal of Microcolumn Separations* **1993**, *5*, 511-516.

(98) Blomberg, J.; Schoenmakers, P. J.; Beens, J.; Tijssen, R. Compehensive two - dimensional gas chromatography (GC× GC) and its applicability to the characterization of complex (petrochemical) mixtures. *Journal of high resolution chromatography* **1997**, *20*, 539-544.

(99) Johnson, E. G.; Nier, A. O. Angular aberrations in sector shaped electromagnetic lenses for focusing beams of charged particles. *Physical Review* **1953**, *91*, 10.

(100)Wiley, W.; McLaren, I. H. Time - of - flight mass spectrometer with improved resolution. *Review of Scientific Instruments* **1955**, *26*, 1150-1157.

(101)Dawson, P. H.: *Quadrupole mass spectrometry and its applications*; Elsevier, 2013.

(102)Schwartz, J. C.; Senko, M. W.; Syka, J. E. A two-dimensional quadrupole ion trap mass spectrometer. *J. Am. Soc. Mass Spectrom.* **2002**, *13*, 659-669.

(103)Comisarow, M. B.; Marshall, A. G. Fourier-Transform Ion-Cyclotron Resonance Spectroscopy. *Chemical Physics Letters* **1974**, *25*, 282-283.

(104)Hertkorn, N.; Ruecker, C.; Meringer, M.; Gugisch, R.; Frommberger, M.; Perdue, E. M.; Witt, M.; Schmitt-Kopplin, P. High-precision frequency measurements: indispensable tools at the core of the molecular-level analysis of complex systems. *Analytical and Bioanalytical Chemistry* **2007**, *389*, 1311-1327.

(105)Hsu, C. S.; Liang, Z.; Campana, J. Hydrocarbon characterization by ultrahigh resolution FT-ICR MS. *Anal. Chem.* **1994**, *66*, 850-855.

(106)Field, F. H.; Hastings, S. H. Determination of unsaturated hydrocarbons by low voltage mass spectrometry. *Anal Chem.* **1956**, *28*, 1248-1255.

(107)Guan, S.; Marshall, A. G.; Scheppele, S. E. Resolution and chemical formula identification of aromatic hydrocarbons and aromatic compounds containing sulfur, nitrogen, or oxygen in petroleum distillates and refinery streams. *Anal. Chem.* **1996**, *68*, 46-71.

(108)Schaub, T. M.; Hendrickson, C. L.; Qian, K.; Quinn, J. P.; Marshall, A. G. High-resolution field desorption/ionization fourier transform ion cyclotron resonance mass analysis of nonpolar molecules. *Anal. Chem.* **2003**, *75*, 2172-2176.

(109)Byrd, H. C. M.; McEwen, C. N. The limitations of MALDI-TOF mass spectrometry in the analysis of wide polydisperse polymers. *Anal. Chem.* **2000**, *72*, 4568-4576.

References

(110)Kim, Y. H.; Kim, S. Improved abundance sensitivity of molecular ions in positive-ion APCI MS analysis of petroleum in toluene. *J. Am. Soc. Mass Spectrom.* **2010**, *21*, 386-392.

(111)Gross, J. H.: *Mass spectrometry: a textbook*; Springer Science & Business Media, 2006.

(112)Marshall, A. G.; Hendrickson, C. L. High-resolution mass spectrometers. *Annu. Rev. Anal. Chem. (Palo Alto Calif)* **2008**, *1*, 579-599.

(113)Chernushevich, I. V.; Loboda, A. V.; Thomson, B. A. An introduction to quadrupole-time-of-flight mass spectrometry. *J. Mass Spectrom.* **2001**, *36*, 849-865.

(114)Scigelova, M.; Makarov, A. Orbitrap mass analyzer--overview and applications in proteomics. *Proteomics* **2006**, *6 Suppl 2*, 16-21.

(115)Hughey, C. A.; Rodgers, R. P.; Marshall, A. G.; Qian, K. N.; Robbins, W. K. Identification of acidic NSO compounds in crude oils of different geochemical origins by negative ion electrospray Fourier transform ion cyclotron resonance mass spectrometry. *Org. Geochem.* **2002**, *33*, 743-759.

(116)Xian, F.; Hendrickson, C. L.; Blakney, G. T.; Beu, S. C.; Marshall, A. G. Automated broadband phase correction of Fourier transform ion cyclotron resonance mass spectra. *Anal. Chem.* **2010**, *82*, 8807-8812.

(117)Ledford Jr, E. B.; Rempel, D. L.; Gross, M. Space charge effects in Fourier transform mass spectrometry. II. Mass calibration. *Anal. Chem.* **1984**, *56*, 2744-2748.

(118)Webb, K.; Bristow, T.; Sargent, M.; Stein, B. Methodology for accurate mass measurement of small molecules. *Best Practice Guide* **2004**.

(119)Viant, M. High mass accuracy and resolution: key specifications in mass spectrometry based metabolomics *University of Birmingham*, http://www.metabolomicssociety.org/tutorials.

(120)Syka, J. E. P.; Marto, J. A.; Bai, D. L.; Horning, S.; Senko, M. W.; Schwartz, J. C.; Ueberheide, B.; Garcia, B.; Busby, S.; Muratore, T.; Shabanowitz, J.; Hunt, D. F. Novel linear quadrupole ion trap/FT mass spectrometer: Performance characterization and use in the comparative analysis of histone H3 post-translational modifications. *Journal of Proteome Research* **2004**, *3*, 621-626.

(121)McLafferty, F. W.: *Interpretation of mass spectra*; Fourth edition ed.; University Science Books, 1993. pp. 42.

(122)Barrow, M. P.; McDonnell, L. A.; Feng, X. D.; Walker, J.; Derrick, P. J. Determination of the nature of naphthenic acids present in crude oils using nanospray Fourier transform ion cyclotron resonance mass spectrometry: The continued battle against corrosion. *Anal. Chem.* **2003**, *75*, 860-866.

(123)Kendrick, E. A Mass Scale Based on CH2= 14.0000 for High Resolution Mass Spectrometry of Organic Compounds. *Anal. Chem.* **1963**, *35*, 2146-2154.

(124)Hughey, C. A.; Hendrickson, C. L.; Rodgers, R. P.; Marshall, A. G.; Qian, K. Kendrick mass defect spectrum: a compact visual analysis for ultrahigh-resolution broadband mass spectra. *Anal. Chem.* **2001**, *73*, 4676-4681.

(125)Corilo, Y.: PetroOrg Software. Florida State University Tallahassee, FL, 2014.

References

(126)Caravatti, P.; Allemann, M. The 'infinity cell': A new trapped - ion cell with radiofrequency covered trapping electrodes for Fourier transform ion cyclotron resonance mass spectrometry. *Organic Mass Spectrometry* **1991**, *26*, 514-518.

(127)Senko, M. W.; Hendrickson, C. L.; Emmett, M. R.; Shi, S. D. H.; Marshall, A. G. External accumulation of ions for enhanced electrospray ionization Fourier transform ion cyclotron resonance mass spectrometry. *Journal of the American Society for Mass Spectrometry* **1997**, *8*, 970-976.

(128)Hendrickson, C.; Quinn, J.; Emmett, M.; Marshall, A. Quadrupole mass filtered external accumulation for Fourier transform ion cyclotron resonance mass spectrometry. *Proceedings of the 48th ASMS Conference on Mass Spectrometry and Allied Topics* **2000**.

(129)Comisarow, M. B.; Marshall, A. G. Frequency-sweep Fourier transform ion cyclotron resonance spectroscopy. *Chemical Physics Letters* **1974**, *26*, 489-490.

(130)Mitchell, D. W.; Smith, R. D. Cyclotron motion of two Coulombically interacting ion clouds with implications to Fourier-transform ion cyclotron resonance mass spectrometry. *Phys. Rev. E. Stat. Phys. Plasmas Fluids Relat. Interdiscip Topics* **1995**, *52*, 4366-4386.

(131)Guisnet, M.; Magnoux, P. Coking and Deactivation of Zeolites - Influence of the Pore Structure. *Applied Catalysis* **1989**, *54*, 1-27.

(132)Qian, K.; Tomczak, D. C.; Rakiewicz, E. F.; Harding, R. H.; Yaluris, G.; Cheng, W.-C.; Zhao, X.; Peters, A. W. Coke Formation in the Fluid Catalytic Cracking Process by Combined Analytical Techniques. 1997, 11, 596-601. *Energy & Fuels* **1997**, *11*, 1108-1108.

(133)Miyabayashi, K.; Suzuki, K.; Teranishi, T.; Naito, Y.; Tsujimoto, K.; Miyake, R. Molecular formula determination of constituents in Arabian mix vacuum residue by electrospray ionization fourier transform ion cyclotron resonance mass spectrometry. *Chemistry Letters* **2000**, 172-173.

(134)McLafferty, F. W.; Tureček, F.: *Interpretation of mass spectra*; Fourth Edition ed.; University Science Books, 1993. pp. 42.

(135)Hughey, C. A.; Rodgers, R. P.; Marshall, A. G. Resolution of 11,000 compositionally distinct components in a single electrospray ionization Fourier transform ion cyclotron resonance mass spectrum of crude oil. *Anal. Chem.* **2002**, *74*, 4145-4149.

(136)Pakarinen, J. M. H.; Teravainen, M. J.; Pirskanen, A.; Wickstrom, K.; Vainiotalo, P. A positive-ion electrospray ionization Fourier transform ion cyclotron resonance mass spectrometry study of Russian and north sea crude oils and their six distillation fractions. *Energy & Fuels* **2007**, *21*, 3369-3374.

(137)Molnarne Guricza, L.; Schrader, W. Electrospray ionization for determination of non-polar polyaromatic hydrocarbons and polyaromatic heterocycles in heavy crude oil asphaltenes. *J. Mass Spectrom.* **2015**, *50*, 549-557.

(138)Bae, E.; Na, J. G.; Chung, S. H.; Kim, H. S.; Kim, S. Identification of about 30 000 Chemical Components in Shale Oils by Electrospray Ionization (ESI) and Atmospheric Pressure Photoionization (APPI) Coupled with 15 T Fourier

Transform Ion Cyclotron Resonance Mass Spectrometry (FT-ICR MS) and a Comparison to Conventional Oil. *Energy & Fuels* **2010**, *24*, 2563-2569.

(139)Sim, A.; Cho, Y.; Kim, D.; Witt, M.; Birdwell, J. E.; Kim, B. J.; Kim, S. Molecular-level characterization of crude oil compounds combining reversed-phase high-performance liquid chromatography with off-line high-resolution mass spectrometry. *Fuel* **2015**, *140*, 717-723.

(140)Cody, R. B.; Laramée, J. A.; Nilles, J. M.; Durst, H. D. Direct analysis in real time (DARTtm) mass spectrometry. *JEOL news* **2005**, *40*, 8-12.

(141)Lobodin, V. V.; Nyadong, L.; Ruddy, B. M.; Curtis, M.; Jones, P. R.; Rodgers, R. P.; Marshall, A. G. DART Fourier transform ion cyclotron resonance mass spectrometry for analysis of complex organic mixtures. *International Journal of Mass Spectrometry* **2015**, *378*, 186-192.

(142)Lide, D. R.: *CRC handbook of chemistry and physics*; CRC press, 2004; Vol. 85.

(143)Henner, P.; Schiavon, M.; Morel, J. L.; Lichtfouse, E. Polycyclic aromatic hydrocarbon (PAH) occurence and remediation methods. *Analusis Magazine* **1997**, *25*, M56-M59.

(144)Baek, S. O.; Field, R. A.; Goldstone, M. E.; Kirk, P. W.; Lester, J. N.; Perry, R. A Review of Atmospheric Polycyclic Aromatic-Hydrocarbons - Sources, Fate and Behavior. *Water Air and Soil Pollution* **1991**, *60*, 279-300.

(145)Mastral, A. M.; Callen, M. S. A review on polycyclic aromatic hydrocarbon (PAH) emissions from energy generation. *Environmental Science & Technology* **2000**, *34*, 3051-3057.

(146)Tan, Y. L.; Heit, M. Biogenic and abiogenic polynuclear aromatic hydrocarbons in sediments from two remote Adirondack lakes. *Geochimica et Cosmochimica Acta* **1981**, *45*, 2267-2279.

(147)Gschwend, P. M.; Chen, P. H.; Hites, R. A. On the Formation of Perylene in Recent Sediments - Kinetic-Models. *Geochimica Et Cosmochimica Acta* **1983**, *47*, 2115-2119.

(148)Golovko, A. K.; Mozzhelina, T. K.; Serebrennikova, O. V. Distribution of perylene hydrocarbons in oils and organic matter of deposits of different age. *Polycyclic Aromatic Compounds* **1999**, *14*, 209-220.

(149)Wenclawiak, B. W.; Hees, T. Optimization of High-Performance Liquid-Chromatography and Solvent Parameters for the Separation of Polycyclic Aromatic-Hydrocarbons Compared with Supercritical-Fluid Chromatography with Uv Detection. *Journal of Chromatography A* **1994**, *660*, 61-65.

(150)Wenclawiak, B.; Rathmann, C.; Teuber, A. Supercritical-Fluid Extraction of Soil Samples and Determination of Polycyclic Aromatic-Hydrocarbons (Pahs) by Hplc. *Fresenius Journal of Analytical Chemistry* **1992**, *344*, 497-500.

(151)Kot, A.; Sandra, P.; David, F. Selectivity tuning in packed column SFC separation of the sixteen priority polycyclic aromatic hydrocarbons as an example. *Journal of High Resolution Chromatography* **1994**, *17*, 277-279.

(152)Paschke, T.; Hawthorne, S. B.; Miller, D. J.; Wenclawiak, B. Supercritical Fluid Extraction of Nitrated Polycyclic Aromatic-Hydrocarbons and Polycyclic

Aromatic-Hydrocarbons from Diesel Exhaust Particulate Matter. *Journal of Chromatography* **1992**, *609*, 333-340.

(153)Itoh, N.; Aoyagi, Y.; Yarita, T. Optimization of the dopant for the trace determination of polycyclic aromatic hydrocarbons by liquid chromatography/dopant-assisted atmospheric-pressure photoionization/mass spectrometry. *J. Chromatogr. A* **2006**, *1131*, 285-288.

(154)Villar, P.; Callejon, M.; Alonso, E.; Jimenez, J. C.; Guiraum, A. Temporal evolution of polycyclic aromatic hydrocarbons (PAHs) in sludge from wastewater treatment plants: Comparison between PAHs and heavy metals. *Chemosphere* **2006**, *64*, 535-541.

(155)Revelskii, I. A.; Yashin, Y. S.; Kurochkin, V. K.; Kostyanovskii, R. G. Mass-Spectrometry with Photoionization at Atmospheric-Pressure and the Analysis of Multicomponent Mixtures without Separation. *Industrial Laboratory* **1991**, *57*, 243-248.

(156)Liu, P.; Shi, Q. A.; Chung, K. H.; Zhang, Y. H.; Pan, N.; Zhao, S. Q.; Xu, C. M. Molecular Characterization of Sulfur Compounds in Venezuela Crude Oil and Its SARA Fractions by Electrospray Ionization Fourier Transform Ion Cyclotron Resonance Mass Spectrometry. *Energy & Fuels* **2010**, *24*, 5089-5096.

(157)Rudzinski, W. E.; Aminabhavi, T. M.; Tarbox, T.; Sassman, S.; Whitney, K.; Watkins, L. M. Liquid chromatography/electrospray ionization/mass spectrometry study of the interactions between palladium and sulfur heterocycles. *Abstracts of Papers of the American Chemical Society* **2000**, *219*, U252-U252.

(158)Roussis, S. G.; Prouix, R. Molecular weight distributions of heavy aromatic petroleum fractions by Ag+ electrospray ionization mass spectrometry. *Anal. Chem.* **2002**, *74*, 1408-1414.

(159)Roussis, S. G.; Proulx, R. Probing the molecular weight distributions of non-boiling petroleum fractions by Ag+ electrospray ionization mass spectrometry. *Rapid Commun Mass Spectrom* **2004**, *18*, 1761-1775.

(160)Gruendling, T.; Hart-Smith, G.; Davis, T. P.; Stenzel, M. H.; Barner-Kowollik, C. Enhanced ionization in electrospray ionization mass spectrometry of labile end-group-containing polystyrenes using silver(I) tetrafluoroborate as doping salt. *Macromolecules* **2008**, *41*, 1966-1971.

(161)Laali, K. K.; Hupertz, S.; Temu, A. G.; Galembeck, S. E. Electrospray mass spectrometric and DFT study of substituent effects in Ag(+) complexation to polycyclic aromatic hydrocarbons (PAHs). *Org. Biomol. Chem.* **2005**, *3*, 2319-2326.

(162)Lobodin, V. V.; Juyal, P.; McKenna, A. M.; Rodgers, R. P.; Marshall, A. G. Silver cationization for rapid speciation of sulfur-containing species in crude oils by positive electrospray ionization fourier transform ion cyclotron resonance mass spectrometry. *Energy & Fuels* **2013**, *28*, 447-452.

(163)Jayaraman, A.; Saxena, R. C. Corrosion and its control in petroleum refineries - A review. *Corrosion Prevention & Control* **1995**, *42*, 123-131.

(164)Jaffe, R.; Gardinali, P. R. Generation and Maturation of Carboxylic-Acids in Ancient Sediments from the Maracaibo Basin, Venezuela. *Org. Geochem.* **1990**, *16*, 211-218.

References

(165)Nascimento, L. R.; Reboucas, L. M. C.; Koike, L.; Reis, F. D. M.; Soldan, A. L.; Cerqueira, J. R.; Marsaioli, A. J. Acidic biomarkers from Albacora oils, Campos Basin, Brazil. *Org. Geochem.* **1999**, *30*, 1175-1191.

(166)Behar, F.; Albrecht, P. Correlations between carboxylic acids and hydrocarbons in several crude oils. Alteration by biodegradation. *Org. Geochem.* **1984**, *6*, 597-604.

(167)Jaffe, R.; Gallardo, M. T. Application of Carboxylic-Acid Biomarkers as Indicators of Biodegradation and Migration of Crude Oils from the Maracaibo Basin, Western Venezuela. *Org. Geochem.* **1993**, *20*, 973-984.

(168)Meredith, W.; Kelland, S. J.; Jones, D. M. Influence of biodegradation on crude oil acidity and carboxylic acid composition. *Org. Geochem.* **2000**, *31*, 1059-1073.

(169)Brient, J. A.; Wessner, P. J.; Doyle, M. N.: Naphthenic acids. In *In Encyclopedia of chemical technology*; 4th ed.; Kroschwitz, J. I. ed.; John Wile & Sons: New York, 1995; pp 1017−1029.

(170)Dzidic, I.; Somerville, A. C.; Raia, J. C.; Hart, H. V. Determination of Naphthenic Acids in California Crudes and Refinery Wastewaters by Fluoride-Ion Chemical Ionization Mass-Spectrometry. *Anal. Chem.* **1988**, *60*, 1318-1323.

(171)Headley, J. V.; Peru, K. M.; Mohamed, M. H.; Frank, R. A.; Martin, J. W.; Hazewinkel, R. R.; Humphries, D.; Gurprasad, N. P.; Hewitt, L. M.; Muir, D. C.; Lindeman, D.; Strub, R.; Young, R. F.; Grewer, D. M.; Whittal, R. M.; Fedorak, P. M.; Birkholz, D. A.; Hindle, R.; Reisdorph, R.; Wang, X.; Kasperski, K. L.; Hamilton, C.; Woudneh, M.; Wang, G.; Loescher, B.; Farwell, A.; Dixon, D. G.; Ross, M.; Pereira Ados, S.; King, E.; Barrow, M. P.; Fahlman, B.; Bailey, J.; McMartin, D. W.; Borchers, C. H.; Ryan, C. H.; Toor, N. S.; Gillis, H. M.; Zuin, L.; Bickerton, G.; McMaster, M.; Sverko, E.; Shang, D.; Wilson, L. D.; Wrona, F. J. Chemical fingerprinting of naphthenic acids and oil sands process waters-A review of analytical methods for environmental samples. *J. Environ. Sci. Health A Tox. Hazard Subst. Environ. Eng.* **2013**, *48*, 1145-1163.

(172)Schindler, D. W. Unravelling the complexity of pollution by the oil sands industry. *Proc. Natl. Acad Sci U S A* **2014**, *111*, 3209-3210.

(173)Barrow, M. P.; Witt, M.; Headley, J. V.; Peru, K. M. Athabasca oil sands process water: characterization by atmospheric pressure photoionization and electrospray ionization fourier transform ion cyclotron resonance mass spectrometry. *Anal. Chem.* **2010**, *82*, 3727-3735.

(174)Headley, J. V.; Peru, K. M.; Barrow, M. P. Mass spectrometric characterization of naphthenic acids in environmental samples: a review. *Mass Spectrom. Rev.* **2009**, *28*, 121-134.

(175)Fan, T. P. Characterization of Naphthenic Acids in Petroleum by Fast-Atom-Bombardment Mass-Spectrometry. *Energy & Fuels* **1991**, *5*, 371-375.

(176)Hsu, C. S.; Dechert, G. J.; Robbins, W. K.; Fukuda, E. K. Naphthenic acids in crude oils characterized by mass spectrometry. *Energy & Fuels* **2000**, *14*, 217-223.

(177)Hao, C. Y.; Headley, J. V.; Peru, K. A.; Frank, R.; Yang, P.; Solomon, K. R. Characterization and pattern recognition of oil-sand naphthenic acids using comprehensive two-dimensional gas chromatography/time-of-flight mass spectrometry. *Journal of Chromatography A* **2005**, *1067*, 277-284.

References

(178)John, W. P. S.; Rughani, J.; Green, S. A.; McGinnis, G. D. Analysis and characterization of naphthenic acids by gas chromatography–electron impact mass spectrometry of tert.-butyldimethylsilyl derivatives. *Journal of Chromatography A* **1998**, *807*, 241-251.

(179)Holowenko, F. M.; MacKinnon, M. D.; Fedorak, P. M. Characterization of naphthenic acids in oil sands wastewaters by gas chromatography-mass spectrometry. *Water Res.* **2002**, *36*, 2843-2855.

(180)Yu, S. K. T.; Green, J. B. Determination of Total Hydroxyls and Carboxyls in Petroleum and Syncrudes after Chemical Derivatization by Infrared-Spectroscopy. *Anal. Chem.* **1989**, *61*, 1260-1268.

(181)Tomczyk, N. A.; Winans, R. E.; Shinn, J. H.; Robinson, R. C. On the nature and origin of acidic species in petroleum. 1. Detailed acid type distribution in a California crude oil. *Energy & Fuels* **2001**, *15*, 1498-1504.

(182)Kauppila, T. J.; Kotiaho, T.; Kostiainen, R.; Bruins, A. P. Negative ion-atmospheric pressure photoionization-mass spectrometry. *J. Am. Soc. Mass Spectrom.* **2004**, *15*, 203-211.

(183)Song, L.; Wellman, A. D.; Yao, H.; Bartmess, J. E. Negative ion-atmospheric pressure photoionization: electron capture, dissociative electron capture, proton transfer, and anion attachment. *J. Am. Soc. Mass Spectrom.* **2007**, *18*, 1789-1798.

(184)Jordan, K. D.; Burrow, P. D. Studies of the temporary anion states of unsaturated hydrocarbons by electron transmission spectroscopy. *Accounts of Chemical Research* **1978**, *11*, 341-348.

(185)Weiss, G.: Hazardous Chemical Data Book Noyes Data Corp. NJ, 1980.

(186)Kim, S.; Stanford, L. A.; Rodgers, R. P.; Marshall, A. G.; Walters, C. C.; Qian, K.; Wenger, L. M.; Mankiewicz, P. Microbial alteration of the acidic and neutral polar NSO compounds revealed by Fourier transform ion cyclotron resonance mass spectrometry. *Org. Geochem.* **2005**, *36*, 1117-1134.

(187)Watson, J. T.; Sparkman, O. D.: *Introduction to Mass Spectrometry: Instrumentation, Applications, and Strategies for Data Interpretation*; 4th ed.; John Wiley & Sons, Ltd, Chichester, UK, 2007.

(188)Jennings, K. R. Collision-induced decompositions of aromatic molecular ions. *Int. J. Mass Spectrom. Ion Phys.* **1968**, *1*, 227-235.

(189)McLuckey, S. A. Principles of collisional activation in analytical mass spectrometry. *J. Am. Soc. Mass Spectrom.* **1992**, *3*, 599-614.

(190)Porter, Q. N.: *Mass Spectrometry of Heterocyclic Compounds* Second Edition ed.; A Volume in the Wiley Series in General Hetrocyclic Chemistry.